A TEXTURAL AND ISOTOPIC STUDY OF IRISH BASE METAL MINERALIZATION OF LOWER CARBONIFEROUS AGE, WITH SPECIFIC REFERENCE TO THE TYNAGH DEPOSIT.

ANTHONY MARK BOAST

A THESIS SUBMITTED FOR THE DEGREE OF
DOCTOR OF PHILOSOPHY

IMPERIAL COLLEGE OF SCIENCE AND TECHNOLOGY - LONDON.

ABSTRACT

A textural and isotopic study of Irish base metal mineralization of Lower Carboniferous age, with specific reference to the Tynagh deposit.

Anthony Mark Boast

At Tynagh mine, Co. Galway, four major stages of mineralization can be recognised that span the diagenetic and post-lithification history of the host Waulsortian limestones:

1) Growth of colloform pyrite clots during early diagenesis.

2) Rapid geopetal precipitation of microcrystalline sulphides, largely sphalerite, within a dilatant fracture system developed in response to tectonism and hydraulic fracturing in the Tynagh fault zone.

3) An epigenetic stage of mineralization dominated by tennantite, galena and barytes.

4) Finally, precipitation of calcite within veinlets and cavities, and dolomitisation of large bodies of Waulsortian limestones.

Sulphur isotope ratios indicate that Lower Carboniferous sea-water acted as the source of sulphate for precipitation of barytes at Tynagh. Stage 1 and 2 sulphides are isotopically light and were precipitated as a result of open-system bacterial reduction of sea-water sulphate. Isotopically heavier reduced sulphur of deep-seated origin was introduced from the fault zone during stage 3, and mixed with bacteriogenic sulphur migrating into the Waulsortian bank limestones. A preliminary investigation of texturally similar ores from the Navan deposit, has revealed a comparable range of $\delta^{34}S$ values.

Mineralized limestones, ore stage and post-ore carbonates at Tynagh are depleted in the heavier isotopes of carbon and oxygen with respect to unmineralized limestones. The depletion in ^{13}C is attributed to the mixing of host derived carbon with bacterially oxidised carbon, and, during stage 4, deep-seated carbon. $\delta^{18}O$ values are tentatively interpreted as indicating an increase in both temperature and the $^{18}O/^{16}O$ ratio of the ore fluid with time.

Tynagh galenas yield a lead isotope model age for mineralization (348 ± 22 m.y.) that agrees precisely with the stratigraphic dating of the deposit. A deep-seated, magmatic source is suggested for the metals. In contrast, lead in galenas from the Navan and Silvermines deposits is comparatively radiogenic, probably indicating a contribution of lead leached from a sedimentary or metasedimentary source.

CONTENTS

page

LIST OF TABLES

LIST OF FIGURES

LIST OF PLATES

ACKNOWLEDGEMENTS

This research was jointly supervised by Dr. Max Coleman (I.G.S.) and Dr. Chris Halls (I.C.) both of whom as well as providing invaluable advice, discussion and comment, instilled an infectious enthusiasm so essential to its successful completion. Additionally I would like to thank my many friends and colleagues within the Isotope Geology Unit (I.G.S.) and the Geology Department (I.C.) for their help and stimulating discussion during the period of research. In particular I am grateful to Dr. Ian Swainbank who provided advice and critical comment during the programme of lead isotope analysis. X.R.F. and Microprobe analyses were carried our by Mr. D. Bland and Mr. N. Wilkinson respectively, and Mr. R. Curtis provided instruction in the X.R.D. lab. Mr. B. Foster, Miss E. Morris and Mr. J. Blount prepared excellent lapped blocks, polished sections and thin sections, and Mrs. H. Richardson and Mr. J. Pulsford assisted with photography.

The project would have been impossible without the co-operation of the various mining companies presently operating within the Irish Republic. I would particularly like to thank Mr. John Hutchings of Irish Base Metal Ltd. for providing me with a free hand at Tynagh, and for pointing out many pertinent geological features. In addition I would like to thank the geological staff of Tara Mines Ltd., Bula Ltd., Mogul of Ireland Ltd., and Magcobar (Ireland) Ltd. for their help and assistance during visits to the Navan and Silvermines deposits.

I will be eternally grateful to my mother for her speedy and accurate typing of both the initial draft and final copy of the

thesis. Last but not least I would like to thank my wife Hilary for her continued encouragement and for helping me through the traumas of writing up.

Financial support was provided by the Natural Environment Research Council.

CHAPTER 1

INTRODUCTION

The discovery of the Tynagh deposit in 1961 opened a new chapter in the history of mineral exploitation within the Republic of Ireland. Prior to 1960 systematic exploration had never been undertaken. Metal production had been minimal and was largely restricted to deposits hosted within pre-Carboniferous lithologies. Minor showings of lead, zinc and copper within Carboniferous limestones were long known to be a common occurrence, but of these only the Abbeytown deposit had yielded a significant output. The Tynagh find, however, induced a phase of intensive exploration that led to the detection and subsequent development of a number of sizeable base metal deposits within the Lower Carboniferous sediments of the Central Plain of Ireland.

The similarity in mineralogy, stratigraphic position and tectonic setting of the major Irish deposits has inevitably led to the postulation of a genetic link between them. However, genetic models so far proposed have been based largely on conjecture, and have been subject to the whims of current geological opinion. Magmatic hydrothermal fluids (Derry et al, 1965; Steed, 1975) migrating formation waters (Patterson, 1971; Barrett, 1975) or both acting in conjunction (Schultz, 1968; Russell, 1968) have been called upon to supply the ore-forming constituents, whilst opinions as to the mode of emplacement have been split between the syngenetic and epigenetic schools of thought.

Against this background the present research project was initiated in the hope that a detailed programme of stable and lead isotope analysis might throw further light on to the genesis of

these economically important deposits. The Tynagh orebody was chosen to provide the basis of the study as, of all the major Irish deposits, it has perhaps been surrounded by the greatest controversy with regard to its origin. In addition, by 1975 underground development had reached a stage whereby much of the orebody was accessible thus enabling the collection of a representative suite of samples.

For an isotopic study of a geological phenomenon to be successful, it is essential that a firm geological foundation has previously been laid, upon which an interpretation of the isotope data can be built. In the case of an ore deposit, this entails the elucidation of the paragenesis or sequence of mineralizing events, and the relationship between these events and the evolution of the host. So as to satisfy this requirement it was considered that an examination of the ore textures at Tynagh was a necessary precursor to the analytical programme.

To extend any conclusions drawn from Tynagh into the broader context of mineralization within the Central Plain, comparative studies of the other producing deposits at Navan and Silvermines have also been attempted. Due to the limited time available these have been necessarily brief. Indeed, the Navan orebody, by far the most important discovery in Ireland to date, clearly warrants detailed investigation in its own right.

CHAPTER 2

GEOLOGICAL AND PALAEOGEOGRAPHICAL SETTING

2.1 REGIONAL SETTING

2.1.1 Introduction

The major and numerous minor base metal deposits of the Central Plain of Ireland are hosted within a gently dipping Lower Carboniferous sequence, through which project inliers of Devonian fluviatile sediments, with cores of highly folded Ordovician and Silurian shales, greywackes and volcanics. A large proportion of the mineralization is fault localised and all the larger deposits occur adjacent to inliers (e.g. Tynagh, Silvermines) or in close proximity to a major Lower Palaeozoic massif (e.g. Navan), - fig. 2.1.

2.1.2 The Caledonian Orogen

During the Lower Palaeozoic, the British Isles were divided into a N.W. and a S.E. foreland by the Iapetus ocean (later to become the Caledonian-Appalachian orogen) which extended from Scandinavia, through N.W. Britain, Ireland, and on into Newfoundland and the eastern United States. In a recent tectonic synthesis, Phillips et al (1976), on the basis of stratigraphic and structural evidence, recognise two distinct belts within the Ordovician and Silurian sequences in Ireland.

Much of the Longford-Down massif, along with the Arra Mountains, Slieve Bernagh and Slieve Aughty inliers, represent a continuation of the Southern Uplands, and are thought to be underlain by a sialic basement which was a part of the N.W. continental

FIG. 2.1 GEOLOGICAL OUTLINE AND PRINCIPAL MINERAL DEPOSITS OF IRELAND.

(Based on Morrissey et al., 1971)

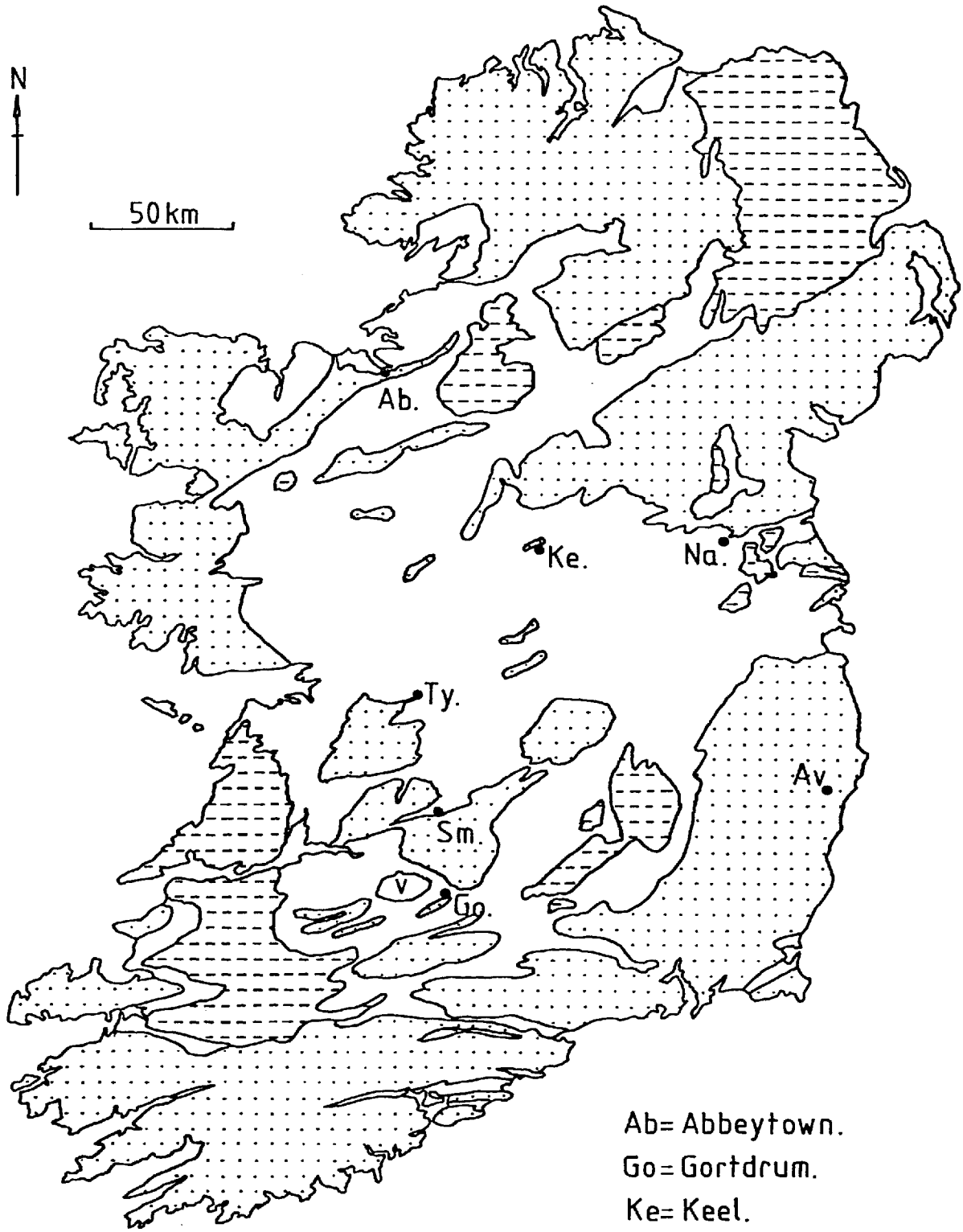

margin. The succession, which is usually overturned with a fairly consistent S.E. dip of both bedding and first cleavage, consists of a sequence of turbidites with local basic volcanics overlying black pelites and cherts.

The volcanic belt of S.E. Ireland, with its numerous rhyolitic and andesitic lavas and tuffs, is related to a continental plate margin associated with a probable south-eastwards subduction of oceanic crust. To the N.W. of the Leinster granite and in the more southerly inliers of the Central Plain, turbidites derived from this volcanic area display upright, gently plunging folds with nearly vertical cleavage.

Oblique closure of the Iapetus ocean resulted in the south-westerly migration of a trench-trench-transform triple junction, and after collision, dextral strike slip on the suture probably arose from continued convergence of the N.W. and S.E. foreland plates. Phillips and co-workers propose that the position of this suture in the British Isles is defined by a line connecting the axis of the Northumberland trough with that of the Shannon trough, via Navan and Silvermines.

Of the Caledonian intrusives, the most notable is the post-tectonic Leinster granite, which is by far the largest granite of any age in the British Isles.

2.1.3 Devonian

The Devonian period saw the peneplanation of the Caledonian orogen in Ireland, O.R.S. facies conglomerates, sandstones, siltstones and mudstones being laid down with marked unconformity upon the highly deformed Lower Palaeozoic succession. These sediments were

derived dominantly from the north, and were deposited on a broad coastal plain which superseded earlier intermontane basins. The total thickness of the Devonian is difficult to gauge, but it may be 1,000 metres in Waterford and as much as 5,000 metres in Cork and Kerry (Charlesworth, 1963).

2.1.4 Lower Carboniferous

The Lower Carboniferous sedimentary sequence of the Central Plain of Ireland is dominated by a diachronous succession of gently dipping limestones that attain a maximum thickness of over 1,000 metres (Charlesworth, 1963). Basal Tournaisian sediments record a transition from an O.R.S. facies fluviatile regime to a shallow water marine environment in which a sequence of silts and calcerous shales were laid down (Lower Limestone Shales). These were subsequently overlain by well-bedded argillaceous limestones (Lower Limestone) which were probably deposited in slightly deeper waters (MacDermot and Sevastopulo, 1972).

During Upper Tournaisian and Lower Visean times a carbonate mud bank complex (Waulsortian limestones) accumulated in an off-shore position and was eventually to cover thousands of square kilometres of the shelf sea. Lees (1961, 1964) considered that the Waulsortian complex occupied a position analogous to that of a barrier reef separating a near shore lagoonal facies lithologically similar to the pre-Waulsortian Lower Limestones, from the mud belt (Culm) on the flanks of the Variscan geosyncline farther to the south (fig. 2.2). The limestones forming the Waulsortian banks are poorly-bedded and lithologically varied, ranging from calcitic mudstones to coarse encrinites. The micrites tend to form the main central portion of the bank structure whilst the crinoidal limestones

envelope or occur marginally to the bank cores. The micritic facies is generally characterized by the presence of irregularly-shaped stromatactis cavities, varying between 1 cm. and 1 metre in lateral extent and infilled by post-depositional generations of lime-mud and sparry diagenetic calcite. Lees attributes the growth of the Waulsortian banks to the sediment baffling action of organisms, possibly plants or sponges, and the formation of stromatactis cavities to subsequent collapse and bridging of cavities following the decay of the organic baffles.

To the north along the margin of the Longford-Down massif, a varied assemblage of near shore sediments ranging from conglomerates and sandstones to oolites and sandy limestones were laid down (fig. 2.2). Parts of the sequence display characteristics of an evaporitic tidal flat environment, although only small amounts of evaporitic minerals have actually been recorded (Sheridan et al, 1967; West et al, 1968).

During Visean times the accumulation of the Waulsortian mud bank complex was abruptly terminated and succeeded by basinal facies argillaceous limestones (Calp).

Volcanics are only of minor importance in the Lower Carboniferous of Ireland, Tournaisian volcanicity being restricted to scattered records of tuffs. The most extensive development of Carboniferous volcanics occurs in the synclinal Limerick basin. These are Visean in age and are composed of olivine - basalts, trachy-basalts, trachy-andesites and trachytes comparable with those of the Midland Valley of Scotland (Ashby, 1939). They occur as sills, tuffs and lavas centered around a number of small vents.

FIG.2.2 UPPER TOURNAISIAN FACIES.

(After MacDermot & Sevastopulo,1972)

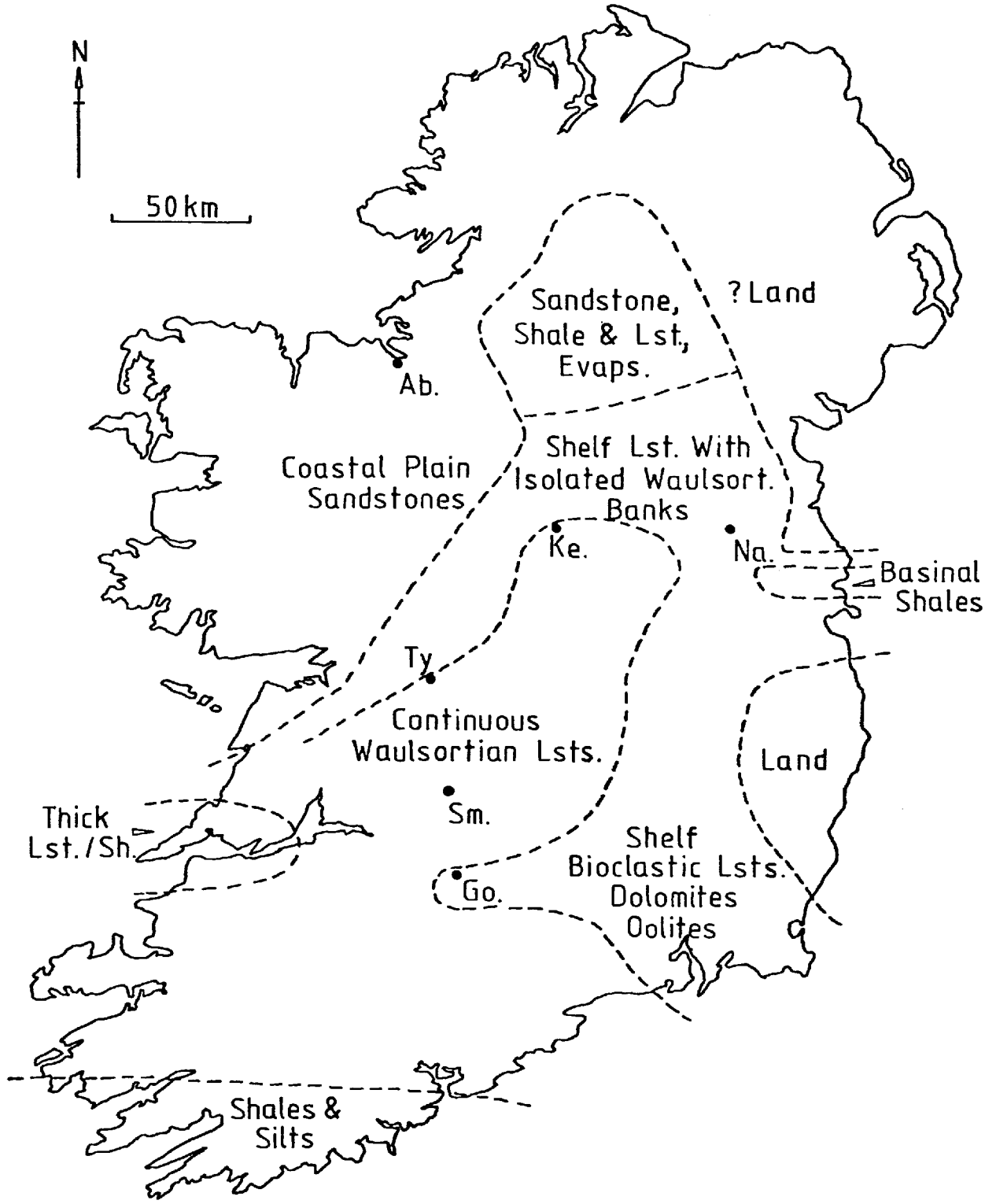

2.1.5 The Hercynian Orogeny

Following the deposition of the Millstone Grit and Coal Measure sequences of the Upper Carboniferous, Ireland was once more involved in major earth movements, which virtually closed the structural history of the greater part of the country. In the extreme south of Ireland, the Hercynian orogeny resulted in the deformation of Devonian and Carboniferous sediments into a series of en échelon anticlines and synclines along approximately east-west axes. The intensity of folding rapidly diminishes northwards on to the foreland, and in the Central Plain is restricted to gentle folds along an inherited Caledonoid trend. Likewise, normal and wrench faulting in the foreland region dominantly follows the E.N.E. - W.S.W./N.E. - S.W. Caledonian trend. This faulting is not entirely post-Carboniferous in age, there being convincing evidence for contemporaneous Lower Carboniferous fault activity, possibly controlled by lines of weakness in the underlying Lower Palaeozoic basement.

2.2 LOCAL SETTING FOR MINERALIZATION AT TYNAGH

2.2.1 Introduction

The Tynagh deposit comprises a primary sulphide body of 9.4 million tons with an average grade* of 3.0% Pb, 3.2% Zn, 0.3% Cu and 1.0 oz/ton Ag. Prior to mining, this was overlain in its western part by a 4.2 million ton residual body (zone I) of metal-rich rubble and sulphide/oxide mud, with a grade* of 9.1% Pb, 7.4% Zn, 0.6% Cu and 3.2 oz/ton Ag.

Morrissey (1970) has demonstrated that the residual orebody was formed by weathering of heavily mineralized limestones, probably

* = grades (short tons) quoted by Morrissey et al, 1971.

late in the Tertiary era. The resultant residuum gravitated into a steep-sided trench produced by the solution and collapse of the Waulsortian limestones.

The bulk of the primary mineralization (zones II and III) occurs within a wedge-shaped mass of Upper Tournaisian and Lower Visean Waulsortian limestones which have been downfaulted to the north of a small inlier of Devonian, O.R.S. facies sediments (figs. 2.3, 2.4). Subordinate mineralization is hosted within the Lower Limestones immediately underlying the Waulsortian limestones, and Schultz (1968) has reported minor veinlets and disseminations within the Calp and the footwall Old Red Sandstone. In all, the primary orebody extends over a vertical distance of approximately 200 metres and has lateral dimensions of 1.6 km. parallel to and 130 metres perpendicular to the strike of the Tynagh fault.

2.2.2 The Lower Carboniferous Succession at Tynagh

2.2.2.1 The Lower Limestone Shales

As is the case elsewhere in the Central Plain of Ireland, the transition from O.R.S. facies sedimentation is gradational via alternations of limestone, shale and sandstone. The basal Carboniferous Lower Limestone Shales (L5)* are composed largely of thinly-bedded dark grey shales, although occasional horizons of crinoid and brachiopod debris are not uncommon. A particularly pure 2.5 metre thick, grey-green shale horizon free from bioclastic debris (the Ballyvergin Shale) provides a distinct marker horizon which can be traced over much of west-central Ireland (thickness = 58 metres).

* (L5). (L4) etc. = mine terminology

FIG.2.3 GEOLOGICAL SECTION 85+00W - TYNAGH. (By permission of Irish Base Metals Ltd.)

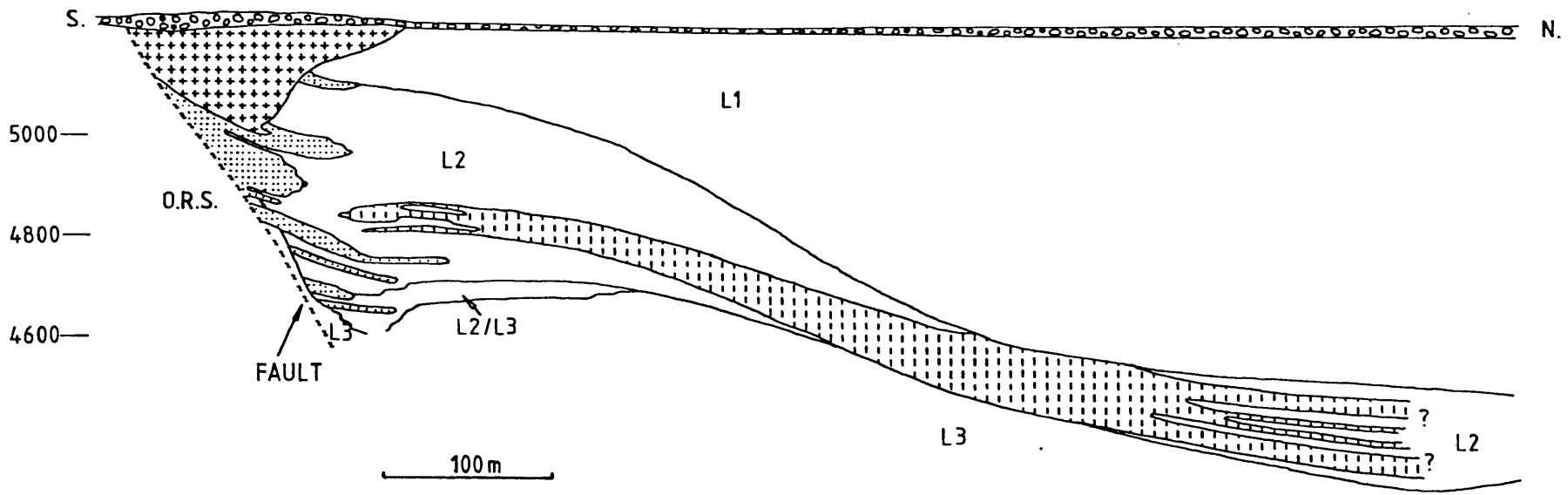

FIG.2.4 GEOLOGICAL MAP OF TYNAGH MINE AREA.

(Based on company maps)

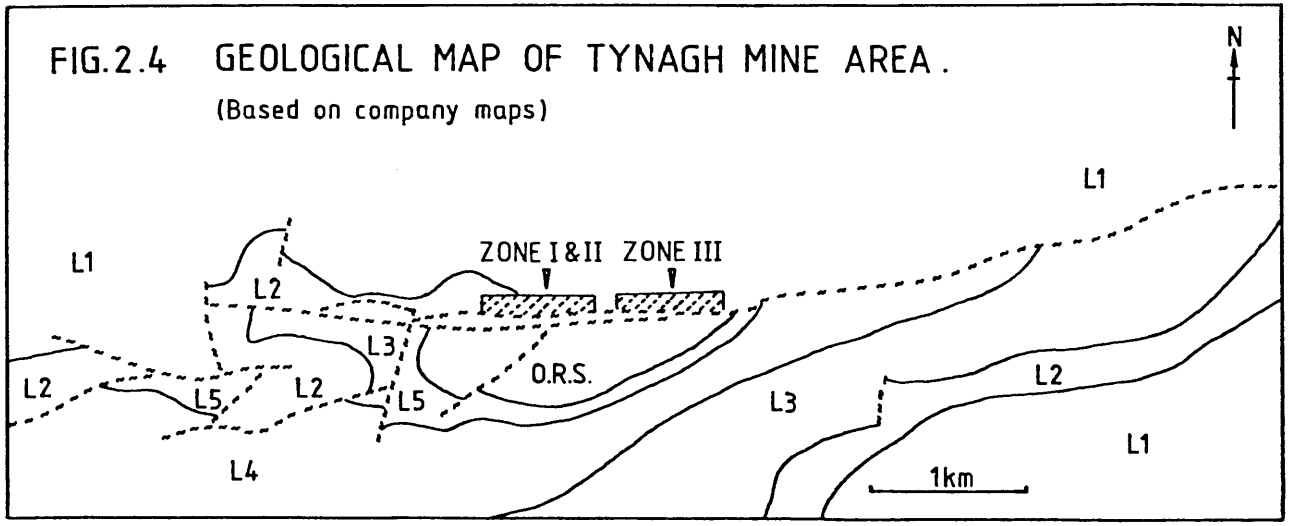

= Glacial drift.

= Residual ore.

= Primary ore.

= Iron formation.

L1 = Calp.

L2 = Waulsortian lst.

L3 = Lower muddy lst.

L4 = Lower bioclastic lst.

L5 = Lower lst. shales.

2.2.2.2 The Lower Limestones

At Tynagh the Lower Limestone can be subdivided into the Lower Bioclastic Limestone (L4) and the Lower Muddy Limestone (L3). The Lower Bioclastic Limestone is a fairly massive, dark bioclastic limestone composed largely of crinoid and brachiopod debris in a micritic and silty matrix with lesser quantities of sparry calcite cement. Shale partings are common, and there is evidence of soft sediment slumping at certain horizons. The overlying Lower Muddy Limestone, the base of which is marked by the first appearance of the colonial coral Syringopora Sp, is very well-bedded, and has a greater proportion of intercalated shale horizons (Pl.2.1A). The contact with the overlying Waulsortian bank complex is often gradational, and interdigitations are common (total thickness 250 to 300 metres).

2.2.2.3 The Waulsortian Limestones

The host Waulsortian Limestones (L2) are associated with the north-eastern margin of the carbonate mud bank complex as defined by Lees (1961, 1964). They vary considerably in both thickness (0 to 200 metres) and sub-facies within the area of the ore deposit, internal correlation often being impossible, even over a few tens of metres. Massive pale to mid-grey, calcitic micrites, often finely laminated or mottled, constitute the nucleus of the bank complex at Tynagh. These are enveloped by biomicrites, consisting largely of crinoidal debris in a matrix of fine grained calcitic mud, and off-bank sedimentary slump breccias. The slump breccias are comprised of rounded lumps of pale grey micrite generally a few centimetres in diameter and often plastically deformed, set within

a dark shaley matrix (Pl.2.1B). Occasional larger blocks of micrite up to several metres in size, and in a similar argillaceous matrix are clearly indicative of the disruption and subsequent transport of more coherent, semi-lithified blocks of bank limestone into an off-bank basinal facies (fig. 2.5).

2.2.2.4 The Iron Formation

To the north, the Waulsortian bank limestones interdigitate with a sedimentary iron formation consisting essentially of finely banded haematite and chert, with intercalated graded bedded limestones, and a few thin tuffaceous beds. The maximum thickness of the Tynagh iron formation is about 50 metres, 40 per cent of which is made up of ironstone beds, and it has a known lateral extent of 600 metres north-south and 1800 metres east-west, (Schultz, 1966a). The tuff horizons in toto only constitute about 1.5 metres (Schultz, 1966b), and Morrissey et al (1971) consider that they could have been wind-borne from the Limerick volcanic centre 70 km. to the south.

2.2.2.5 The Calp

The Calp (L1) in the vicinity of the orebody, overlies and interdigitates with the upper Waulsortian Limestones, but away from the main bank structure there is a gradual transition into the underlying Lower Muddy Limestones via off-bank slump breccias. The Calp consists of a monotonous sequence of dark grey calcilutites with carbonaceous black shale partings. Occasional thin bioclastic horizons composed largely of comminuted crinoid and brachiopod debris occur, and pale mottled horizons sometimes define a crude lamination (Pl.2.1C).

PLATE 2.1 TYPICAL INFRA AND OFF-BANK LITHOLOGIES - TYNAGH

A) Crinoidal Lower Muddy Limestone (L3)

DDH 178, 156 - 163 m.

B) Soft sediment slump breccia - clasts of brecciated and plastically deformed Waulsortian micrite, plus crinoidal debris, within a dark argillaceous matrix.

DDH 387, 160 - 166 m.

C) Calp (L1) displaying pale mottling.

DDH 387, 82 - 88 m.

PLATE 2.1

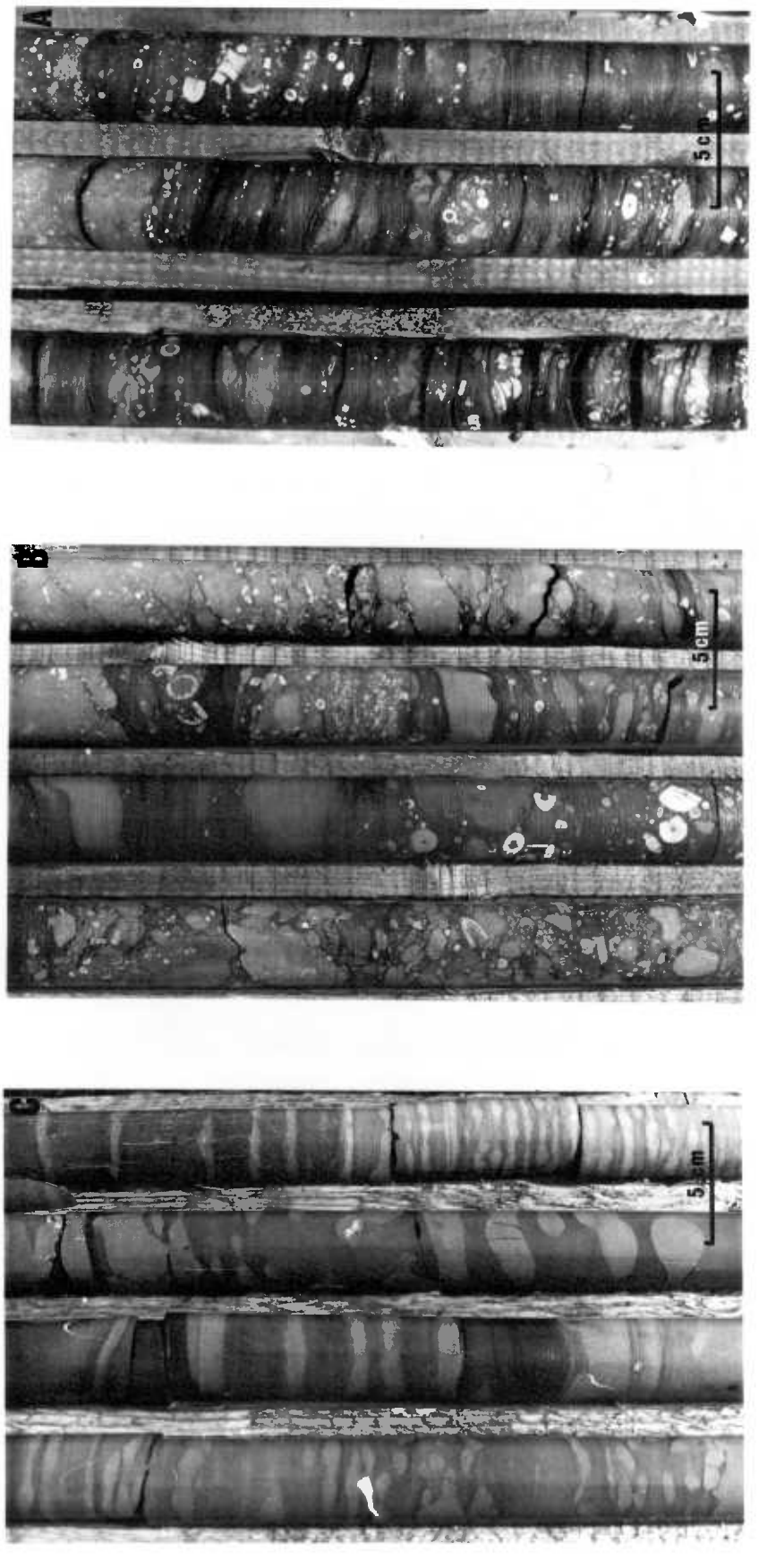

FIG.2.5 SLUMPED BLOCKS OF WAULSORTIAN MICRITE.

4912 Level 66+30W.

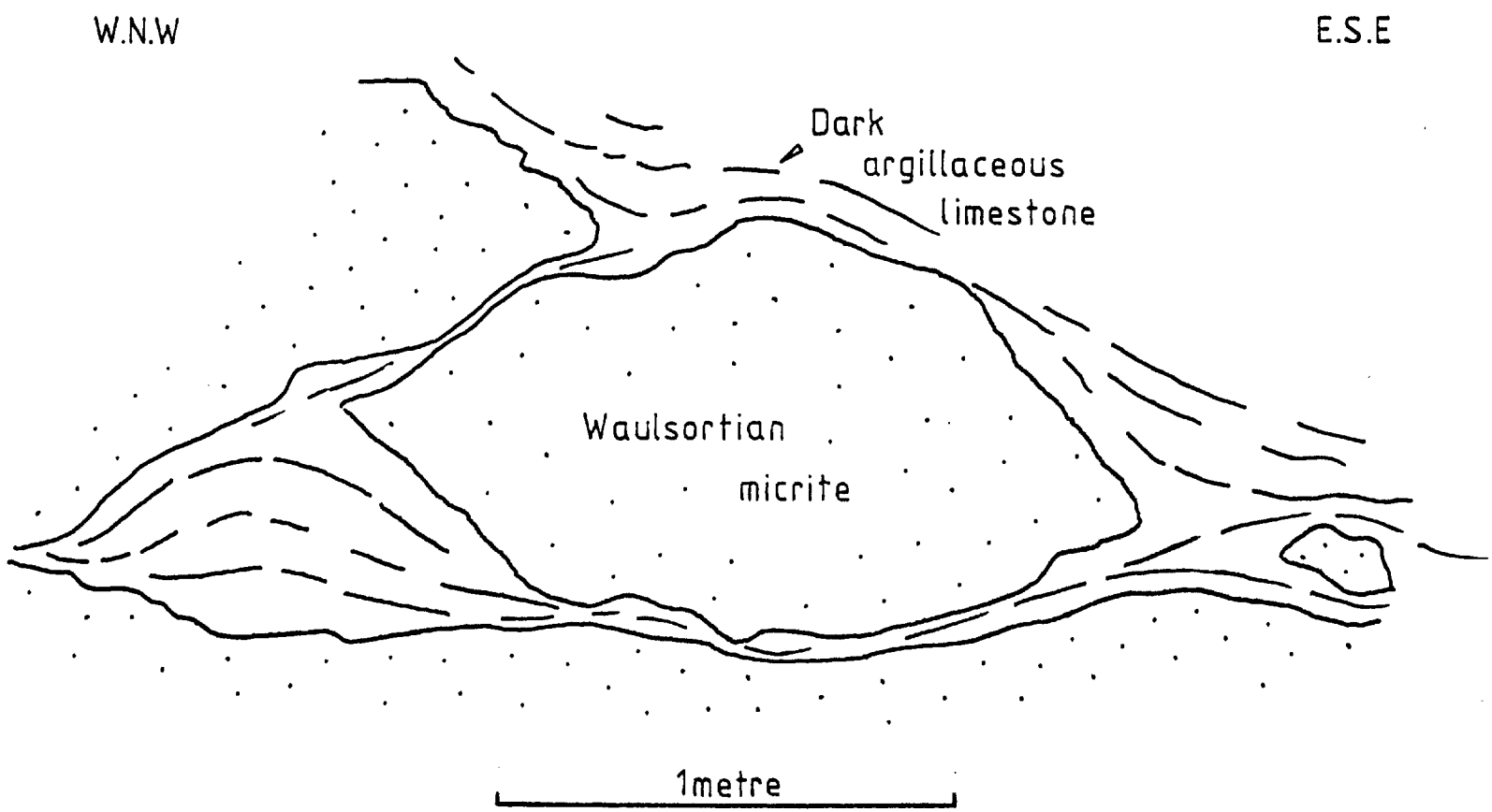

2.2.3 Structure

The most important structural feature is the Tynagh fault which has an approximate east-west trend, and a northward dip of 60 to 65° (Pl.2.2A). Normal displacements are estimated to exceed 600 metres in the mine area (Morrissey and Whitehead, 1970), the dip and throw both diminishing towards the east. The orebody is rarely juxtaposed against the actual fault plane, but is separated from it by a tectonically emplaced slice of Lower Muddy Limestone, generally no more than a few metres in width (Pl.2.2B). The abundance of synsedimentary slump breccias throughout much of the Lower Carboniferous sequence at Tynagh, and especially in association with the Waulsortian bank complex, is strongly suggestive of contemporaneous movement along the fault plane. Indeed the rapid facies changes may in part have been the result of fault controlled variations in sub-marine topography.

The Lower Carboniferous strata are gently folded along approximately E.N.E. axes, dips rarely exceeding 15°. In the north wall of the open pit, a number of small, northward plunging cross folds can be observed within the well bedded Calp. These are interpreted by Moore (1975) as having been associated with late stage (Hercynian ?) compressional movements on the fault plane.

2.3 PREVIOUS WORK ON THE TYNAGH DEPOSIT

Hypotheses as to the mode of emplacement of the primary base metal deposits have essentially been divided between the syngenetic and epigenetic schools of thought. Derry et al (1965) in a preliminary geological study regarded the association of sulphides with a banded iron formation and volcanic ash as being significant.

PLATE 2.2 THE TYNAGH OPEN PIT AND FAULT

A) View of the open-pit, Tynagh, looking west along the strike of the fault plane. Benches to the left of the photograph (south) within Devonian sandstones, conglomerates and shales. To the right, thinly bedded Calp limestones dipping towards the north.

B) Slickensided surface of the Tynagh fault plane, overlain by sheared fault gouge (Lower Muddy Limestone lens) - east end of the open pit.

PLATE 2.2

A

B

They proposed that sulphide deposition was contemporaneous with the formation of the mud bank complex, and that both the sulphide assemblage and the iron formation were precipitated from solfataric solutions issuing from fissures that may have followed the line of the present Tynagh fault.

Schultz (1966a) favoured the view that iron and silica were derived by intensive chemical weathering of Lower Dinantian sediments that had been exposed on newly emergent land. He considered the association between the iron formation and the sulphide deposit to be coincidental, and went on to describe the orebody as "an epigenetic cavity-filling and replacement deposit" (Schultz, 1968). He proposed a paragenetic sequence to illustrate the main trend of mineralization (fig. 2.6), but stated that ..... " Because of the complex nature of much of the ore, more precise definition of the age relations of some of the minerals and possible distinction of two or more separate generations of some species would require examination of a much larger number of polished and thin sections selected from various parts of the deposit."

Schultz tentatively favoured the conclusion that the ore components were derived largely from deep-seated magmatic sources with a possible contribution of metal extracted from country rocks by circulatory connate and/or meteoric waters.

Russell (1974, 1975) demonstrated the presence of an extensive manganese halo centered on the iron formation, and attributed an exhalative origin to them both. He further showed that anomalous levels of Zn, Ba and Pb existed within the iron formation, and on these grounds considered that the sulphide orebody was deposited from the same mineralizing solutions.

Fig. 2.6 Paragenesis of Mineralization at Tynagh - Schultz (1968)

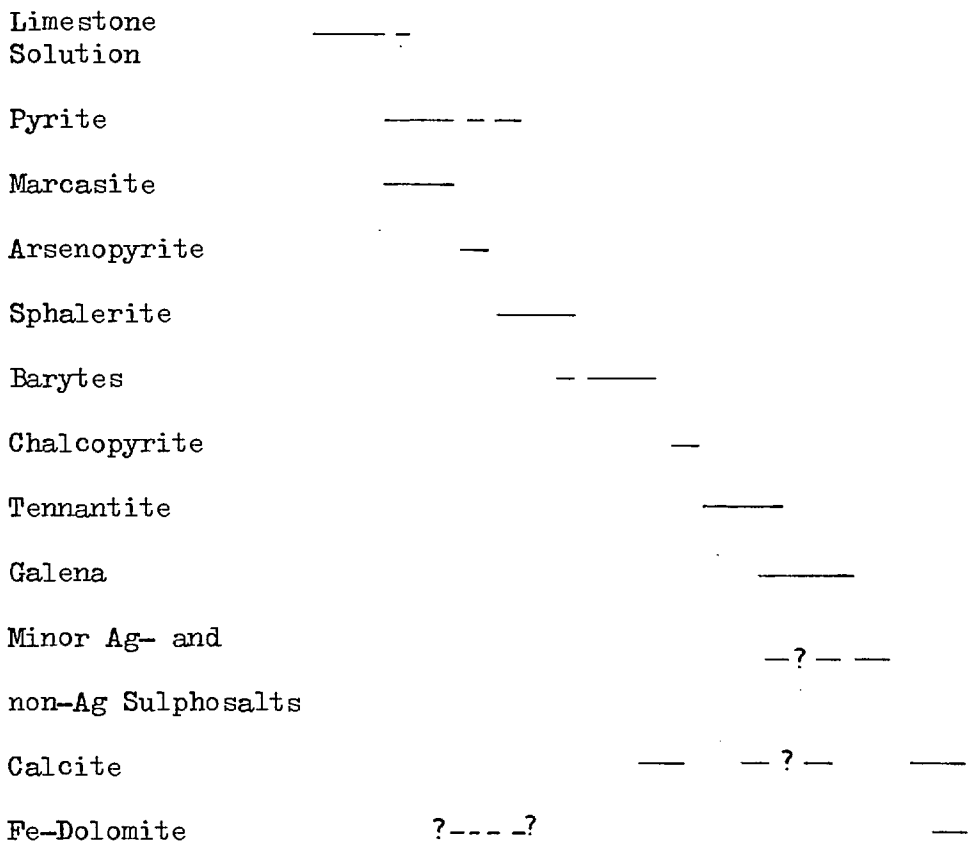

Riedel (1977) went on to further develop the syngenetic model, by suggesting that decaying organisms provided the reducing conditions necessary for sulphide precipitation. He considered that fault movement synchronous with the accumulation of the Waulsortian limestones was a vital factor in establishing a suitable environment for ore deposition and preservation, but did not consider the fault to be a conduit for metalliferous fluids.

To conclude, neither of the two basic hypotheses alone satisfactorily explain the genesis of the primary orebody. The epigenetic model is clearly in conflict with the known association with an iron formation of undoubted sedimentary affiliations. However, it is difficult to envisage how euxinic conditions necessary for sulphide deposition could be established in a relatively shallow

water, active environment, whilst oxidising conditions existed in a basinal and presumably more restricted environment.

CHAPTER 3

THE STYLE AND PARAGENESIS OF MINERALIZATION AT TYNAGH

3.1 INTRODUCTION

Although Schultz (1968) carried out a mineralogical study of drill core material obtained from the primary ore, it was felt that in view of the strong geological control required by an isotopic study, an extension of his work was justified. Although a certain degree of repetition has been unavoidable, the subsequent discovery of the eastern-extension (zone III) orebody and access to extensive underground workings not available to Schultz, has aided in the re-appraisal of many ore textures.

In studying the Tynagh deposit, greatest attention was paid to those areas where relationships between the ore mineralization and the host could be ascertained. A mineralogical and textural study has led to the recognition of four major stages of mineralization:-

(i) An initial stage, dominated by the growth of clots of colloform and granular pyrite, possibly during the early diagenetic history of the Waulsortian micrites.

(ii) The rapid geopetal precipitation of microcrystalline sulphides, largely sphalerite, within a dilatant fracture system developed in response to tectonic activity in the fault zone.

(iii) An epigenetic stage of mineralization, dominated by tennantite, medium to coarsely crystalline galena and sparry barytes.

(iv) Finally, the post-ore precipitation of calcite within veinlets and cavities, and the dolomitisation of large bodies of unmineralized Waulsortian limestones.

Hydrothermal alteration of the host Waulsortian limestones, associated with primary sulphide mineralization, is only occasionally evident and restricted in its extent.

Sub-economic mineralization within the underlying Lower Muddy Limestones is of interest in that it demonstrates the strong lithological control on the style of mineralization.

3.2 STAGE 1 - SULPHIDE MINERALIZATION OF POSSIBLE SYNSEDIMENTARY OR EARLY DIAGENETIC AGE

3.2.1 Macrotextural Features

Sporadically distributed within the micritic Waulsortian bank limestone of zone II are clots and irregular bands of colloform and granular pyrite. These comprise a minor component of the total sulphide assemblage, and have not been observed within the zone III micrites or the underlying Lower Muddy Limestones. They often consist of compact, approximately spherical masses of banded pyrite, up to 20 cms. in diameter. Individual bands of pyrite are no more than 1 or 2 cms. in width, are usually highly convoluted and frequently display colloform textures (Pl. 3.1A). Fine grained black carbonate, clearly distinguishable from the much paler grey Waulsortian micrites, encloses and forms the matrix to these pyrite agglomerations, the contact between the black carbonate and the micrite being usually sharp and distinct. Where sedimentary banding can be distinguished within the host micrites, it can be seen that these pyritic masses bear a discordant relationship.

Minor stratiform horizons of fine grained sulphides occur within thin shale beds that interdigitate with the bank limestones.

3.2.2 Microtextural and Mineralogical Observations

Two main types of colloform texture can be recognised within the pyrite aggregates:-

(i) Concentrically banded hemispherical bodies displaying a fibrous radiating texture perpendicular to the growth surfaces (Pl.3.8B)

and

(ii) elongated frond or plumose-shaped colloform structures (Pl.3.8C).

However, the pyrite is more often granular in appearance and can be seen to be composed of a polycrystalline aggregation of anhedral crystal a few μm in size. Incipient colloform banding can sometimes be discerned within the aggregates (Pl.3.8A) and occasional horizons displaying well developed euhedral crystal faces are observed.

The black carbonate matrix to the pyrite clots consist of a fine grained mosaic of anhedral to euhedral dolomite and calcite, individual crystals being 10–30 μm in size. X-ray diffraction studies have shown that the proportion of dolomite to calcite is highly variable, and frequently the carbonate is composed entirely of one phase. Disseminations of pyrite form an important component of the matrix (up to 10%), the concentration decreasing away from the main pyrite aggregates. These disseminations, consisting of euhedra and zoned spheres 1–30 μm in size, may be a contributory factor to the carbonate's dark colouration. Alternatively this could be due to the presence of minute hydrocarbon inclusions within

or intergrown with the calcite and dolomite.

The occasional occurrence of pyritised crinoid ossicles in close proximity to colloform pyrite aggregates provides a further indication of an association between organic matter and the early stages of sulphide mineralization. In certain instances pyrite has totally replaced crinoid fragments a few mms. in diameter, preserving the fine detail of the internal structure in the process (Pl.3.8D).

Framboids are rarely observed in association with granular and colloform pyrite but are a common component of the sulphide assemblage within the Lower Muddy Limestone. The framboids (up to a few 10s of μm in size) tend to be concentrated within argillaceous bands or as interstitial components of bioclastic horizons, and occur in isolation or as small clusters, several 100s of μm across.

Euhedral pyrite often forms drusy overgrowths upon colloform, granular and framboidal aggregates (Pl.3.9A; 3.11A). In addition, pyrite euhedra, 60 to 120 μm in size, are a common component of thin shale horizons that interdigitate with the Waulsortian carbonate mud banks. These are often concentrated into specific horizons that are conformable with the laminations of the enclosing shale. Within the Waulsortian limestones themselves, minor disseminations (<1%) of fine grained (generally ≤ 5 μm) anhedral and euhedral pyrite are ubiquitous.

Marcasite is only a minor component of stage 1 intergrowths, occurring in anhedral intergrowth with granular and colloform pyrite. Marcasite spherulites have only been noted at one locality (89+00W[1], 4800 level[2]), in a thin shale band within a sequence of micrites and

biomicrites interdigitated with the iron formation. The spherulites are 60 to 120 μm in diameter, display a well developed internal radial structure, and along with euhedral pyrite are concentrated into and define stratiform horizons within the shale (Pl.3.9B).

The bulk of the zinc mineralization at Tynagh can be demonstrated to post-date the precipitation of syngenetic/diagenetic iron sulphides. However, rare conformable layers and lenses of microcrystalline sphalerite within shale horizons interdigitated with Waulsortian micrites beg a syngenetic interpretation (Pl.3.9C). The sphalerite occurs intergrown with rhombs of carbonate ≤120 μm in size, identified as ankerite and siderite by X-ray diffractometry, and bundles of acicular chlorite crystals. Individual chlorite needles tend to be only 20 to 30 μm in length and display a random orientation. Although chlorite is a common component of unmineralised argillaceous limestones in the area, the lack of alignment parallel to bedding suggests authigenic growth within the sphaleritic sediment rather than a detrital origin.

Complex interbandings between sphalerite and colloform pyrite have been observed in one section only (Pl.3.9D). Both the sphalerite and the pyrite display atoll textures which, if interpreted as a replacement phenomenon, would suggest the phases had simultaneously replaced one another. More likely this indicates post-depositional re-equilibration between co-precipitated sphalerite and pyrite.

1: Westings refer to section lines perpendicular to the mine base line (the mine base line is approximately parallel to the trend of the Tynagh fault). Zone II extends from 96+00W to approximately 78+00W; zone III falls between 67+00W and 44+00W. Sections are at 100' intervals e.g. 89+00W is 100' west 88+00W. (See Appendix 3)

2: Level elevations, in feet. 0 level = 5000' below S.L.; surface elevation ≃ 5200 level.

3.2.3. Cataclasis and Replacement of Diagenetic Pyrite

Colloform and granular pyrite often display evidence of brittle fracture and cataclasis, possibly in response to increasing sedimentary load during late diagenesis or seismic disturbance triggered by tectonic activity in the fault zone (Pl.3.9E). Later sulphides of stages 2 and 3 are frequently observed to penetrate along these fractures, and indeed their introduction may have been synchronous with brecciation (Pl.3.9F). This fracturing and later penetration aided subsequent replacement, three major types of textures being recognised:-

(i) Replacement of large areas of the pyrite by euhedra and subhedra of galena, and, to a lesser extent, sphalerite and tennantite. This ultimately results in the almost total digestion of the pyrite, skeletal remnants being preserved within a matrix of the later sulphides (Pl.3.10A,B,E).

(ii) Replacement of the core regions of colloform and granular pyrite, by large, single euhedra of galena, often several mms. in size, giving the false impression that the pyrite postdates precipitation of the galena (Pl.3.10C,D).

(iii) Preferential replacement of specific horizons within colloform banded and euhedral pyrite by anhedral intergrowths of later sulphides (Pl.3.11C,D).

As well as being overgrown by later generations of euhedral pyrite, relic framboids are commonly observed to be overgrown and replaced by chalcopyrite (Pl.3.11A) and less commonly sphalerite, galena and tennantite (Pl.3.10F;3.11B).

3.3 STAGE 2 - SULPHIDE DEPOSITION WITHIN A DILATANT FRACTURE/BRECCIA SYSTEM

3.3.1 Macrotextural Features

The deposition of stage 2 sulphides, largely sphalerite, did not occur within a conventional vein system or as synsedimentary stratiform horizons, but in a complex dilatant fracture/breccia system, within which textural characteristics of both mineralization styles were developed. The dilatant fractures are of variable width - from a few mms. to several 10s of cms.- and attitude - vertical, horizontal and sub-horizontal - and appear to display no consistent directional relationship with major tectonic structures. Careful observation shows that the dilatant fracture system post-dates the early diagenetic evolution of the Waulsortian bank limestones. Sulphides related to this stage penetrate and replace diagenetic pyrite (3.2.3). Cavities infilled with sparry diagenetic calcite are observed to be cut and displaced, and stylolite surfaces are abruptly terminated against fracture infillings of sulphides (Pl.3.2A,B). Replacement of the host micritic limestones by sulphides was minimal and largely restricted to minor disseminations in the immediate contact zone with the fractures.

There are many textural features displayed by these sulphide infillings which clearly illustrate that sedimentary processes were operating within an interconnected and open fracture system. The sulphides are frequently finely banded in the horizontal plane on a scale of a few mms. to a cm. or two in width (Pl.3.1B). The banded sulphides are composed largely of a very fine grained inter-growth of sphalerite and carbonate, which in hand specimen often has

the appearance of a varved mudstone, individual crystals being indiscernible even with the aid of a hand lens . The banding within the sphalerite/carbonate intergrowths is distinguished by contrasts in colour, which is variable from pale yellow-brown to dark orange-brown. Parallel to and conformable with the sphalerite/carbonate banding, horizons rich in fine grained galena, usually intimately intergrown with sphalerite, are commonly observed. Included clasts of micrite and crinoidal debris along with cataclased fragments of sulphide/carbonate intergrowths are common within the banded sulphide sequences (Pl.3.3A,B; 3.12C). The included micrite fragments are poorly sorted, a few mms. to several cms. in size, angular to sub-rounded in shape and often occur preferentially concentrated within a specific horizon. The sulphide clasts tend to be much smaller in size (up to 2 or 3 mms. across) less common, and have diffuse margins. Together, these various fragments display a variety of geopetal textures:-

(i) Minor graded bedding,

(ii) load depressions,

(iii) preferred orientation of elongated micrite clasts and crinoid ossicles parallel to sulphide banding,

(iv) pinching out of sulphide bands against large micrite clasts.

There is evidence to suggest that during and soon after the precipitation of the banded sulphide sequences, there were periods of physical disruption and remobilisation whilst the sulphides were in a plastic, semi-consolidated state. This is manifested in the form of microfaults which displace the banded texture of the sulphides (Pl.3.1B), but which are terminated at the contact with the carbonate host, highly disrupted and folded banding and vertical remobilisation

and flow of sulphides into mud volcanoes erupting at higher levels within the dilatant fracture (Pl.3.2A,B). Pressure solution surfaces are frequently noted parallel to associated vertical flow zones, and also around the margins of larger clasts (Pl.3.3A).

Vertical fracture infillings occasionally display crustiform textures more typical of a vein system, however many also exhibit strong geopetal influences and evidence of internal slumping (Pl.3.6A,B).

Brecciation of the host Waulsortian micrites is often observed to increase in intensity as the fault zone is approached, culminating in zone (III) in the massive breccia ore. The breccia is located against the tectonically emplaced fault zone lens of Lower Muddy Limestone facies sediments, and where exposed by mining activity between 64+60W and 66+50W, 5000 level, extends to a maximum of 25 metres to the north of the fault zone. It is a wedge-shaped body diminishing rapidly northwards, laterally and vertically, only being present as a 1 metre wide zone at the 5050 elevation and not being observed at the 4912 level. The breccia ore consists of angular clasts and blocks of micrite up to 1 metre across, enclosed within a matrix of microcrystalline sphalerite and minor fine grained galena that displays no gross internal fabric. The micrite fragments are extremely poorly sorted and their angular nature plus the abundance of clasts composed of diagenetic calcite, shows that the Waulsortian limestones had reached an advanced stage of diagenesis and lithification prior to brecciation (Pl.3.4). Pressure solution activity is indicated by the occurrence of interlocking fragments of dissimilar carbonate host. However the majority of the breccia fragments occur in isolation, being totally enclosed by an envelope

of the matrix. Less commonly, sphalerite and galena form the matrix to clasts of Waulsortian micrite which may have been in a semi-consolidated state during brecciation. The clasts appear coherent but have margins which are rounded and diffuse (Pl.3.5).

3.3.2 Microtextural and Mineralogical Observations

3.3.2.1 Sphalerite, Galena, Carbonate, Barytes Intergrowths

The banded sphalerite/carbonate intergrowths are composed essentially of microcrystalline sphalerite, occasionally displaying metacolloid textures, and fine grained dolomite. The dolomite occurs as rhombs, 10 to 150 μm in size, which are often corroded in appearance and contain numerous rounded inclusions of sphalerite (Pl.3.12A). The size and distribution of rhombs within a given band of microcrystalline sphalerite is usually uniform but variations in size, and the ratio of sphalerite to dolomite from band to band produce the colour variation seen in hand specimen. Paler bands often have up to 70 or 80% dolomite, whilst dark horizons can be almost devoid of non-opaques. Calcite is a rare component of these intergrowths, and where present displays an anhedral habit.

Two types of metacolloid textures within the sphalerite can be recognised, (i) colloform banding (Pl.3.12E) and (ii) globular aggregates (Pl.3.15B). Colloform sphalerite is generally free from inclusions of other phases and displays concentric banding, with an internal porous texture (Pl.3.15E), or a fibrous texture orientated perpendicular to the banding. The globular aggregates consist of compact masses of spherical sphalerite bodies, 25 to 250 μm in diameter, but of uniform size within a given specimen. The globules often exhibit an internal banding distinguished by

variations in colour, and careful observation occasionally reveals growth surfaces displaying minute euhedral crystal faces or druses.

The fine grained galena, conformably interbanded with the sphalerite, is usually irregularly intergrown with sphalerite and dolomite, with which it appears to have been coevally precipitated. The contacts between sphalerite and galena are always tortuous, embayed and often cuspate, whilst dolomite intergrown with galena often displays a near perfect rhombic habit, and has fewer inclusions of sulphides (Pl.3.12B). Galena displaying identical textural relationships also occurs as scattered, anhedral patches of variable size within the sphalerite/dolomite intergrowths. Intergrowths of sphalerite and galena pseudomorphing barytes are suggestive of its earlier precipitation or, more likely, post-depositional replacement of co-precipitated barytes. The intergrowths mimic the habit of barytes, occurring as discrete or interlocking blades, 250 to 500 μm in length, within a finer grained sphalerite/dolomite intergrowth (Pl.3.13C).

The bulk of the barytes mineralization at Tynagh post-dates the dilatant fracture infillings. Nevertheless it is ubiquitous within the sphalerite/dolomite intergrowths, and in certain bands comprises the major component. Where barytes is subordinate to sphalerite, it rarely displays its euhedral bladed habit, occurring as anhedral patches, or as poikilitic or skeletal crystals approximately 500 μm in length (Pl.3.13A,B). As the percentage of barytes increases the euhedral habit becomes dominant, and crystal size increases (up to 1.5 mms.).

3.3.2.2 Subordinate Sulphide Components

Disseminations of pyrite, 1 to 80 μm in size, are

a ubiquitous but minor (rarely in excess of 1%) component of the sphalerite/dolomite intergrowths. Two basic types can be recognised, relic stage 1 granular and colloform pyrite, and subhedral to euhedral pyrite which appears to be coeval with the enclosing matrix.

Chalcopyrite is a rare component, but occasional minor disseminations within sphalerite/carbonate intergrowths are observed. It occurs as anhedral patches, a few 10s of μms in size, and displays no evidence of replacing or of being replaced by the matrix.

Siegenite $(Ni,Co,Fe)_3S_4$ again occurs as rare disseminations and displays a number of unusual and variable textural associations, often with chalcopyrite and galena. Four different types of intergrowth have been recognised:-

(i) Irregular intergrowths with galena as large (up to 200 μm), discrete, anhedral patches in a finer grained matrix of sphalerite and dolomite.

(ii) Zoned crystals, approximately 10 μm in size, with spherical cores of siegenite overgrown by subhedral galena, in turn overgrown by a rim of, or replacing the core of, euhedral pyrite.

(iii) Discrete patches with contained (exsolved ?) lamellae of galena (P1.3.11E) and chalcopyrite (P1.3.11F).

(iv) In intimate irregular intergrowth with sphalerite, galena and chalcopyrite.

Optical identification of siegenite was verified by semi-quantitative microprobe analysis:-

Section No. Ty 12 (i)

Fe	-	8.50
S	-	43.31
Ni	-	48.04
Co	-	15.67
Total	-	115.52%

Small anhedral inclusions of gersdorffite (NiAsS) and tennanite occasionally occur within conformable stage 2 galena horizons, however these two phases are more commonly associated with stage 3.

3.3.2.3 Subordinate Silicate Phases

Although silicate phases only comprise a minor component of the intergrowths that infill the dilatant fractures, a surprisingly wide variety have been identified.

Plagioclase occurs as subhedral and euhedral lath-shaped crystals, $\leqslant 70$ µm in length, most commonly within the darker orange-brown microcrystalline sphalerite bands where the percentage of intergrown dolomite is low. Some crystals display simple twins and more rarely polysynthetic twinning, and have been identified as albite. However, indistinct twinning in conjunction with small size often precludes positive identification. The presence of other members of the plagioclase series, therefore, cannot be ruled out.

Potassium feldspars have been tentatively identified in thin section, and positively identified by X-ray diffractometry, as being a minor component of some sphalerite/dolomite intergrowths. So as to try and specify the identity more precisely, a concentrate

was prepared by digesting, in hot 50% HCl, a sample in which several per cent potassium feldspar formed a fine grained anhedral intergrowth with sphalerite. The d spacings matched those of hyalophane, a barium potassium feldspar. It is interesting to note that where hyalophane was found to be present, barytes was never detected, perhaps indicating the preferential location of barium in the silicate lattice, at the expense of the formation of barytes.

Quartz, like plagioclase , most commonly occurs within the darker orange-brown microcrystalline sphalerite. It is subordinate in abundance to plagioclase , and occurs as subhedra and euhedra up to 200 μm across, but generally <50 μm in size (Pl.3.15E).

Acicular crystals of muscovite up to 60 μm in length but usually < 10 μm, are commonly observed to be intergrown with microcrystalline sphalerite, and can locally comprise several per cent of the intergrowths (Pl.3.12D). The optical identification of muscovite type mica has been verified by X-ray diffractometry. It occurs as randomly orientated needles within sphalerite intergrowths, but more commonly defines an oriented fabric parallel to the direction of flow in zones of remobilisation. These flow textured intergrowths often flank solution surfaces, a few 10s of μms in width, defined by a black, amorphous, non-reflective material within which occur concentrations of disseminated pyrite and siegenite. The best development of this flowage/solution phenomenon is observed within the breccia ore, where it comprises the dominant microtexture. Bands of flow textured sphalerite and muscovite envelope and are constricted between breccia clasts of Waulsortian micrite and more coarsely crystalline sphalerite/dolomite intergrowths (Pl.3.14A,B,C).

Muscovite has been observed in thin sections of un-

mineralized Waulsortian micrites, and X.R.D. analysis of an acid insoluble residue from such a limestone demonstrated that it was the second most common component after quartz. It is therefore, possible that the muscovite is entirely derived from the host. However, evidence has been presented supporting the growth of authigenic muscovite from montmorillonite and kaolinite by reaction with potassium, and a product approaching muscovite has been produced by the hydrothermal reaction of illite with potassium salts (see Yoder and Eugster, 1955). Growth of muscovite during ore deposition as a result of reaction between clay minerals within the sediment and potassium, possibly from the mineralizing fluid, is, therefore, not totally out of the question.

The occurrence of chlorite intergrown with stratiform sphalerite within an argillite band has already been described (section 3.2.2). Chlorite does occasionally occur intergrown with microcrystalline sphalerite infilling dilatant fractures, but only where the mineralization is hosted within an argillaceous facies. This spatial relationship suggests that either chlorite or its component elements have been derived from the argillite and have recrystallised within the sphalerite intergrowth.

3.4 STAGE 3 - EPIGENETIC Pb, Cu, Ba, MINERALIZATION

3.4.1 Macrotextural Features

Tennantite, medium to coarsely crystalline galena, and coarse sparry barytes, dominate the latest stage of base metal mineralization, with chalcopyrite being occasionally observed as an important component of the intergrowths. The mineralization occurs as irregularly-shaped massive bodies, often several metres in dimension, inter-connected by

thin veinings and pipes several cms. to 10s of cms. in width or as discrete vertical to sub-vertical veins up to 10 cms. in width. Veinlets and isolated euhedra (up to 5 mms. in size) of stage 3 galena, are frequently observed to cross cut and replace the host Waulsortian micrites, colloform pyrite and banded dilatant fracture infillings (fig. 3.1; Pl.3.7A, B; Pl.3.1B). Contacts between mineralization and the host are often diffuse and characterised by zones of disseminated replacement and alteration. Cockade textures are developed where replacement has resulted in the enclosure of relic ovoid bodies of microcrystalline sphalerite by galena, which is in turn overgrown by coarse intergrowths of barytes (fig. 3.2). There is little evidence of sequential deposition or crustification within the veins. However barytes, although clearly spatially related, often appears to post-date sulphides and sulphosalts.

3.4.2 Microtextural and Mineralogical Observations

3.4.2.1 Galena, Tennantite, Chalcopyrite, Barytes Intergrowths

The sequence of mineral deposition as indicated by the ore textures is often confusing and ambiguous. Generally the sulphides and sulphosalts of this stage display allotriomorphic mutual intergrowths with one another (Pl.3.16C,D). However, in certain instances distinct age relationships can be deduced: chalcopyrite rimming and replacing galena; chalcopyrite overgrowing tennantite; chalcopyrite replacing and pseudomorphing barytes (Pl.3.17A); tennantite overgrowing and replacing chalcopyrite (Pl.3.17B). Where galena is the dominant phase, tennantite, and less frequently chalcopyrite, commonly occur as anhedral inclusions, generally 100 - 200 μm in size within the galena.

FIG. 3.1 STAGE 3 GALENA REPLACING BANDED SPHALERITE. 5000 63+00W.

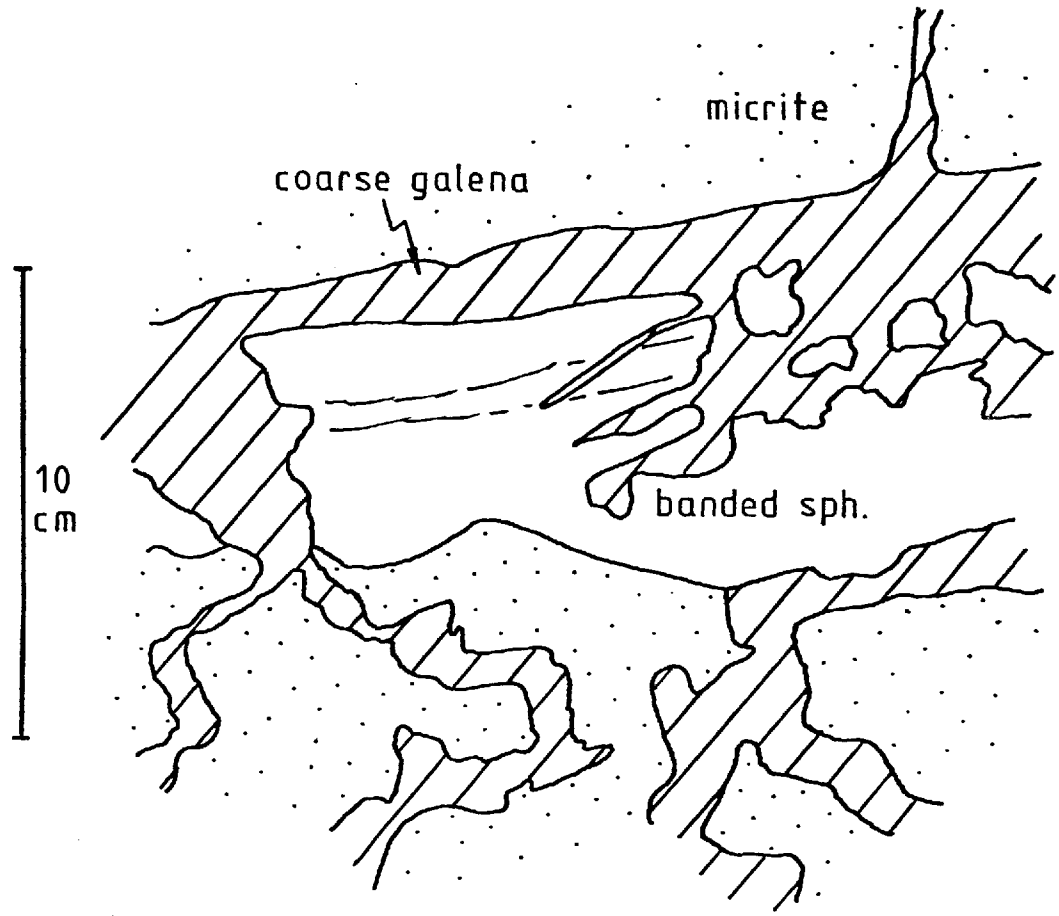

FIG. 3.2 COCKADE TEXTURE. 4912 63+90W.

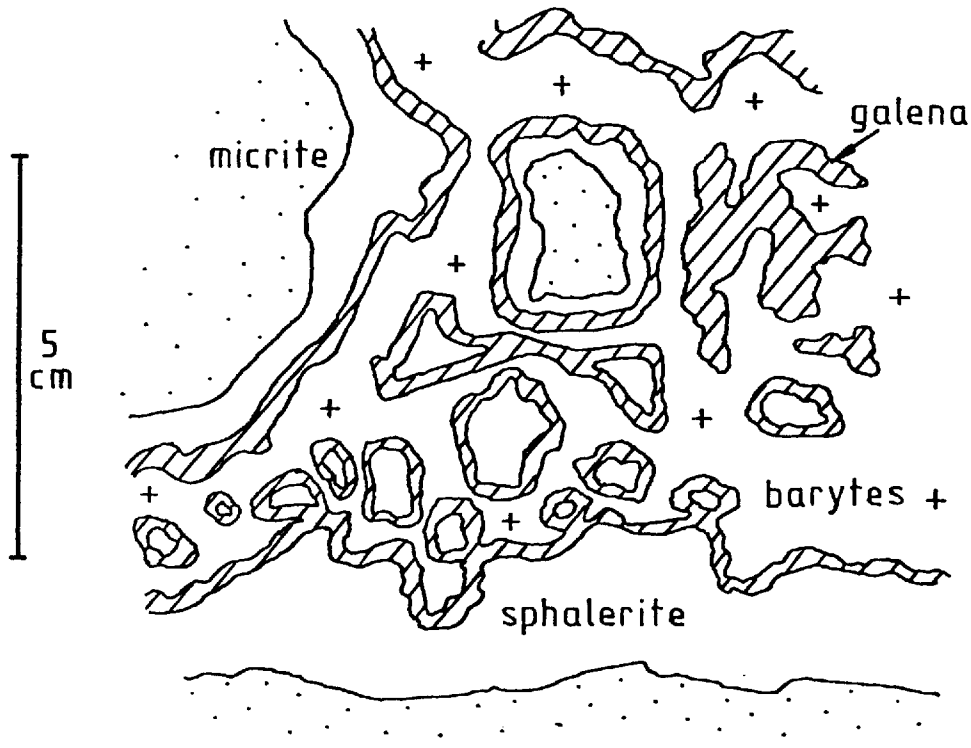

Both X-ray diffraction and qualitative micro-probe analyses have confirmed that tennantite, although not a pure end member, is indeed from the As rich end of the tennantite - tetrahedrite series, and has detectable amounts of Fe, Zn and Ag, but no Hg or Bi. A detailed study of the tennantites was beyond the scope of this project, however compositional variations were apparent from the optical properties alone. The majority of the tennantites had a dark green-grey streak and in reflected light displayed no evidence of internal reflections. However, specimens from 90+00W and 91+00W, 4700 level, gave a red-brown streak, had abundant ruby-red internal reflections, and were translucent in thin section. Ramdohr (1969) states that internal reflections are more visible in the pure Cu, As varieties and rare in types rich in Ag, Hg and Bi.

As mentioned above, barytes in hand specimen often appears to enclose and replace associated stage 3 sulphides and sulphosalts. Similar relationships are commonly observed in section, large bladed crystals of barytes projecting into and apparently replacing the intergrowths. Alternatively, this relationship could be interpreted as being an expression of barytes' inherent ability to crystallise in its euhedral habit, and indeed would be more consistent with the spatial relationships observed.

3.4.2.2 Associated Subordinate Phases

Bornite has only been observed by the writer in specimens collected from 90+00W and 91+00W, 4700 level, in association with pure Cu, As varieties of tennantite, and in loose blocks of primary ore from the residual orebody. It usually occurs in mutual intergrowth with other stage 3 sulphides and sulphosalts (Pl.3.11C,D; 3.16C,D) but is also observed to be rimmed and penetrated by later

chalcopyrite and can contain (exsolved ?) flame-like lamellae of chalcopyrite (Pl.3.11C).

Arsenopyrite is only noted as a relatively abundant phase in areas proximal to the Tynagh fault. It occurs as diamond-shaped and acicular crystals up to 3 mms. in size, both as replacements of the host limestones (Pl.3.17C), and as intergrowths with other stage 3 sulphides and sulphosalts. In certain instances the arsenopyrite clearly pre-dates the associated phases, fractured acicular crystals being penetrated by and enclosed within a later matrix of galena (Pl.3.17E,F).

The majority of the sphalerite intergrown with stage 3 sulphides is obviously of a relic nature. However, sphalerite is occasionally observed to be mutually intergrown (Pl.3.16C,D). At three locations, all of which are in the fault zone, individual crystals of sphalerite can be seen to contain numerous rounded inclusions of chalcopyrite (< 10 µm in size generally), displaying a typical emulsion texture (Pl.3.16F).

Gersdorffite occurs as small (generally $\leqslant 20$ µm), rounded inclusions within galena. Semi-quantitative micro-probe analysis verified that gersdorffite is present as the pure end member of the gersdorffite - ullmannite series, Sb not being detected:-

	Section No. Ty 3	
	1	2
Ni	40.10	40.74
As	44.41	44.41
S	12.60	12.60
Total	97.11%	97.75%

Stage 3 galenas as well as being characterized by an abundance of included tennantite often contain inclusions of other sulphosalts. Of these bournonite, $2PbS.Cu_2S.Sb_2S_3$, is by far the most common. It occurs as small (< 80 μm, usually 10-30 μm), oval or elongate blebs that often exhibit a preferred orientation parallel to cleavage directions of galena (Pl.3.16E). Dufrenoysite, $2PbS.As_2S_3$, occurs as rare lozenge-shaped inclusions (⩽ 125 μm) that display abundant polysynthetic twin lamellae. Two sub-rounded inclusions of pearceite/arsenopolybasite, $(Ag, Cu)_{16}(As, Sb)_2S_{11}$, approximately 300 μm in size, have been noted within a single specimen of galena. Qualitative S.E.M. analysis demonstrated that Sb is subordinate to As. Unfortunately, it is not possible to distinguish between the pearceite and polybasite solid solution series on the basis of optical properties and chemical composition alone (Uytenbogaardt and Burke, 1971).

Carbonates and silicates are not a common component of stage 3 intergrowths, and a relic or derivative origin in many cases cannot be ruled out. Dolomite is the most common non-opaque phase, however it does not occur in the nearly same abundance as in stage 2 intergrowths, and usually tends to be restricted to the contact zones with the host limestone.

3.4.3 Microtextural Evidence for the Replacement and Recrystallisation of Stage 2 Intergrowths

A variety of microtextural relationships have been observed supporting a post-dilatant fracture-fill age for stage 3 intergrowths: typical stage 2 intergrowths of sphalerite and dolomite occur as corroded relic patches within a matrix of later tennantite (Pl.3.15A); euhedra of arsenopyrite form overgrowths over disseminated

sphalerite, the sphalerite being enclosed within the arsenopyrite to produce a sieve texture (Pl.3.17D). However, it is galena that displays the best sequence of replacement textures: galena truncates and selectively replaces colloform banded sphalerite (Pl.3.15E); relic patches of banded sphalerite occur completely enclosed within galena (Pl.3.15C); euhedral and subhedral crystal faces of galena project into and replace microcrystalline sphalerite intergrowths (Pl.3.10E); sphalerite displaying atoll textures, commonly interpreted as a replacement phenomenon, occurs as inclusions within galena (Pl.3.15D).

There is also evidence to suggest that recrystallisation of previously precipitated phases has occurred in response to the influx of later mineralizing fluids. Corroded patches of microcrystalline sphalerite, characterized by a porous texture and intergrown with minor silicate, barytes and carbonate, can be seen to have recrystallised along the contact zones with later discordant galena (Pl.3.16A). The recrystallised sphalerite no longer displays a porous texture, lacks inclusions of non-opaque phases and displays straight or gently curved margins, suggesting mutual intergrowth with galena. Ultimately small areas of recrystallised sphalerite occur in isolation within galena and are indistinguishable from co-precipitated phases (Pl.3.16B). It is, therefore, possible that the sphalerite described above (3.4.2.2) as being in mutual intergrowth with stage 3 sulphides and sulphosalts, is in fact recrystallised stage 2 sphalerite.

3.5 THE STYLE OF MINERALIZATION WITHIN THE LOWER MUDDY LIMESTONES

Although all three stages of sulphide mineralization can be

recognised within the Lower Muddy Limestone sequence, the style of mineralization is quite different to that observed within the major host. The lithology of the Lower Muddy Limestone, briefly described in chapter 2, essentially consists of a sequence of thinly bedded, dark, crinoidal limestones with intercalated shales. The sulphides occasionally occur as conformable stratiform horizons of massive sulphides, largely microcrystalline sphalerite, up to 10 or 20 cms. in thickness. More commonly the sulphides are present as interstitial disseminations forming the matrix to bedded crinoid debris. The stratiform nature of the sulphides suggests a synsedimentary origin, but there are a number of textural features which do not support this hypothesis. In hand specimen, the crinoidal limestones are fresh and unaltered in appearance, however, a more detailed examination of a number of specimens in section has revealed a sequence of alteration and replacement textures indicative of a post-diagenetic age for ore sulphide mineralization.

The original rock consisted of close packed organic detritus, comprised largely of crinoid fragments with minor amounts of brachiopod debris in a matrix of sparry calcite and minor argillite. The sparry cement overgrew the organic fragments with optical continuity producing a tightly interlocking mosaic of anhedral calcite (Pl.3.18A) with minor interstitial patches of mud. Subsequent to the cementation of the rock, the introduction of, and replacement by ferroan calcite, rhombic dolomite, barytes and sulphides, led in places to the almost complete destruction of the primary sedimentary and diagenetic textures. In many cases the original calcite cement of the rock has been completely replaced, remnants of sparry calcite and crinoid ossicles being totally

enclosed by the later matrix (Pl.3.18B,C,D). Crinoid fragments proved more resistant to replacement, but even so provide ample evidence of corrosion and alteration. This initially takes the form of marginal alteration of the calcite to ferroan calcite, the original outline and internal texture of the crinoid fragments being preserved (Pl.3.18C). In the more advanced stages of replacement, the margins of the ossicles appear ragged and diffuse, and the cores become infilled by sulphides and associated non-opaques of an identical nature to that of the matrix. Ultimately this results in the almost complete digestion of the crinoid fragments into the matrix.

Examination of the upper contacts of the stratiform massive sulphide horizons with the enclosing host, reveals that, as the contact is approached, there is ever increasing evidence of alteration and replacement of an identical nature to that described above for the disseminated sulphide/crinoid horizons. This suggests a post-sedimentation/diagenetic age for the stratiform horizons within the Lower Muddy Limestones.

3.6 ALTERATION AND REPLACEMENT OF THE WAULSORTIAN MICRITES ASSOCIATED WITH PRIMARY SULPHIDE MINERALIZATION

3.6.1 Dolomitisation

Dolomitisation is only occasionally evident, restricted in its extent, and is localised to the immediate contact zone between sulphide mineralization and the host Waulsortian limestones. It is associated with both stage 2 and 3 mineralization, but is best developed and most commonly associated with stage 3.

Macroscopically the dolomitisation appears as a bleached zone,

generally no more than 2 or 3 cms. in width, sometimes displaying a lamination perpendicular to the host/mineralization contact (Pl.3.7A). Microscopically it can be seen to consist of a granular mosaic of anhedral dolomite crystals, 10 to 60 μm in size, with minor amounts (<1%) of interstitial ferroan calcite. Crystal size increases (100 to 150 μm) as the dolomite/micrite contact is approached, and a subhedral to euhedral habit becomes more evident. The contact between the dolomite and the micrite is usually distinct, although corroded relics of partially dolomitised calcitic micrite and crinoid fragments often occur within the dolomite close to the contact zone (Pl.3.18E).

3.6.2 Barytisation

Fine grained barytes replacement has been noted in association with both stages 2 and 3, but as in the case of dolomitisation, is largely developed in association with stage 3 mineralization. The barytes, associated with disseminated sulphides, occur as lenses within the micrites, up to 30 cms. in width and several metres in lateral extent, and also as zones of replacement adjacent to sulphide/sulphosalt veins (Pl.3.7B).

The barytes occurs as uniformly sized blades, clustered together to form rosette structures 0.4 to 1.5 mms. in diameter. An equigranular mosaic of anhedral to subhedral dolomite, with minor interstitial ferroan calcite, similar to that described above (3.6.1), forms the matrix of the barytes rosettes. Contacts between the rosette barytes/dolomite intergrowths and unaltered micrites are usually gradational and ill-defined.

3.6.3 Replacement by Silicates

Albite, occasionally displaying simple and polysynthetic

twinning, occurs as euhedral and subhedral laths 20 to 50 μm in size within an otherwise unaltered micritic host. Its abundance increases as dilatant fractures and stage 3 veinlets are approached, but never forms more than a few per cent of the rock. Potassium feldspars, possibly hyalophane, are less commonly observed as small scattered euhedra. Anhedral to subhedral feldspars, displaying weak albite twinning, have been noted in Waulsortian micrites collected well away from known areas of mineralization, it is therefore possible that some of the feldspars may be detrial or authigenic in origin. Indeed, Kastner (1971) found that authigenic albite was a common component of micrites. However, as their abundance generally increase towards dilatant fracture infillings and veinlets, a hydrothermal origin seems more probable.

Plagioclase also occurs in association with rosette barytes replacement, where subhedral and euhedral crystals up to 70 μm in size can compromise up to 5% of the total intergrowth. Similarly, it has been noted as a component of dolomitised zones, where, in association with disseminated pyrite, subhedral intergrowths define a narrow suture zone 60 to 80 μm in width along the contact between unaltered and dolomitised micrite (Pl.3.18E). Individual crystals within the suture zone are 40 to 50 μm in size, and only occasionally display weak albite twinning.

Although quartz comprises the most common non-carbonate component of unmineralized Waulsortian micrites, it is less abundant than plagioclase within the mineralized micrites at Tynagh. Euhedra of quartz have been observed as overgrowths and replacements of bioclastic fragments infilled by sparry calcite, clearly indicating a post-diagenetic age for their crystallisation (fig. 3.3).

FIG. 3.3 QUARTZ OVERGROWING BIOCLASTS.

Ty10, 66+10W 5050.

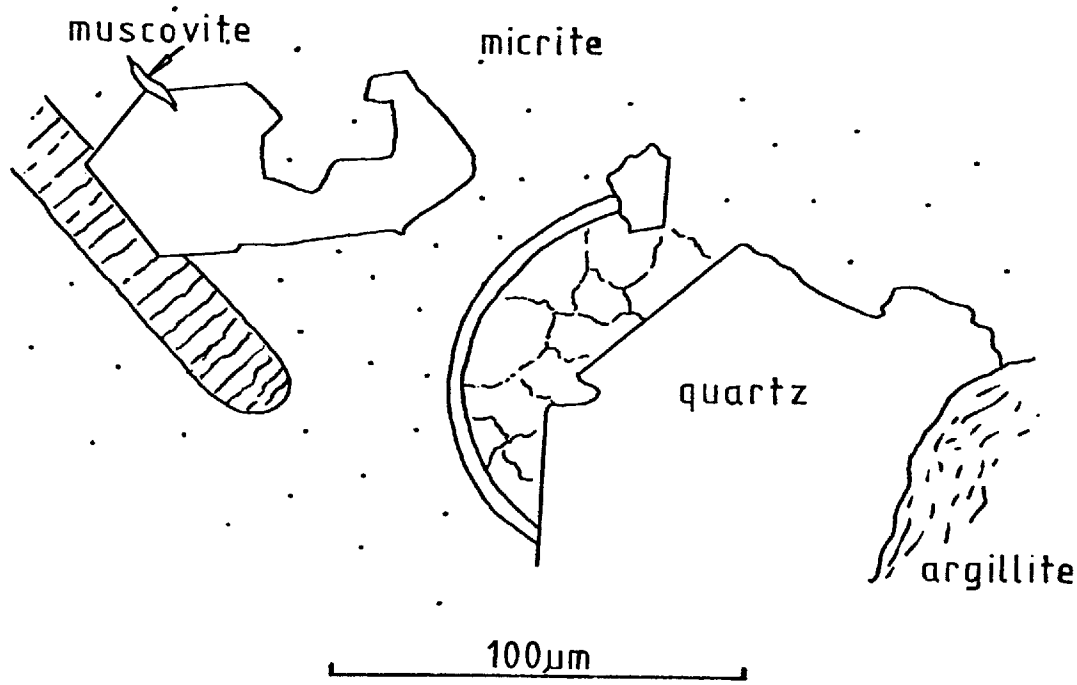

FIG. 3.4 FRAGMENTED BOTRYOIDAL PYROBITUMENS. 89+00W 4900.

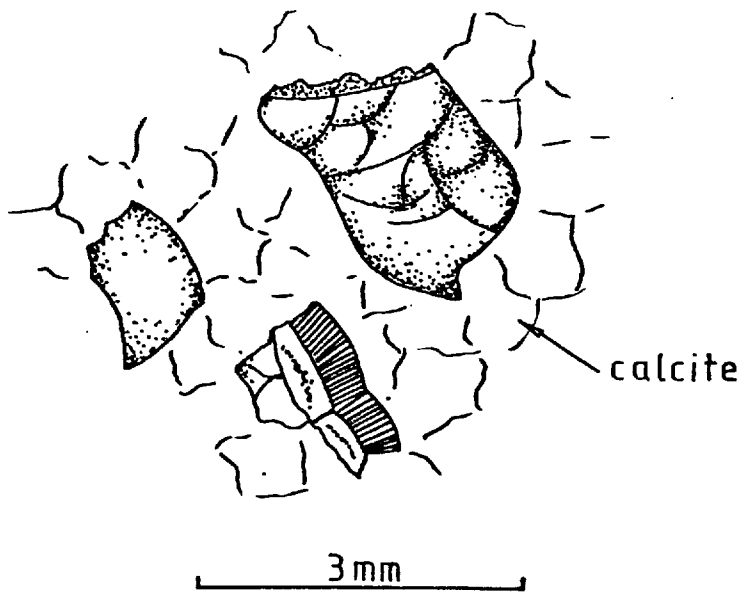

Silicification has only been noted in abundance at one locality, adjacent to an area of arsenopyrite replacement. In this particular example the quartz occurs as euhedra, up to 200 μm in size, that are intergrown with lesser amounts of albite and which together form up to 10 or 15% of the rock. The centre of the quartz crystals are clouded due to the presence of numerous rounded inclusions of calcite, 1 to 10 μm in size, presumably incorporated from the host during crystal growth. An outer rim, approximately 10 μm in width, tends to be free of these solid inclusions, however tiny (≤ 5 μm) two phase fluid inclusions have occasionally been noted. The gas-liquid ratio within these inclusions is variable, the liquid phase often only forming a thin outer rim to the gas bubble.

3.7 STAGE 4 - PRECIPITATION OF POST-ORE CARBONATES AND ASSOCIATED PHASES

3.7.1 Veinlet and Cavity Infillings by Calcite

Distributed throughout the Tynagh ore zones are veinlets and cavities infilled with anhedral intergrowths of coarse, white calcite. Dolomite is a rare component. The veinlets are generally no more than 1 or 2 cms. in width, and many display distinct structural controls on their alignment. The dominant set are vertical and have a N - S orientation; however, as the fault zone is approached, horizontal gashes become more common. Moore (1975) suggested that the N - S veins correspond with post-tectonic relaxation joints, whilst he relates the horizontal calcite veining in the fault zone to reverse movements tentatively correlated with Hercynian deformation farther to the south.

Cross cutting relationships clearly demonstrate a post-ore age for the calcite veins. Sulphides, largely sphalerite and galena, are recrystallised into the veinlets along contact zones with primary mineralization. Minor amounts of purple fluorite have been observed to be intergrown with vein calcite, but at only two localities. At 89+00W 4900 level, fragments of pyrobitumen up to several mms. in size occur enclosed within a matrix of coarse sparry calcite infilling a post-ore cavity. Careful examination reveals that their solidification pre-dated the introduction of the calcite, and that they must have been derived from the enclosing host (fig. 3.4). The pyrobitumens have a botryoidal outer 'skin', less than 0.5 mm. thick, that in section displays a perpendicular fibrous texture. This encloses a brittle vitreous core that exhibits a conchoidal fracture.

In an attempt to further define the parameters of post-ore carbonate precipitation, homogenisation temperatures of two phase fluid inclusions in calcite and fluorite were determined. Unfortunately, the poor quality of the material precluded the confirmation of their primary nature. The three specimens examined each exhibited an excessive range of values and, therefore, cannot be regarded as an accurate indication of the temperature of deposition. However, this temperature possibly falls somewhere within the total range exhibited ($58^{o}C$ - $158^{o}C$).

3.7.2 Dolomitisation

Scattered at intervals along the Tynagh fault are zones or "plugs" of Waulsortian micrite that have been extensively dolomitised. One such "plug" occurs between the zone II and zone III orebodies.

The primary texture of the micrites can be seen to have been completely destroyed, having recrystallised into a sugary intergrowth of pale grey dolomite with spectacular cavernous vugs up to 0.5 metres in diameter, lined with pink euhedral dolomite. Zebra textures are extensively developed consisting of sub-horizontal interbandings of the grey sugary dolomite and pink euhedral dolomite. The surfaces of the dolomite crystals lining the large vugs are often overgrown by euhedra of calcite, up to 2 cms. across, and peppered with smaller euhedral crystals of chalcopyrite, 1 to 2 mms. in size. Radiating out to the north of the "plug" a system of N. to N.W. trending vertical veins, up to half a metre in width and containing coarse anhedral intergrowths of pink dolomite and white calcite, have been observed at the 4700 and 4880 elevations.

A contact between the dolomitisation and the sulphide mineralization has been exposed at the 5000 and 5050 elevations, zone III (Pl.3.19). Although the cavernous dolomite would provide an ideal host for mineralization, even where directly in contact with the ore, it is devoid of sulphide infillings, bar the minor chalcopyrite overgrowths described above. Veinlets of dolomite can be seen to emanate out of the dolomitised zone into the sulphides, but quickly die out due to the unsuitable nature of the sulphide host for replacement. It is clear, therefore, that the "plug" dolomitisation post-dates sulphide mineralization.

3.7.3 Gypsum

White massive gypsum has been observed at only one locality where it occurs as an infilling to a larger cavity. The occurrence of mineralized micrite fragments within the gypsum indicates a post-ore age for its precipitation, however the temporal relationship to the calcite veinlets and the "plug" dolomite cannot be ascertained.

PLATE 3.1 COLLOFORM PYRITE AGGREGATE (STAGE 1) AND DILATANT FRACTURE INFILLING (STAGE 2)

A) Aggregate of colloform pyrite within black carbonate matrix.
Ty 34; 4900, 86+00W.

B) Dilatant fracture infilling of horizontally banded micro-crystalline sphalerite. The banding within the sphalerite is displaced by a reversed microfault that has been utilised by later (stage 3) discordant coarse grained galena. The later mineralizing fluids were dammed at the contact between the banded sphalerite and the overlying Waulsortian micrite, resulting in lateral replacement by disseminated and euhedral galena. Recrystallisation of the host carbonate occurred along this contact, and coarsely crystalline galena partially replaced the finely banded micrite.
Ty 16; 5050, 66+80W.

PLATE 3.1

A

B

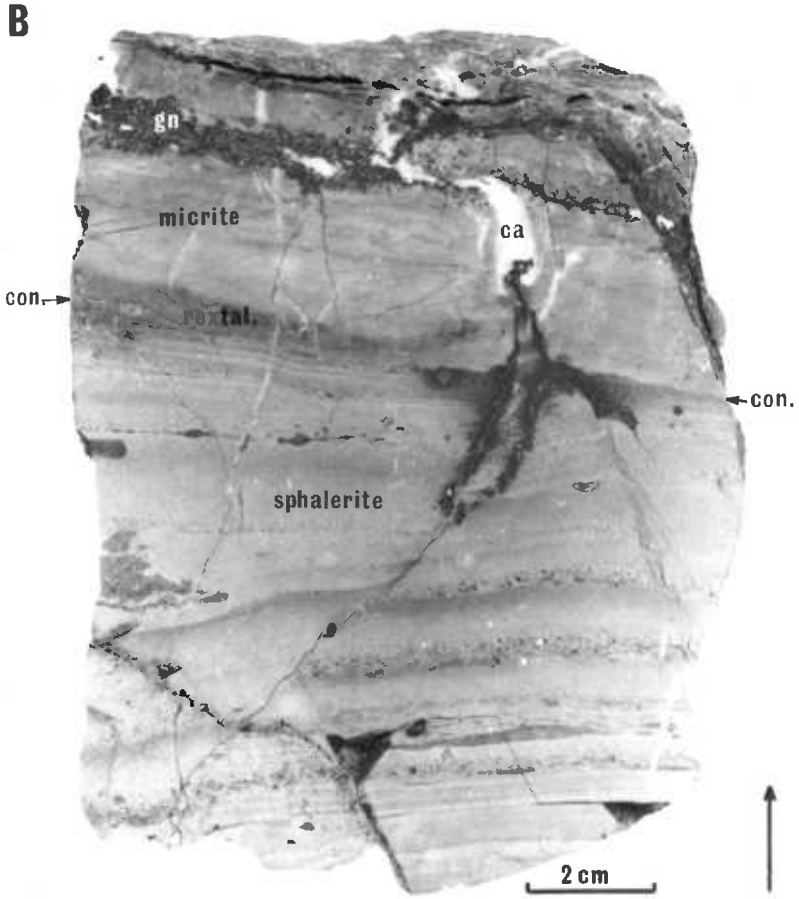

PLATE 3.2 DILATANT FRACTURE INFILLING (STAGE 2)

A), B) Dilatant fracture infilling of microcrystalline sphalerite and galena within mottled biomicrite. The banded sulphides within the lower half of the specimens have been plastically deformed and have undergone vertical flow and remobilisation, erupting as a sphalerite mud volcano at a higher level. Horizontal stylolite surfaces within the host limestone are terminated at the contact with the sulphides, and have acted as a locus for replacement by disseminated sphalerite.

Ty 29; 5050, 66+80W

PLATE 3.2

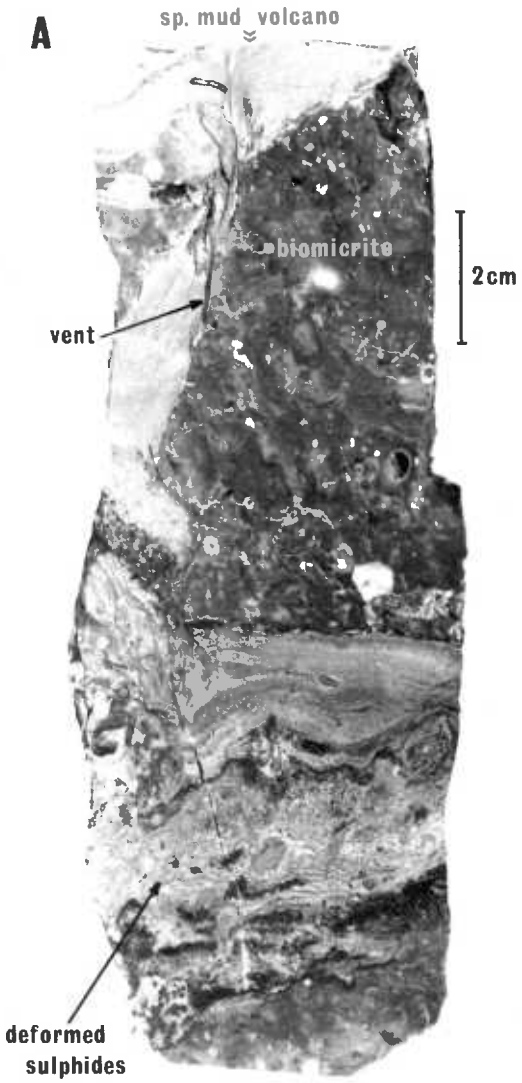
A
sp. mud volcano
biomicrite
2cm
vent
deformed
sulphides

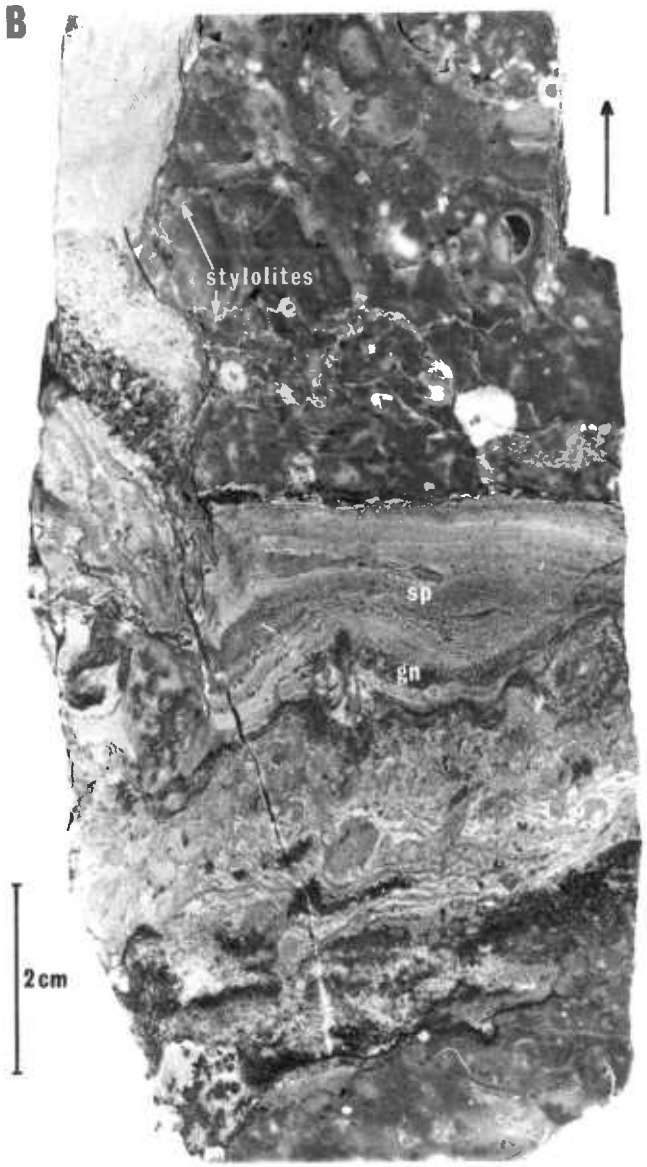
B
stylolites
sp
gn
2cm

PLATE 3.3 DILATANT FRACTURE INFILLINGS (STAGE 2)

A) Banded microcrystalline sphalerite/dolomite intergrowth with numerous included sub-rounded clasts of Waulsortian limestone, infilling dilatant fracture. Numerous vertical and sub-vertical stylolite surfaces cross-cut the sulphide banding, the most pronounced occurring along the contact with the limestone. The host is a mottled biomicrite, the bioclastic components including crinoid ossicles, brachiopods and fenestellid bryozoa.
Ty 31; 5050, 65+40W

B) As above. Darker horizons within the banded infilling are comprised dominantly of carbonate, whilst paler horizons contain a higher proportion of microcrystalline sphalerite. Note how the banding pinches over the elongate micrite clast (a), and the load depression beneath the smaller sub-rounded clast (b). Incipient dolomitisation of the Waulsortian host has occurred along the upper contact with the dilatant fracture.
Ty 37; 5050, 65+40W

PLATE
3.3

A

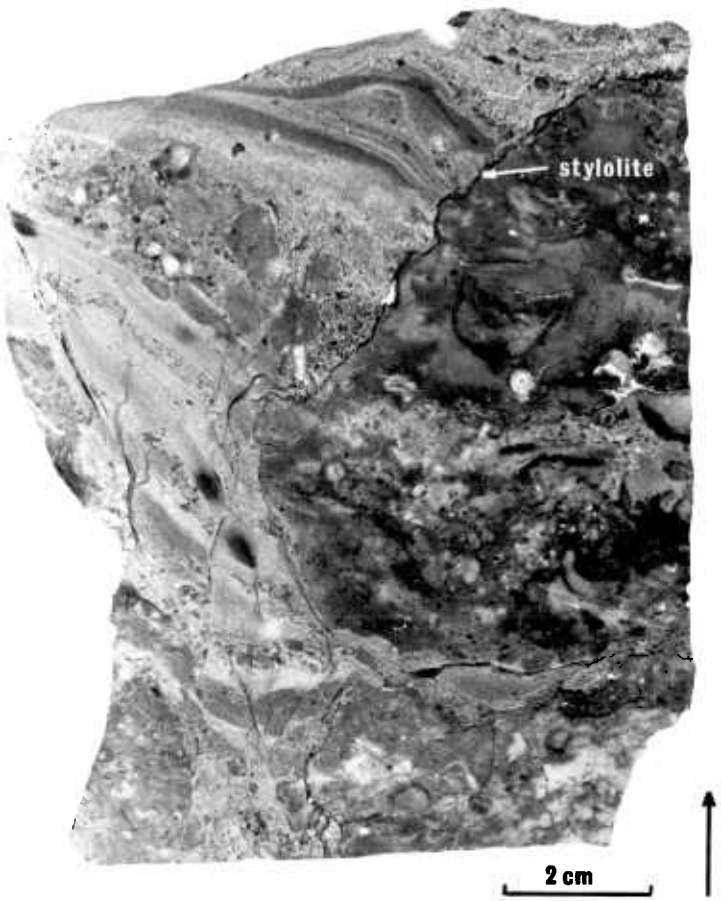

B

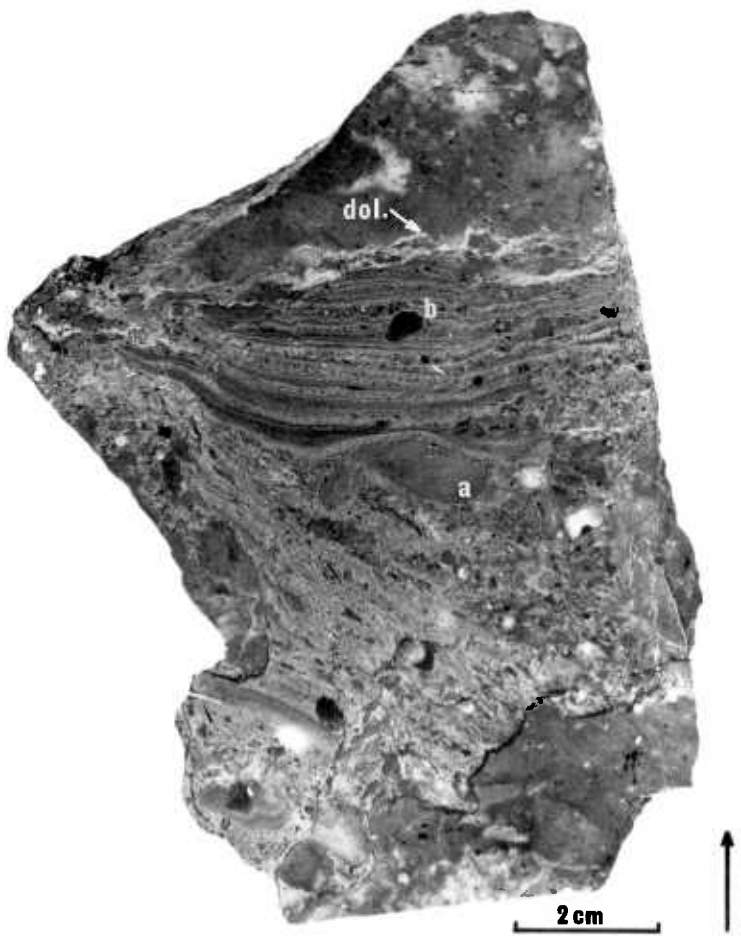

PLATE 3.4 BRECCIA ORE (STAGE 2)

Angular fragments of laminated micrite in a matrix of microcrystalline sphalerite. The angular nature of the fragments, the presence of fibrous diagenetic calcite (a), and cavity infillings of lime mud (b) indicate that brecciation post-dates the early history of lithification of the Waulsortian bank limestones.

Ty 15; 5000, 64+85W

PLATE 3.4

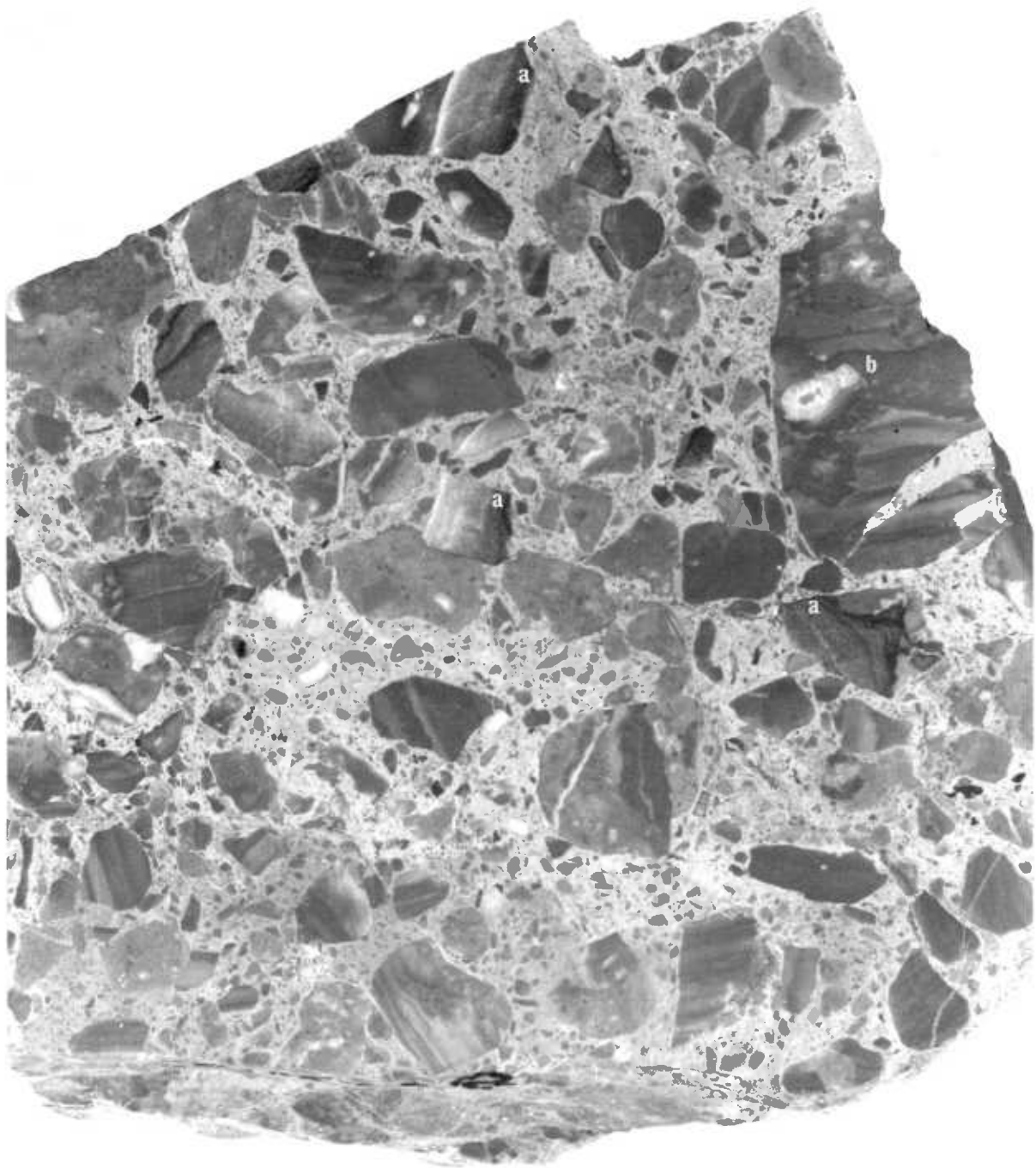

PLATE 3.5 BRECCIA ORE (STAGE 2)

Clasts of Waulsortian biomicrite in a matrix of micro-crystalline sphalerite, and later coarse galena. The sub-rounded and diffuse nature of the clast margins may indicate that brecciation of the host occurred whilst it was in a semi-coherent state.

Ty 2; 4900, 89+20W

PLATE 3.6 DILATANT FRACTURE INFILLINGS (STAGE 2)

A) Discordant fracture infilled with microcrystalline sphalerite and galena displaying crude banding. The mineralized fracture cross-cuts, and is aligned perpendicular to an horizon of stromatactis cavities dipping towards the left of the photograph. Mineralization clearly post-dates the early diagenetic history of the host carbonate sequence.

4912, 63+90W, looking south.

B) Irregular shaped pod of microcrystalline sphalerite and galena within Waulsortian limestones. The gross textural appearance of the sulphide 'mud' suggests that internal slumping and flow occurred prior to lithification.

4800, 89+00W, looking east

PLATE
3.6

A

B

PLATE 3.7 EPIGENETIC VEININGS (STAGE 3)

A) Coarse grained galena cutting and replacing micrite. The host in the immediate contact zone with the veinlets and disseminations has been bleached and dolomitised. The white dolomite displays a wispy horizontal lamination, and the contact with the unaltered calcitic micrite is sharply defined in places by a narrow suture. Small cavities contain microcrystalline sphalerite.

Ty 6; 5050, 66+10W

B) Tennantite veinlets in barytised Waulsortian bank limestones. Two types of barytes can be observed - a fine grained variety intergrown with disseminated tennantite that has replaced the limestone, and a coarse euhedral variety in close association with the veinlets.

Ty 88; 4800, 80+80W

PLATE 3.7

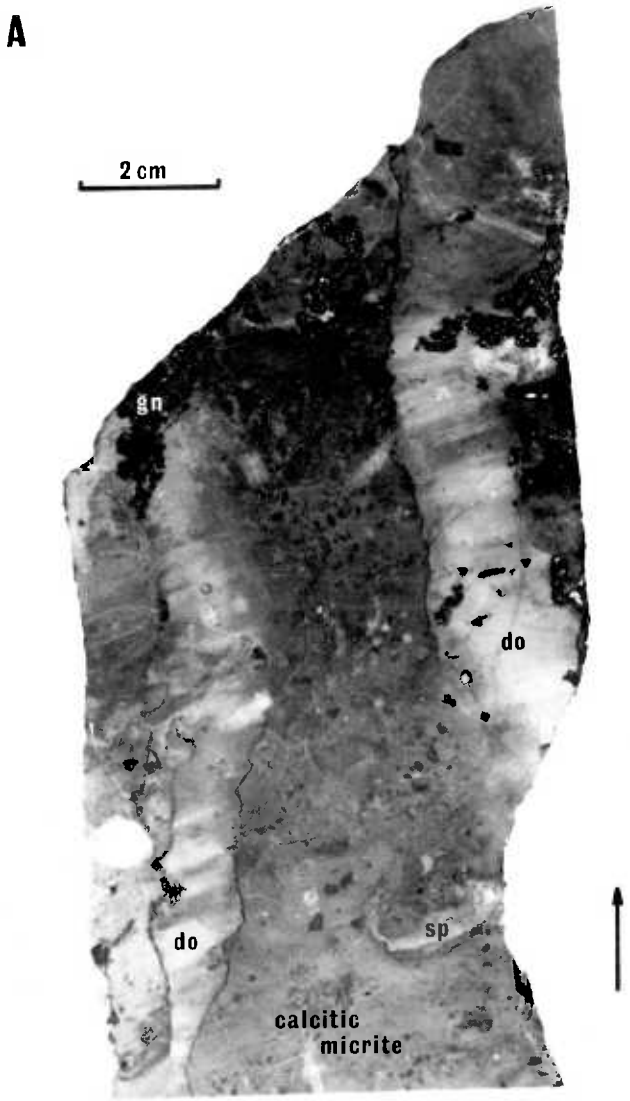

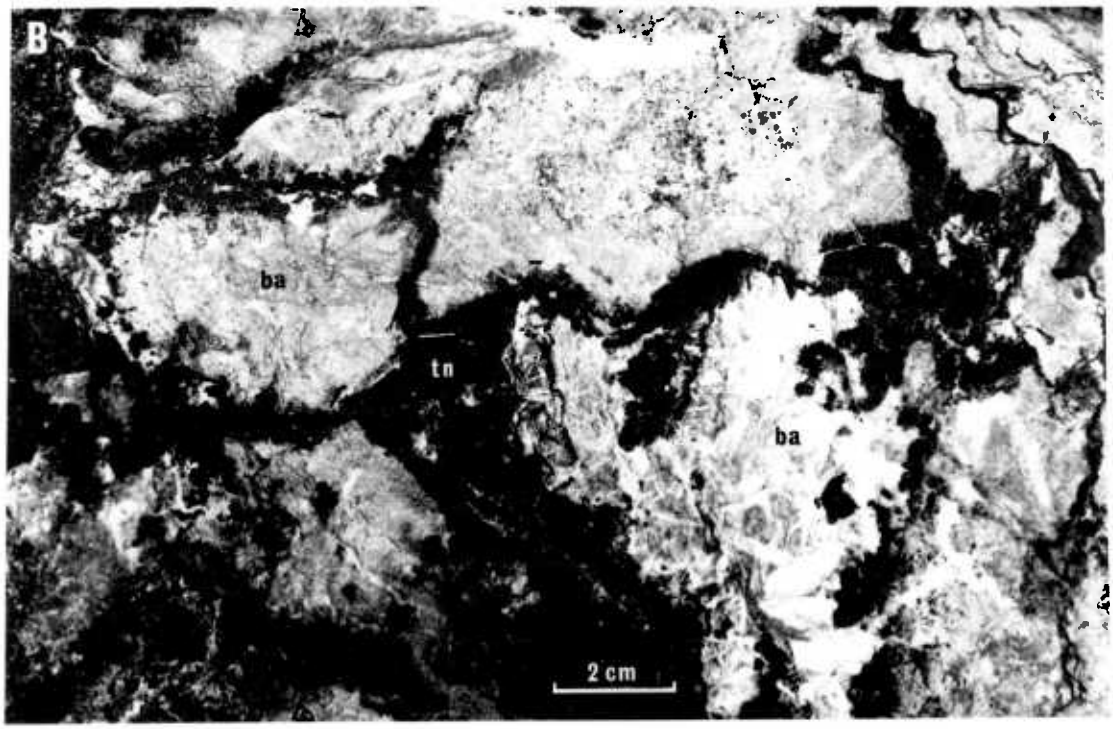

PLATE 3.8 TEXTURES IN STAGE 1 PYRITE

A) Granular pyrite exhibiting incipient colloform texture. A stylolite surface cutting the calcitic micrite is deflected around the pyrite aggregate. (Reflected light).
Ty 82; open pit - 4900, 84+00W

B) Concentrically banded colloform pyrite. (Reflected light).
Ty 18; open pit - 4900, 85+20W

C) Plumose colloform pyrite. (Reflected light).
Ty 18; open pit - 4900, 85+20W

D) Internal structure of pyritised crinoid ossicle.
(Reflected light).
Ty 19 (ii); 4900, 86+00W

PLATE 3.8

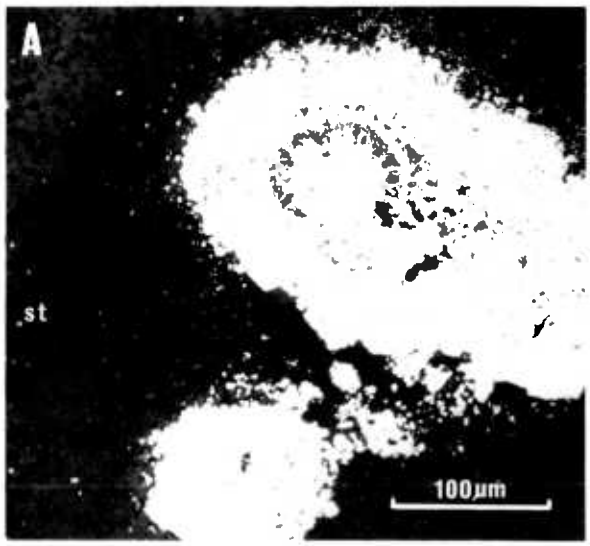

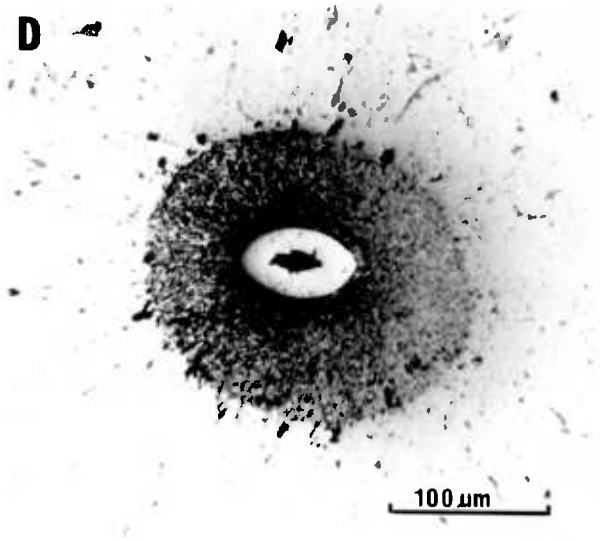

PLATE 3.9 STAGE 1 MICROTEXTURES AND REPLACEMENT OF PYRITE

A) Euhedral pyrite overgrowing colloform pyrite. (Reflected light).
Ty 70; 4800, 89+50W

B) Spherulitic marcasite and euhedral pyrite within argillite horizon. (Reflected light).
Ty 65; 4800, 89+00W

C) Conformable horizons of sphalerite, colloform pyrite and finely crystalline euhedral pyrite (lower half of photograph) within argillite overlying biomicrite.
Ty 70; 4800, 89+50W

D) Interbanded sphalerite and pyrite. Note apparent atoll replacement of pyrite by sphalerite and sphalerite by pyrite.
(Reflected light; oil immersion).
Ty 69; 4800, 90+10W

E) Brecciated pyrite and marcasite within black carbonate matrix.
(Reflected light).
Ty 22; 4900, 87+80W

F) Galena penetrating brecciated pyrite. (Reflected light).
Ty 19 (ii); 4900, 86+00W

PLATE 3.9

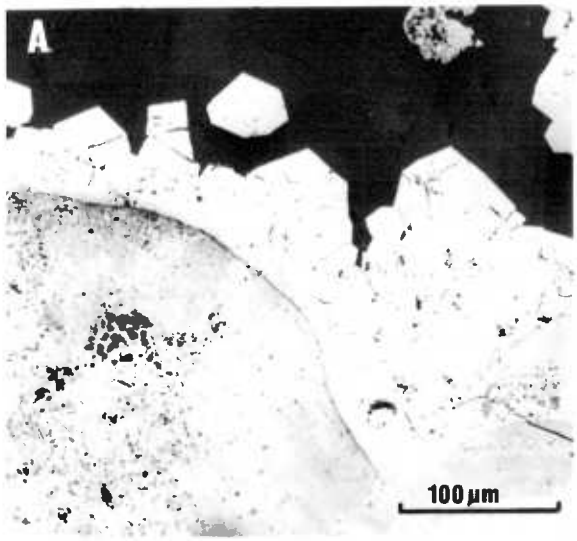
A
100 µm

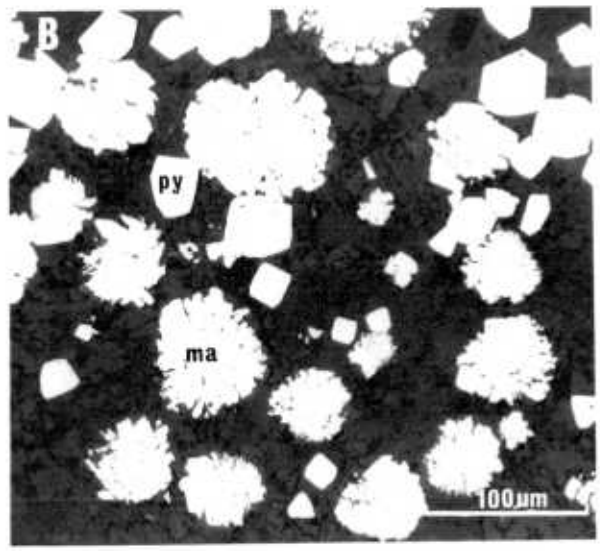
B
py
ma
100µm

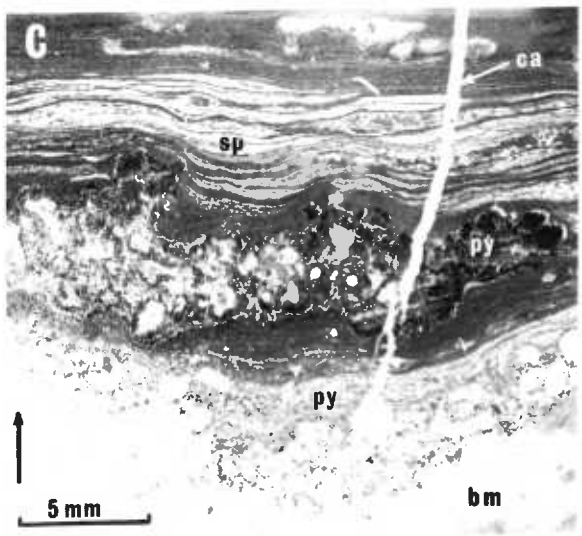
C
ca
sp
py
py
5 mm
bm

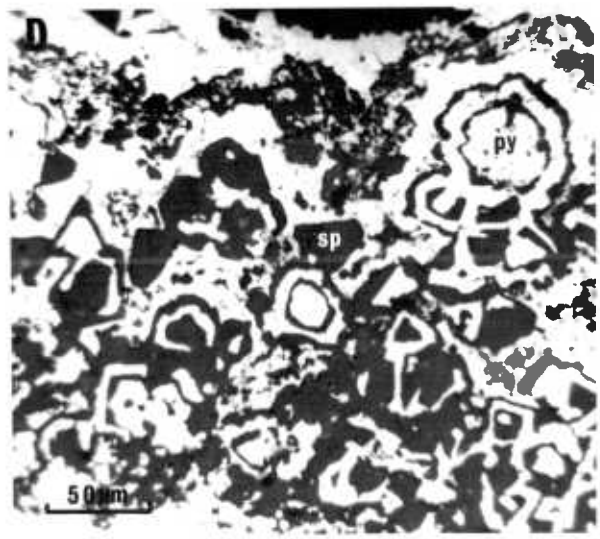
D
py
sp
500µm

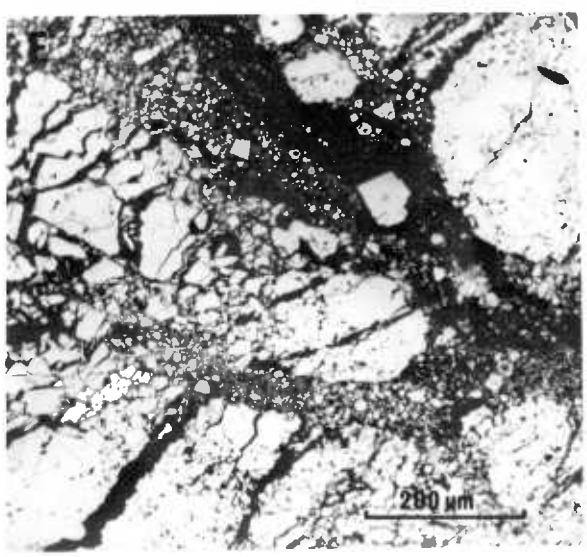
E
200 µm

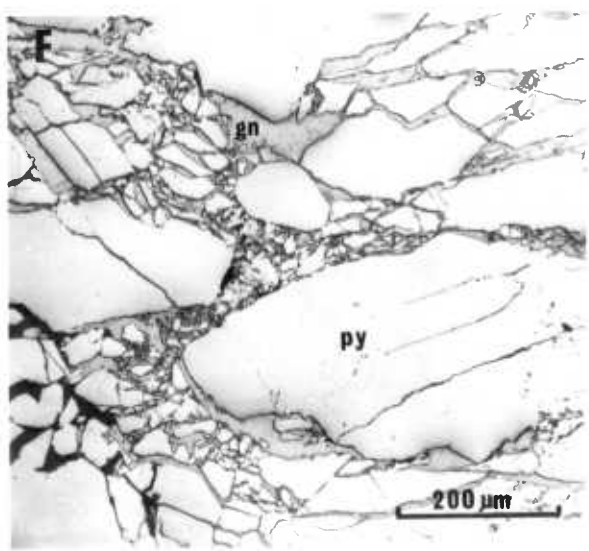
F
gn
py
200 µm

PLATE 3.10 REPLACEMENT OF STAGE 1 PYRITE

A) Subhedral sphalerite replacing granular pyrite. (Reflected light).
Ty 82; open pit - 4900, 84+00W

B) Replacement of pyrite by euhedral galena. (Reflected light).
Ty 19 (i); 4900, 86+00W

C) Core of granular pyrite aggregate being replaced by euhedral galena. Minor disseminations of sphalerite and pyrite within fine grained carbonate matrix. (Reflected light).
Ty 22; 4900, 87+80W

D) Detail of contact between euhedral galena and granular pyrite. Note termination of colloform banding and replacement of core regions by later galena. (Reflected light; oil immersion).
Ty 22; 4900, 87+80W

E) Sphalerite replacing pyrite, and in turn being replaced by galena. (Reflected light).
Ty 19 (ii); 4900, 86+00W

F) Framboidal pyrite within a matrix of tennantite and sphalerite. (Reflected light; oil immersion).
Ty 24; loose block of primary ore from residual deposit.

PLATE 3.10

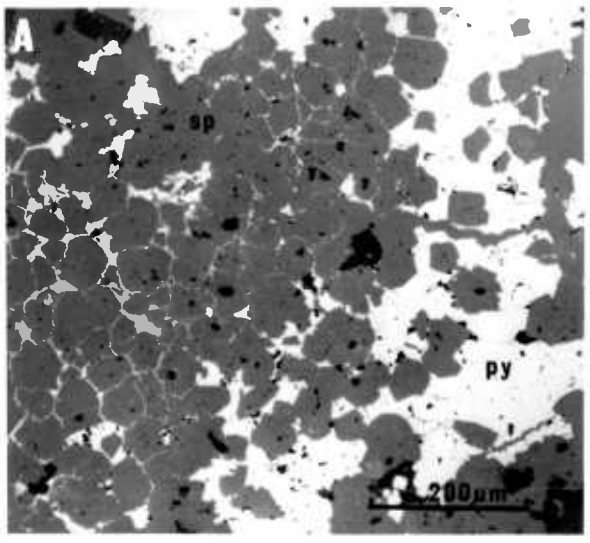
A
sp
py
200µm

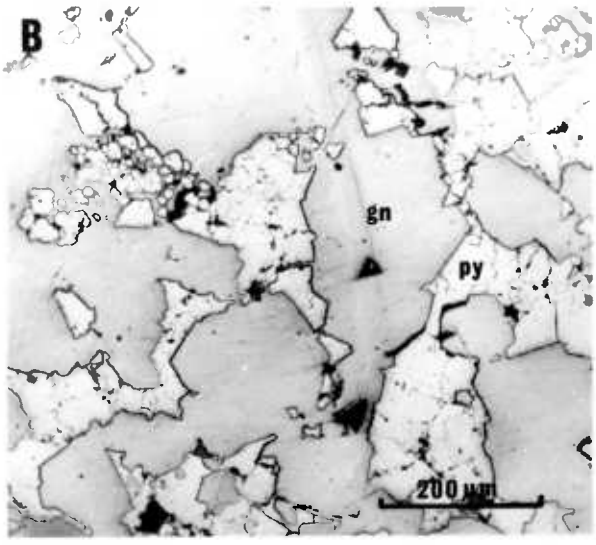
B
gn
py
200µm

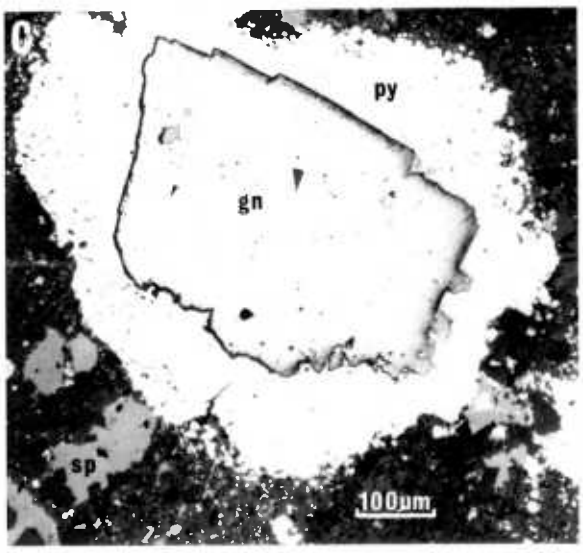
C
py
gn
sp
100µm

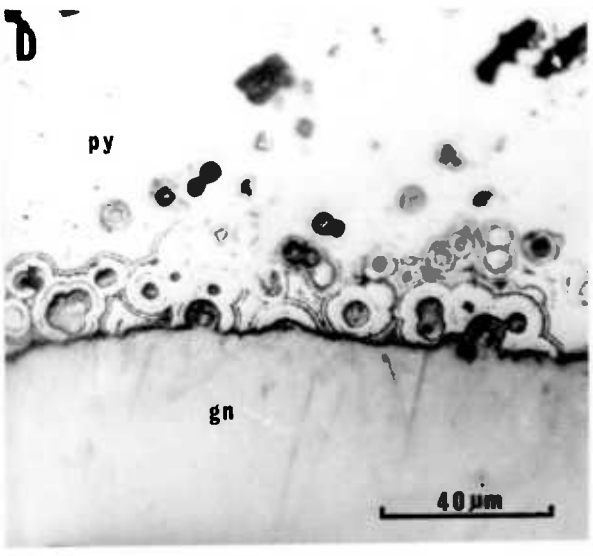
D
py
gn
40µm

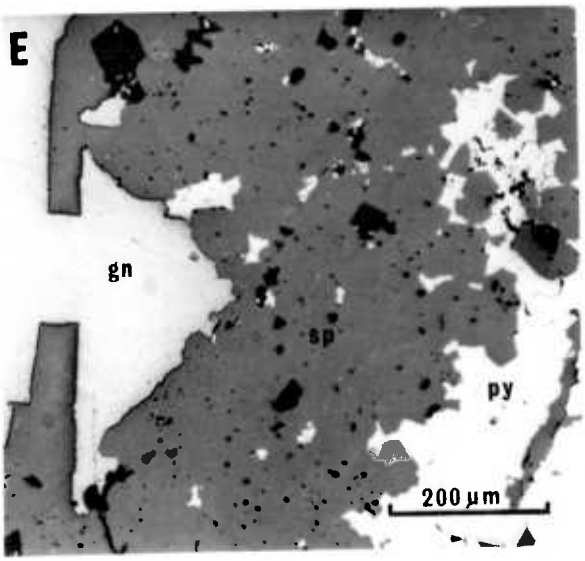
E
gn
sp
py
200µm

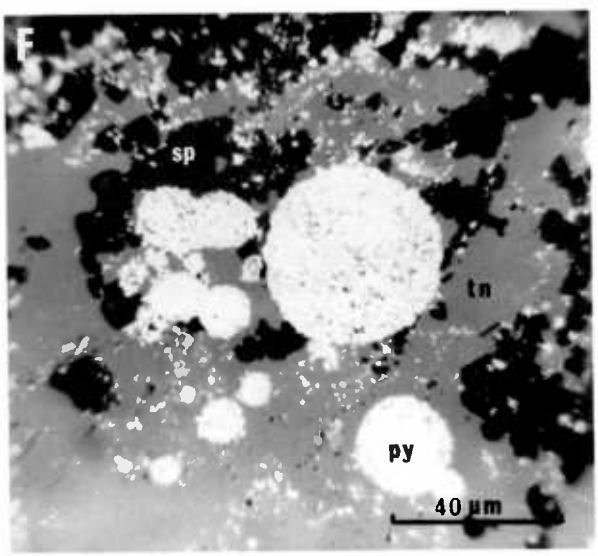
F
sp
tn
py
40µm

PLATE 3.11 REPLACEMENT OF STAGE 1 PYRITE;

SIEGENITE INTERGROWTHS

A) Framboid overgrown by euhedral pyrite, providing a locus for later chalcopyrite precipitation. Host:- Lower Muddy Limestone. (Reflected light; oil immersion).

Ty 40; 4620, 89+80W

B) Pyrite framboid being replaced by an intergrowth of tennantite and sphalerite. Matrix:- barytes/carbonate intergrowth. (Reflected light; oil immersion).

Ty 49; 4700, 91+10W

C) Selective replacement of euhedral pyrite by a mutual intergrowth of bornite, galena, tennantite and barytes. Note chalcopyrite lamella within bornite. (Reflected light; oil immersion).

Ty 51; 4700, 90+00W

D) Colloform pyrite with euhedral overgrowths, being replaced by a mutual intergrowth of bornite, galena, tennantite and barytes. In the lower half of the specimen bornite and tennantite are pseudomorphing the banded texture of the pyrite - (Reflected light).

Ty 51; 4700, 90+00W

E) Siegenite with replacement lamellae of galena. (Reflected light; oil immersion).

Ty 29 (i); 5050, 66+80W

F) Siegenite with replacement lamellae of chalcopyrite. (Reflected light; oil immersion).

Ty 6 (iii) 5050, 66+10W

PLATE 3.11

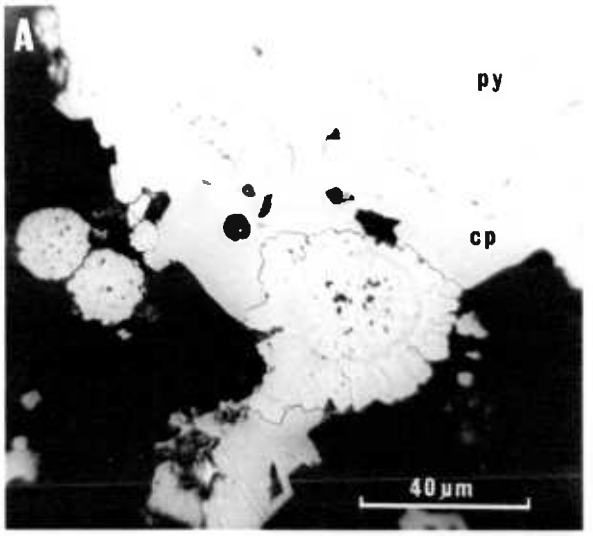
A
py
cp
40 µm

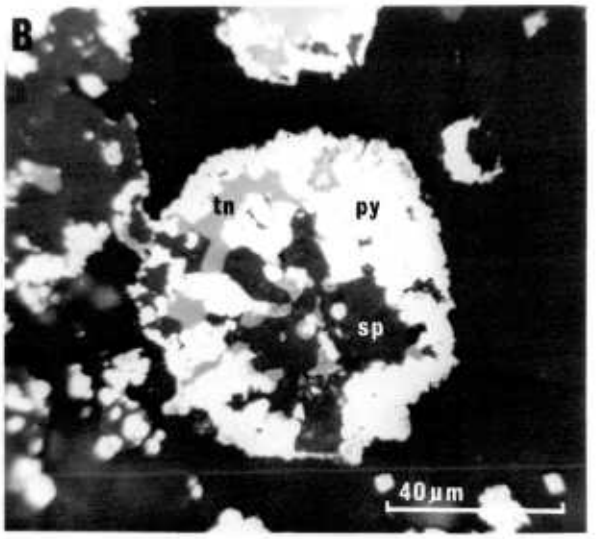
B
tn
py
sp
40 µm

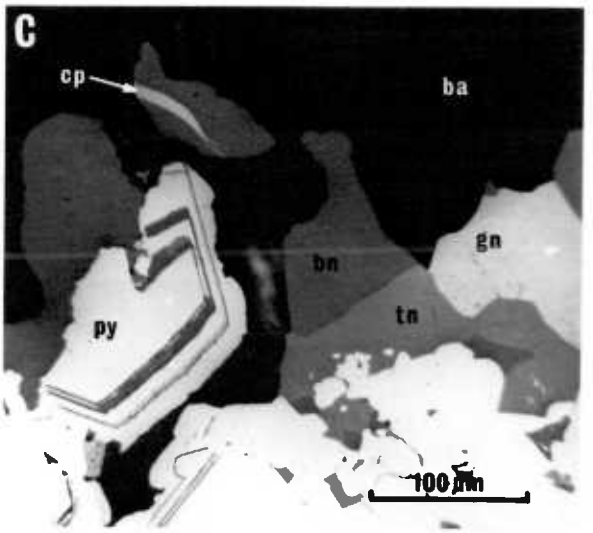
C
cp
ba
gn
bn
tn
py
100 µm

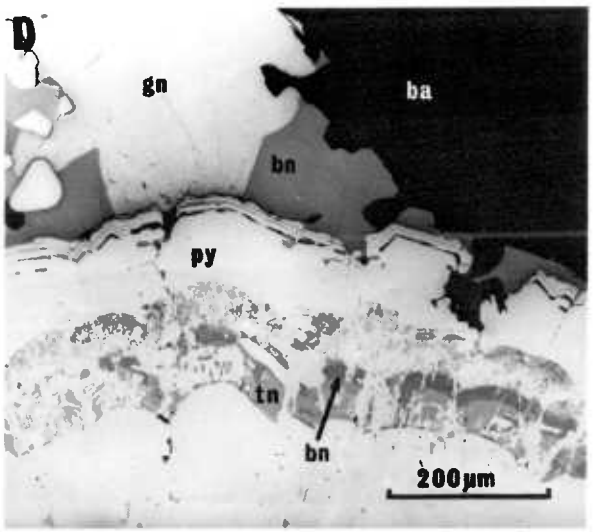
D
gn
ba
bn
py
tn
bn
200 µm

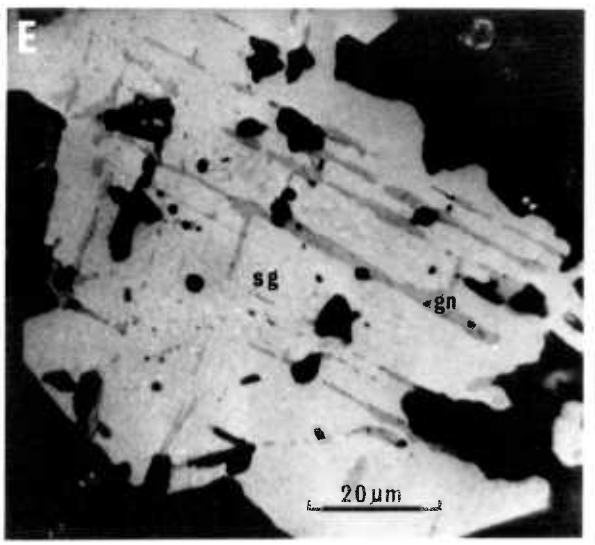
E
sg
gn
20 µm

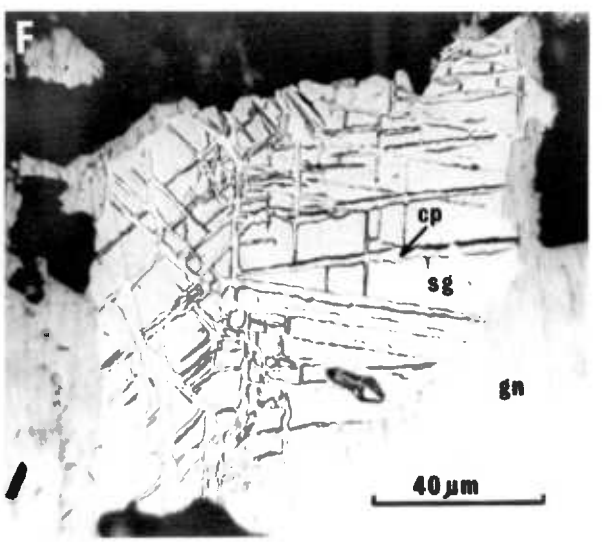
F
cp
sg
gn
40 µm

PLATE 3.12 STAGE 2 MICROTEXTURES

A) A typical sphalerite/dolomite intergrowth. (Reflected light).
Ty 66; 4800, 87+10W

B) Sphalerite, galena, dolomite intergrowth. (Reflected light).
Ty 9; 5050, 66+10W

C) Crinoid ossicle within a fine grained matrix of sphalerite, dolomite and hyalophane, with minor galena. The highest concentration of sulphides occur as marginal replacements of the crinoid fragment and the small micrite clast above. (Reflected light).
Ty 9; 5050, 66+10W

D) Sphalerite intergrown with acicular crystals of muscovite. (Reflected light).
Ty 14; 5000, 64+85W

E) Colloform banded sphalerite interbanded with anhedral calcite. (Reflected light).
Ty 52; 4700, 87+00W

PLATE 3.12

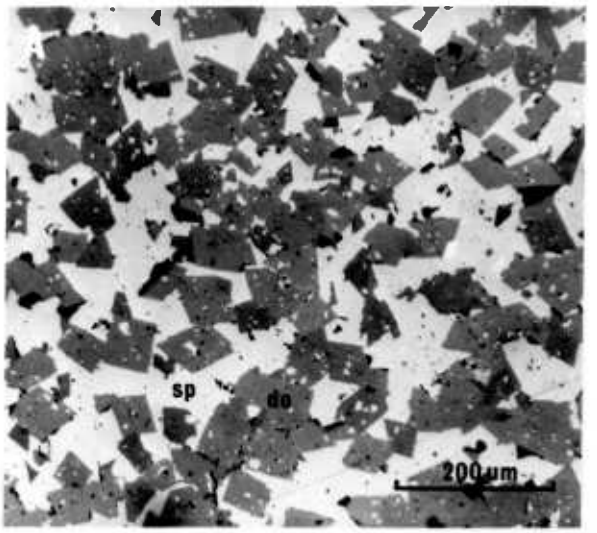

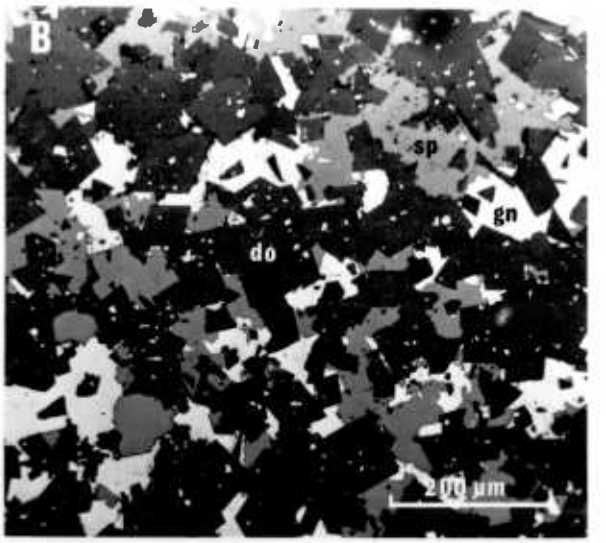

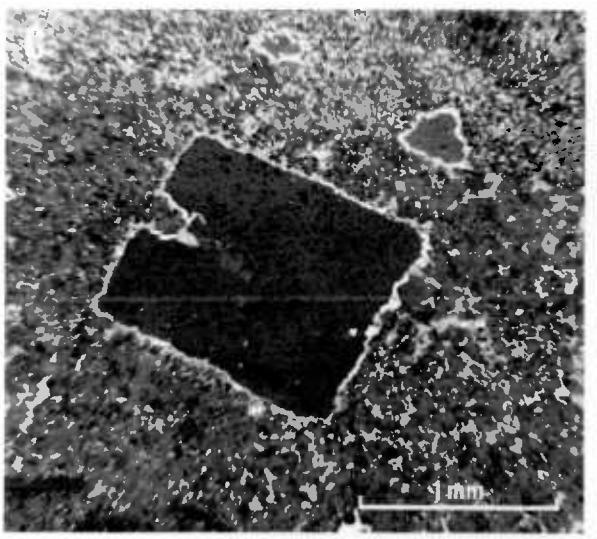

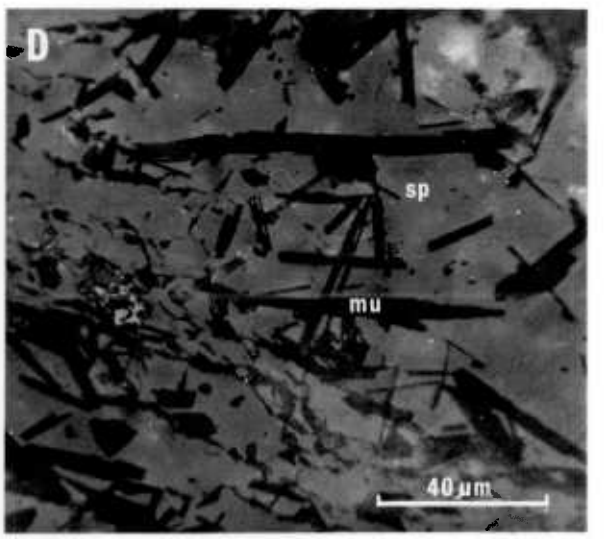

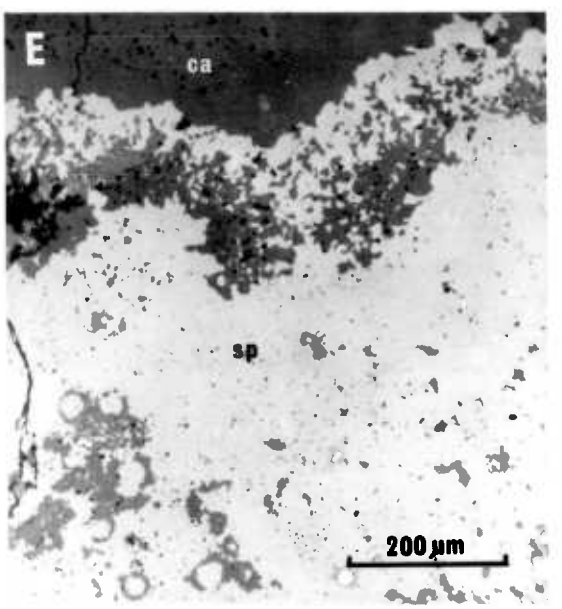

PLATE 3.13 STAGE 2 MICROTEXTURES

A) Poikilitic crystals of barytes in a matrix of micro-crystalline sphalerite. (Reflected light).

Ty 3; 5050, 65+40W

B) Skeletal barytes intergrown with microcrystalline sphalerite. (Reflected light).

Ty 52; 4700, 87+00W

C) Sphalerite and galena pseudomorphing barytes. Matrix - dolomite. (Reflected light).

Ty 12; 5050, 66+10W

PLATE 3.13

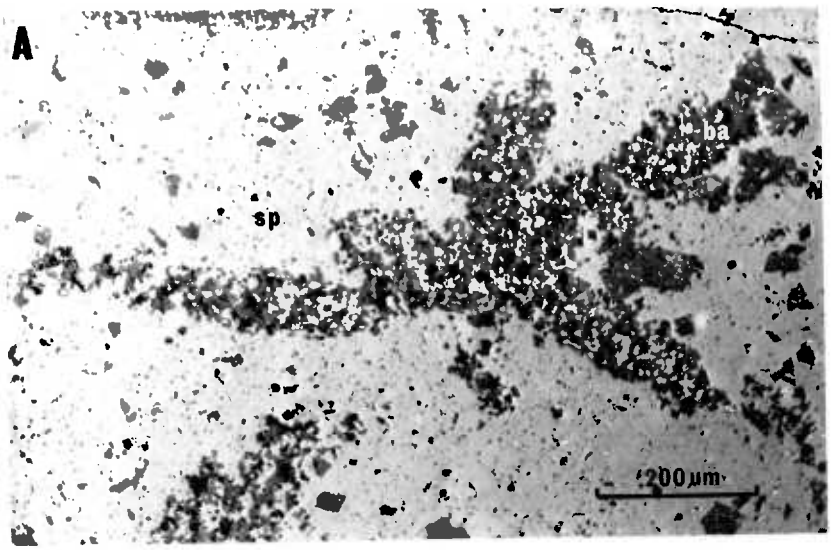

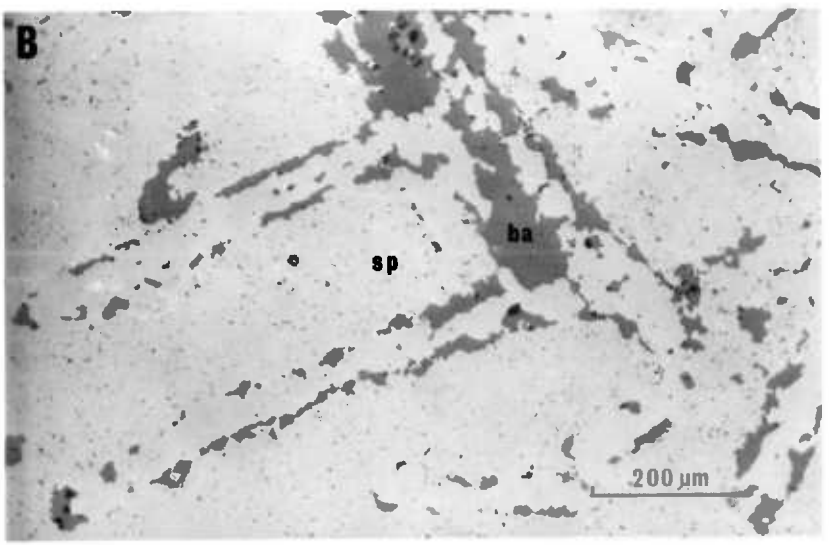

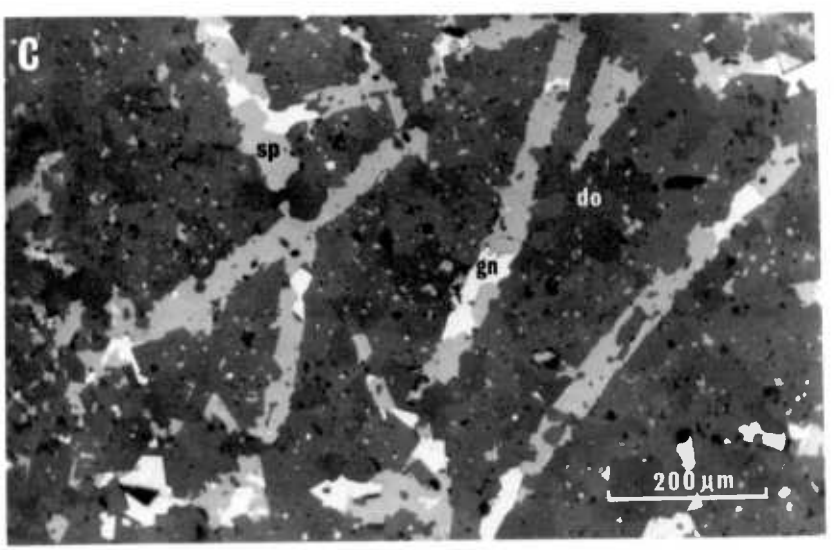

PLATE 3.14 STAGE 2 MICROTEXTURES

A) Flow textured sphalerite constricted between two micrite clasts. Minor disseminations of pyrite occur within the micrite; chalcopyrite occurs as a marginal replacement. (Reflected light).
Ty 14; 5000, 64+85W

B) Clasts of Waulsortian micrite and fine grained rosette barytes in a matrix of flow textured sphalerite. The large micrite clast has been partially replaced by disseminated sphalerite. (Reflected light).
Ty 14; 5000, 64+85W

C) Clasts of microcrystalline sphalerite with intergrown subhedral dolomite, in a finer grained matrix of sphalerite, dolomite and muscovite. (Reflected light).
Ty 14; 5000, 64+85W

PLATE 3.14

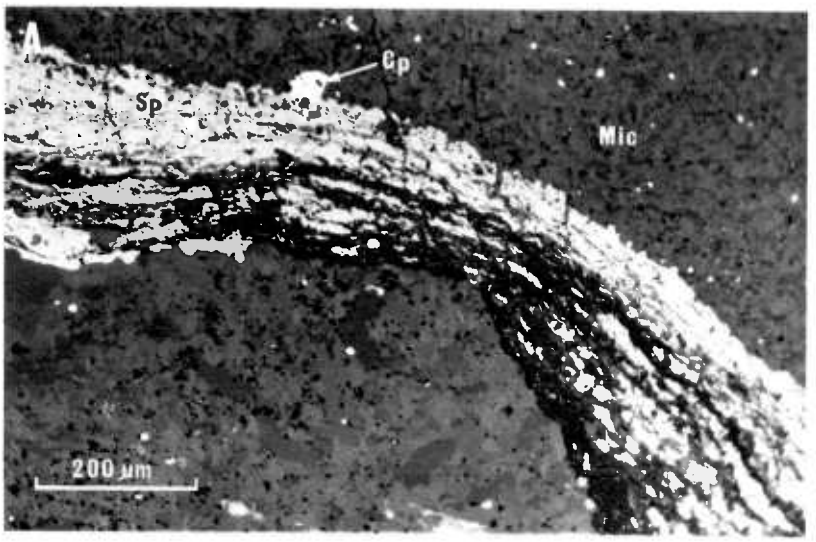

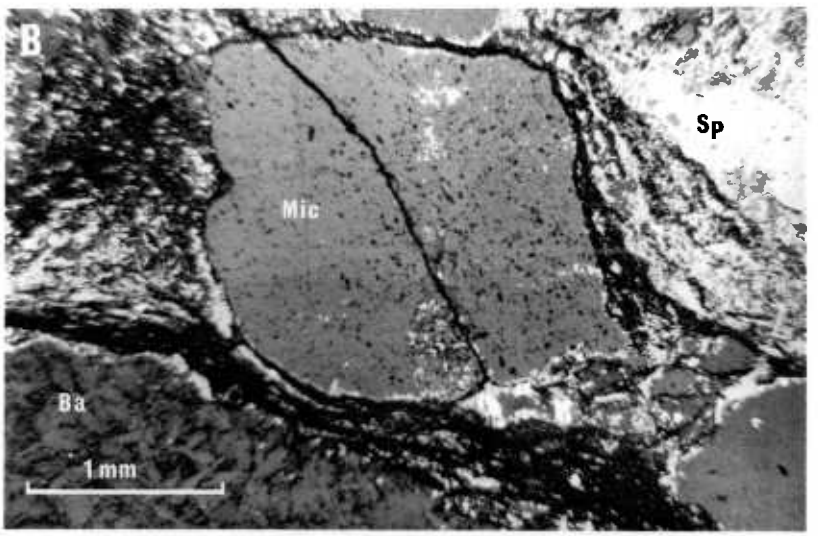

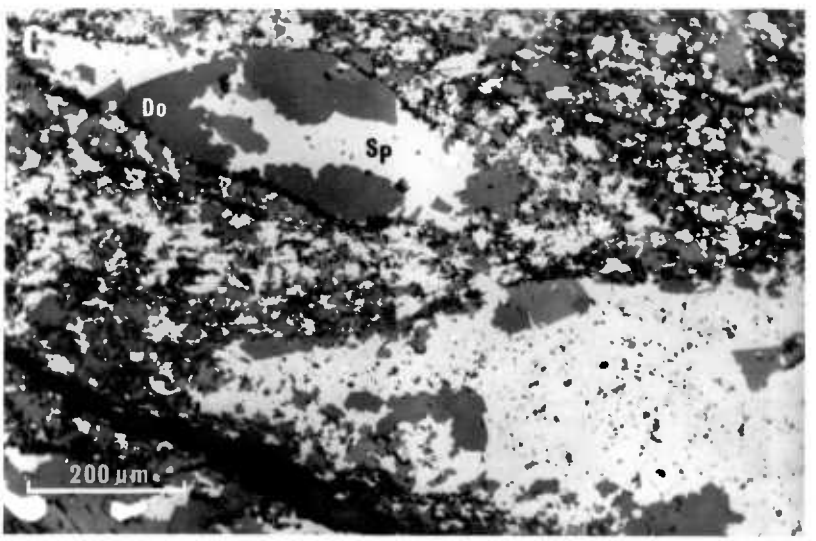

PLATE 3.15 REPLACEMENT OF STAGE 2 INTERGROWTHS

A) Relic sphalerite/dolomite intergrowth with minor disseminated pyrite, within a matrix of later tennantite.
(Reflected light)
Ty 59; 4800. 82+90W

B) Globular sphalerite with interstitial pyrite and dolomite, being replaced by galena. (Reflected light).
Ty 30 (i); 5050, 66+80W

C) Relic banded sphalerite included within coarsely crystalline galena. (Reflected light).
Ty 6 (iv); 5050, 66+10W

D) Atoll shaped inclusions of sphalerite in galena with minor intergrown tennantite. (Reflected light).
Ty 28; loose block of primary ore from residual deposit.

E) Selective replacement of colloform sphalerite by galena. Note the poor polishing qualities of the sphalerite resulting in a characteristic porous texture. Small isolated crystals of quartz included within the sphalerite.
Ty 75; 4800, 91+00W

PLATE 3.15

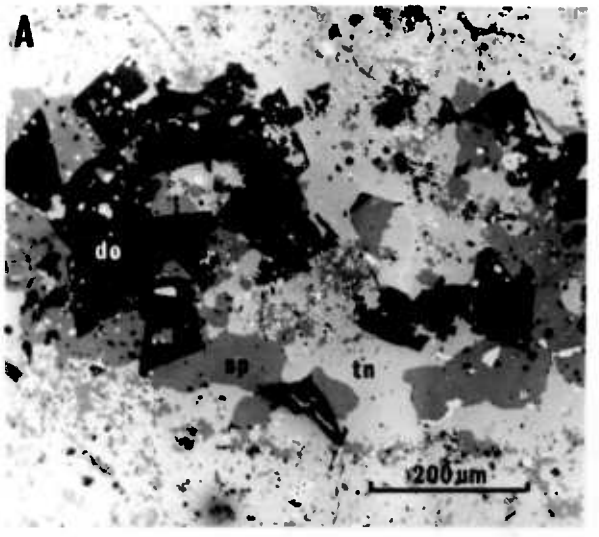
A
do
sp
tn
200µm

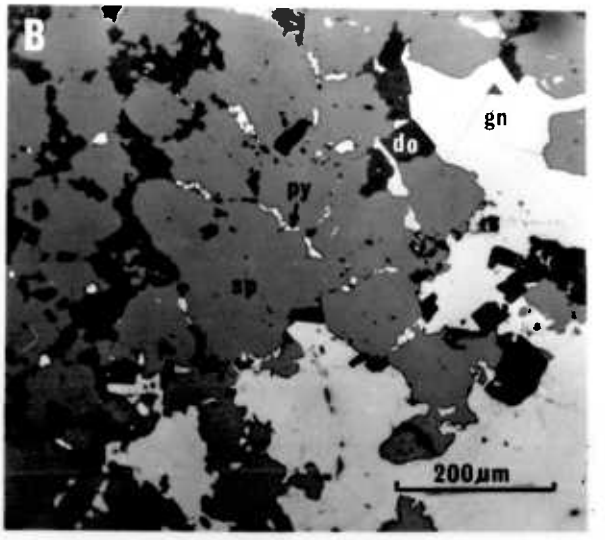
B
gn
do
py
sp
200µm

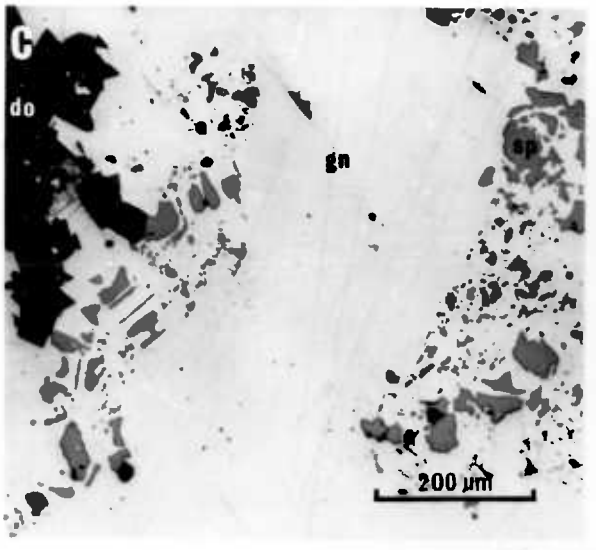
C
do
gn
sp
200 µm

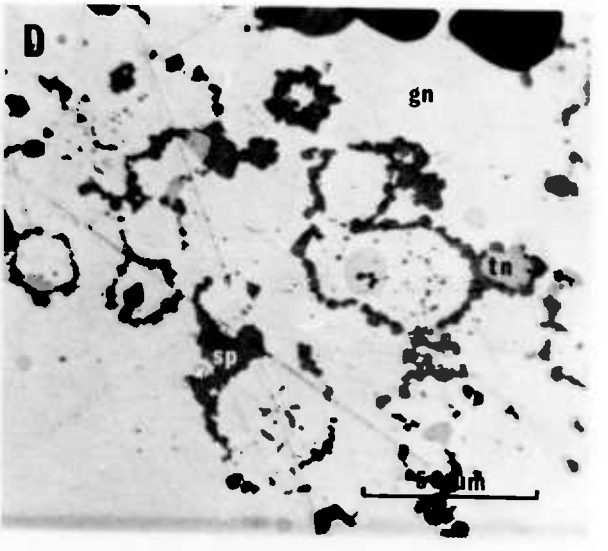
D
gn
tn
sp

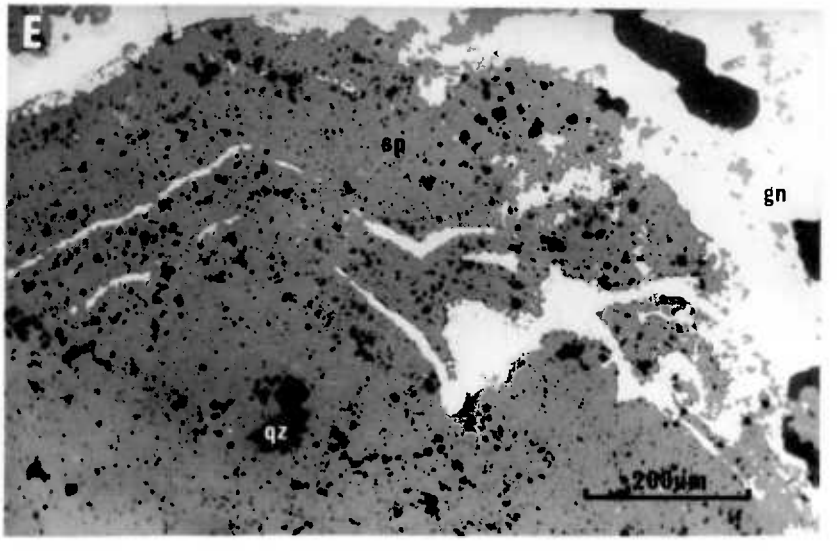
E
sp
gn
qz
200µm

PLATE 3.16 SPHALERITE RECRYSTALLISATION TEXTURES AND STAGE 3 INTERGROWTHS

A) Porous microcrystalline sphalerite [sp] recrystallising [sp(r)] at contact with later galena. (Reflected light).
Ty 30 (iii); 5050, 66+80W

B) Relic microcrystalline sphalerite [sp] intergrown with anhedral barytes, within a matrix of later galena in mutual intergrowth with recrystallised sphalerite [sp(r)] (Reflected light).
766D; 5000, 53+00W

C) Mutual intergrowth of sphalerite (recrystallised ?), tennantite, galena, bornite, chalcopyrite and barytes. (Reflected light; oil immersion).
Ty 24; loose block of primary ore from residual deposit.

D) Lobate intergrowth between sphalerite (recrystallised ?) and bornite. Minor tennantite, galena and relic pyrite. (Reflected light).
Ty 51; 4700, 90+00W

E) Oriented inclusions of bournonite in galena. (Reflected light; oil immersion).
Ty 20; 4900, 86+00W

F) Chalcopyrite blebs in sphalerite, displaying emulsion texture. (Reflected light).
Ty 57; 4700, 89+00W

PLATE 3.16

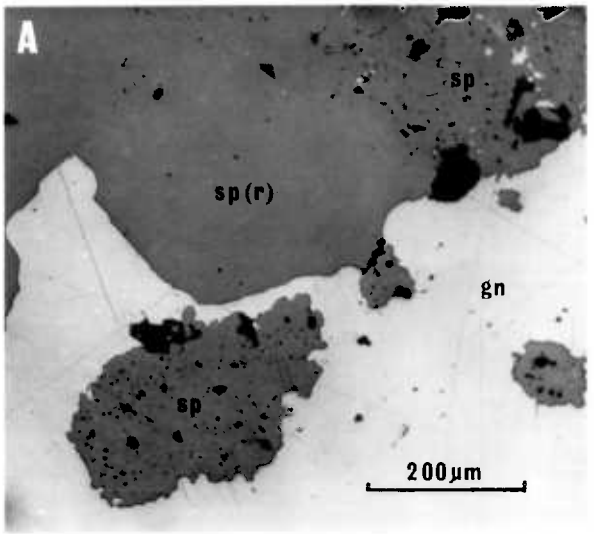
A
sp
sp(r)
gn
sp
200µm

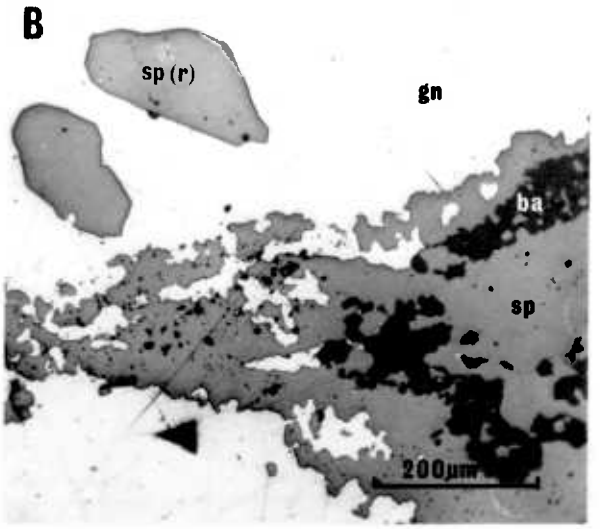
B
sp(r)
gn
ba
sp
200µm

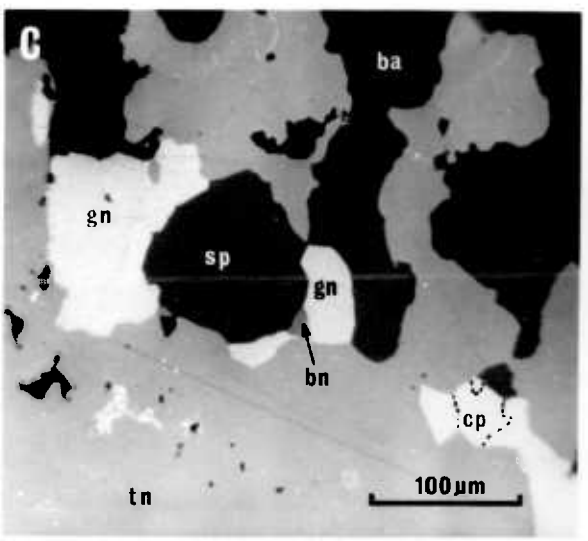
C
ba
gn
sp
gn
bn
cp
tn
100µm

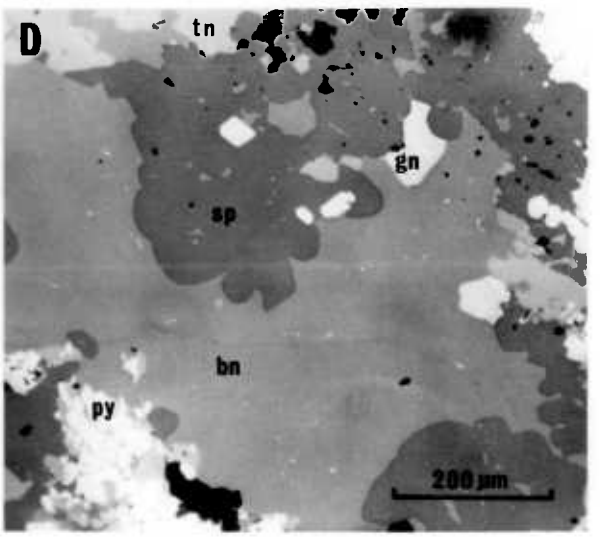
D
tn
gn
sp
bn
py
200µm

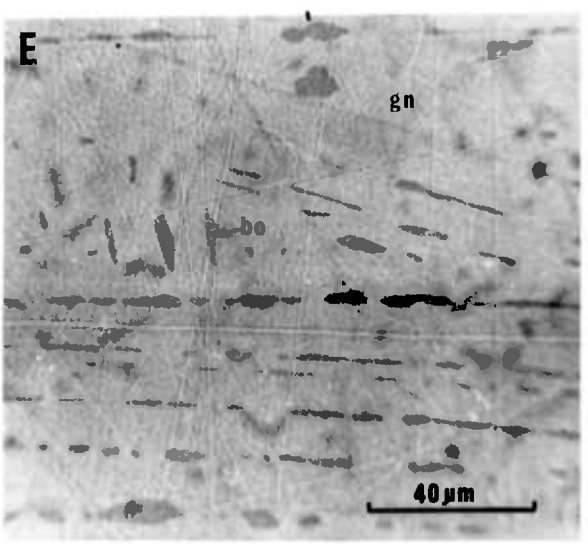
E
gn
bo
40µm

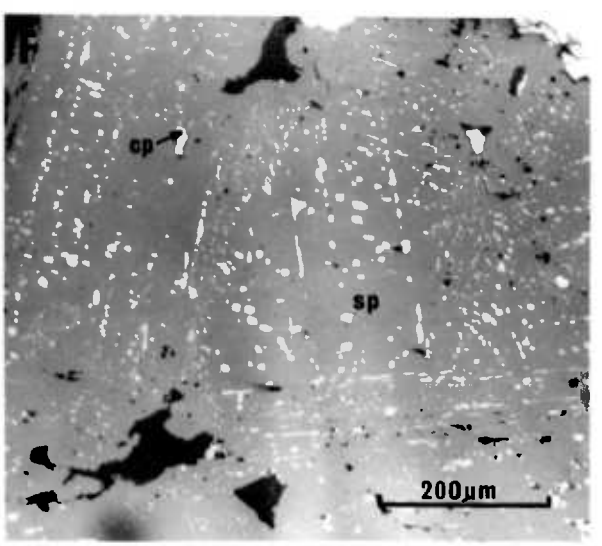
F
cp
sp
200µm

PLATE 3.17 STAGE 3 INTERGROWTHS

A) Bladed crystals of chalcopyrite overgrowing and pseudomorphing barytes. Host:- Lower Muddy Limestone. (Reflected light).
Ty 46; 4620, 88+90W

B) Replacement of chalcopyrite by tennantite. Matrix - dolomite. (Reflected light; oil immersion).
Ty 62 (ii); 4800, 78+50W

C) Arsenopyrite replacing partially recrystallised micritic limestone. (Reflected light).
Ty 77; 4900, 89+10W

D) Arsenopyrite overgrowing disseminated sphalerite. (Reflected light).
Ty 77; 4900, 89+10W

E) Broken arsenopyrite needle within a matrix of later galena. (Reflected light).
Ty 76; DDH 386 - 158 metres.

F) Arsenopyrite with small inclusions of galena, overgrown by quartz, which is in turn included within galena. (Reflected light).
Ty 76; DDH 386 - 158 metres

PLATE 3.17

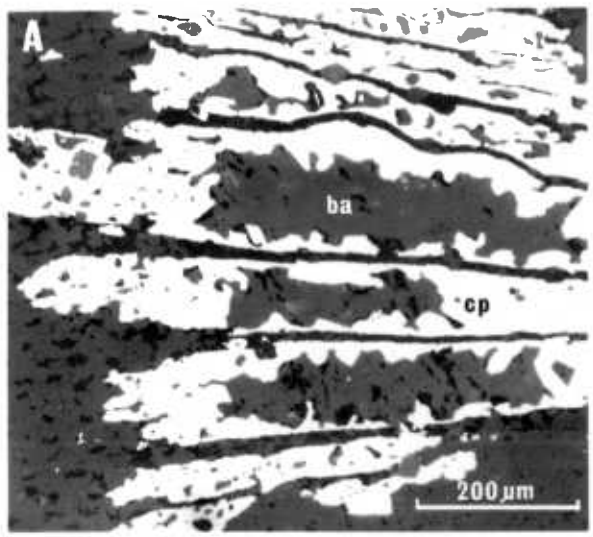
A
ba
cp
200 µm

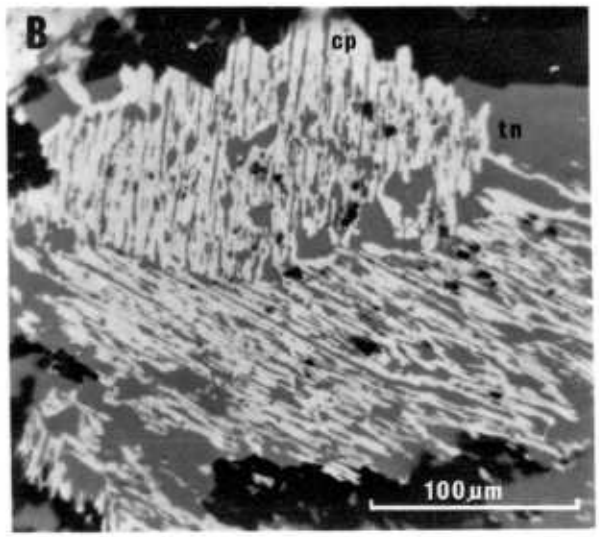
B
cp
tn
100 µm

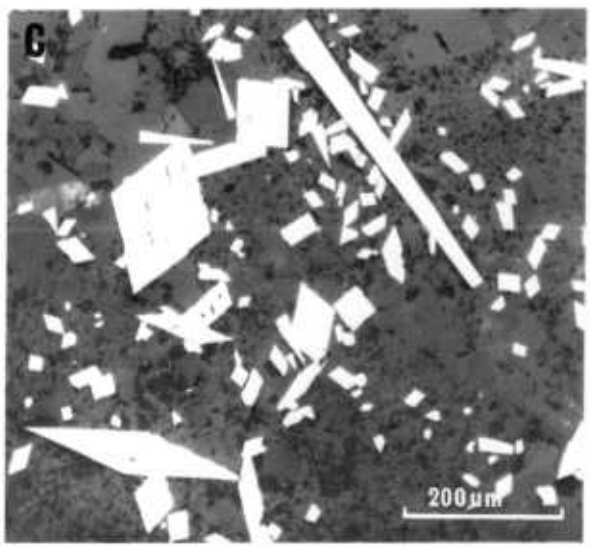
C
200 µm

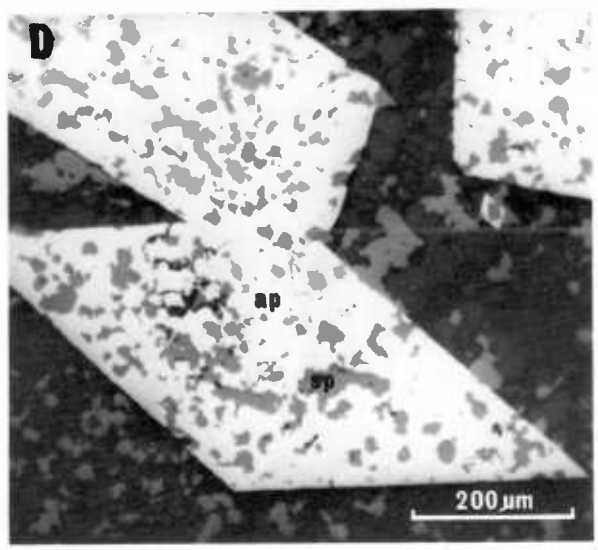
D
ap
sp
200 µm

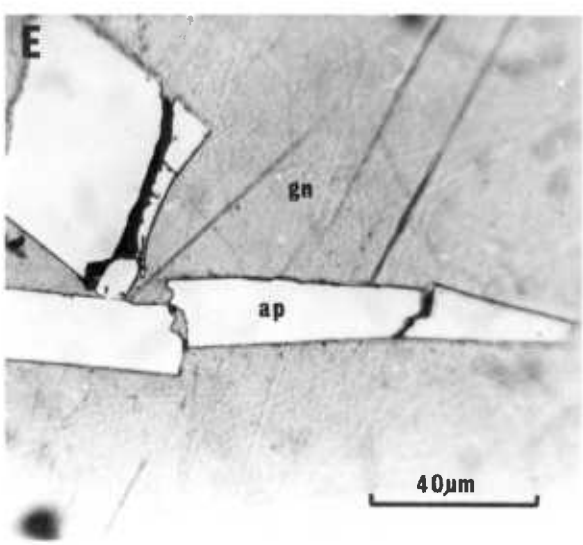
E
gn
ap
40µm

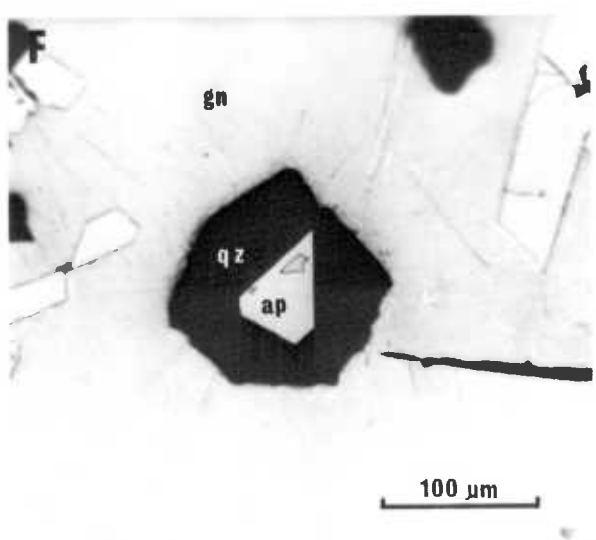
F
gn
qz
ap
100 µm

PLATE 3.18 TEXTURES ILLUSTRATING REPLACEMENT OF LOWER MUDDY LIMESTONE AND DOLOMITISATION OF WAULSORTIAN LIMESTONES

A) Unaltered crinoidal horizon from Lower Muddy Limestone. Crinoid fragments overgrown by coarse sparry calcite cement. (Transmitted light).
Ty 42; 4620, 93+20W

B) Relic crinoid fragments overgrown by calcite cement in a matrix of later microcrystalline sphalerite.
(Transmitted light).
Ty 42; 4620, 93+20W

C) Relic crinoid fragments in a matrix of later sulphides, dolomite and euhedral barytes. Marginal darkening of crinoid fragments due to alteration of calcite to ferroan calcite. (Transmitted light).
Ty 45; 4620, 86+70W

D) Crinoid ossicle in a matrix of microcrystalline sphalerite and rhombic dolomite. Core of ossicle replaced by disseminated sphalerite. (Reflected light).
Ty 45; 4620, 86+70W

E) Contact between unaltered calcitic micrite and dolomitised micrite. Contact defined by a pyrite/silicate suture zone. The crinoid fragment has proven resistance to dolomitisation. (Transmitted light).
Ty 6 (ii); 5050, 66+10W

PLATE 3.18

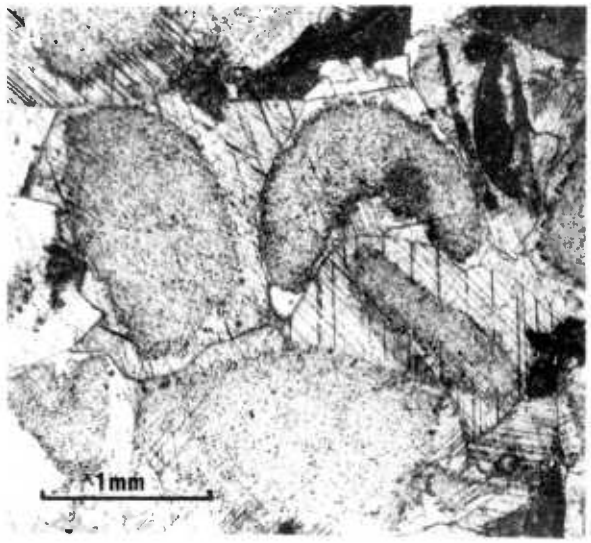

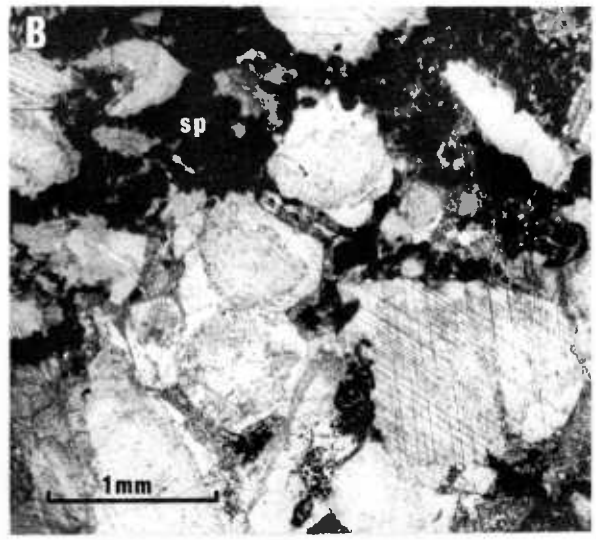

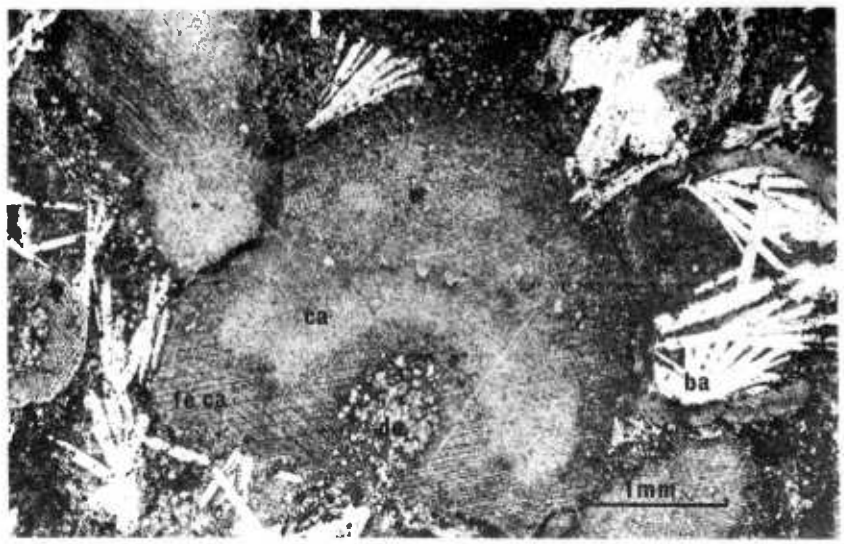

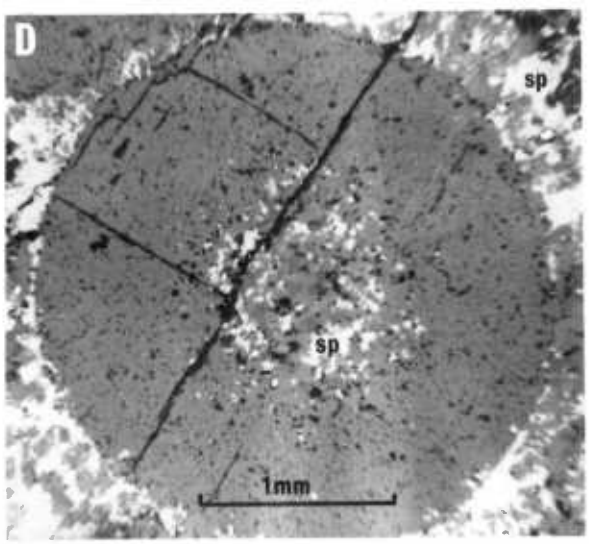

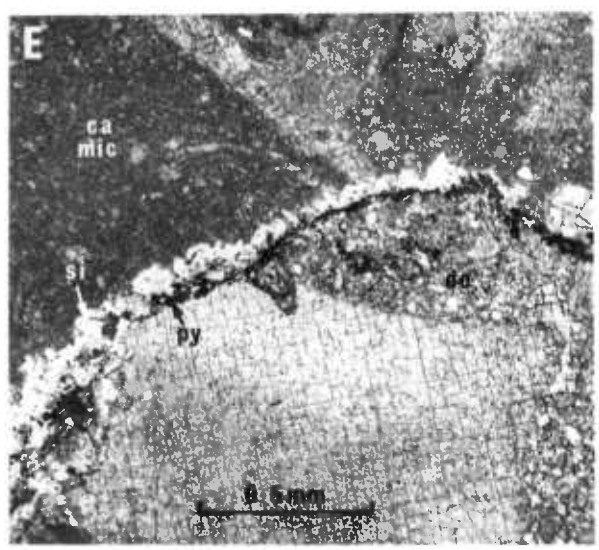

PLATE 3.19 POST-ORE DOLOMITE (STAGE 4)

Contact between 'plug' dolomite and zone III orebody. The large cavities lined with pink euhedral dolomite are devoid of sulphide infillings and irregular dolomite replacements can be seen to extend into the massive brown sphalerite to the right.

5000, 67+10W, looking west.

3.8 GENETIC SIGNIFICANCE OF THE ORE TEXTURES

3.8.1 Colloform Textures in Pyrite and Sphalerite

The term colloform was first coined by Rogers in 1917 to describe rounded, more or less spherical forms that he thought were indicative of a colloidal, gel-like stage during ore formation. However, the genetic interpretation of colloform aggregates is not unambiguous, and many workers attach no importance to the role of colloids in their formation. Roedder (1968), studied colloform textures in sphalerite from a number of deposits and revealed:- "crystal growth features that cannot have been formed by crystallisation from gels, and indicate that most, and perhaps all, grew directly as minute druses of continuously euhedral crystals projecting into an ore fluid". However, Lebedev (1967) obtained globular zinc sulphide aggregates in the laboratory from zinc sulphide gels. He suggests that the presence of granular, fibrous and radial textures is not evidence of crystalline accretion, but are the result of re-crystallisation of metastable gels, and that it is preferable to place greater emphasis on the interpretation of gross morphological features.

As the colloform and granular pyrite aggregates at Tynagh occur as isolated bodies within the Waulsortian micrites, it is difficult to envisage a situation in which crystalline accretion from a passing ore fluid could have occurred. If they had formed as a result of precipitation from fluids diffusing through the sediment, one might expect the resultant concretions to be more compact, to display greater symmetry, and to have disturbed the enclosing sediment. Crystallisation from a colloidal gel during the early diagenetic

history of the Waulsortian bank limestones seems to be the most plausible hypothesis.

The occurrence of colloform sphalerite within an interconnected fracture system at Tynagh, would allow a mechanism of formation similar to that described by Roedder to operate. Indeed, the observation of euhedral crystal faces within sphalerite globules (see 3.3.2.1) would seem to support such a mechanism. However, the morphological similarity of the aggregates of globular sphalerite observed at Tynagh to those produced by Lebedev in the laboratory prevents the total rejection of a colloidal origin.

3.8.2 Framboidal Pyrite

Pyrite framboids are a common component of many sediments, particularly shales and mudstones (Love, 1964), however, as in the case of colloform pyrite, the discussion of their origin is surrounded by controversy. Love (1957) suggested that they represented the fossilised remains of micro-organisms on the basis of the presence of an organic matrix within the spheres. Vallentyne (1963) challenged this after the discovery of numerous framboids in recent sediments that lacked an organic matrix. This was subsequently supported by Berner (1969), who successfully synthesised framboidal pyrite in the laboratory, by the reaction of FeS with elemental sulphur in saturated H_2S solution.

It is generally agreed though that pyrite framboids are of primary sedimentary origin, precipitated by bacteriogenic H_2S during diagenesis. The common occurrence of framboidal pyrite within the Lower Muddy Limestones, and more rarely in association with colloform pyrite within the Waulsortian micrites is, therefore, strongly suggestive of the existence of anaerobic conditions during the

diagenesis of the carbonate sequence at Tynagh.

3.8.3 The Dilatant Fracture/Breccia System - The Creation of Space

The location of the Tynagh orebody against a major fault suggests that the fault was a controlling factor in ore formation. One important role that the fault could have taken is in the creation of space for the precipitation of the stage 2 intergrowths. Halls (1975) proposed a syndiagenetic model for Irish mineralization, involving the injection of mineralizing fluids into unlithified Waulsortian mudbanks whose internal cavity geometries had been modified by fault tectonism. Tectonic activity in league with hydraulic fracturing seems a highly plausible mechanism for formation of the dilatant fracture/breccia system.

Phillips (1972) explained normal fault located mineralized breccia zones in Cardiganshire as being a direct result of hydraulic fracturing. He suggests that low density hydrothermal solutions build up on the fault plane and set up a pressure gradient between the solution at the top of the fault and the pore water in the adjacent rocks. Permeation of the hydrothermal solution into the pore spaces of the adjacent rock results in the decrease of the effective principal stresses in the rocks at the top of the fracture, and the fault extends by hydraulic fracturing. The abrupt decrease in the pressure of the hydrothermal solution when fracturing occurs causes the bursting apart of the rock into which the hydrothermal solution has permeated to form angular breccias. Furthermore, he suggests that the preferential location of these breccias in the hangingwall (c.f. Tynagh) is a result of preferential upward movement of the fluids due to their low density.

Certain textural features of ores formed in such a way are consistent with those observed at Tynagh. Phillips describes the breccias as being characterized by extremely angular fragments which are generally not in contact (see 3.3.1), and states that, as solutions enter, the brecciated area might become a fluidized sheet. Although coarsely crystalline quartz and sulphides form the matrix to the Cardiganshire breccias, the flow textured sulphides forming the matrix to the breccias at Tynagh may be a "fossilised" expression of such a fluidized zone. The dilatant fracture system may be representative of areas where the effects of hydraulic fracturing were less intense, moreover, the presence of fluids under pressure would have maintained such a system which under conditions of normal lithostatic load would not have been possible. Within the Lower Muddy Limestones bedding surfaces, a feature rarely developed in the Waulsortian limestones, may have acted as planes of weakness. Injection of high pressure fluids along these surfaces could explain the pseudo-stratiform appearance of the mineralization within this sequence. The presence of distinct bands of sulphides within the dilatant fractures is suggestive of a pulsatory or episodic precipitation from, and/or introduction of, ore fluids into the system. The latter would clearly be consistent with a mechanism involving periodic build up and release of stress. Tectonism resulting in the disruption and fluidization of semi-consolidated sulphide muds was clearly prevalent during the precipitation of stage 2 sulphides, being manifested in the form of highly disrupted and folded banding, micro-faulting, mud volcanoes and flow banding. Again tectonic activity was probably responsible for the periodic detachment of fragments of the host from the walls of the fracture system, to be incorporated as clasts within the banded sulphide

sequences.

An indication as to the minimum depth at which the fracture system developed may be gained from a study of the diagenetic state of the host micrite prior to dilatancy. It was maintained in section 3.3.1 that stylolite development within the host pre-dates the formation of the dilatant fractures. Stylolites have been found in limestones that cannot have been buried under an overburden greater than about 90 metres (Schlanger, 1964). Unfortunately, the formation of stylolites is not solely dependent on the magnitude of directed stress. The problem is complicated by the influence of other variables such as the nature of the pore fluid, porosity, permeability, surface area of pore walls, rates of fluid flow, temperature and the concentration of clay in the rock (Bathurst, 1971). However, the occasional occurrence of breccias showing evidence of soft sediment deformation of the host during mineralization, does suggest that mineralization extended at least to the sediment/rock interface.

3.8.4 Rates and Possible Mechanisms of Precipitation of Stage 2 Intergrowths

The extremely fine grained and irregular nature of the stage 2 sulphide/carbonate intergrowths infilling the dilatant fracture/breccia system is highly indicative of their rapid precipitation. The establishment of numerous crystal nuclei would have led to rapid precipitation, which in turn prevented the attainment of textural equilibrium between coeval phases. Relatively slower rates of deposition would have favoured the establishment of more extensive crystal growth surfaces which, by a process of sequential accretion, could have led to the formation of larger, possibly euhedral crystals

projecting into the ore fluid. The presence of sphalerite displaying metacolloid textures provides further support for this hypothesis. Roedder (1968) suggests that the maintenance of the large number of crystal nuclei responsible for colloform textures in sphalerite is attributed to relatively high supersaturation and hence relatively high nucleation and growth rates. Rapid rates of precipitation may also explain the occurrence of Ni, Co and As bearing phases (namely siegenite and gersdorffite) within these intergrowths. Anderson (1975) in consideration of unusual mineral assemblages (including Ni and As bearing sulphides) in mines of the New Lead belt in S.E. Missouri, suggested that under conditions of rapid "dumping", metals present in small amounts may be precipitated which under conditions of slower precipitation would pass through the ore zone without precipitating.

Solubility data for galena and sphalerite in NaCl brines at 100°C, indicate that if lead, zinc and reduced sulphur are transported together to the site of deposition, the solution must be quite acid (Anderson, 1973, 1975; Hamann and Anderson, 1978). If calcite and dolomite can be demonstrated to have been co-precipitated with sphalerite and/or galena such acid conditions are ruled out, and the only reasonable precipitation mechanism is addition of reduced sulphur to the metal bearing brine (Anderson, 1975; Beales, 1975). Similarly, if chalcopyrite is stable during deposition of galena, sphalerite and carbonates, increase in reduced sulphur is called for (Anderson, 1975).

Dolomite and lesser amounts of chalcopyrite were clearly stable during the deposition of the banded sulphides at Tynagh, and there is little evidence of dissolution of the host limestone. It

therefore seems highly improbable that stage 2 mineralizing fluids were of an acid nature. Taking the above discussion into consideration the transport of reduced sulphur along with the metals to the site of ore deposition does not seem to be a very plausible theory. Unfortunately, the lack of information as to the temperature at which mineralization occurred prevents the total rejection of this hypothesis. However, Anderson's extrapolation of the solubility values to higher temperatures indicates that none of his conclusions will be changed up to at least 150°C. A mechanism for rapid precipitation involving the mixing of two solutions, one rich in base metals and the other rich in reduced sulphur resulting in a relatively high degree of supersaturation, therefore seems possible.

3.8.5 Emulsion Textures

It has been considered that the presence or absence of chalcopyrite bodies within sphalerite can be used as a geothermometer. Buerger (1934) found that they are capable of some degree of solid solution at temperatures of 350 to 400°C, solutions of chalcopyrite in sphalerite unmixing at about these temperatures. However, many high temperature sphalerites contain no such bodies despite the presence of abundant chalcopyrite, and other low temperature sphalerites contain numerous exsolved blebs of chalcopyrite (see Ramdohr, 1969). The occurrence of sphalerite exhibiting emulsion textures in association with stage 3 intergrowths cannot, therefore, be used as a reliable indication of the temperature of deposition. Indeed, Ramdohr points out that similar exsolution textures can be produced by tectonic pressure, a hypothesis which would be consistent with the restriction of these intergrowths to the Tynagh fault zone.

3.8.6 Textural Variation with Time

The transition from Fe and Zn dominated mineralization during stages 1 and 2, to the later precipitation of Cu, Pb, As and Ba rich phases raises important questions as to the controlling factors influencing such changes, questions which are difficult to answer without reference to corroborative geochemical data. Is this transition reflecting the evolution of the source region, the influence of a completely separate source for the metal bearing solutions, or is it the manifestation of changing physico-chemical conditions within the ore fluid ? Replacement and alteration of the host rocks during sulphide mineralization appears to have been more prevalent during stage 3, and relatively slower crystallisation (and higher temperatures ?) may have aided the attainment of greater textural equilibrium. Changing conditions within the mineralizing fluids, therefore, do appear to have played a role. However, the contrast in style of mineralization may simply be a result of the continued evolution of the host. It has been argued above that pyrite was precipitated as a colloid or gel within an unconsolidated sediment, and that later sphalerite mineralization occurred after the host had been buried to fairly shallow depths and had achieved a state of lithification where it would remain coherent on brecciation. Obviously in a regime of continuing sedimentation, subsequent mineralizing events will be emplaced into a host which will be at ever increasing depths and will display features more characteristic of an epigenetic deposit. It is suggested, therefore, that changes in the style of mineralization with time at Tynagh, is a reflection of the lithification state of the host, and the depth to which it had been buried.

CHAPTER 4

AN OUTLINE OF THE GEOLOGY AND METALLOGENY OF THE NAVAN AND SILVERMINES DEPOSITS

4.1 NAVAN

4.1.1 Introduction

The Navan stratabound Zn-Pb orebody occurs within a succession of Tournaisian carbonates, sandstones, siltstones and shales along the southern margin of the Longford-Down massif. The deposit is currently being worked by Tara Mines Limited, whose reserves exceed 67 million tons with an average grade of 11.0% Zn and 2.4% Pb.* An updip extension is being developed by Bula, whose proven reserves are 15 million tons at 9.2% Pb-Zn, plus additional probable reserves estimated at 6.6 million tons with a grade of 5.2% Pb-Zn.*

4.1.2 Local Stratigraphic Setting

The basal Carboniferous in the Navan area marks a transition from terrestrial sandstones and conglomerates into shallow water finely banded, grey argillites and siltstones that display abundant evidence of bioturbation (Laminated Beds). These are in turn overlain by a succession of dark grey argillites and bioclastic limestones (Muddy Limestone) that are lithologically comparable with the Lower Limestones at Tynagh. Crinoid and brachiopod debris dominates the bioclastic horizons; however beds comprised entirely of fragmented Syringopora Sp. corals have been noted. Soft sediment slumping during the deposition of the Muddy Limestones is indicated by the presence of rounded and contorted clasts of pale grey calciferous

* Source - Mining International Year Book, 1978.

siltstone within the dark argillitic matrix.

The mineralization is entirely hosted within a 30 to 150 metre thick sequence of limestones and dolomites (Pale Beds) which succeed the Muddy Limestones. The limestones are pale grey in colour and are silty, arenaceous or bioclastic in parts. Dolomitisation is spatially related to the mineralization, occurring as a darkened, irregular envelope, that thickens and thins in conjunction with the orebody (Byrne et al, 1971).

The Tournaisian-Visean boundary is defined by a marked unconformity, on the surface of which rests a conglomerate horizon containing boulders of mineralized limestones (D.Downing, pers. comm.). A series of thin limestones and intercalated black shales (Upper Dark Limestone ≡ Calp), cap the Lower Carboniferous succession.

4.1.3 Structure

The host sediments dip to the south west at an angle of approximately 20^{o}, and are cut by a north east trending reversed fault ('A' fault) which has a throw of about 75 metres. Two approximately E - W trending branch faults ('B' and 'C' faults) have normal displacements and are terminated at the Tournaisian-Visean unconformity (fig. 4.1).

4.1.4 Style and Paragenesis of Mineralization

The mineralization varies from being massive to fairly disseminated, and occurs as a series of stacked lenses which parallel the dip of the host and which are displaced by pre-Visean faulting. Maximum mineral development is to the N.E. where the lenses merge into a continuous vertical thickness in excess of 60 metres.

FIG. 4.1 GENERALISED GEOLOGICAL SECTION THROUGH NAVAN DEPOSIT. (By permission of Tara Mines Ltd.)

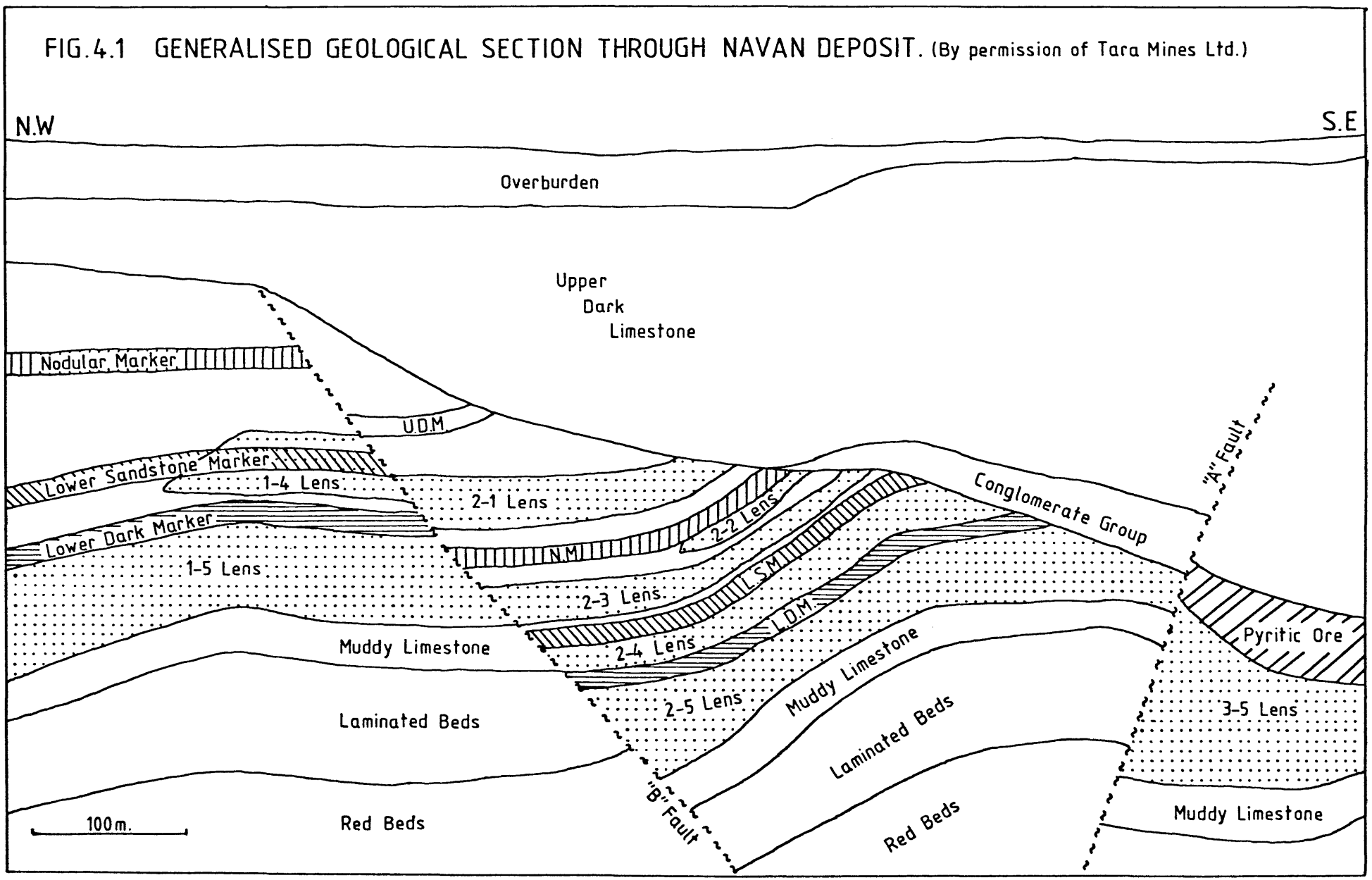

Sphalerite with lesser quantities of galena dominates the sulphide assemblage. The sphalerite is microcrystalline, pale orange-brown in colour and, together with intercalated galena and barytes horizons, often displays fine banding that parallels the bedding of the enclosing host (fig. 4.2A). Horizontal stylolites cross cut the sulphide banding, and intraformational slump breccias point to the disruption of the fine grained sulphides soon after their deposition (Pl.4.1). A spectacular feature of these banded sequences is the occurrence of horizons comprised entirely of dendritic galena and sphalerite (fig. 4.2A). The dendrites are generally oriented perpendicular to banding, and individual crystals can be several cms. in length. These are often interpreted as indicating rapid precipitation and have been reproduced experimentally. Leleu and Goni (1974) precipitated dendritic galena from aqueous lead chloride by supplying bacteriogenic H_2S to the solution. This does not necessarily imply that the Navan dendrites were precipitated by bacterially reduced sulphate. Nevertheless, it is of interest that pyrobitumens, which could be the remnants of an organic substrate, were observed as late stage cavity infillings (fig. 4.2B) within the specimen illustrated in fig. 4.2A.

Microscopic examination reveals a variety of colloform textures within the sulphide intergrowths. Sphalerite often forms concentrically banded, hemispherical masses, in which the banding is picked out by variations in both colour and opacity. These structures are frequently brecciated and overgrown by later generations of similar colloform sphalerite, or cemented by paler and more coarsely crystalline sphalerite (Pl.4.2A,B). A second type of metacolloid structure has cores of dendritic galena, which are often overgrown

FIG.4.2 MASSIVE BANDED AND DENDRITIC SPHALERITE - NAVAN.

A)

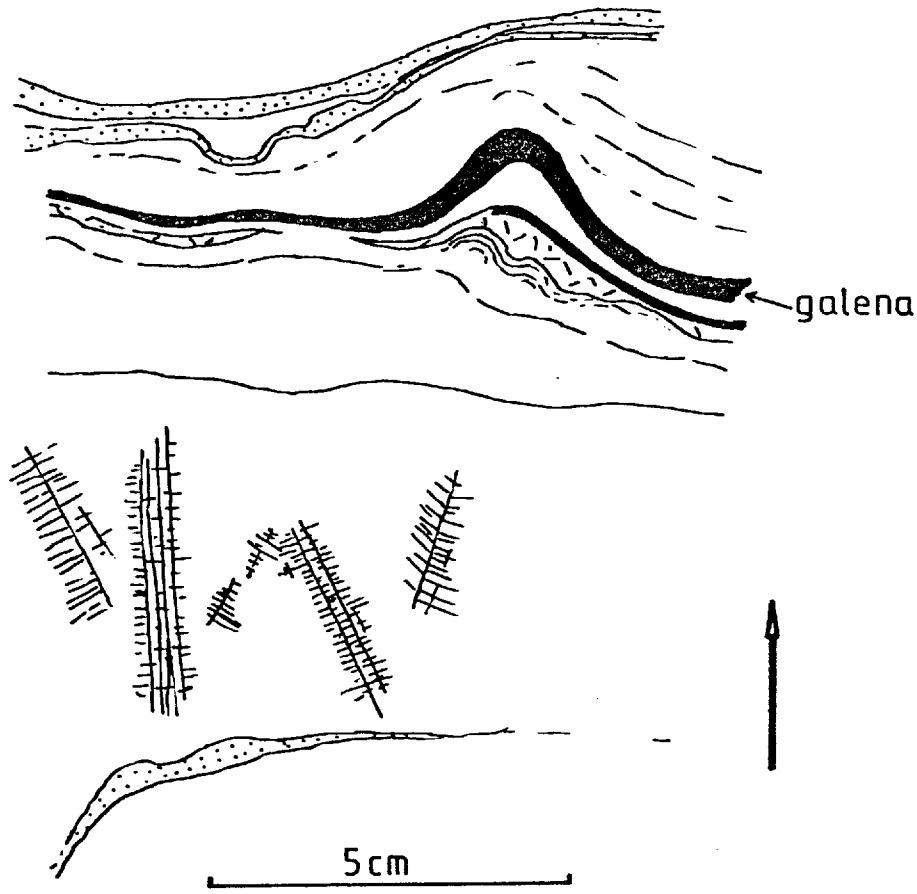

B)

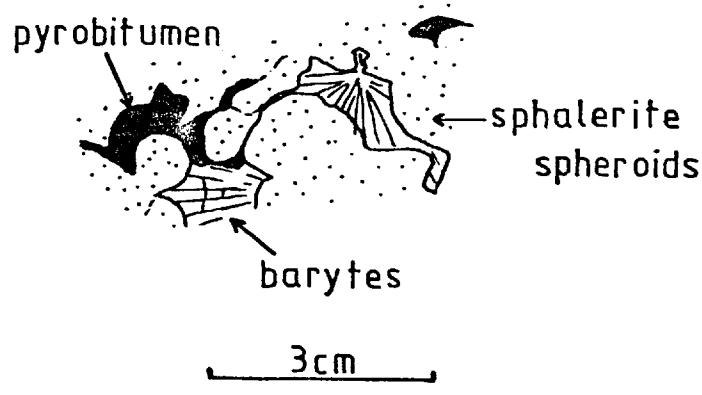

PLATE 4.1 SLUMPED SULPHIDES - NAVAN

Slump structures in banded sequence of microcrystalline sphalerite and galena. Brecciated fragments in centre of specimen cemented by an intergrowth of microcrystalline sphalerite and fine grained euhedral barytes.

N8; TARA 2 - 1 lens, 812.0 NW, 503.9 NE, 1378 El.

5 cm

PLATE 4.1

PLATE 4.2 ORE TEXTURES - NAVAN

A) Colloform sphalerite overgrown by paler, coarsely crystalline sphalerite (white). Note termination of colloform banding by later generations. (Transmitted light).
N4; TARA 2-5 lens, 841.7 N.W., 495.2 N.E., 1375 Elev.

B) Colloform sphalerite. (Transmitted light).
N4; TARA 2-5 lens, 841.7 N.W., 495.2 N.E., 1375 Elev.

C) Dendritic galena overgrown in turn by barytes and colloform sphalerite. Interstices occupied by acicular barytes and pale crystalline sphalerite. (Transmitted light).
N12; TARA 2-4 lens, 822.5 N.W., 498.0 N.E., 1348 Elev.

D) Bladed euhedral barytes intergrown within a calcerous and dolomitic arenite. (Transmitted light; + Nicols).
N12; TARA 2-4 lens, 822.5 N.W., 498.0 N.E., 1348 Elev.

E) Dendritic galena, overgrown by barytes and colloform sphalerite. (Reflected light).
N6; TARA 2-5 lens, 826.5 N.W., 493.8 N.E., 1350 Elev.

PLATE 4.2

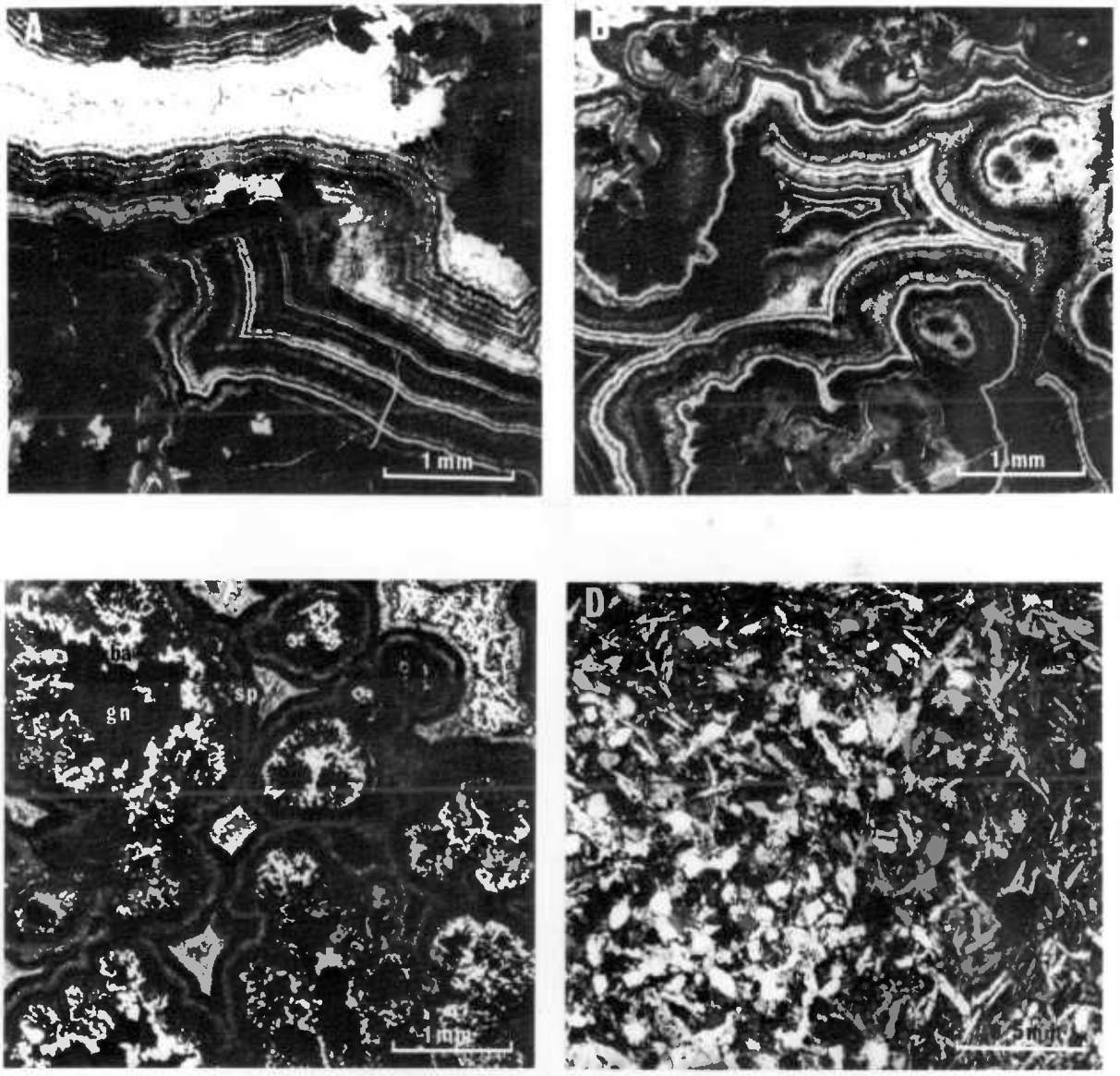

by a narrow rim of barytes, and in turn enclosed by colloform sphalerite. Small cavities between these structures are usually lined by a drusy overgrowth of sphalerite crystals, and infilled by later generations of barytes and calcite (Pl.4.2C,E).

Careful observation reveals that galena invariably has inclusions of jordanite ($27PbS.7As_2S_3$) within it, usually occurring as oriented acicular crystals <20 μm in length, or as lamellae. Larger anhedra up to 500 μm in size are more rarely observed.

As at Tynagh, iron sulphides are a minor component of the sulphide assemblage. However, at the top of the ore section, pyrite forms a cap up to 12 metres thick. Generally though, pyrite and marcasite occur as minor brecciated and replaced fragments within a matrix of sphalerite. Scattered framboids have occasionally been observed enclosed within microcrystalline sphalerite and the host sediments.

As well as occurring as thin bands and cavity infillings within the sulphide sequences, barytes has been observed as disseminations within the enclosing host. In one particular example acicular crystals of barytes up to 250 μm in length occur dispersed within a calciferous arenite that encloses isolated colloform sphalerite structures. The arenite consists of well sorted, sub-angular to rounded particles of quartz, plagioclase , microcline and muscovite, 100 to 150 μm in size, cemented by a matrix of anhedral and rhombic carbonate. The barytes euhedra display a random orientation which suggests that they grew within the sediment after its deposition (Pl.4.2D).

Co-precipitated silicates and carbonates are a minor component of the massive sulphide intergrowths, quartz and dolomite occurring

as scattered, isolated euhedra, $\leqslant 300$ µm in size. The occurrence of brecciated fragments of banded sulphide enclosed within an undisturbed mosaic of 150 µm sized euhedral dolomite crystals, indicates that, at least locally, crystallisation of the enclosing dolomite must have taken place after deposition of the sulphides.

In conclusion, the displacement of the ore lenses by pre-Visean faulting, and the occurrence of mineralized boulders along the Tournaisian-Visean unconformity, clearly indicates a Tournaisian age for mineralization at Navan. Additionally, the conformable attitude of the ore lenses to the enclosing host and the abundance of geopetal textures would support a synsedimentary mode of deposition. The occurrence of a dolomitised envelope around the orebody could suggest a post-sedimentation age for mineralization. However, this may be the product of interaction between the host and fluids expelled from the sulphide sequences during their diagenesis.

4.2 SILVERMINES

4.2.1 Introduction

In the vicinity of the village of Silvermines, County Tipperary, scattered Pb, Zn, Cu, Ag, Ba mineralization occurs in a belt approximately 4 km. in length, close to the line of a major fault which downthrows Lower Carboniferous limestones to the north of Devonian sandstones. The bulk of the mineralization occurs as a number of conformable stratiform bodies (Mogul's Upper G and B zones, Magcobar's barytes deposit) at a single stratigraphic horizon within an Upper Tournaisian limestone sequence. Two smaller discordant bodies (Mogul's Lower G and K zones), also hosted within

Tournaisian limestones, are located against, and parallel to the Silvermines fault (fig. 4.3). Together these deposits constitute an orebody comparable in size to that at Tynagh:

Deposit	Million tons	% Zn	% Pb	oz/ton Ag	Source
Upper G	9.3	9.2	2.4	0.7	Graham (1970)
Lower G	2.1	3.4	4.5	1.1	" "
B zone	2.0	6.0	4.0	1.0	" "
K zone	0.5	6.5	1.0	0.5	" "
Magcobar	4.0	85-95% $BaSO_4$			Barrett (1975)

Minor disseminations, veinlets and fault breccias within O.R.S. facies Devonian sandstones were mined until 1958.

The Silvermines deposits have been the subject of a number of geological studies in the past (Rhoden, 1958; Graham, 1970; Fillion, 1973; Barrett, 1975), which have been freely drawn upon in the discussion below.

4.2.2 Local Stratigraphic Setting

The stratiform sulphide/barytes orebodies conformably overlie a succession of thinly bedded, dark crinoidal limestones and shales (Muddy Limestone and Muddy "Reef" Limestone). These sediments are lithologically comparable with the Tynagh Lower Limestones and were probably deposited in a similar lagoonal environment. The lower half of this sequence has been dolomitised and is the host rock of the Lower G zone mineralization. Waulsortian facies limestones see their expression as the Dolomite Breccia which comprises the hanging-wall succession to the stratiform bodies. This sequence is extremely variable in lateral extent and horizons of brecciation intercalate with massive dolomites and bank limestones. The dolomitisation and

FIG.4.3 GEOLOGICAL SECTION THROUGH G ZONE - SILVERMINES. (Simplified from Fillion, 1973)

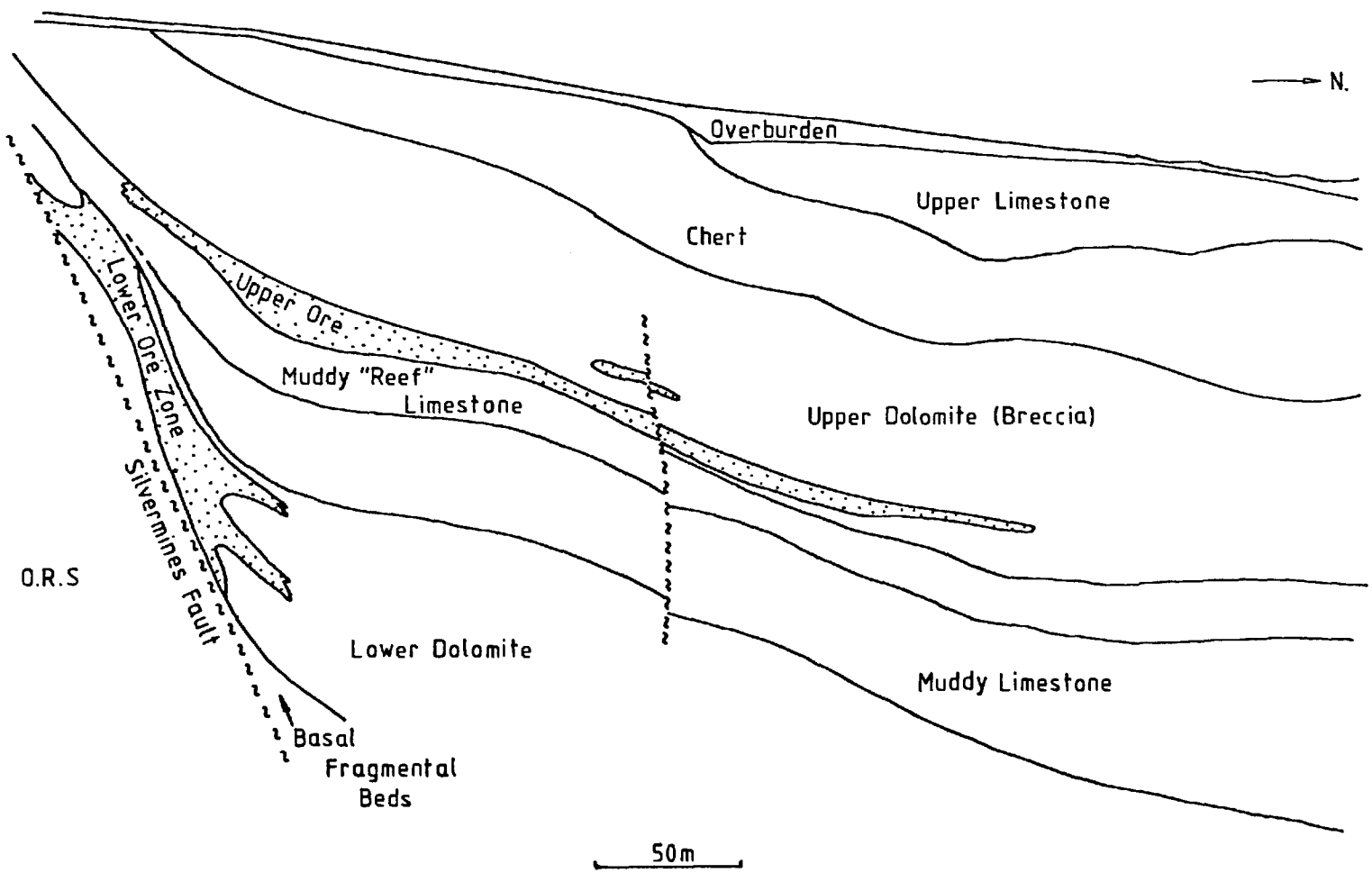

brecciation of the carbonate mud banks lessens considerably to the north of the Silvermines orebodies (Fillion, 1973). Graham (1970) interpreted the brecciation as being the product of soft sediment slumping induced by fault tectonism.

4.2.3 Structure

The Devonian and Lower Carboniferous strata are folded into a broad syncline between the Lower Palaeozoic inliers of the Silvermines Mountains to the south, and the Arra Mountains to the north. Except for those disturbed by faulting, beds along the southern limb strike E - W and have a maximum dip of 20°N. The major structural feature is undoubtedly the E.N.E. - W.S.W. trending Silvermines fault, which has a normal displacement of approximately 200 metres in the mine area, and which can be traced along strike for about 40 km.

4.2.4 Style and Paragenesis of Mineralization

The mineralogy of the Silvermines sulphide orebodies is similar to that of the Tynagh deposit, the economic sulphides being sphalerite and galena. However, unlike Tynagh, iron sulphides are a major component of the mineral assemblage, especially in the Upper G zone where pyrite forms an impressive massive horizon. Minor and trace sulphides include tennantite, tetrahedrite, chalcopyrite, arsenopyrite and bournonite.

The stratiform sulphides are generally fine grained, display a wide variety of colloform and framboidal textures, and exhibit abundant evidence of brecciation during various stages of consolidation. Likewise the massive barytes deposit is finely crystalline, and in its western part is capped by a pyritic horizon which occupies depressions in its upper surface. The mineralization within the

Lower G zone, however, is relatively coarsely crystalline, and occurs as fracture infillings, disseminations and replacements.

The consensus of opinion is that the stratiform pyritic and barytic bodies are synsedimentary and that local disruption and slumping occurred in response to tectonic activity along the Silvermines fault. The discordant ore zones have been interpreted as both an epigenetic stockwork to the stratiform mineralization, and as a recrystallised and remobilised synsedimentary deposit.

Opinion is divided as to the relative ages of economic sulphide mineralization and pyrite/barytes deposition. Graham (1970) found the mineral paragenesis within the Upper G zone to be repetitive and inconsistent, and concluded that the ore sulphides were precipitated along with pyrite. Fillion (1973) and Barrett (1975) considered that deposition of the stratiform pyrite and barytes preceded the precipitation of Pb, Zn and Cu sulphides. Indeed occurrences of coarsely crystalline galena that appear to be replacing massive pyrite, are not uncommon within the B and Upper G zones. However, the presence of conformable horizons of micro-crystalline sphalerite and galena within the shaley footwall sequence, that have undergone soft sediment deformation along with their host, is in clear support of a synsedimentary age for at least a part of the Pb-Zn mineralization (fig. 4.4).

4.3 MAJOR SIMILARITIES AND DISSIMILARITIES OF THE NAVAN, SILVERMINES AND TYNAGH DEPOSITS

(i) The most obvious difference between Navan and the other major base metal deposits is one of size, Navan being 5 or 6 times larger than Tynagh and Silvermines.

FIG.4.4 STRATIFORM SULPHIDES IN FOOTWALL MUDDY "REEF" LIMESTONE – MOGUL B ZONE, 4931 HAULAGE.

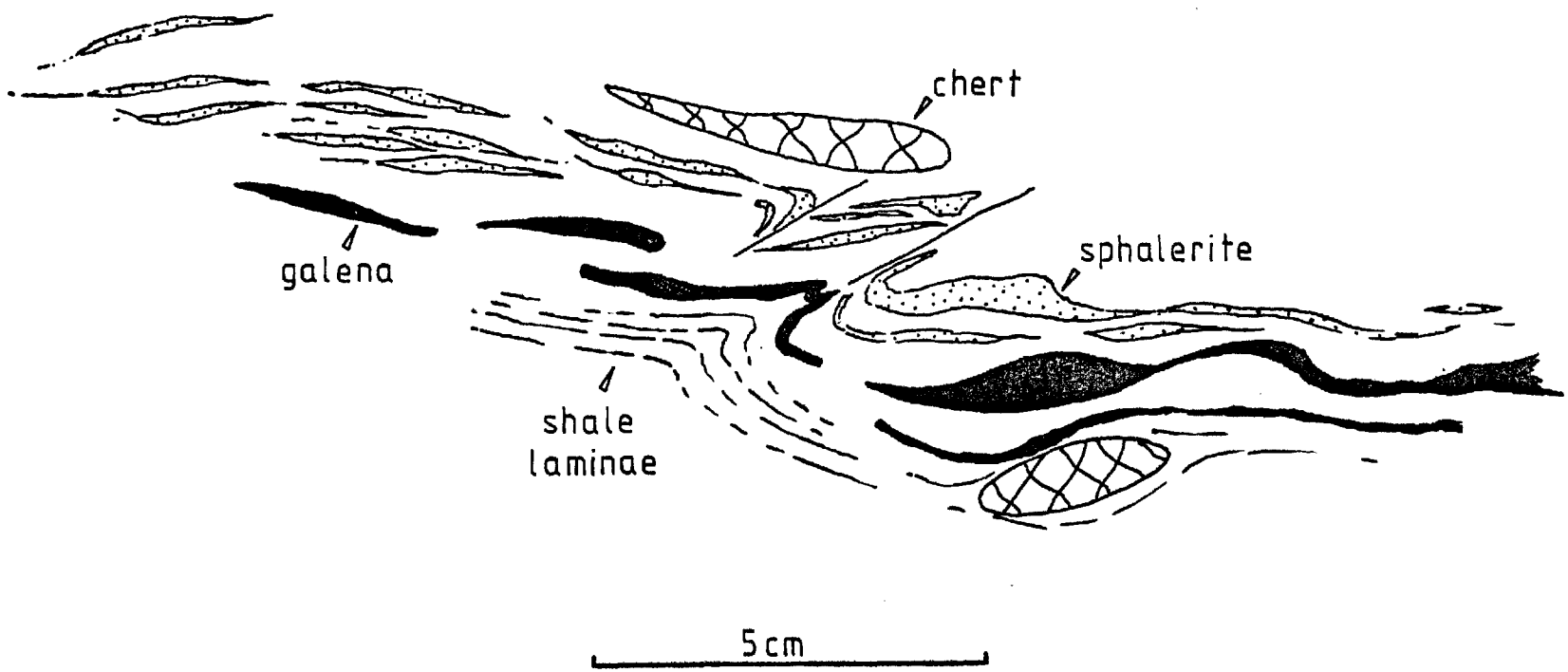

(ii) All three deposits are associated with faulting possibly controlled by lines of weakness in the Caledonian basement. Tynagh and Silvermines are located against major approximately E - W trending normal faults with a downthrow to the north, whilst the Navan deposit is cut by a N.E. trending reversed fault.

(iii) They are all in close proximity to the outcrop of the Lower Palaeozoic sequence. Tynagh and Silvermines are adjacent to major inliers with cores of Ordovician and Silurian sediments and volcanics, whilst the Navan orebody occurs along the southern margin of the Longford-Down massif.

(iv) All three deposits occur within a carbonate dominated Lower Carboniferous sedimentary sequence. Although there are major differences between the actual host lithologies, they all occur at the top of a succession of thinly bedded, dark, argillaceous and bioclastic limestones, possibly laid down under lagoonal conditions.

(v) The available geological evidence points to a Lower Carboniferous age for each deposit. At Navan and Silvermines sulphide deposition occurred during Upper Tournaisian times. However at Tynagh mineralization possibly extended into the Lower Visean.

(vi) The Navan orebody and the bulk of mineralization at Silvermines is stratiform and both exhibit convincing textural evidence for a synsedimentary mode of deposition. At Tynagh sulphide emplacement was initiated during early diagenesis and continued through the early lithification and post-lithification stages of host evolution.

(vii) All three deposits have a broadly similar mineralogical and textural composition. Sphalerite and galena are the major

economic sulphides, and abundant metacolloid and microcrystalline textures are indicative of their rapid precipitation. However, pyrite is much more important at Silvermines than at Tynagh and Navan, and Cu sulphosalts and sulphides, which are important accessory components of the Silvermines and Tynagh deposits, are absent at Navan.

(viii) Disruption and soft sediment slumping, most probably induced by fault tectonism, was synchronous with sulphide deposition at Tynagh, Navan and Silvermines.

CHAPTER 5

METHODS OF ISOTOPIC ANALYSIS

5.1 STABLE ISOTOPE MEASUREMENT AND DATA PRESENTATION

In stable isotope analysis, it is not the absolute abundances of given isotopes that are measured, but the ratio (R) of the most abundant trace isotope, to the major isotope. The reason for this is that a ratio can be measured more precisely than absolute abundances, and any instrumental error that could be introduced during the measurement of individual masses is cancelled. For carbon, oxygen and sulphur the isotopes measured are as follows:-

Most abundant trace isotope	Major isotope	R^x
^{13}C	^{12}C	$R^{13} = {}^{13}C/{}^{12}C$
^{18}O	^{16}O	$R^{18} = {}^{18}O/{}^{16}O$
^{34}S	^{32}S	$R^{34} = {}^{34}S/{}^{32}S$

The above elements also have other stable isotopes, however it has been shown that the variations in their abundances are related. For systems in thermodynamic equilibrium (Craig, 1954) and similarly for kinetic effects (Bigeleisen, 1952), the fractionation factor for the distribution of an isotope between two compounds is a function of the mass difference:-

e.g. $$\left[\frac{R^{18}\text{Sample}}{R^{18}\text{Standard}}\right]^{1/2} = \frac{R^{17}\text{Sample}}{R^{17}\text{Standard}}$$

Since the ratio differences measured are small, they are expressed in the del notation as per mille, or parts per thousand ($^{o}/_{oo}$) differences from a standard where:-

$$\delta^{x}\ (^{o}/_{oo}) = \left[\frac{R^{x}\text{Sample}}{R^{x}\text{Standard}} - 1 \right] \times 1000$$

If a sample has a positive del value it is enriched in the heavier trace isotope with respect to the standard, and is said to be isotopically heavy. Conversely, if a sample has a negative del value it is depleted in the trace isotope and is said to be isotopically light. Samples with a del value of zero per mille have the same isotopic composition as the standard.

The international standards to which all carbon, oxygen and sulphur isotope analyses are now related are:-

Element	Standard	Description
C, O	PDB	Carbonate from Peedee Bellemnitella (Urey et al, 1951)
O, (H/D)	SMOW	Standard Mean Ocean Water (Craig, 1961a)
S	CDT	Troilite phase from the Cañon Diablo meteorite (Jensen and Nakai, 1963)

The methods used for the production of CO_2 for isotopic analysis from carbonates and waters involve different oxygen isotope fractionation effects, the absolute values of which are uncertain. Different standards are, therefore, used for the different types of sample. PDB is the accepted oxygen isotope standard for palaeo-temperature determinations on planktonic foraminifera, and for studies of carbonate diagenesis, as it closely approximates the average isotopic composition of marine carbonates of all ages. SMOW is the standard generally adopted for all other oxygen bearing phases, and is especially useful in studies of oxygen and hydrogen exchange between waters and silicates. PDB oxygen is + 30.86$^{o}/_{oo}$ on the SMOW scale.

All isotopic ratio measurements were made on carbon and oxygen in the form of CO_2, and on sulphur in the form of SO_2. Analyses of both these gases were carried out on separate Micromass 602 C double collector mass spectrometers, with a standard reproducibility better than $0.1^{o}/oo$ (CO_2), and $0.15^{o}/oo$ (SO_2). The two collectors enable the simultaneous measurement of signals from two ion beams of different mass to produce a ratio. Sample gas and a laboratory reference gas of known isotopic composition were alternately admitted into the ion source via a solenoid valve operated inlet system, thus allowing continuous standardisation of the sample. The sample and reference gas were each measured six times, and the reference gas was calibrated at the beginning and end of each day by measurement against separately prepared aliquots of itself.

The isotopic ratios of carbon (R^{13}) and oxygen (R^{18}) in CO_2 were determined by measuring the ratios of the related molecular masses 45/44 and 46/(44 + 45) respectively. Since the solenoid valves of the inlet system do not seal perfectly, approximately 0.1% of the reference gas enters the ion source while the sample is analysed and vice versa. A correction was therefore applied to the data for inlet valve mixing (Deines, 1970) - Appendix 1a. To convert the measured molecular mass ratio differences to specific isotope ratio differences, the isobaric correction factors derived by Craig (1957) were subsequently applied - Appendix 1b. The carbon correction factor corrects for the $^{12}C^{16}O^{17}O$ component of the mass 45 beam, and the oxygen correction factor corrects for the $^{13}C^{16}O^{17}O$ component of the mass 46 beam, and for the mass 45 beam collected along with the mass 44 beam. The corrections are small but significant, 1% of the ^{13}C difference entering into the oxygen correction factor, and 3% of

^{18}O difference entering into the carbon correction factor.

Similarly, in the measurement of SO_2, the ratio of the molecular masses 66/64 was determined, valve leakage (Deines, 1970) and isobaric (M.L. Coleman - unpub.) correction factors being applied to convert the measured δ^{66} value to a corrected δ^{34} value with respect to the CDT standard.

5.2 SAMPLE PREPARATION FOR STABLE ISOTOPE ANALYSIS

5.2.1 Mineral Separation

Monomineralic microsamples were obtained from hand specimens either by means of a dental drill, or by hand picking fragments broken from the specimen with a steel probe. This method has a number of advantages over other standard mineral separation techniques. Firstly it allows samples to be taken from small areas thus enabling comparisons between individual depositional or growth bands within a single specimen. Secondly, it was found to be the quickest and most efficient method of separating the small quantity of sample required. Pyrite concentrates from unmineralized limestone and shale were prepared by dissolution of the carbonate component in 0.2 M di-ammonium EDTA. Smear mounts of the samples were prepared and analysed by X-ray diffractometry, to determine their mineralogical purity. The fine grained and complex nature of many of the ore intergrowths often precluded complete segregation of the various sulphide and gangue phases present. As a result, in certain instances it was found to be necessary to subject the samples to further purification processes, and where this was not possible, to discard them.

The majority of the sphalerite samples prepared for sulphur isotope analysis were contaminated by trace to minor amounts of

barytes, carbonate and silicate. The carbonate and silicate components present no problem. However, as barytes will contribute sulphur during the gas extraction process, it was of prime importance to separate it. A chemical separation of the two was achieved by an adaptation of the sulphate reduction system (fig. 5.2). The samples were reacted with hot 50% HCl, in a stream of nitrogen. The resultant H_2S produced from the sulphide was precipitated as CdS, after washing in 0.1 M HNO_3, and the barytes was left as an unreacted residue. Experimentation with equal weight mixtures of sphalerite and barytes of known isotopic composition, demonstrated that the sulphur liberated from the sphalerite was unaffected isotopically (table 5.1).

Table 5.1 Sphalerite/Barytes Separation Data

Reagents	$\delta^{34}S$ (°/oo)
Sphalerite F (direct Cu_2O oxidation)	-12.61
" " " " "	-12.76
Sphalerite F + EDH $BaSO_4$ (50% HCl extraction)	-12.70
" " " " " "	-12.50
" " " " " "	-12.63
Residual EDH $BaSO_4$	+14.36

5.2.2 Oxidation of Sulphides to SO_2

The method as described by Robinson and Kusakabe (1975), was used to oxidise sulphides, producing SO_2 free from impurities and in 100% yield (fig. 5.1). Failure of the sulphur to undergo 100%

FIG. 5.1 SO_2 EXTRACTION LINE.

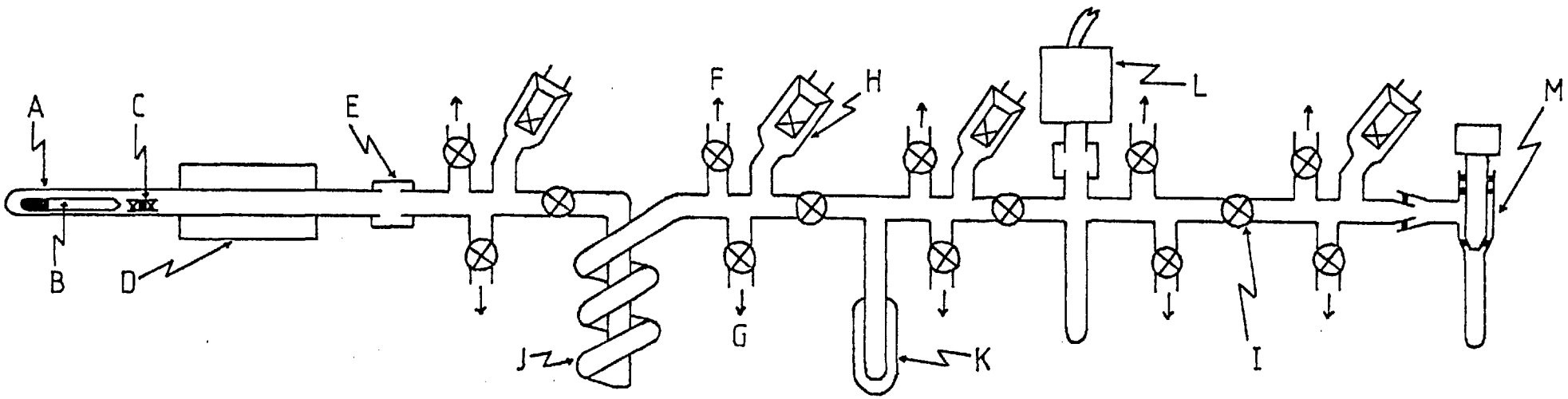

KEY

A) Quartz glass reaction tube.

B) Magnetic pusher.

C) Quartz glass sample tube with quartz wool retaining plugs.

D) Furnace.

E) Cajon joint.

F) To rotary pump.

G) To diffusion pump.

H) Thermocouple gauge.

I) High vacuum valve.

J) Solid CO_2/acetone trap.

K) N-pentane trap.

L) Capacitance manometer.

M) Collection vessel.

reaction leads to fractionation, the SO_2 being depleted in ^{34}S with respect to the sample. The reason for this is that the lighter isotope forms weaker chemical bonds than the heavier isotope and therefore reacts more readily. Although all the sulphur may have reacted, in practice natural samples rarely produce 100% yields due to the presence of impurities.

Enough sulphide to liberate 2 to 3 standard ccs. of SO_2 (e.g. 5 mgs. of sulphur or 10 mgs. of pyrite) was taken and intimately mixed with excess (200 mgs.) Cu_2O. The reaction was carried out in a quartz glass tube at 1070°C, for 15 minutes, in vacuo. As the reaction proceeded the SO_2 and CO_2 impurity produced were frozen into an n-pentane cryogenic trap, via a solid CO_2/acetone trap which freezes out any water vapour. The CO_2 originates from carbon impurities in the sample or on the walls of the silica tube, and/or absorbed gases on the Cu_2O and sample (Rafter, 1957; Robinson and Kusakabe, 1975), and can be removed by differential sublimation at -130°C (Oana and Ishikawa, 1966). The liquid nitrogen used to freeze the gas into the trap, also freezes the n-pentane which is contained in an outer jacket. At the freezing point of n-pentane (-129.7°C), the vapour pressure of CO_2 (2.35 torr) greatly exceeds that of SO_2 (3.47×10^{-3} torr). On removal of the liquid nitrogen, the n-pentane warmed to -129.7°C and the solid CO_2 impurity sublimated and was frozen into a liquid nitrogen trap, while the SO_2 remained frozen. The pressure of CO_2 was monitored by a thermocouple vacuum gauge, and when all the CO_2 was observed to have been frozen over, the liquid nitrogen trap was isolated, prior to sublimation of the SO_2. The CO_2 was then pumped away and the volume of the purified SO_2 was measured by means of a capacitance manometer,

before being transferred to a vacuum tight collection vessel.

5.2.3 Reduction of Sulphates to Sulphide

Approximately 60 mg. sulphate samples, enough for two sulphide oxidations, were reduced to H_2S by a boiling mixture of HI, H_3PO_2 and HCl in the manner described by Thode et al (1961). The reaction was carried out in a 250 ml. flask provided with a reflux condenser (fig. 5.2). The H_2S was swept out of the reaction flask by a stream of nitrogen and washed in 0.1 M HNO_3 to remove any acid fumes present. The H_2S was precipitated as CdS by reaction with 0.05 M Cd acetate/0.05 M acetic acid solution. The CdS was converted to Ag_2S by adding 0.5 M $AgNO_3$, and washed once in deionised water and twice in concentrated NH_4OH, before being dried in an oven at 110°C. The dried Ag_2S was converted to SO_2 in the manner described above.

5.2.4 Extraction of CO_2 from Carbonates

CO_2 samples were prepared using a method similar to that of McCrea (1950), fig. 5.3. Samples of approximately 10 mgs. in weight were reacted with 100% phosphoric acid, in vacuo, at 25.18°C, for two hours in the case of calcite, and fifteen days for dolomite. Prior to collection, the CO_2 evolved, was passed through a solid CO_2/acetone trap to remove any water vapour present.

Phosphoric acid is used for the reaction, as it has a low vapour pressure, enabling it to be more readily handled in a vacuum, and the activity of water in its concentrated solution is less than that for other acids, leading to a low oxygen isotope exchange rate between the solution and the CO_2 (McCrea, 1950). The reaction yields only two-thirds of the total oxygen of the carbonate as CO_2, and involves a large kinetic isotope effect, the CO_2 being enriched in

FIG.5.2 SULPHATE REDUCTION LINE.

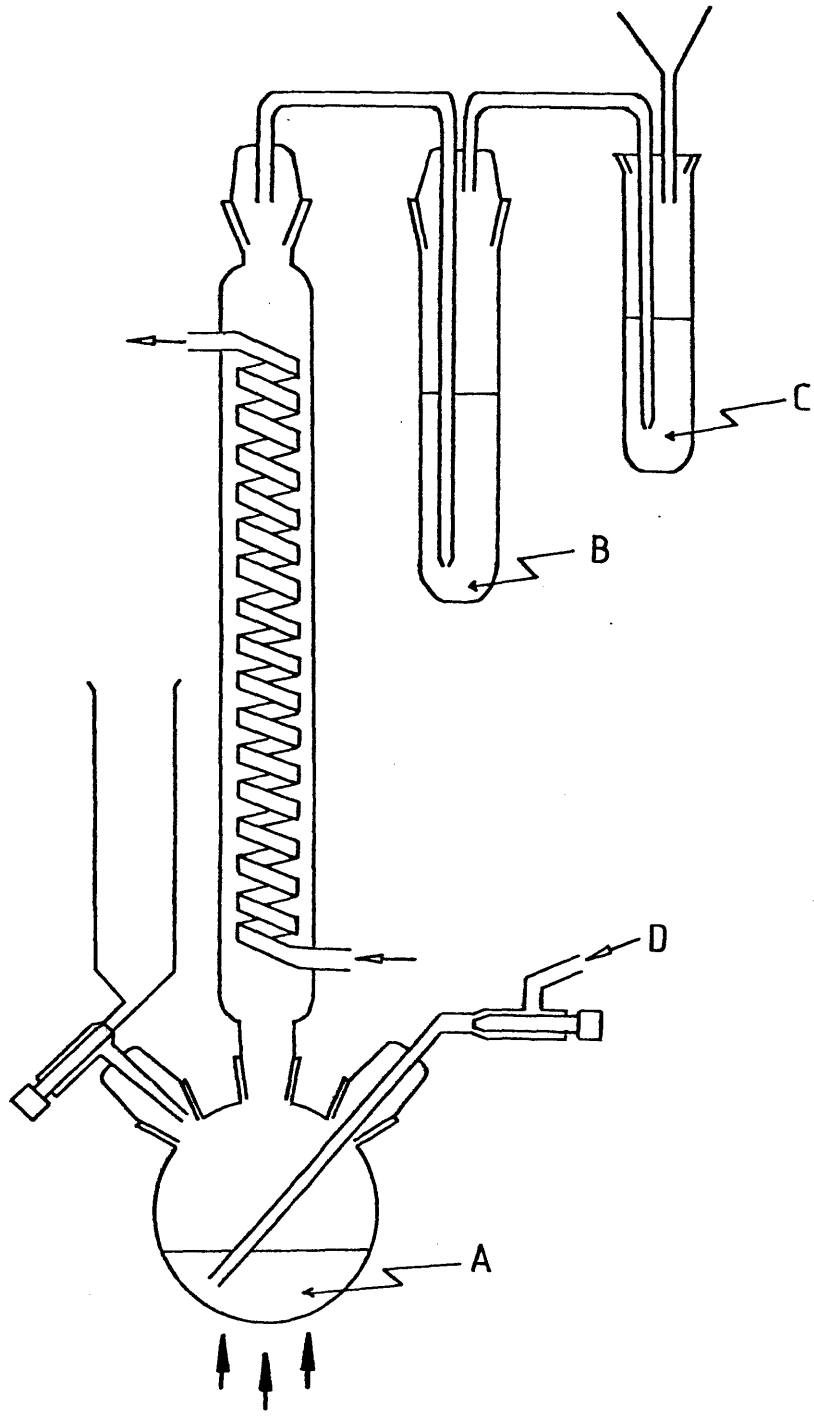

KEY

A) Sample & boiling HI, HCl, H_3PO_2.

B) 0·1M HNO_3.

C) 0·05M Cd acetate / 0·05M acetic acid.

D) Nitrogen.

FIG. 5.3 CO_2 EXTRACTION LINE.

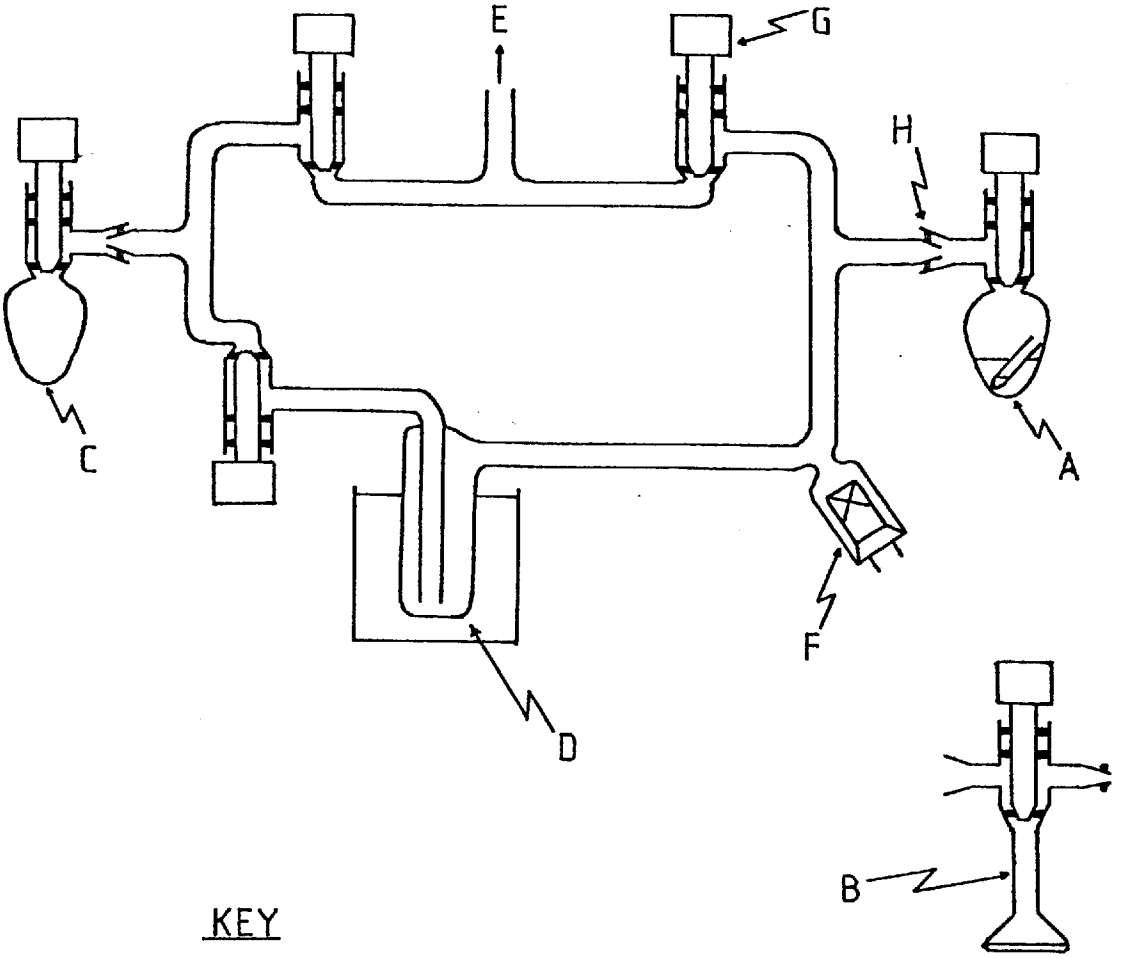

KEY

A) Reaction vessel containing 100% phosphoric acid and sample tube.

B) 'T' tube containing lead acetate.

C) Collection vessel.

D) Solid CO_2 / acetone trap.

E) To rotary and diffusion pumps.

F) Thermocouple gauge.

G) High vacuum stopcock in closed position.

H) B14 joint fitted with Viton 'o' ring ('T' tube inserted for H_2S separation)

^{18}O with respect to the carbonate. The extent of the fractionation (α) is dependent upon the composition of the carbonate, and at the temperature quoted above, has been found to be 10.25°/oo and 11.07°/oo for CO_2 evolved from calcite and dolomite respectively (Sharma and Clayton, 1965). A correction was therefore applied for the difference in fractionation factors when dolomite CO_2 was analysed with respect to the reference calcite CO_2.

5.2.5 Extraction of CO_2 from Sulphide/Carbonate Mixtures

It was often not possible to completely segregate carbonate intergrown with associated ore sulphides. Unfortunately, phosphoric acid also reacts with sphalerite and galena to produce H_2S which interferes with accurate isotopic analysis. The similarity in freezing point and vapour pressure of CO_2 and H_2S prohibits the use of a cryogenic trap to segregate them. Wet chemical methods can be ruled out also as oxygen isotope exchange readily occurs between CO_2 and water, e.g. Epstein and Mayeda (1953). Reaction of H_2S with anhydrous lead acetate or lead formate provides a quick and effective method of separation.

A series of experiments was devised to test whether isotopic exchange occurs between CO_2 and the reagents during the reaction.

Anhydrous lead acetate was prepared by dehydrating laboratory reagent lead acetate, trihydrate at 110°C. Anhydrous lead formate was prepared by neutralising aqueous formic acid with lead carbonate and crystallising lead formate from the solution by evaporation. The reagent was then recrystallised from water and dried at 110°C.

Two samples of calcite of different isotopic composition were taken and each mixed with an equal weight of galena. Aliquots of

approximately 15 mgs. were taken from both mixtures and from control samples of uncontaminated calcite and allowed to react with phosphoric acid for fifteen days (the longest period of time required for complete decomposition of any carbonate usually analysed).

The CO_2 from the control samples and one mixture were extracted normally: that is without exposure to lead acetate or formate. To remove H_2S, the gas evolved from the other mixtures was frozen into the 'T' tube (fig. 5.3), which contained 50 mgs. of lead acetate or formate, and isolated from the rest of the system. For the reaction to go to completion, it was found that it was necessary to carry out the reaction within a confined volume, anything up to about 45 mls. being suitable, and with the reagent dispersed over the base of the 'T' tube so as to expose a large surface area. The reaction starts as soon as the tube has warmed to room temperature, but to ensure completion it was heated with a hot air gun to approximately 100°C for about 20 seconds, the H_2S reacting to produce lead sulphide and acetic or formic acid. The procedure was then completed as usual allowing the vapour of the organic acid and water to be frozen out together in the solid CO_2/acetone trap. All gas samples were subsequently analysed on the mass spectrometer, and the results are shown in table 5.2.

The gas sample that had not had H_2S removed was difficult to measure precisely the ratio value being erratic and variable. An examination of the complete mass-spectrum revealed large peaks at mass 34 (H_2S) and 48 and 64 (SO_2), whose intensities relative to mass 44 were 0.9%. 1.3% and 2.5% respectively. The presence of SO_2 suggests a reaction between H_2S and CO_2 in the source of the mass-spectrometer, which could produce the instability that was observed.

Table 5.2 CO_2/H_2S Separation Data

Sample	Reagent	δ^{45}(‰)	error (2 S.E.M.)	δ^{46}(‰)	error (2 S.E.M.)
Calcite I	-	-0.166	0.006	-0.060	0.006
"	-	-0.281	0.011	-0.296	0.027
Calcite I + PbS	-	+7.002	0.228	+1.082	0.032
"	Pb acetate	-0.154	0.005	-0.102	0.021
"	Pb formate	-0.130	0.006	-0.265	0.022
"	"	-0.161	0.028	-0.105	0.008
Calcite II	-	-20.571	0.006	-4.003	0.026
"	-	-20.561	0.004	-3.915	0.027
Calcite II +PbS	Pb acetate	-20.605	0.014	-4.001	0.016
"	"	-20.584	0.023	-4.035	0.016
"	Pb formate	-20.595	0.006	-3.996	0.019
"	"	-20.564	0.012	-4.087	0.032

In contrast, all the other samples showed only traces of the extraneous peaks and were measured normally.

The isotopic compositions of the CO_2 extracted from the calcite/galena mixture are not significantly different from the non-contaminated controls. Although formic acid gives a mass spectrum with peaks at masses 46 and 45, and acetic acid also at mass 45, any residual acid vapour, if present in the CO_2 samples, had no effect on its measured isotopic composition. However, as mass 46 would be more sensitive to such contamination, lead acetate was used.

The success of this method allowed analyses to be made of dolomite and calcite intimately intergrown with microcrystalline sphalerite and galena.

5.2.6 Extraction O_2 from Silicates

Quantitative liberation of oxygen from silicates was achieved by reaction with BrF_5 in the manner described by Clayton and Mayeda (1963). This procedure normally involved overnight reaction of the sample ($\sim$ 10 mgs.) within evacuated nickel tubes at a temperature of 580°C. However, the differential reactivity of certain mineral phases was taken advantage of to yield oxygen from an inseparable quartz-albite pair. Clayton and Mayeda (1963) found that it was possible to get good oxygen isotope analyses from feldspars in the presence of equal amounts of quartz, by conducting the reaction at 100°C. Quartz is unaffected by BrF_5 at this low temperature. J.J. Durham (pers. comm.) has confirmed this for temperatures of up to 140°C.

After passage through two liquid nitrogen traps to remove any bromine or fluorine compounds, the oxygen was converted to CO_2

by reaction with carbon at a temperature of 550 to 600°C. The CO_2 was transferred to an evacuated collection vessel and analysed in the normal manner.

5.3 LEAD ISOTOPE RATIO MEASUREMENT

Unlike stable isotope analysis, absolute lead isotope abundances are determined by the individual measurement of the masses 208, 207, 206 (radiogenic lead) and 204. All lead isotope analyses were carried out on a Thomson 206 solid source mass spectrometer, using an adaptation (I.G. Swainbank - pers. comm.) of a method developed by Cameron et al (1969). Approximately 5 µg of sample in the form of lead nitrate was mounted on to a rhenium filament along with a drop of silica gel/phosphoric acid solution. The presence of the silica gel/phosphoric acid aids thermal ionisation of the sample on the filament and produces a beam current of around 2×10^{-11}A for a few hours. Where possible, 50 or 60 measurements were made on an individual sample and a number of replicate analyses were made to check reproducibility. The NBS 981 Common Lead Standard (Catanzaro et al, 1968) was analysed at regular intervals, and corrections were applied for the variation in the measured value from its absolute value. For correction to the absolute value, sample ratios were multiplied by the following factors:-

$\frac{206}{204}$	$\frac{207}{204}$	$\frac{208}{204}$	
1.00041	1.00097	1.00120	(C402 - C442)
1.00118	1.00162	1.00216	(C466 - C511)

The error (2 x S.E.M.) on the reproducibility of the standard over the period of measurement was $\pm$0.008 (206/204), $\pm$0.009 (207/204) and $\pm$0.016 (208/204). However measurement errors on samples were

generally better than those quoted above.

An additional correction for atmospheric and reagent contamination was applied to the whole rock data (Appendix 1C). Unfortunately, due to the lack of clean laboratory facilities, blank levels for lead were high (7.2 µg), and as a consequence the correction large. As only single analyses were carried out on the whole rock samples and because the isotopic composition of the blank has to be estimated, the error on this correction is also large - probably of the order of 1%.

5.4 SAMPLE PREPARATION FOR LEAD ISOTOPE ANALYSIS

5.4.1 Galenas

10 mg. samples of galena were dissolved in 1 ml. of Aristar HCl and evaporated to dryness. 1 or 2 mls. of Aristar HNO_3 were added to convert the lead to the nitrate, and again evaporated to dryness. The lead nitrate was then dissolved and diluted down in 85 mls. of 0.1 M HNO_3. At this concentration one drop of solution contained sufficient lead for one analysis.

5.4.2 Whole Rocks

Enough powdered sample to yield approximately 30 µgs of lead was placed in a teflon beaker, digested overnight in $HF/HNO_3/HClO_4$, and evaporated to dryness. The residue was dissolved in 25 mls. of 1M HCl, centrifuged, and the solution decanted off prior to passage through a 20 cm. column of Dowex - 1 x 8 anion exchange resin onto which the lead adsorbed (Nelson and Kraus, 1954). After washing with a further 20 mls. of 1M HCl, 20 mls. of 6M HCl was passed through the column to extract the lead from the resin, collected and evaporated to

dryness in a clean beaker. The lead was further purified using the standard dithizone technique which involves the extraction of lead into a chloroform solution of dithizone, and its subsequent stripping into a dilute HNO_3 solution (e.g. see Powell and Kinser, 1958).

CHAPTER 6

SULPHUR ISOTOPES

6.1 SULPHUR ISOTOPE VARIATION IN GEOLOGICAL SYSTEMS

6.1.1 Introduction

The important sources of sulphur in ore deposits are deep-seated sources (mantle or homogenised crust), local country rocks and sea-water or marine evaporites. However, the two primary sources from which all sulphur has ultimately been derived are the deep-seated and sea-water reservoirs on which fractionation processes have operated to produce the wide range of isotopic compositions observed in nature. Of course sea-water sulphur is fundamentally of deep-seated origin, however it has been present as a vast and isotopically distinct reservoir for most of geological time.

6.1.2 Isotopic Composition of the Major Sulphur Reservoirs

Meteoritic troilite has been shown to display uniform isotopic compositions ranging from -0.1 to $+0.6^{o}/oo$ (mean $+0.2^{o}/oo$) (Jensen and Nakai, 1963; Kaplan and Hulston, 1966; Jensen, 1967), and it is widely accepted that this is representative of the value for deep-seated terrestrial sulphur.

Likewise, present day sea-water sulphate has a remarkably consistent isotopic composition, the most recent determination of the mean value being $+20.99^{o}/oo$ with a total spread of $0.38^{o}/oo$ (Rees et al, 1978). However, the sulphur isotope composition of sea-water sulphate has varied considerably with geological time (fig. 6.1), estimates of this variation being based on the analysis of marine evaporites of various ages.

FIG. 6.1 VARIATION IN $\delta^{34}S$ OF SEA-WATER SULPHATE WITH GEOLOGICAL TIME. (After Holser, 1977).

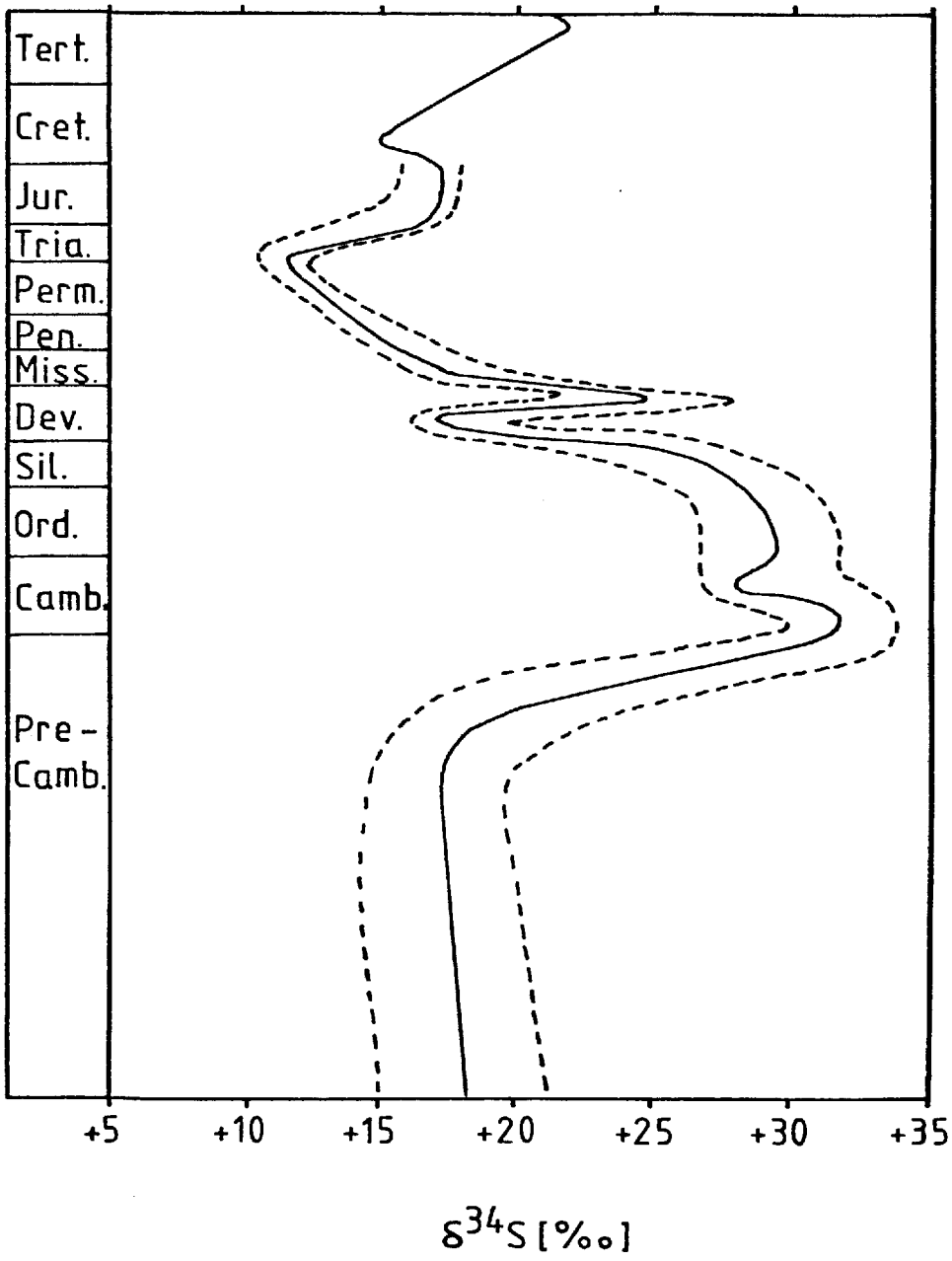

Thode and Monster (1965) found that gypsum precipitated at room temperature under equilibrium conditions was enriched in ^{34}S by 1.7°/oo with respect to the brine. However, they considered that even this small fractionation would seldom be realised due to the inflow of ocean water and outflow of brine from the system, and that evaporites indeed reflect the isotopic composition of contemporaneous sea-water sulphate.

A variety of models have been proposed to explain the variation in isotopic composition of the ocean with geological time. Holser and Kaplan (1966) attributed this to an imbalance between the rate of supply and rate of removal of sulphur from the oceans. They suggest that the preferential removal of isotopically light sulphur and its fixation as sedimentary sulphides results in a corresponding enrichment in ^{34}S of the ocean sulphate reservoir. Conversely, the inflow of isotopically light sulphate derived from shale sulphide causes a depletion in ^{34}S of the ocean sulphate.

Rees (1970) proposed that competition between isotopically heavy evaporite and isotopically light sulphide formation played an important role, the $\delta^{34}S$ of the ocean tending to high values in periods when evaporite formation was of minor importance and to low values in periods of major evaporite formation.

Holser (1977) postulated that brine generated by evaporite deposition is stored in deeps of Mediterranean-type basins. Beneath this brine the precipitation of isotopically light pyrite builds a store of brine enriched in heavy sulphate. Destruction of the basins causes the catastrophic mixing of the brine and surface ocean resulting in a sudden increase in ^{34}S content of surface ocean sulphate.

6.1.3 Controls on Sulphur Isotope Variation

6.1.3.1 Fractionation

Two processes act upon the major sulphur reservoirs to provide a wide spectrum of observed values. These are equilibrium fractionation, involving the partitioning of the trace isotope relative to the major, and kinetic fractionation, which depends on the relatively faster rate of reaction of the lighter isotope.

Equilibrium fractionation provides the basis of isotope geothermometry, the partitioning of the isotopes between various phases being dependent on temperature alone. If two co-existing phases are precipitated in equilibrium with one another, the lighter isotope, which forms a weaker bond, is preferentially located in the more weakly bonded site, an effect which increases with decrease in temperature. Numerous attempts, both theoretical and experimental, have been made at calibrating equilibrium fractionations between various sulphide and sulphate phases (fig. 6.2). Unfortunately, it is difficult to achieve isotopic equilibrium at low temperatures, and the curves have to be extrapolated from results obtained at higher temperature (generally $>250^{\circ}C$).

The published equilibrium fractionation curves must be used with care as it is all too easy to manipulate them. For example Ohmoto (1972) uses Sakai's (1968) data for his H_2S - ZnS fractionation, but takes the mean value of Sakai's (1968) theoretical and Kajiwara and Krouse's (1971) experimental data for his FeS_2 - ZnS fractionation factors. Following Ohmoto an enrichment factor of $-0.3^{\circ}/oo$ for FeS_2 in equilibrium with H_2S would indicate a temperature of $250^{\circ}C$. However, taking Sakai's data alone, the same fractionation

FIG. 6.2 ISOTOPIC ENRICHMENT FACTORS FOR SOME IMPORTANT SULPHUR SPECIES.

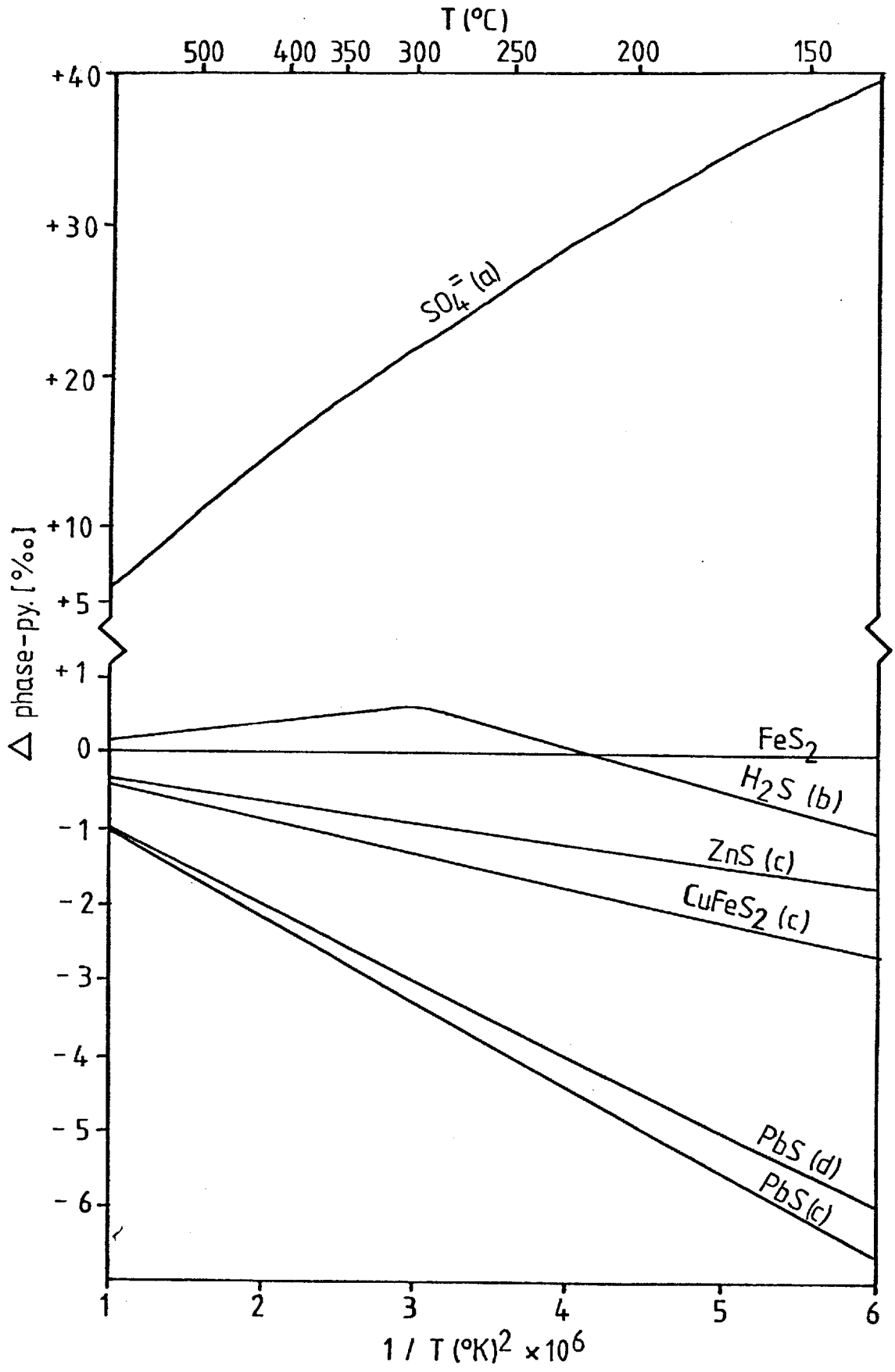

(a) Sakai, 1968.

(b) Ohmoto, 1972, after Sakai, 1968.

(c) Kajiwara & Krouse, 1971.

(d) Czamanske & R e 1974.

factor gives a temperature of 327 °C!

The most important type of kinetic fractionation effect within the sulphur cycle involves the bacterial reduction of sea-water sulphate to sulphide. It has been demonstrated that in the purely chemical reduction of sulphate, $^{32}SO_4^{2-}$ will react 2.2% faster than $^{34}SO_4^{2-}$ (Harrison and Thode, 1957), thus given an infinite source of sulphate any sulphide produced as a result of such a kinetic reaction will be depleted in the heavier isotope by 22°/oo. In close agreement with this, are results produced from artificial laboratory cultures of the sulphur reducing bacterium Desulfovibrio desulfuricans and related species (Kemp and Thode, 1968; Smejkal et al, 1971; McCready, 1975). These experiments mostly produced a maximum fractionation of 25°/oo in favour of the lighter isotope in the resultant H_2S, with respect to the original source sulphate. However, bacterial reduction of sea-water sulphate in present day anaerobic sedimentary environments has been observed to produce depletions in ^{34}S of up to about 50°/oo (Kaplan et al, 1963; Nakai and Jensen, 1964).

Various mechanisms have been proposed to explain the discrepancy between natural and experimental observations. Kemp and Thode (1968) proposed a double kinetic isotope effect involving an intermediate sulphite ion. Similarly, Smejkal et al (1971) suggested that reduction by a symbiotic pair of organisms, one reducing sulphate to sulphite and the other sulphite to sulphide, could produce larger fractionations. Rees (1973) developed expressions which relate overall isotope effects to diffusion mechanisms within the bacterium. He speculates that fractionations of 50°/oo are brought about by the bacterial population having grown

to the point where it utilises all suitable organic nutrients as they are supplied. Goldhaber and Kaplan (1974) demonstrated that there is an antipathetic relationship between the rate of reduction and the degree of the kinetic isotope effect (fig. 6.3). Furthermore, they showed that there is a positive correlation between rate of sulphate reduction and sedimentation rate (fig. 6.4), high rates of sedimentation favouring the preservation of suitable organic matter required for bacterial metabolism.

The type of distribution in sulphur isotope ratios produced by a process of bacterial reduction, is dependent upon whether an open or closed system has been operating (Kemp and Thode, 1968; Schwarcz and Burnie , 1973). In a closed system where there is a limited sulphate source, $\delta^{34}S$ of the residual sulphate increases as the reduction proceeds and, therefore, assuming the fractionation factor remains constant, each successive batch of reduced sulphur will be heavier than the previous. If the reduced sulphur is immediately precipitated as metallic sulphides, these will display a range of values ranging from $\delta^{34}S$ (sea-water sulphate - fractionation factor) to $\delta^{34}S$ (residual sulphate - fractionation factor). Correspondingly any sulphate phase precipitated will display a wide range of δ values which are heavier than $\delta^{34}S$ (sea-water). If sulphide precipitation is not immediate, the H_2S will have the opportunity to homogenise, and, if sulphate reduction goes to completion, the resultant sulphide will have an isotopic composition equal to that of the initial sulphate. An open system is one in which there is an unlimited reservoir of sulphate, an infinitesimal amount of which is reduced to sulphide. Therefore, the variation in isotopic composition of the resultant sulphide is only dependent on fluctuations in the fractionation factor. Sulphate phases will

FIG.6.3 VARIATION IN KINETIC ISOTOPE EFFECT WITH RATE OF REDUCTION. (After Goldhaber & Kaplan, 1974)

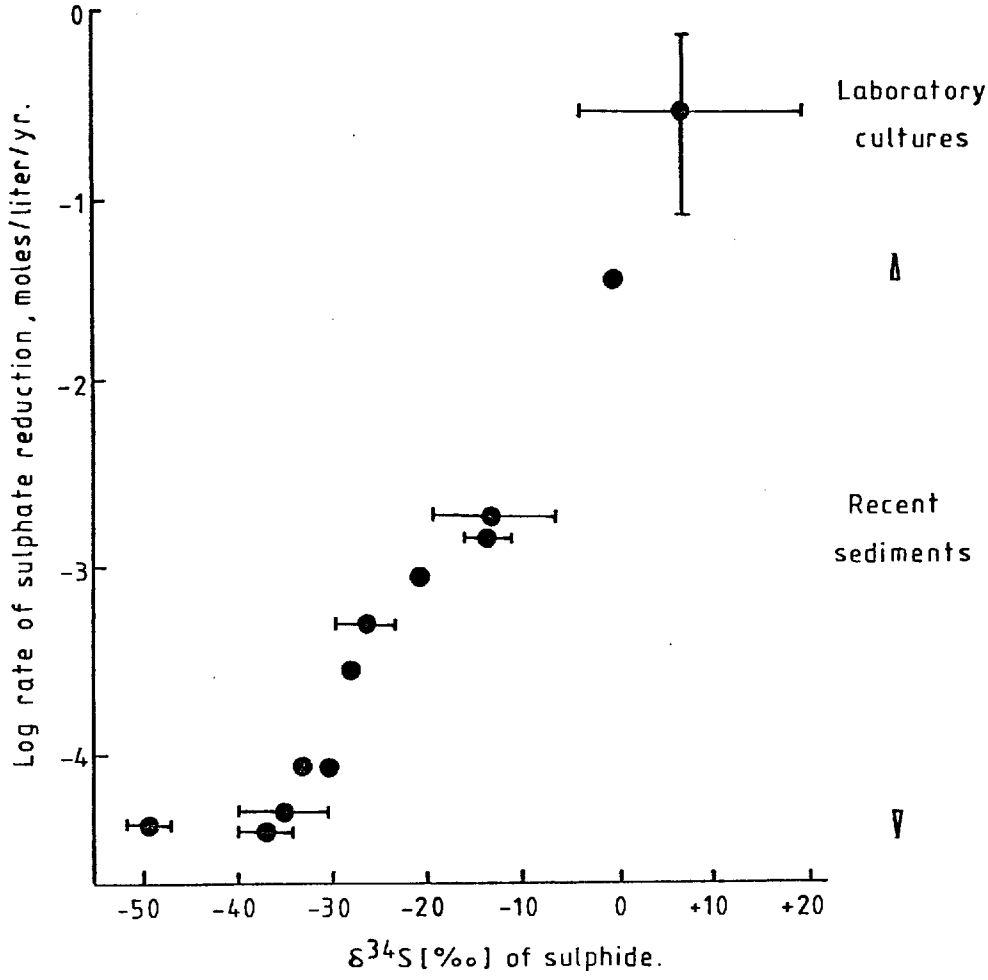

FIG.6.4 VARIATION IN RATE OF REDUCTION WITH SEDIMENTATION RATE. (After Goldhaber & Kaplan, 1974)

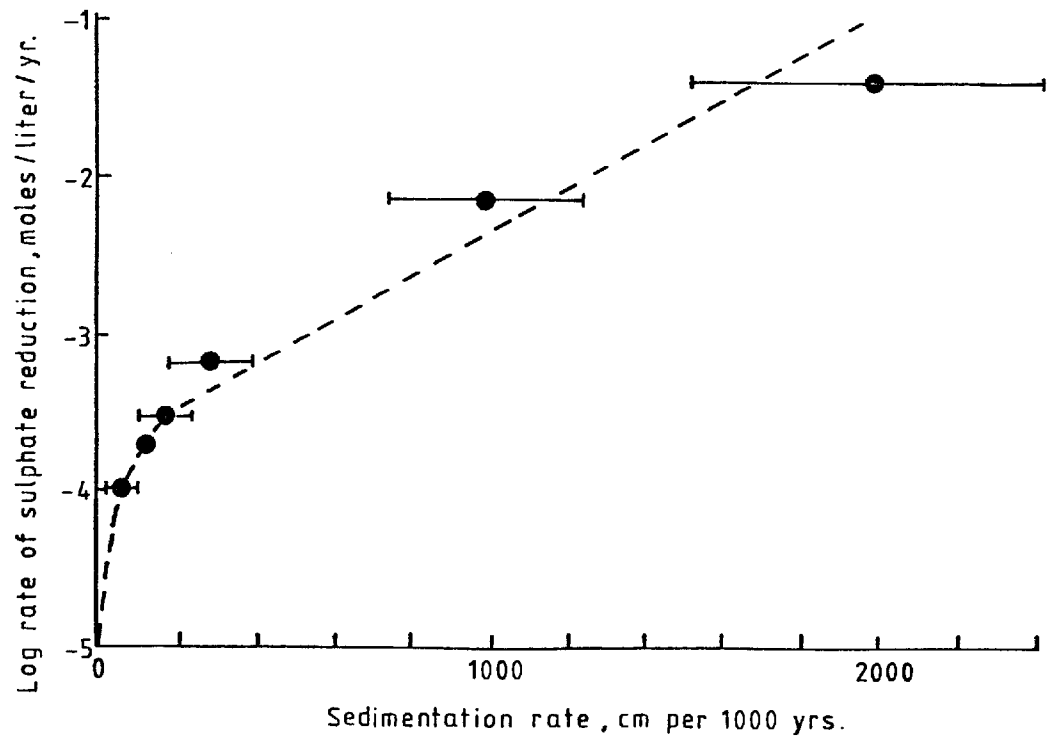

display δ values around that of the contemporaneous sea-water sulphate.

6.1.3.2 Fluid Chemistry

Until recently sulphides which displayed a narrow range of $\delta^{34}S$ values around $0^{o}/oo$ were regarded as having a deep-seated origin, and those which displayed a wide range of negative $\delta^{34}S$ values were thought to have been precipitated from bacterially reduced sulphate. However, the sulphur isotope composition of a mineral phase is controlled not only by the mode of fractionation, temperature of deposition and by the isotopic composition of the source, but also, in the case of equilibrium fractionation, by the proportion of oxidised (SO_4^{2-}, HSO_4^-, KSO_4^-, $NaSO_4^-$) and reduced (H_2S, HS^-, S^{2-}) species in solution (Sakai, 1968; Ohmoto, 1972). At a given temperature the equilibrium fractionation between a mineral phase (e.g. galena) and the species in solution from which it was precipitated (e.g. S^{2-}) will be a constant (see 6.1.3.1). If S^{2-} is the only sulphur-bearing species in solution then $\delta^{34}S\ (S^{2-}) = \Sigma\delta^{34}S$ ($\delta^{34}S$ for total sulphur present in all species). However, if a proportion of the S^{2-} is oxidised to SO_4^{2-}, the SO_4^{2-} will be enriched in ^{34}S with respect to S^{2-} (e.g. approximately + $30^{o}/oo$ at $200^{o}C$), and the S^{2-} will be correspondingly depleted in ^{34}S. As the oxidation process continues successive batches of SO_4^{2-} will be isotopically lighter than the previous, as the source S^{2-} becomes progressively depleted in ^{34}S. If oxidation goes to completion then $\delta^{34}S\ (SO_4^{2-}) = \Sigma\delta^{34}S$ (fig. 6.5).

Small changes in the parameters controlling the proportions of reduced and oxidised species in solution, namely pH

and fO_2 will therefore result in large ranges in $\delta^{34}S$ of mineral phases precipitated under equilibrium conditions. Greatest variation in isotopic composition will occur in the vicinity of the boundary between the stability fields of oxidised and reduced mineral phases, as isotopic fractionations between sulphate and sulphide are very large and in this region the activities of oxidised and reduced sulphur species in solution will be most variable. For example, at 150°C in this region, an increase in fO_2 by one log unit or in pH by one unit can cause a decrease in $\delta^{34}S$ of a phase by more than 20°/oo (see fig. 6.6). This effect becomes slightly less pronounced at higher temperatures due to the decrease in the equilibrium fractionation factor.

6.2 SULPHUR ISOTOPE VARIATION WITHIN THE TYNAGH DEPOSIT

6.2.1 Results

Sulphur isotope analyses for the Tynagh deposit are presented in table 6.1. Greatest emphasis has been placed upon the analysis of phases precipitated during stage 2 and stage 3, as the bulk of the sulphides, including all those of economic importance, were precipitated during these two mineralizing events. The samples analysed were collected over a total vertical distance of 130 metres, and have a lateral spread of 130 metres perpendicular to, and 1.30 km. parallel to the strike of the Tynagh fault. In addition, a number of samples were taken from mineralized drill core obtained at distances of 1.34 km. and 3.62 km. along strike from the eastern extremity of the orebody. The distances north of the Tynagh fault quoted in table 6.1 were measured horizontally from the intersection of the fault plane with the elevation at which the

FIG.6.5 VARIATION OF $\delta^{34}S$ WITH SULPHIDE/SULPHATE RATIO.

(After Coleman, 1977)

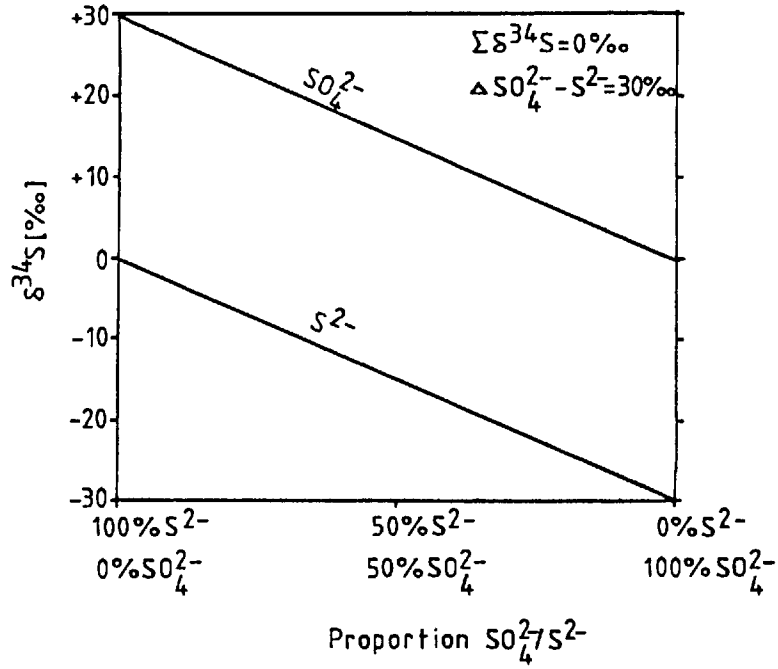

FIG.6.6 VARIATION OF $\delta^{34}S$ AS A FUNCTION OF fO_2 & pH.

(After Ohmoto, 1972)

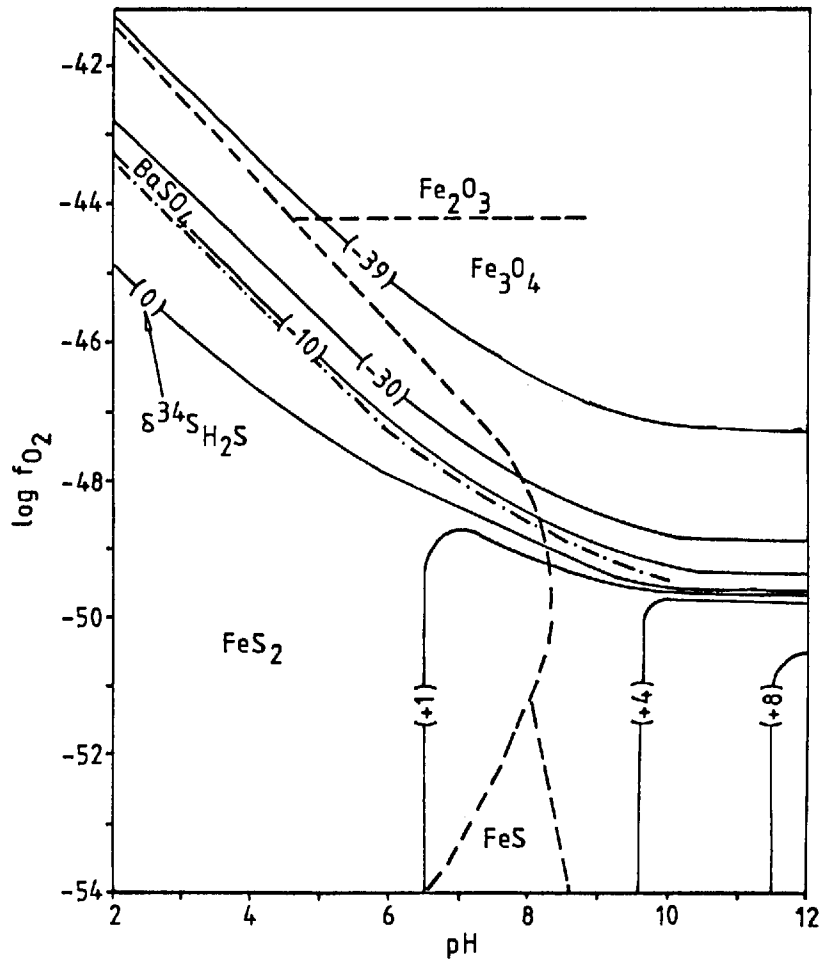

T=150°C ; Ionic strength=1molar ; $\Sigma\delta^{34}S=0‰$.

— — =Fe-S-O mineral boundaries at $\Sigma S=0{\cdot}001$ moles/kg H_2O.

—·— =Barytes soluble/insoluble boundary at $m_{Ba^{2+}}.m_{\Sigma S}=10^{-5}$.

sample was collected. The majority of samples, unless otherwise stated, are of mineralization hosted within Waulsortian facies limestones. For comparison, analyses were carried out on trace syngenetic/diagenetic pyrite separated from samples of Lower Limestone collected well away from known areas of mineralization (table 6.3). The most important features of the data can be summarised as follows:-

(i) With the exception of one sample ($\delta^{34}S = -15.51^{o}/oo$), stage 1 sulphides display a narrow range of isotopic compositions from $-3.11^{o}/oo$ to $-8.01^{o}/oo$ (mean: $-5.76^{o}/oo$, σ:2.61):- fig. 6.7.

(ii) Stage 2 sulphides closely approximate a normal distribution ranging from $-4.06^{o}/oo$ to $-25.98^{o}/oo$ (mean: $-17.19^{o}/oo$, σ:3.92):- fig. 6.7.

(iii) There is no correlation of variation in isotopic composition of stage 2 sulphides with elevation, distance along the strike of the Tynagh fault, or distance perpendicular to the fault, (figs. 6.8, 6.9). However, the isotopically lightest ($< -20^{o}/oo$) sulphides occur at the 4800 and 4900 elevations (zone II) and 5000 elevations (zone III) at a distance of 10 to 50 metres from the fault (fig. 6.10).

(iv) Serial samples taken from hand specimens of stage 2 dilatant fracture infillings display small (up to $3.43^{o}/oo$) but significant variations between individual sulphide bands (figs. 6.11A, B,C,D). However, no consistent trends can be recognised.

(v) Stage 3 sulphides have a very broad, approximately normal distribution, ranging from $+11.13^{o}/oo$ to $-23.02^{o}/oo$, (mean: $-8.66^{o}/oo$, σ:6.68).

(vi) As for stage 2 sulphides, there is no relationship between isotopic composition of stage 3 sulphides and elevation (fig. 6.12).

TABLE 6.1 SULPHUR ISOTOPE RESULTS - TYNAGH

Extraction No.	Location			Distance N of fault (Metres)	Mineral	Stage No.	$\delta^{34}S$ (°/oo)
S738	5050	66+80W		61.0	sphalerite	2	-14.80
S702	"	"		"	"	2	-15.36
S550	"	"		"	galena	2	-16.98
S551	"	"		"	"	2	-17.42
S666	"	"		"	sphalerite*	4	-14.59
S614	"	66+30W		76.0	galena	3	-15.37
S743	"	"		"	barytes	3	+19.04
S412	"	66+10W		67.0	galena	2	-16.46
S413	"	"		"	" (rpt.)	2	-16.34
S703	"	"		"	sphalerite	2	-15.16
S714	"	"		"	"	2	-14.52
S569	"	66+00W		36.5	"	4	-17.55
S704	"	65+80W		70.0	"	2	-13.18
S613	"	"		"	galena	3	-11.02
S742	"	"		"	barytes	3	+20.02
S747	"	"		"	"	3	+20.42
S410	"	65+40W		64.0	galena	3	-12.96
S411	"	"		"	"	3	-10.79
S615	"	64+50W		24.5	"	3	-18.71
S582	5000	67+10W		49.0	chalcopyrite+	4	- 7.77
S710	"	66+95W		55.0	sphalerite	2	-14.13
S545	"	66+85W		39.5	"	4	-17.59
S544	"	"		"	chalcopyrite*	4	-17.67
S546	"	"		"	galena	4	-19.75
S719	"	"		47.0	sphalerite	2	-20.96
S705	"	"		"	galena	3	-21.63
S724	"	66+65W		38.0	sphalerite	2	-21.53
S709	"	66+55W		50.0	"	2	-14.53
S734	"	66+50W		30.5	"	2	-19.61
S730	"	66+00W		12.0	"	2	-17.03
S711	"	"		30.5	"	2	-17.28
S717	"	"		"	"	2	-18.06
S712	"	"		"	"	2	-16.17
S718	"	"		"	"	2	-17.59
S736	"	65+00W		35.0	"	2	-16.44
S562	"	64+85W		18.0	"	2	- 9.21
S552	"	"		"	galena	2	-11.33
S731	"	63+95W		91.5	sphalerite	2	-15.04
S724	"	63+90W		82.0	"	2	-15.28
S908	"	63+35W		38.0	gypsum	4	+23.63
S732	"	63+00W		79.0	sphalerite	2	-15.02
S839	"	51+50W	DDH 1	3.0	galena	3	-11.23
S824	"	"	"	5.5	"	3	+ 2.65
S833	"	"	"	9.0	sphalerite	2	-15.41
S840	"	"	"	"	galena	3	- 7.51
S825	"	"	"	13.5	"	3	- 6.18
S834	"	"	"	14.0	"	3	- 6.91
S841	"	"	"	20.0	sphalerite	2	-15.76
S820	"	"	"	20.0	galena	3	- 4.28
S819	"	"	"	24.5	"	3	- 9.24
S832	"	"	"	30.5	sphalerite	2	-12.18
S823	"	"	"	"	galena	3	-12.42
S822	"	"	"	33.5	"	3	-10.48
S843	"	"	DDH 8	16.0	"	3	- 8.00
S842	"	"	"	19.0	"	3	-13.45
S827	"	"	"	21.0	"	3	- 6.77
S826	"	"	"	28.0	"	3	- 8.24
S844	"	"	"	31.0	"	3	- 7.09
S722	4912	66+30W		21.0	sphalerite	2	-15.62
S733	"	65+55W		18.0	"	2	-19.67
S584	"	65+35W		36.5	"	4	-16.30
S585	"	"		"	galena	4	-19.08
S737	"	64+85W		20.0	sphalerite	2	-17.09
S736	"	63+90W		15.0	"	2	-17.35
S752	"	"		"	barytes	2	+20.18
S739	4890	63+50W		30.5	sphalerite	2	-18.43
S725	"	63+40W		46.0	"	2	-15.29
S744	"	"		"	barytes	2	+18.15

cont. over

TABLE 6.1 cont.

Extraction No.	Location	Distance N of fault (Metres)	Mineral	Stage No.	$\delta^{34}S$ (°/oo)
S726	4890 63+40W	46.0	sphalerite	2	-16.45
S727	" "	"	"	2	-17.37
S728	" "	"	"	2	-18.72
S720	" 62+80W	32.0	"	2	-13.27
S708	" "	"	galena	3	-13.66
S830	" 62+65W	81.0	barytes	3	+18.92
S628	4900 91+00W	30.5	pyrite	1	- 7.01
S1115	" 90+00W	15.0	sphalerite	2	-23.65
S1120	" "	"	galena	2	-24.04
S871	" "	30.5	sphalerite	2	-17.57
S892	" 89+80W	41.0	"	2	- 4.06
S616	" 89+20W	50.5	"	2	-20.82
S1129	" 89+10W	1.5	"	2	-12.76
S1128	" "	"	galena	3	- 3.48
S1127	" "	"	arsenopyrite	3	+ 1.76
S635	" 88+90W	24.5	pyrite	1	- 5.28
S661	" "	"	"	1	- 5.38
S723	" "	"	sphalerite*	2	-24.18
S745	" "	"	barytes*	2	+17.90
S746	" "	"	" *	2	+17.36
S650	" "	"	galena	3	- 2.51
S625	" "	7.5	pyrite	1	- 5.26
S564	" "	"	sphalerite*	4	- 2.67
S563	" "	"	galena*	4	- 4.81
S626	" 88+80W	15.0	pyrite	1	- 5.22
S1144	" 88+00W	33.5	sphalerite	2	-24.99
S1149	" "	"	galena	3	- 6.82
S640	" 87+80W	46.0	pyrite	1	- 5.24
S662	" "	"	"	1	- 5.79
S408	" "	"	galena*	3	- 7.56
S831	" "	"	barytes*	3	+20.93
S1255	" 87+00W	21.0	sphalerite	2	-21.02
S1182	" "	"	galena	3	- 5.45
S589	" 86+00W	23.0	pyrite	1	- 3.11
S378	" "	"	"	1	- 4.67
S363	" "	"	sphalerite	2	-20.30
S586	" "	"	"	2	-19.95
S409	" "	"	galena	3	- 3.85
S406	" "	"	"	3	- 6.59
S365	" 85+20W	20.0	pyrite*	1	- 3.62
S364	" "	"	" *	1	- 4.25
S1146	" "	"	sphalerite	2	-20.89
S1179	" "	"	galena	3	- 7.57
S812	" "	"	barytes	3	+19.41
S627	" 84+40W	49.0	pyrite	1	-15.51
S1143	" "	"	sphalerite*	2	-24.85
S641	" "	"	galena	3	- 1.98
S1145	4800 94+00W	33.5	sphalerite	2	-21.06
S1187	" 92+00W	52.0	"	2	-16.23
S1148	" 91+00W	24.5	"	2	-25.98
S1150	" "	"	galena	3	- 7.67
S713	" 90+10W	4.5	sphalerite (FW L3)	2	-10.60
S1122	" "	12.0	pyrite	1	- 3.56
S867	" "	"	sphalerite	2	-20.76
S1119	" "	"	galena	3	- 7.29
S587	" "	21.0	pyrite*	1	- 6.34
S890	" "	"	sphalerite*	2	-18.12
S872	" "	"	" *	2	-15.83
S898	" "	"	"	2	-20.23
S873	" "	"	galena	3	-10.60
S891	" "	43.0	sphalerite	2	-23.26
S897	" "	50.0	"	2	-19.23
S588	" 89+50W	79.0	pyrite (sh)	1	- 6.79
S665	" "	"	sphalerite (sh)	1	- 8.01
S610	" 89+00W	21.0	pyrite	1	- 3.70
S611	" "	"	"	1	- 4.06
S1140	" 88+90W	30.5	sphalerite	2	-19.76
S1175	" "	"	galena	3	- 5.52
S590	" 88+80W	21.0	pyrite	1	- 7.40
S567	" "	"	sphalerite*	4	- 9.25
S828	" 88+20W	35.0	barytes	3	+19.93

cont. over

TABLE 6.1 cont.

Extraction No.	Location	Distance N of fault (Metres)	Mineral	Stage No.	$\delta^{34}S$ (°/oo)
S1139	4800 88+20W	39.5	sphalerite	2	-24.23
S1176	" 87+10W	18.0	galena	3	- 9.45
S1147	" "	30.5	sphalerite	2	-22.04
S1101	" 82+90W	61.0	tennantite	3	-10.46
S815	" "	61.0	barytes	3	+18.59
S1184	" 82+20W	76.0	galena	3	-20.80
S1124	" 81+40W	79.0	"	3	-18.70
S740	" "	"	barytes	3	+18.63
S909	" 80+80W	88.5	"	3	+21.09
S1183	" 80+60W	85.0	galena	3	-18.27
S868	" 80+30W	58.0	sphalerite	2	-16.45
S1103	" "	"	chalcopyrite	3	-20.39
S1117	" "	"	galena	3	-20.47
S813	" "	"	barytes	3	+18.30
S1185	" 78+50W	39.5	tennantite	3	-16.43
S829	" "	"	barytes	3	+20.00
S910	4725 88+60W	91.5	"	3	+18.54
S1177	" 86+20W	85.5	galena	3	- 5.98
S866	" "	122.0	sphalerite	2	- 8.67
S1121	" "	"	galena	3	- 1.93
S814	" "	"	barytes	3	+20.61
S1254	" 86+10W	82.5	sphalerite	2	-18.45
S1142	" 86+00W	94.5	"	2	-14.65
S1261	" 85+80W	128.0	"	2	-18.82
S1178	" "	"	galena	3	-23.02
S1253	" 85+60W	107.0	sphalerite	2	-15.84
S1251	" "	"	galena	3	- 9.97
S612	4700 91+10W	9.0	pyrite	1	- 6.47
S664	" "	"	sphalerite	2	-15.91
S617	" "	"	"	2	-15.07
S753	" "	"	barytes	3	+19.92
S870	" 90+00W	0.5	sphalerite (FW L3)	2	-17.85
S900	" "	1.5	sphalerite (FW L3)	2	-11.13
S1123	" "	4.5	pyrite	1	- 4.32
S899	" "	"	sphalerite	2	-19.47
S741	" "	11.0	barytes	3	+19.12
S1099	" "	14.0	tennantite	3	- 6.27
S1100	" "	15.0	"	3	- 8.91
S1118	" "	"	galena	3	-10.78
S869	" "	24.5	sphalerite	2	-15.12
S1141	" 87+00W	61.0	"	2	-19.43
S1136	4620 92+10W	24.5	"	2	-16.74
S1104	" 90+80W	7.5	chalcopyrite (L3)	3	- 4.42
S893	" 90+30W	15.0	sphalerite	2	-13.10
S1102	" 90+20W	9.0	chalcopyrite (L3)	3	- 4.54
S1116	" 90+10W	39.5	sphalerite (L3)	2	-12.33
S1133	" 89+20W	30.5	sphalerite (L3)	2	-14.31
S1130	" 88+90W	12.0	galena (L3)	3	- 9.04
S1105	" "	"	chalcopyrite (L3)	3	- 3.38
S1131	" 87+60W	14.0	galena (L3)	3	- 5.07
S1087	" 86+70W	39.5	sphalerite (L3)	2	-15.44
S1259	DDH 368 (125m) 1.34 km. E of Zone III	6.0	sphalerite	2	-16.74
S1235	" "	"	galena	3	- 3.78
S1260	DDH 376 (136m) 1.34 km. E of Zone III	7.5	sphalerite (L3)	2	-18.92
S1234	DDH 386 (158m) 3.62 km. E of Zone III	0.0	galena (L4)	3	+ 7.02
S1231	" "	"	arsenopyrite (L4)	3	+11.13

KEY TO TABLE 6.1

* Sample from same locality, but different hand specimen (s).

\+ Overgrowing euhedral 'plug' dolomite.

(sh) From shale horizon interdigitating with Waulsortian limestones.

(FW L3) Hosted within tectonically emplaced footwall lense of Lower Muddy Limestone.

(L3) Lower Muddy Limestone host.

(L4) Lower Bioclastic Limestone host.

TABLE 6.2 SULPHUR ISOTOPE FRACTIONATION TEMPERATURES

Location	Mineral Pair	Stage	1000 lnα (°/oo)	Inferred Temperature (°C)
4900 90+00W	sphalerite-galena	2	0.40	1050* } disequilibrium
5000 64+85W	" "	2	2.14	299* }
4800 80+30W	chalcopyrite-galena	3	0.08	2577+ } non
4620 88+90W	" "	3	5.70	65+ } co-precipitated
5000 66+85W	sphalerite-galena	4	2.20	291*
4912 65+35W	" "	4	2.83	224*
4900 88+90W	" "	4	2.15	298*

* Experimental calibration of Czamanske and Rye, 1974.

\+ " " Kajiwara and Krouse, 1971.

TABLE 6.3 ISOTOPIC COMPOSITION OF TRACE PYRITE

Extraction No.	Location	Description	Wt. % Pyrite	$\delta^{34}S$ (°/oo)
S1232	11.3 km. W.N.W. Tynagh mine	Dark bioclastic limestone (Lower Lst.)	1.21	-18.49
S1236	" " " "	Limestone shale (Lower Lst.)	1.78	- 8.62
S1228	14.9 km. W Tynagh mine	Dark bioclastic limestone (Lower Lst.)	0.96	-21.72

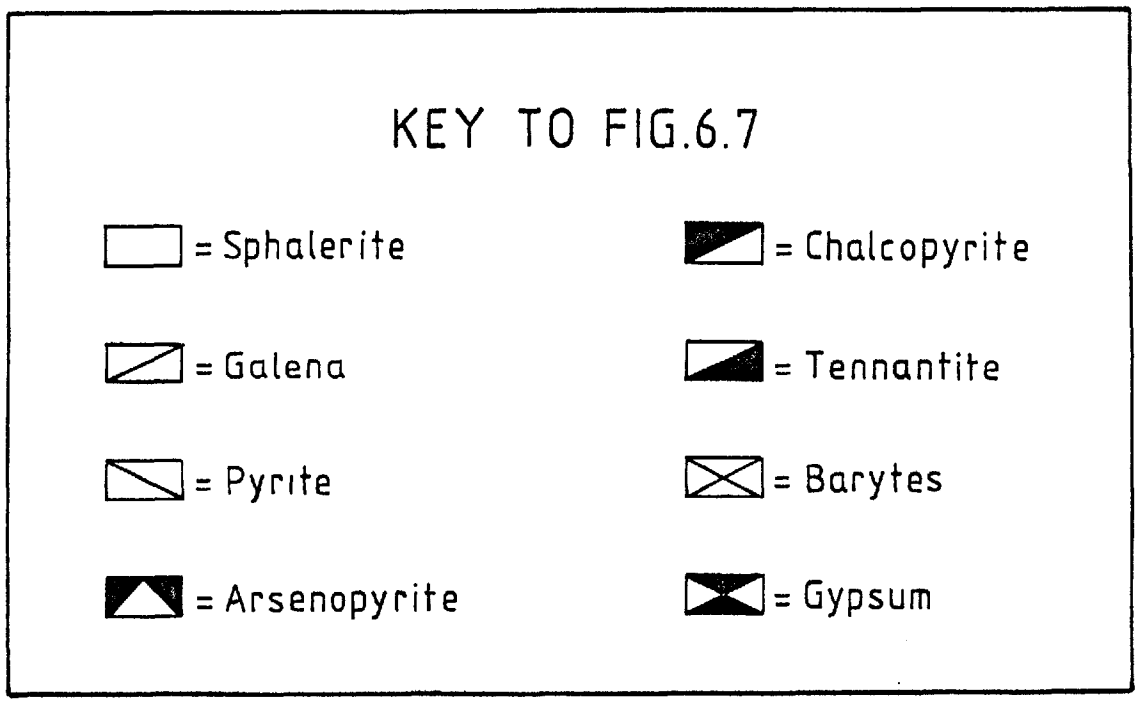
KEY TO FIG.6.7
= Sphalerite
= Galena
= Pyrite
= Arsenopyrite
= Chalcopyrite
= Tennantite
= Barytes
= Gypsum

FIG. 6.7 SULPHUR ISOTOPE VARIATION – TYNAGH.

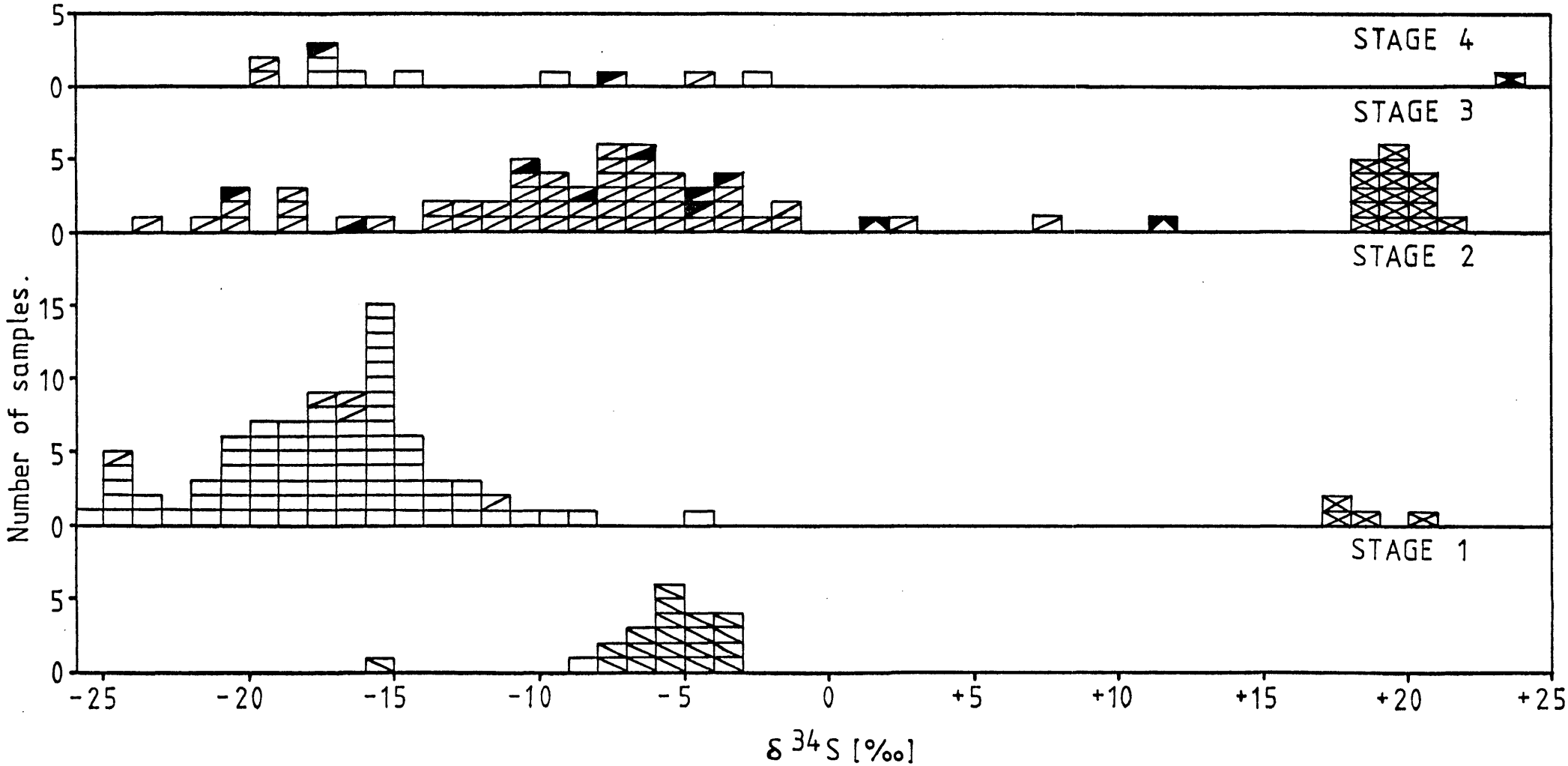

(vii) In the vicinity of the Tynagh fault (0 to 24 metres north) there is a marked negative correlation (r = 0.6, slope = -0.44) between isotopic composition of stage 3 sulphides and distance from the fault, the heaviest samples analysed being located in the actual fault plane. Distal samples, however, display a much wider range in $\delta^{34}S$ composition, with a tendency towards lighter values, the variation being in no way related to proximity to the fault (fig. 6.13). The comparatively wide spread of values away from the fault plane is partially accounted for by the fact that variation is not solely related to perpendicular distance from the fault. In the central region of the orebody (eastern and western extremes of zone II and zone III respectively) there is a marked 'bulge' towards the fault plane of lighter $\delta^{34}S$ values (fig. 6.14).

(viii) Neither for stage 2 nor stage 3 is there any significant difference in isotopic composition of those sulphides hosted within the Waulsortian Limestones and those hosted within the Lower Muddy Limestone (L3).

(ix) All sulphides recrystallised into later calcite veins (stage 4) have isotopic compositions similar to those displayed by the primary ore in the immediate vicinity (table 6.1). However, a chalcopyrite sample (S582 - 5000, 67+10W) collected from the dolomitised 'plug' between zones II and III has an isotopic composition ($-7.77^{o}/oo$) markedly different from that of the adjacent ore sulphides ($\delta^{34}S = -14.13 \rightarrow -21.63^{o}/oo$).

(x) There is no significant difference in the spread of $\delta^{34}S$ values displayed by stage 2 barytes and those of stage 3, the total range being $+17.36^{o}/oo$ to $+21.09^{o}/oo$ (mean: $+19.35^{o}/oo$, σ: 1.06). The late stage gypsum is isotopically heavier

($\delta^{34}S$ = +23.63°/oo) than ore stage barytes samples.

(xi) Sulphide samples taken from a single hand specimen but representing different stages of mineralization display a wide variation in sulphur isotope composition reflecting the overall trend ('heavy' - 'light' - 'heavy') exhibited by fig. 6.7 (e.g. 4900, 86+00W - stage 1 pyrite: -3.11°/oo, -4.67°/oo; stage 2 sphalerite: -20.30°/oo, -19.95°/oo; stage 3 galena: -3.85°/oo, -6.59°/oo).

(xii) Co-precipitated stage 2 sphalerite-galena pairs yield widely differing fractionation factors that would infer geologically unreasonable temperatures and, therefore, cannot be considered to be in isotopic equilibrium (table 6.2).

(xiii) Co-existing stage 3 chalcopyrite-galena pairs can be shown on textural grounds to be non-co-precipitated and, therefore, cannot be used as geothermometers. If so used they would again infer geologically unrealistic temperatures (table 6.2).

(xiv) Stage 4 recrystallised sphalerite-galena pairs appear to be co-precipitated, in textural equilibrium, and yield consistent fractionation factors suggesting a temperature of deposition between 224°C and 298°C for post-ore carbonate veins.

(xv) Trace syngenetic/diagenetic pyrite samples separated from the Lower Limestones, exhibit a range of $\delta^{34}S$ values (-8.62°/oo to -21.72°/oo, table 6.3) similar to that of the stage 2 ore sulphides.

Nine samples from the Tynagh deposit analysed by Greig et al (1971), are within the overall range of analyses produced in this study. However, as their spatial and temporal relationships

are unknown, they are not considered in the following discussion.

6.2.2 Interpretation and Discussion

6.2.2.1 The Source of Sulphate

The narrow range of sulphur isotope compositions displayed by barytes and the agreement of these values with those exhibited by Lower Carboniferous evaporites from various parts of the world (compare fig. 6.1) is indicative of a contemporaneous sea-water or evaporitic source for the sulphate.

6.2.2.2 Stage 1 and 2

If the mean value (+19.35°/oo) for all Tynagh barytes samples is taken as being the isotopic composition of Lower Carboniferous sea-water sulphate at the time of mineralization, then stage 1 sulphides are depleted in ^{34}S by 25°/oo (±2°/oo) with respect to sea-water sulphate. This difference closely approximates a simple one-step kinetic fractionation effect calculated by Harrison and Thode (1957) and matches precisely the maximum observed experimental fractionation produced in open-system bacterial reduction of sulphate (see 6.1.3.1).

Stage 2 sulphides are isotopically lighter by 23 to 45°/oo with respect to co-existing sulphate, which is well within the range of depletions produced by open-system bacterial reduction in present day euxinic environments (see 6.1.3.1). Isotopic disequilibrium amongst co-precipitated phases, as exhibited by stage 2 sulphides, is another feature common to ore deposits precipitated from bacterially reduced sulphur (Rye and Ohmoto, 1974). (Equilibrium is not attained due to the low temperatures involved). The

FIG.6.8 VARIATION IN $\delta^{34}S$ OF STAGE 2 SULPHIDES WITH ELEVATION.

Key as for fig.6.7 ; DDH samples E. of Zone III omitted.

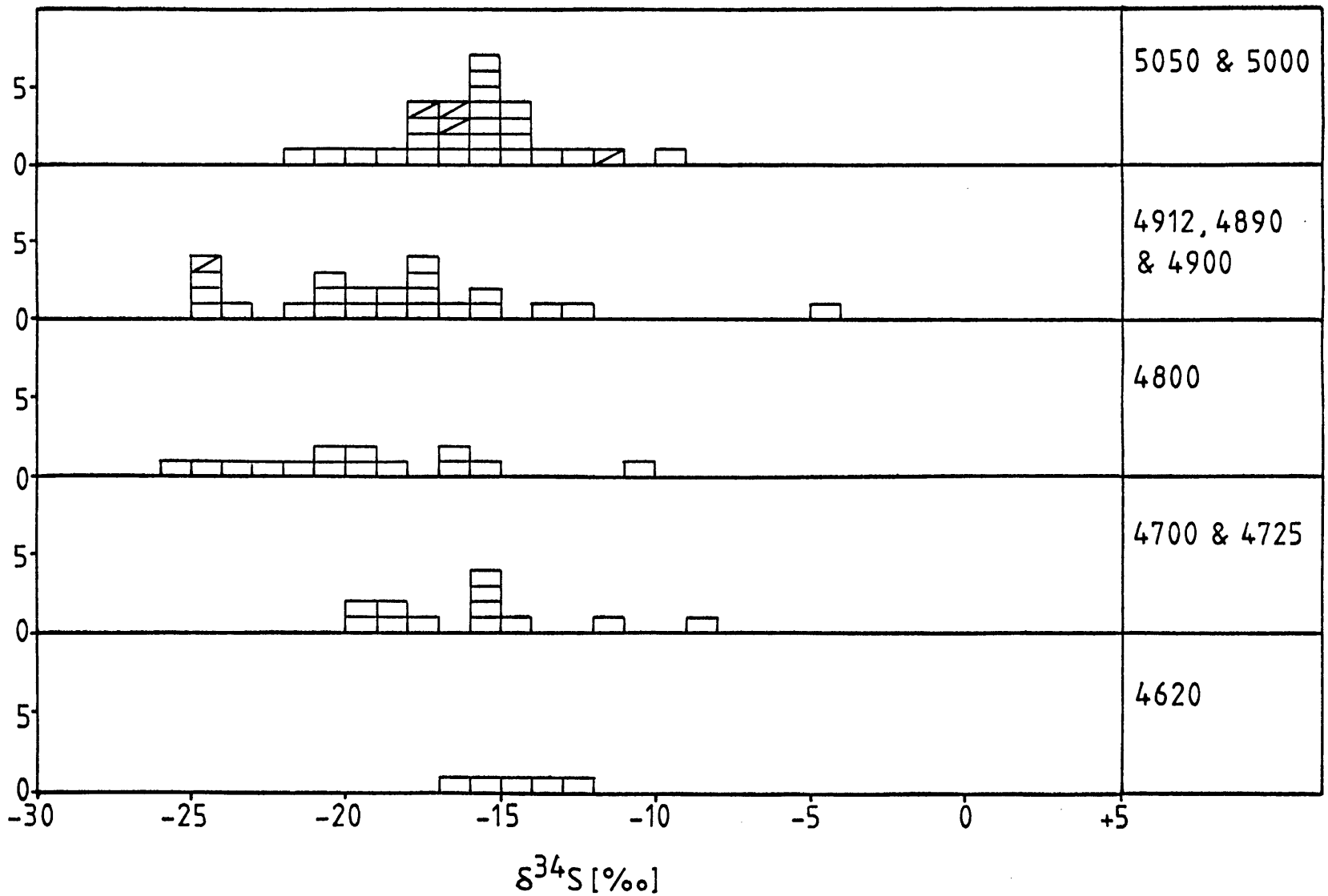

FIG.6.9 $\delta^{34}S$ OF STAGE 2 SULPHIDES v DISTANCE FROM FAULT.

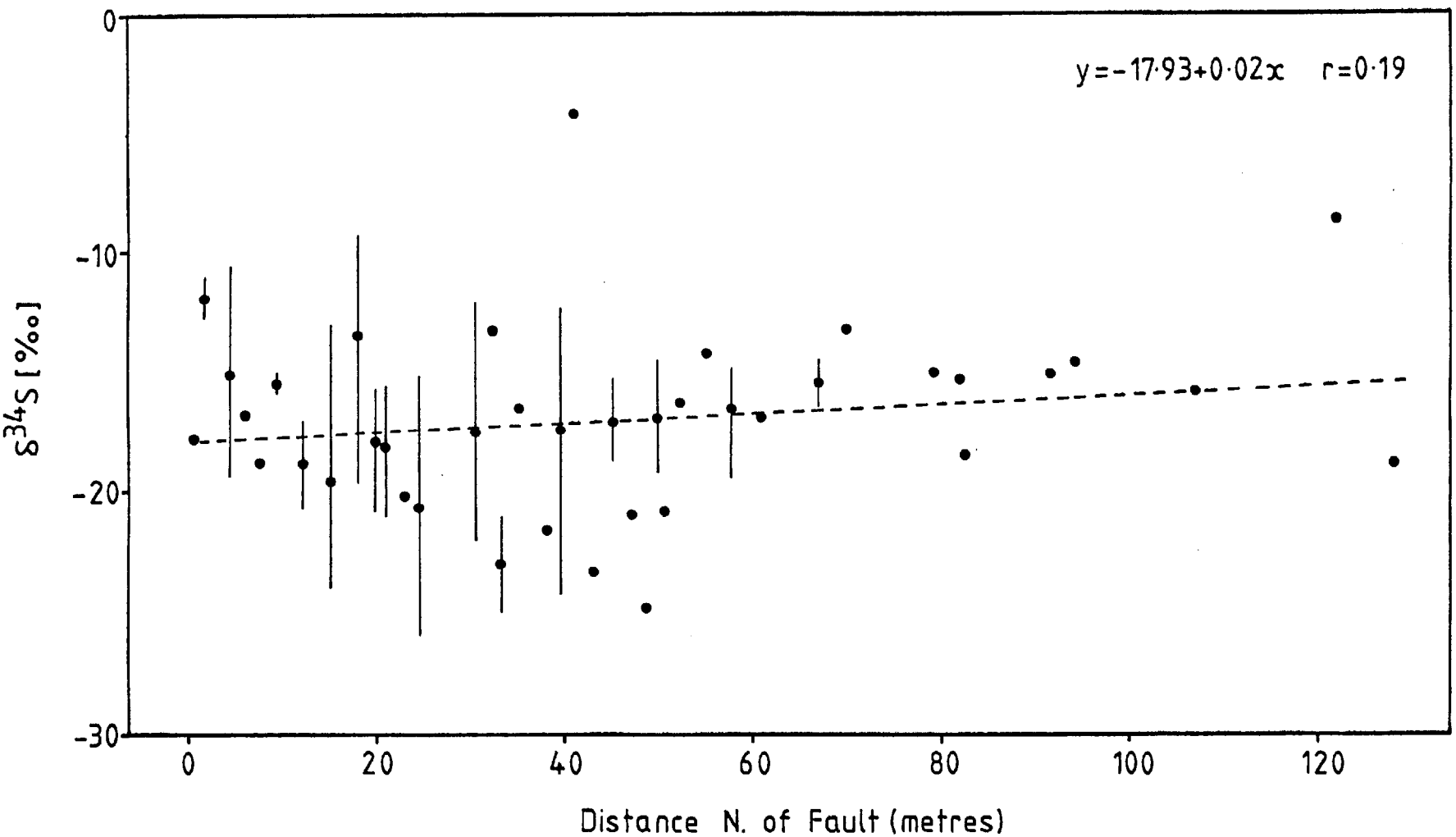

FIG.6.10 LATERAL VARIATION IN $\delta^{34}S$ OF STAGE 2 SULPHIDES.

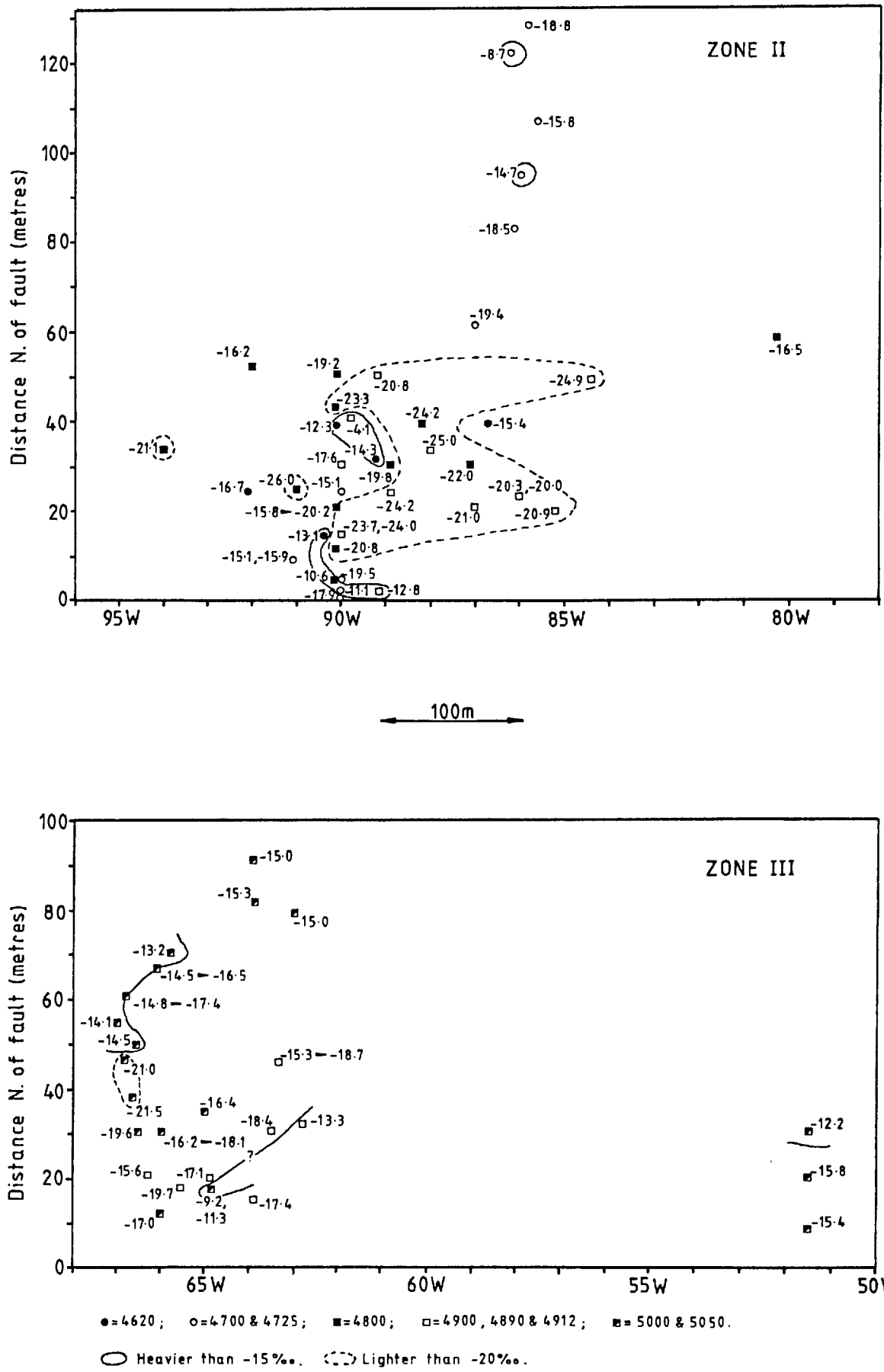

FIG.6.11 SULPHUR ISOTOPE VARIATION WITHIN BANDED STAGE 2 SEQUENCES.

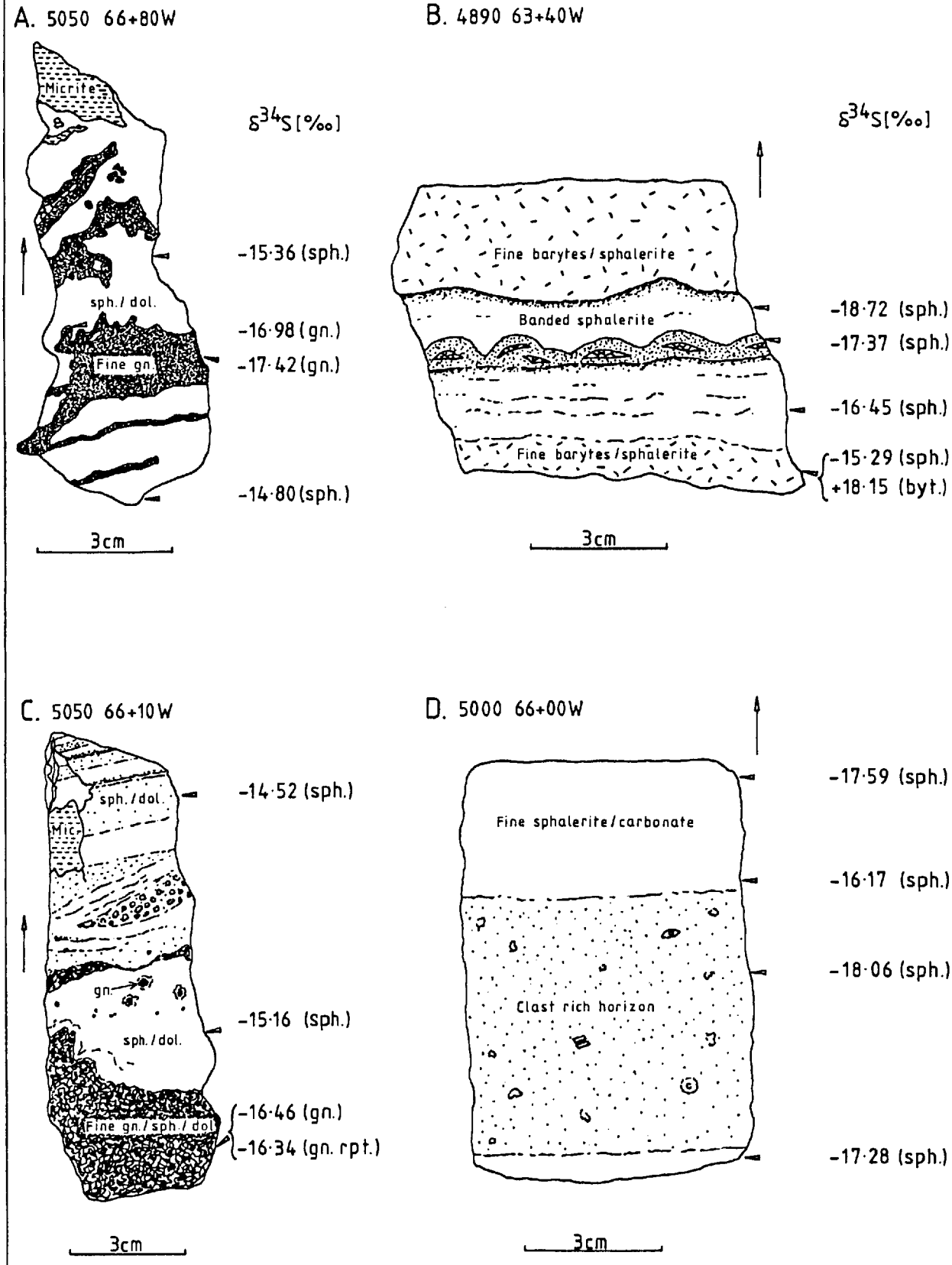

range of $\delta^{34}S$ values displayed by stage 2 sulphides could be produced by equilibrium fractionation between sulphate and sulphide over a temperature range of approximately 300°C to 100°C. However, if this were the case, one would expect to observe a zonation in sulphur isotope ratios with respect to a feeder zone, fractionation factors increasing as hydrothermal solutions cooled on permeation outwards into the host rock. The Tynagh fault provides the most likely candidate for such a feeder zone, and as can be seen from examination of fig. 6.9 and 6.10, isotopic variation is highly sporadic and unrelated to distance from the fault. Similarly, if the partitioning of sulphur between oxidised and reduced species in response to changing physico-chemical conditions were the cause of variation, one would expect this variation to be more systematic, and there would be a corresponding range in the isotopic comosition of co-precipitated barytes.

In consideration of the above discussion, precipitation of stage 1 and 2 sulphides from bacterially reduced contemporaneous sea-water sulphate seems highly probable. During stage 1 environmental conditions, namely temperature, sulphate concentration, availability of suitable nutrients and rate of sulphate reduction must have remained constant so as to maintain a stable physiological state, and hence consistent kinetic fractionation effect within the bacterium cells. However, the difference in the extent of the kinetic isotope effect during stage 2 as compared to that pertaining during stage 1 suggests that there were fundamental environmental dissimilarities between the two stages. Consideration of the possible sites of sulphate reduction may resolve the problem.

In chapter 3 it was argued on textural grounds that stage 1 colloform and granular pyrite crystallised from colloidal gels during the early diagenetic history of the Waulsortian limestones. If this is so, an explanation has to be proposed for the initiation and preservation of localised reducing conditions within these otherwise rather pure carbonate muds soon after their sedimentation, thus enabling the establishment and continued support of sulphate reducing anaerobes. Lees (1964) attributed the growth of the Waulsortian banks to the sediment baffling action of organisms, possibly plants or sponges, and the formation of stromatactis cavities to subsequent collapse following decay of the organic baffles. Local conditions of rapid burial of the Waulsortian micrites under thicknesses of synsedimentary slump breccias, which are abundant at Tynagh, would have been favourable to the preservation of such organic matter until buried below the oxidation/reduction interface. This trapped organic matter may have provided the locus for subsequent bacterial reduction and hence precipitation of iron sulphides during early diagenesis. Indeed, the replacement of crinoid ossicles by diagenetic pyrite has been described and it was suggested that the dark discolouration of the carbonate enclosing colloform and granular pyrite bodies may be due to the presence of minute hydrocarbon inclusions (3.2.2). In addition, this hypothesis would further explain the paucity of stromatactis structures within the Tynagh micrites (Schultz, 1968; Whitehead, 1971), the undecayed organic matter and subsequent iron sulphide precipitations preventing the establishment of cavity systems.

The above mechanism could explain the small

volumes of reduced sulphur involved in the precipitation of stage 1 sulphides. However it is difficult to envisage how such a process would produce the vast amounts required for the precipitation of the ore sulphides of stage 2. Indeed, Anderson (1975), points out that an orebody represents a concentration of reduced sulphur much too great to have been at the site of deposition before the advent of metal-bearing brine, which implies that there must be transport not only of metal but also of sulphur to the site of deposition. It may be possible that diffusion of reduced sulphur out of the bioclastic and shaley Lower Limestones and/or the carbonaceous basinal Calp (both ideal environments for reduction of contemporaneous sea-water sulphate) has taken place. Indeed, the similarity in isotopic composition of stage 2 ore sulphides and syngenetic/diagenetic pyrite from the Lower Limestone is suggestive of a common source of sulphur. Differences in the degree of the kinetic isotope effect between stage 1 and stage 2 sulphides could be explained by differences in the sedimentary regime at the sites of reduction. High rates of sedimentation within the Waulsortian bank system suggested above would lead to rapid rates of sulphate reduction and correspondingly a relatively small kinetic isotope effect (see figs. 6.3, 6.4). Conversely, comparatively slower rates of sedimentation within the thinly bedded lagoonal and basinal facies limestone and shales would lead to slower rates of sulphate reduction and hence a relatively large kinetic isotope effect. Although no independent evidence can be presented in support, spatial variations in $\delta^{34}S$ within individual banded sulphide sequences may be a reflection of geographical or secular variations in reducing conditions within the source region.

Although the above hypotheses are compatible with the sulphur isotope data, it has to be considered whether they are geologically feasible. The comparatively narrow, approximately normal distributions in isotopic compositions of both stage 1 and stage 2 sulphides, and the small spread of values for barytes, are indicative that sulphate reduction took place within an open system in which there was an infinite source of sulphate. Therefore, the permeability of the sediment within which bacterial reduction took place must have been great enough to allow the diffusion of the sulphate and so prevent the establishment of local closed systems. It is generally known that carbonate sediments are subject to lithification early in their burial history (Hunt, 1967), and Ginsburg (1957) has pointed out that most of the water in carbonate muds is lost in the first half metre or so. As permeability will decrease with increasing lithification, it is more likely that free diffusion of sulphate through the Waulsortian micrites would have occurred at shallow depths during early diagenesis. In addition, Lindbloom and Lupton (1961) observed that bacteria living on the organic matter in carbonate muds from Florida and Cuba practically died out within the first metre and a half of sediment. It would seem, therefore, in close agreement with textural observations, that sulphate reduction during stage 1 most probably occurred within the upper few metres of the Waulsortian micrites during their early diagenetic history.

If reduction only took place within the top one and a half metres of the lagoonal/basinal sediments, how would any reduced sulphur have migrated into the Waulsortian bank system ? The presence of a large detrital component within these sediments

manifested as numerous intercalated shale horizon may have aided the preservation of both a bacterial population and permeability to greater depth, viable bacteria having been found to depths of 45 metres in clay muds from the Orinoco Delta (Lindbloom and Lupton, 1961). Trapped sea-water sulphate migrating through the bioclastic limestone/limestone shale sequence during de-watering or permeating down from the sediment/water interface could have been reduced by contained bacteria, and assuming that the hydro-geologic situation was right, diffused into any suitable reservoir. As long as only an infinitesimal amount of the sulphate was reduced, the sulphate reservoir would retain its isotopic integrity, and movement of fluids through the system would aid the migration of any reduced sulphur not precipitated in situ.

Alternatively, in both the bank and off bank environments, sulphate reduction could have taken place at shallow depths, the resultant H_2S being trapped within the sediment on burial to be released and utilised at a later date. Indeed, Hunt (1967) states that in pure carbonates relatively free of iron, there is a build-up in H_2S content which remains in the sediment even at great depths. However, within the lagoonal and basinal limestones and shales any resident H_2S would probably be precipitated by iron associated with clay minerals, and in such a static environment closed systems would develop within sediment interstices.

If the deduction that stage 1 sulphides were precipitated by H_2S produced by in situ bacterial reduction is correct, then this imposes strict limitations on the temperature of their deposition. Optimum temperatures for microbial reduction of sulphate are between 30 and 45°C, and their activity is believed

to be reduced drastically at temperatures above 60°C (Orr, 1974), although Zo Bell (1963) reported some strains which survive temperatures up to 104°C. However, no such constraints are placed on stage 2 if, as is suggested, reduced sulphur was not generated in situ.

6.2.2.3 Stage 3

Stage 3 sulphides display a distinct variation in $\delta^{34}S$ with respect to the Tynagh fault (fig. 6.13), thus a mechanism solely involving bacterial reduction cannot adequately explain the observed distributions. Equilibrium fractionation between sulphate and sulphide over a temperature range of 730°C to 155°C could produce the observed range in isotopic compositions. However, such a temperature range is geologically unrealistic, and fluctuations in $\delta^{34}S$ are too sporadic. An explanation involving the partitioning of sulphur between oxidised and reduced species in response to changing physico-chemical conditions is precluded by the narrow range of $\delta^{34}S$ values displayed by barytes. The mixing of two sources of sulphur, therefore, seems to be the only plausible hypothesis, isotopically heavier sulphur being introduced along with stage 3 metals from the fault zone, mixing with light bacteriogenic sulphur already present within the host, or migrating into the host from other sedimentary facies. Examination of fig. 6.15 reveals that there is an off-bank trough that may have influenced the migratory paths of solution diffusing out of the limestone/shale sequence into the Waulsortian complex. Indeed, this may account for the bulge in this region of isotopically lighter sulphides towards the fault plane.

The derivation of light sulphur from pre-existing sulphide phases is unlikely as even where stage 3 sulphides can be seen to be replacing earlier pyrite or sphalerite, their isotopic compositions are often markedly different. For example at 84+40W, 4900 level, galena (S641) is 13.5°/oo heavier than the pyrite (S627) which it has replaced (table 6.1).

The trend in $\delta^{34}S$ values of stage 3 sulphides towards 0°/oo as the fault is approached points to an influx of deep-seated sulphur. However, sulphide samples collected from within the actual fault plane, the most likely uncontaminated representatives of the isotopic composition of the heavy source, have $\delta^{34}S$ values of +7.02°/oo and +11.13°/oo. It is unlikely that such heavy values could be produced under geologically reasonable conditions from a sulphur source with a $\Sigma\delta^{34}S$ of 0°/oo, simply by variations in pH and fO_2. Nevertheless, the fractionating effect of closed system precipitation under equilibrium conditions as the solution rose from depth could have enriched the deep-seated sulphur in the heavier isotope.

An alternative process that may possibly produce isotopically heavy reduced sulphur involves the abiogenic reduction of sea-water or connate sulphate. Toland (1960) has shown that reduction of sulphate by various organic compounds is very rapid at temperatures of 300 to 350°C when H_2S is present in the system. Orr (1974) suggests that thermal maturation of oil in high temperature reservoirs (>80-120°C) may involve non-microbial reduction of sulphate with negligible isotopic fractionation. However, this proposal is purely conjectural, being based on the presence of heavy sulphur in mature oils isotopically similar to associated

FIG.6.12 VARIATION IN $\delta^{34}S$ OF STAGE 3 SULPHIDES WITH ELEVATION.

Key as for fig.6.7 ; DDH samples E. of Zone III omitted.

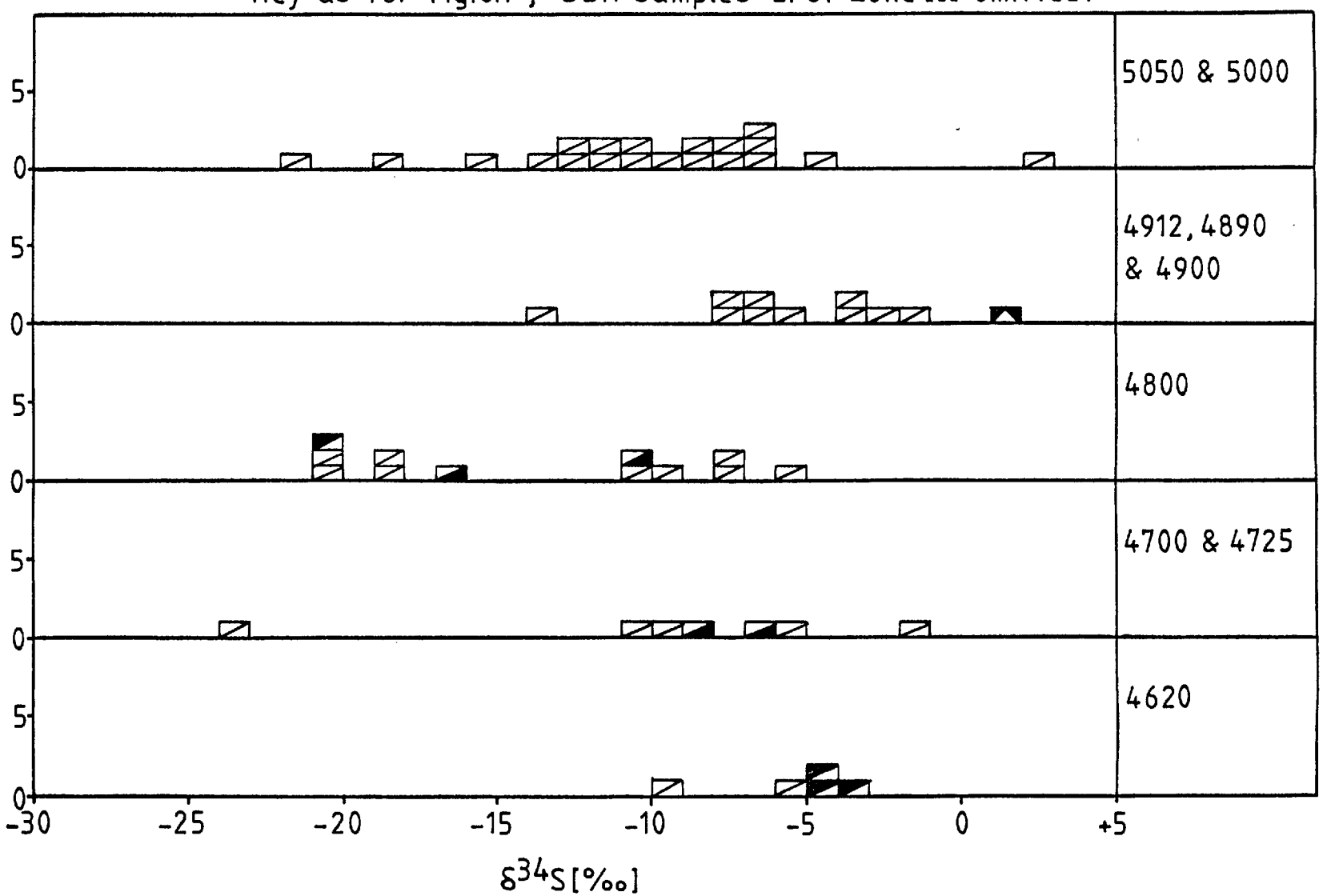

FIG.6.13 $\delta^{34}S$ OF STAGE 3 SULPHIDES v DISTANCE FROM FAULT.

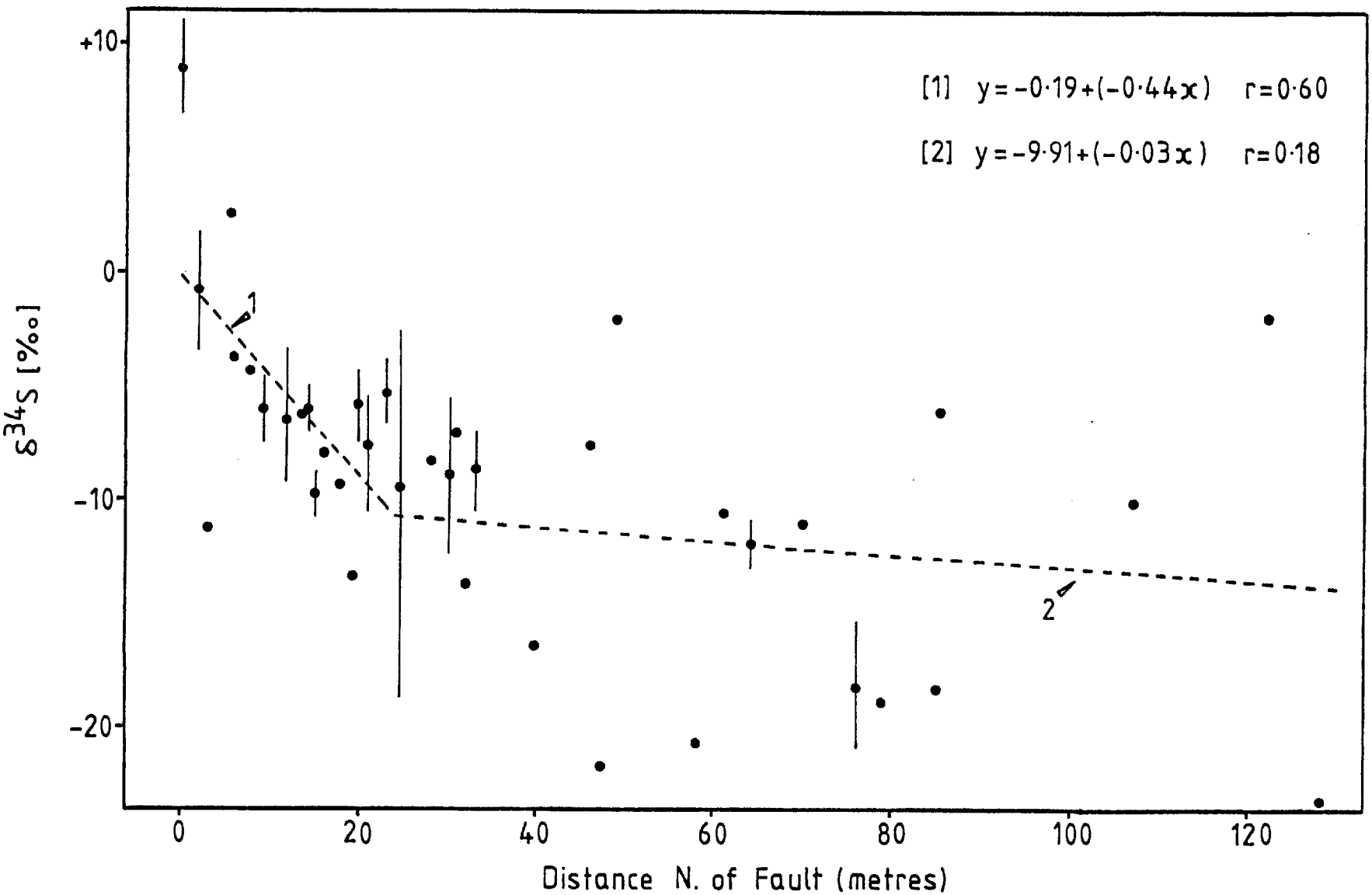

FIG.6.14 LATERAL VARIATION IN $\delta^{34}S$ OF STAGE 3 SULPHIDES.

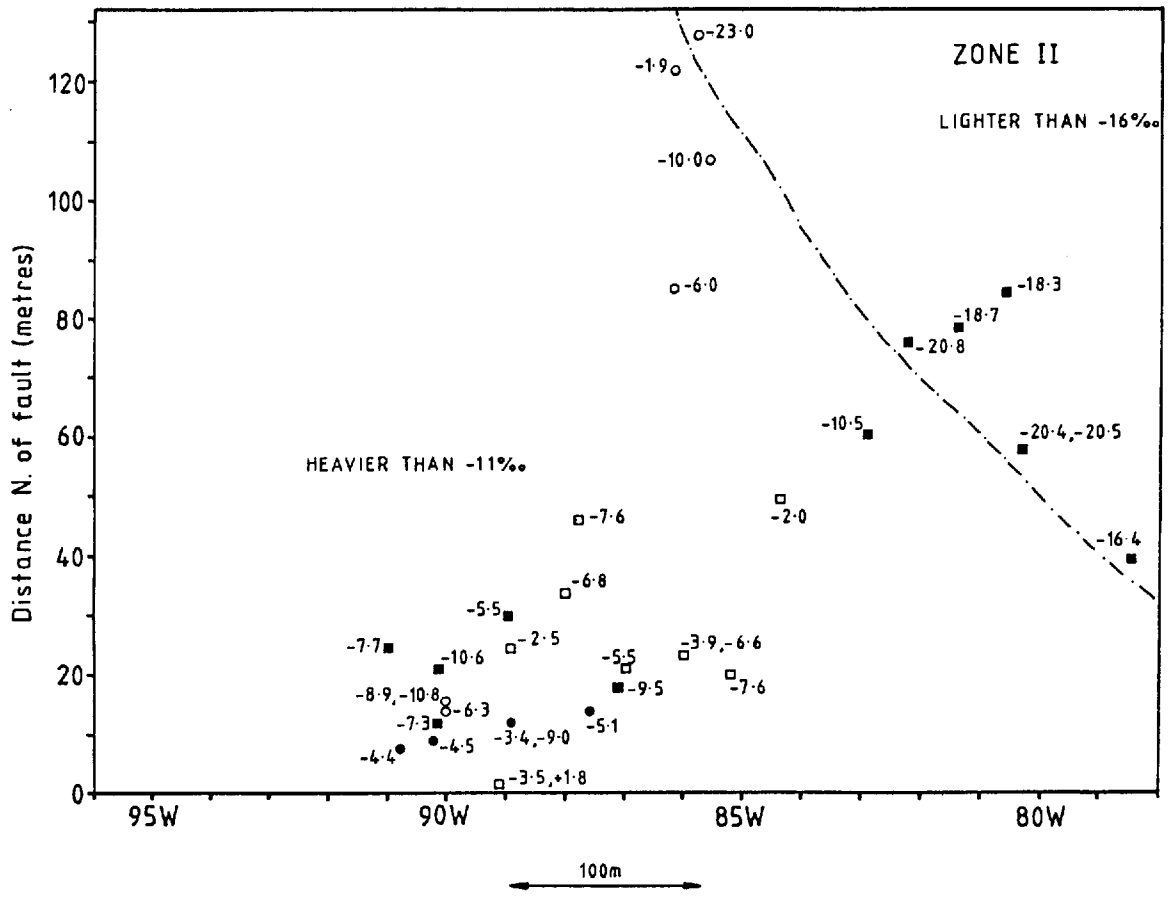

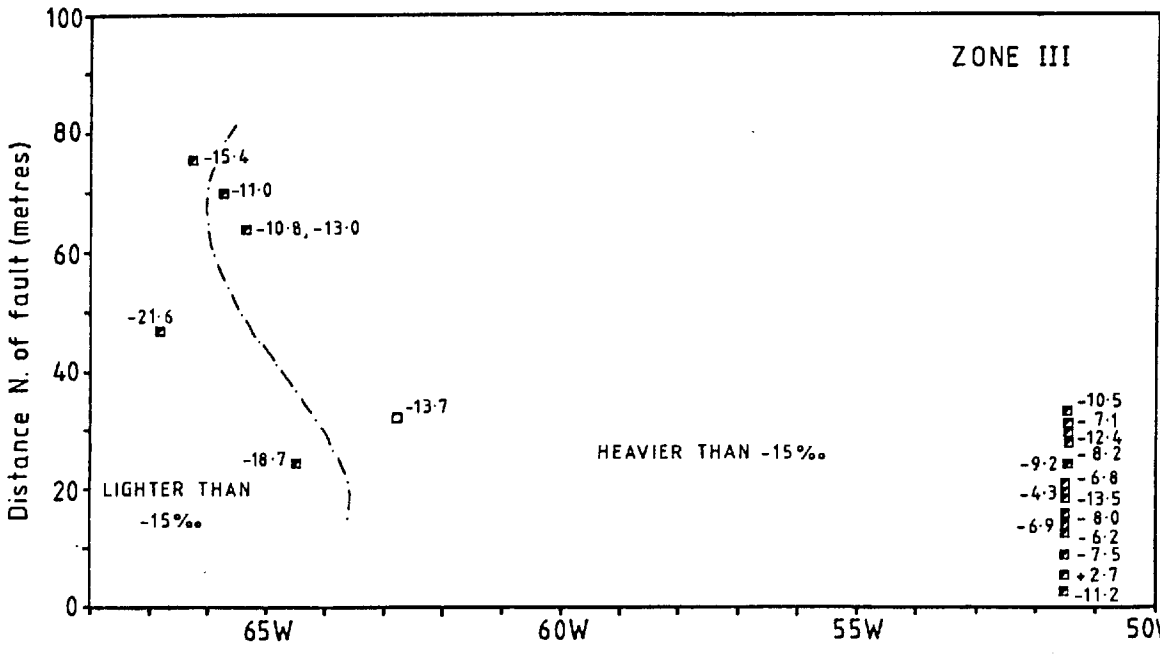

Key as for FIG. 6.10

FIG. 6.15 RELATIONSHIP BETWEEN $\delta^{34}S$ OF STAGE 3 SULPHIDES AND OFF-BANK TROUGH.

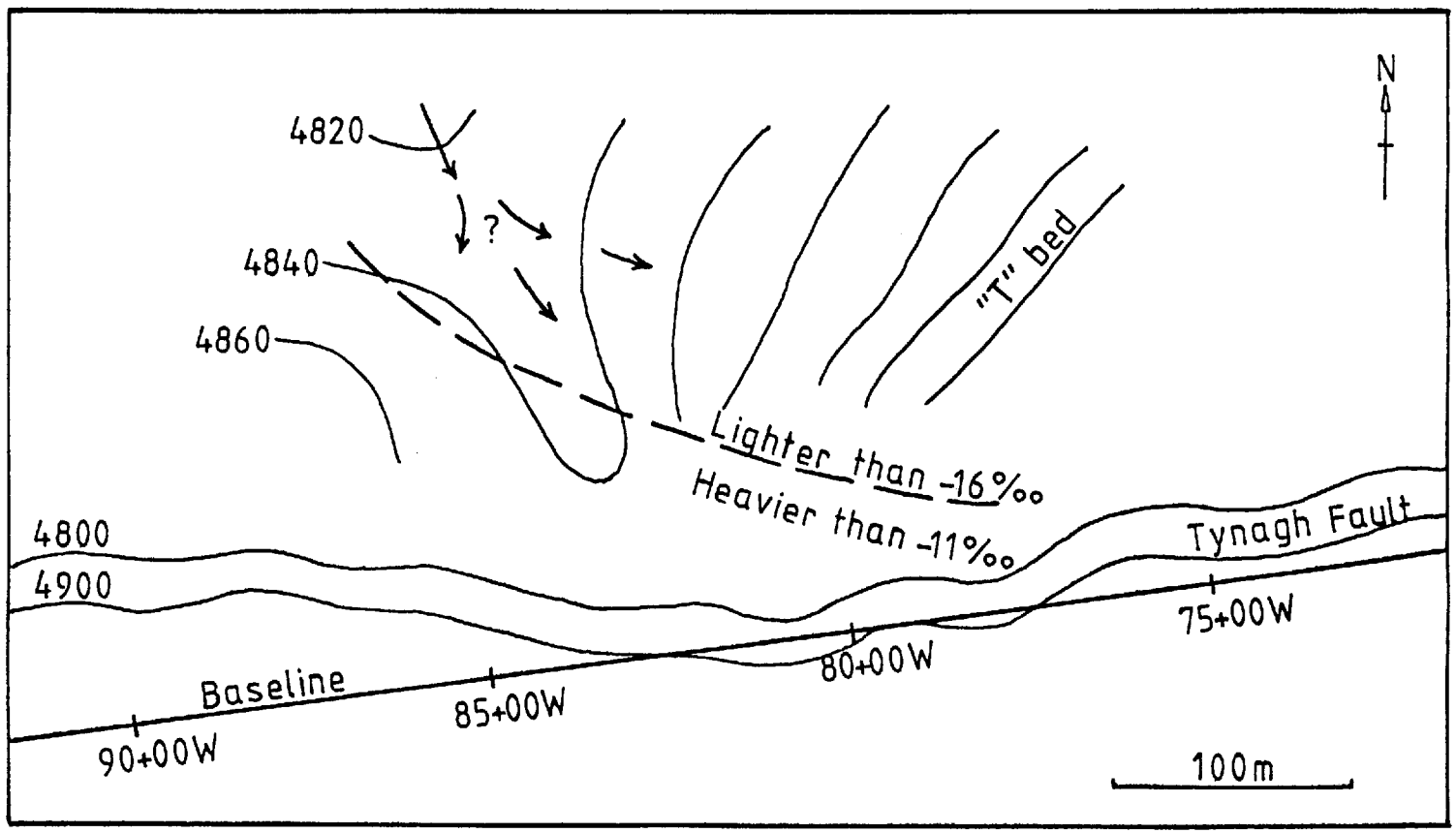

——$\delta^{34}S$ boundary projected to 4800 level.

⟶ Postulated migration paths of bacteriogenic sulphur.

Structure contours from Schultz, 1968.

sulphates. Nevertheless, it may be possible that sulphate diffusing through and being reduced by carbonaceous sediments at depth could have provided a source of isotopically heavy reduced sulphur. If this were the case though, one would expect to see sulphides with $\delta^{34}S$ compositions close to that of the source sulphate. It is therefore concluded that the heavier sulphur introduced from the fault zone was of deep-seated origin.

The introduction of sulphur from the fault zone along with the metals has important implications with regard to the chemistry of the ore fluid. The solubility data presented by Anderson (1973, 1975) and Hammann and Anderson (1978) indicates that at temperatures of up to 150°C, reduced sulphur and lead can only be transported together if the solution is quite acid (see 3.8.4). Although the available temperature data is at best scanty, a temperature of less than 150°C is suggested for stage 3 precipitation (see 7.4). Moreover a decrease in the pH of the ore fluids would explain the greater abundance of replacement textures, and the comparative paucity of carbonates in stage 3 intergrowths.

6.2.2.4 Stage 4

It was stated above that the sulphides recrystallised into post-ore carbonate veins have retained the isotopic identity of the parental primary ore. The uniformity of fractionation factors between co-precipitated sphalerite and galena indicates that isotopic exchange must have occurred during recrystallisation. However, as the calculated temperatures are far in excess of those indicated by the preliminary fluid inclusion investigation equilibrium could not have been completely attained (see 3.7.1).

The dissimilarity in isotopic composition of chalcopyrite overgrowing late stage dolomite, from that of the primary ore stage sulphides in the immediate vicinity does not support a derivative origin.

The post-ore gypsum is isotopically heavier than ore stage barytes, possibly indicating a different source of sulphate or alternatively late stage, closed system kinetic fractionation.

6.3 COMPARISON WITH OTHER MAJOR DEPOSITS

6.3.1 Navan

A limited number of sulphur isotope analyses were carried out on banded sulphide ores from the Navan deposit (table 6.4) which, although of similar mineralogical composition and textural appearance to Tynagh stage 2 sulphides, have been precipitated in a different environment and are possibly slightly earlier in age (see chapter 4). The analyses presented here can only be regarded as constituting a pilot study and any inferences drawn must be considered tentative.

Sulphides (+2.93°/oo to -23.75°/oo) and barytes (+19.63°/oo, +22.56°/oo) display similar values and ranges to their counterpart at Tynagh. An origin involving the bacteriogenic reduction of Lower Carboniferous sea-water sulphate is, therefore, possible. The slightly heavier value for one of the barytes samples could be a product of localised closed system reduction. The lighter sample (+19.63°/oo) was collected from a stratiform horizon interbanded with microcrystalline sphalerite, whilst the isotopically heavier sample infilled a late stage cavity within pre-existing sphalerite, and could

TABLE 6.4 SULPHUR ISOTOPE RESULTS – NAVAN

Extraction No.	Location	Mineral	$\delta^{34}S$ (°/oo)
S1239	2–5 Lens, 835.7 N.W., 494.8 N.E., 1388 El, 83 m. from 'B' Fault	sphalerite	+ 2.93
S1250	" " " " "	galena	– 2.30
S1241	2–5 Lens, 826.2 N.W., 492.7 N.E., 1350 El, 90 m. from 'A' Fault	sphalerite	– 8.99
S1267	" " " " "	barytes	+22.56
S1242	2–5 Lens, 837.7 N.W., 483.0 N.E., 1398 El, 3 m. from 'A' Fault	sphalerite	–14.38
S1240	2–5 Lens, 846.8 N.W., 496.8 N.E., 1388 El, 5 m. from 'B' Fault	"	–12.08
S1252	2–5 Lens, 841.7 N.W., 495.2 N.E., 1375 El, 45 m. from 'B' Fault	"	–14.52
S1243	2–4 Lens, 822.5 N.W., 498.0 N.E., 1348 El, 110 m. from 'B' Fault	"	– 1.77
S1266	" " " " "	barytes	+19.63
S1244	2–3 Lens, 820.0 N.W., 500.6 N.E., 1347 El, 100 m. from 'B' Fault	sphalerite	–23.75
S1245	2–1 Lens, 812.0 N.W., 503.9 N.E., 1378 El,	"	– 8.01
S1246	145 m. from 'B' Fault	"	– 3.92

have been precipitated from sulphate trapped within the sulphide sediment. Alternatively, the sulphur isotopic composition of sea-water sulphate at the time of formation of the Navan deposit may have slightly differed from that of sea-water contemporaneous with the Tynagh deposit. Indeed, extrapolation from fig. 6.1 would suggest Tournaisian sea-water was heavier than Visean sea-water.

6.3.2 Silvermines

The Silvermines deposits have been the subject of a number of individual sulphur isotope investigations, all of which arrived at widely different conclusions. Graham (1970) as part of a much broader geological study produced a limited number of analyses, mostly from the Mogul G orebody and concluded that the sulphides were precipitated from bacterially reduced Lower Carboniferous sea-water sulphate. Greig et al (1971) made a more systematic collection and demonstrated a progressive decrease in δ values of sulphides, upwards in the Lower G orebody, and outwards into Upper G orebody, from around $0^{o}/oo$ to $-35^{o}/oo$. They favoured a model involving equilibrium deposition of sulphides and sulphates, from a mineralizing fluid originating at depth, under conditions of progressively increasing fO_2 and pH, and decreasing temperature. In conflict with the geological evidence, this implied an epigenetic origin for all the Silvermines deposits. Coomer and Robinson (1976) in an attempt to reconcile these differing interpretations extended the data coverage and proposed a model involving the mixing of deep-seated sulphur ($\sim 0^{o}/oo$) introduced from the fault zone, and bacterially reduced sea-water sulphate.

The Coomer and Robinson model is clearly comparable with that

FIG.6.16 SUMMARY OF SULPHUR ISOTOPE ANALYSES FROM THE SILVERMINES DEPOSITS.

(After Coomer & Robinson, 1976)

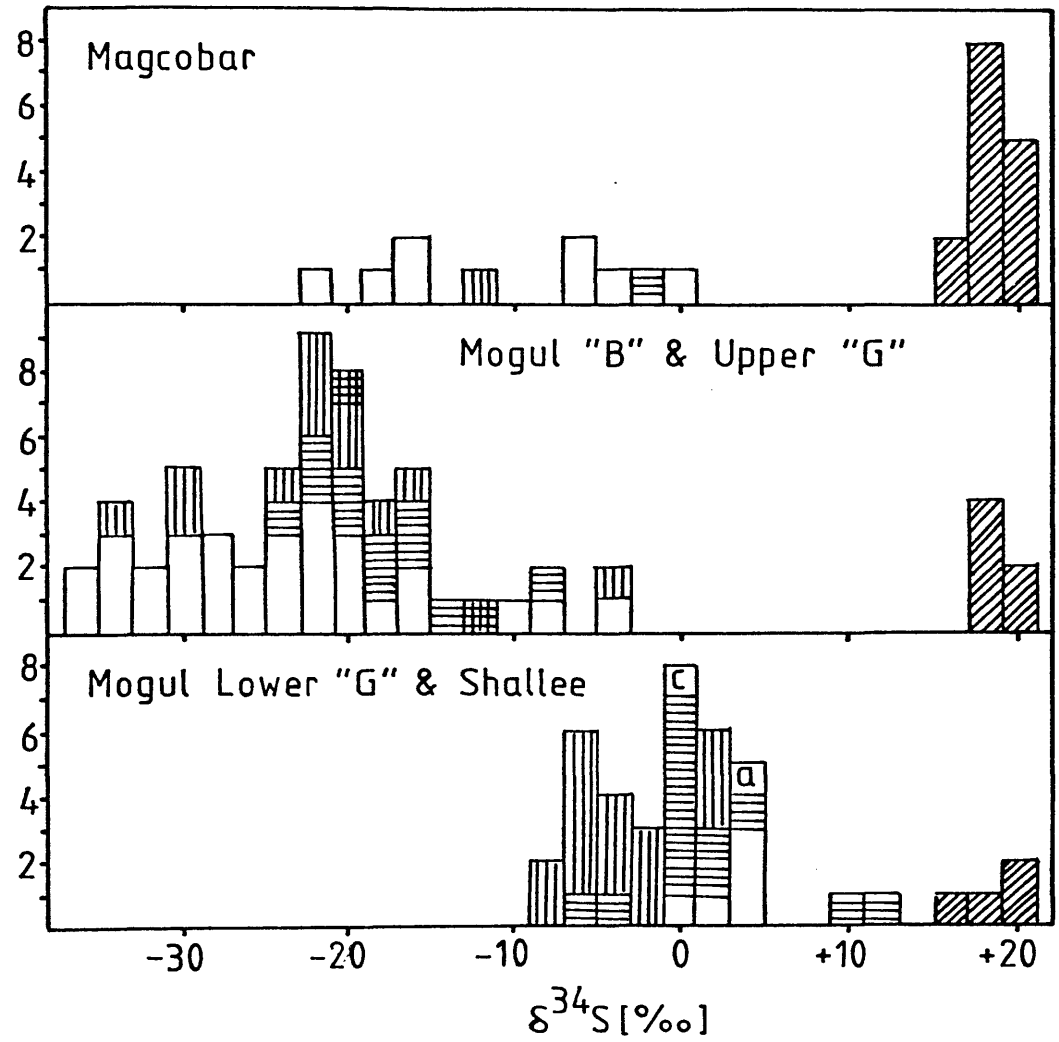

barytes
pyrite
c chalcopyrite
a arsenopyrite
sphalerite
galena
sphalerite & galena

proposed above for Tynagh, and provides further support for a genetic link between them.

A summary of previously published sulphur isotope data from the Silvermines deposits is presented in figure 6.16.

6.4 CONCLUSIONS

$\delta^{34}S$ values of barytes precipitated during stages 2 and 3 at Tynagh are indicative of a Lower Carboniferous sea-water source for the sulphate ($\delta^{34}S \simeq +19^{o}/oo$). Stage 1 sulphides were precipitated by reduced sulphur produced during in situ open-system bacterial reduction of this sulphate reservoir during the early diagenesis of the Waulsortian bank limestones. Reduced sulphur generated by the same mechanism and from the same sea-water sulphate source, but within the lagoonal facies Lower Limestones and/or the basinal Calp, migrated into the Waulsortian carbonate mud banks and precipitated stage 2 sulphides. Differing sedimentological regimes operating at the two sites of bacterial reduction were fundamental in controlling the metabolic state and thus the degree of the kinetic isotope effect within the bacterium cell.

The range and spatial distribution of sulphur isotope compositions displayed by stage 3 sulphides are indicative of the late stage mixing of deep-seated sulphur introduced from the Tynagh fault zone, and isotopically light sulphur already present or migrating into the Waulsortian Limestones. The transport of reduced sulphur and metals together to the site of ore deposition probably indicates that stage 3 metalliferous fluids were quite acid.

Sulphides recrystallising into post-ore carbonate veins (stage 4) retained the isotopic identity of the parental primary ore.

Although fractionation factors between co-existing sphalerite-galena pairs are fairly consistent, the inferred temperatures are far in excess of those suggested by preliminary fluid inclusion investigations. It is suggested that isotopic equilibrium was not completely attained.

A pilot study of banded stratiform ores from the Navan deposit indicates their precipitation from bacterially reduced Lower Carboniferous sea-water sulphate. However, further work is needed to refine the model.

Comparison of the new sulphur isotope data from the Tynagh deposit with previously published analyses from Silvermines provides further support for a genetic link between these two major ore-bodies.

CHAPTER 7

CARBON AND OXYGEN ISOTOPES

7.1 THE MAJOR CARBON RESERVOIRS AND CONTROLS ON VARIATION

The important reservoirs of carbon are deep-seated sources (mantle or homogenised crust), limestones, organic matter in sedimentary rocks and the biosphere.

Deep-seated carbon is considered to have a uniform isotopic composition of around $-7^{o}/oo$ with respect to PDB. The basis of this supposition is that fresh, unaltered carbonatites display a narrow range in $\delta^{13}C$ of -5 to $-8^{o}/oo$ (Taylor et al, 1967). In addition, CO_2 rich inclusions within low-alumina tholeiitic glasses collected from the mid-Atlantic Ridge have been shown to have an isotopic composition of $-7.6 \pm 0.5^{o}/oo$, (Pineau et al, 1976).

The average carbon isotopic composition of normal marine carbonates has remained fairly uniform through geological time, at around $0^{o}/oo$ (Keith and Weber, 1964; Veizer and Hoefs, 1976).

The isotopic composition of carbon within the biosphere varies considerably, the total range being approximately $0^{o}/oo$ to $-35^{o}/oo$ (Schwarcz, 1969). However, organic carbon in sedimentary rocks has a more restricted range of $\delta^{13}C$ values of around $-25^{o}/oo$ (Eckelmann et al, 1962), and is a potential source of isotopically distinct CO_2. In low temperature environments where bacterial reduction of sulphate or bacterial oxidation is occurring, CO_2 is produced from the organic matter which is consumed as an energy source. This process is generally considered to be non-fractionating, therefore any carbonate phase that has incorporated bacterially

oxidised organic matter will be depleted in ^{13}C. However, the process of bacterial fermentation in which both CH_4 and CO_2 are produced, imposes very large fractionations, values of $-75^{o}/oo$ being common for bacterial methane (Claypool et al, 1973). Consequently CO_2 produced by the reaction will be enriched in ^{13}C with respect to the source organic matter. There is no reliable data as to the isotopic composition of CO_2 produced in this manner; however Irwin et al (1977) estimate a value of around $+15^{o}/oo$ to be reasonable.

In hydrothermal systems the isotopic composition of carbon bearing phases precipitated from solution is controlled by the chemistry of the fluid (Ohmoto, 1972). The principles of the application of carbon isotope data to hydrothermal deposits are similar to those for sulphur (see chapter 6). There are large equilibrium fractionations between reduced and oxidised carbon species and the abundance of these species in solution is largely a function of temperature, pH and fO_2 (fig. 7.1).

Carbon isotope fractionation amongst the various carbonate species (HCO_3^-, CO_3^{2-} and calcite) is not well established, but theoretical considerations indicate that they are small (1 or $2^{o}/oo$), and almost independent of temperature between 0 and $400^{o}C$. However, there are large temperature dependent fractionations between the above species and CO_2/H_2CO_3 (fig. 7.2). As the relative abundances of the various oxidised species in solution is controlled largely by temperature and pH, large ranges in isotopic compositions can be obtained by varying both or either of these parameters alone.

7.2 OXYGEN ISOTOPE VARIATION IN THE DOLOMITE-CALCITE - WATER SYSTEM

The oxygen isotope composition of any carbonate precipitated

FIG.7.1 VARIATION OF $\delta^{13}C$ AS A FUNCTION OF fO_2 & pH. (After Ohmoto, 1972)

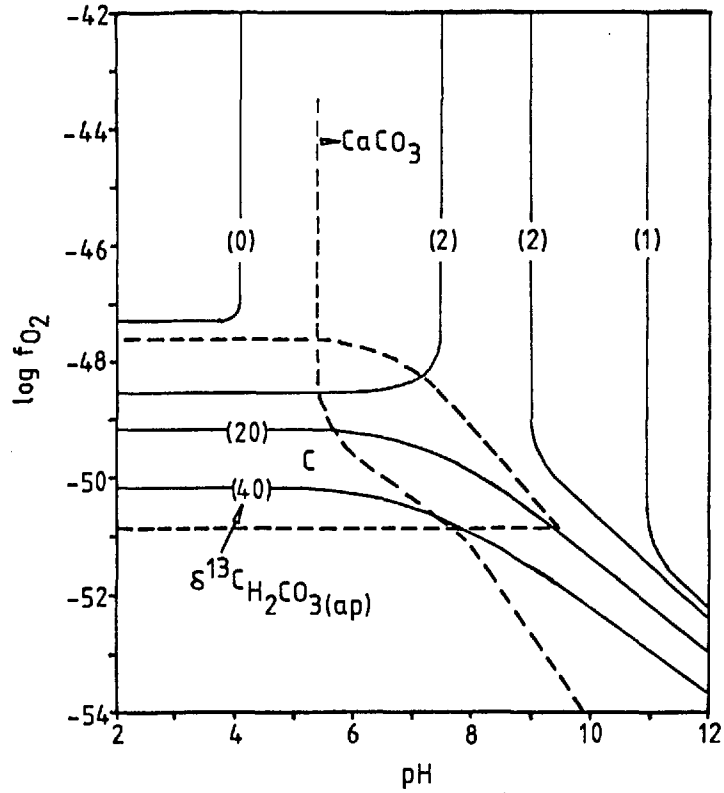

T=150°C ; Ionic strength=1molar ; $\Sigma\delta^{13}C$=0‰ ; $H_2CO_{3(ap)}=CO_{2(aq)}+H_2CO_3$.

——:Stability boundaries for calcite & graphite at ΣC=0·1moles/kg H_2O.

FIG.7.2 ISOTOPIC ENRICHMENT FACTORS FOR IMPORTANT CARBON SPECIES. (After Ohmoto, 1972)

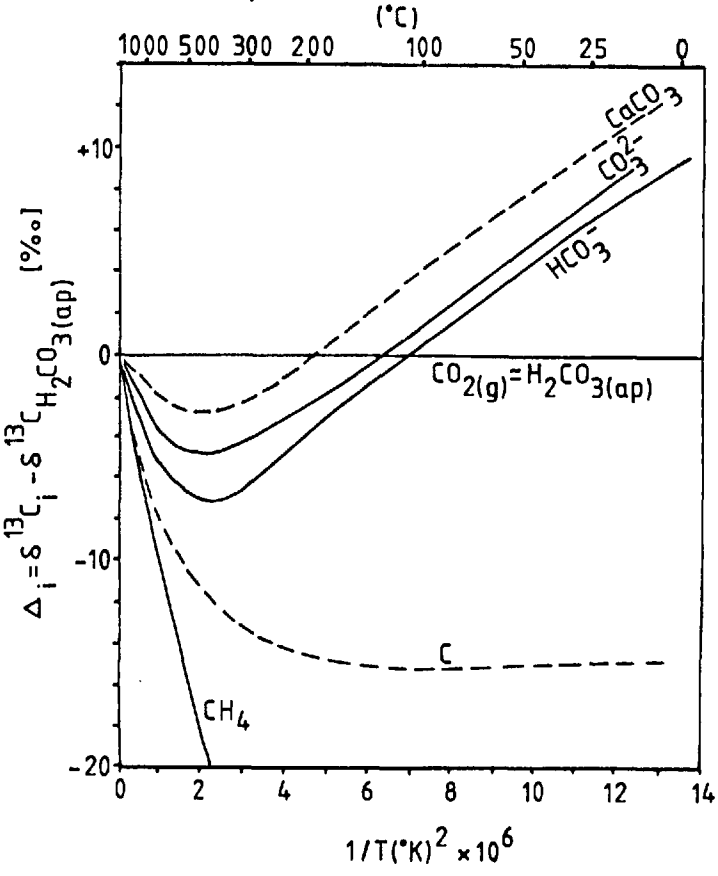

in isotopic equilibrium from a liquid depends on the oxygen isotope composition of that liquid, and the temperature of formation.

At low temperature, oxygen isotope equilibrium fractionations between carbonate phases and water are considerable (fig. 7.3), and large variations in $\delta^{18}O$ can be produced by changes in temperature alone. A decrease in the $^{18}O/^{16}O$ ratio exhibited by successive generations of carbonate precipitated from water of the same isotopic composition indicates an increase in temperature. For example at 25°C, calcite precipitated in equilibrium with water which has an isotopic composition of 0°/oo (SMOW), will have a $\delta^{18}O$ value of +28.8°/oo (SMOW). At 100°C, calcite precipitated in equilibrium with the same water will have a $\delta^{18}O$ value of 16.6°/oo (SMOW). Oxygen isotope fractionation between dolomite and water is greater than that which occurs between calcite and water. Thus, if a calcite–dolomite pair can be demonstrated to have been precipitated in equilibrium, they can be used as an isotope geothermometer. However, this difference is small, and as a consequence calculated temperatures are very susceptible to analytical error. In addition, there are considerable discrepancies between the various published experimental fractionation factors. The enrichment factors in figure 7.3 are high temperature (>200°C) experimental calibrations, and have to be extrapolated to lower temperatures.

In palaeotemperature studies of fossil carbonates, the low temperature calibration of Epstein et al (1953), subsequently modified by Craig (1965), is used. Their experimental procedure involved oxygen isotope analysis of calcium carbonate from shells of invertebrates grown at known temperatures. The temperature coefficient of the calcite–water exchange reaction is:-

FIG. 7.3 DOLOMITE-WATER, CALCITE-WATER OXYGEN ISOTOPE FRACTIONATION FACTORS.

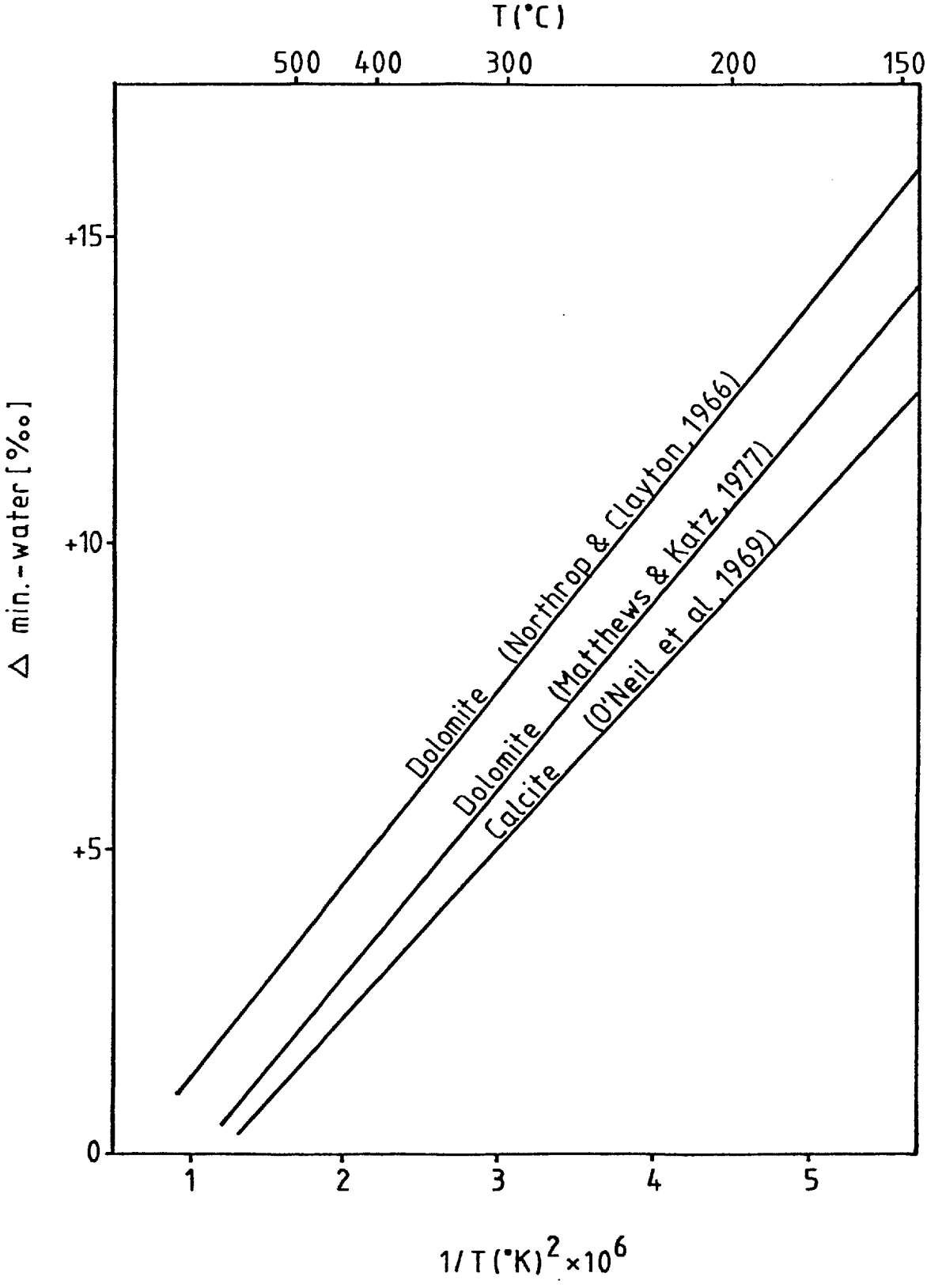

$$T(^{\circ}C) = 16.9 - 4.21\ (\delta c - \delta w) + 0.14\ (\delta c - \delta w)^2$$

where $\delta c = \delta^{18}O$ sample (w.r.t. PDB)

$\delta w = \delta^{18}O$ CO_2 in equilibrium with water at 25.2°C (w.r.t. CO_2/PDB).

A similar relationship has been proposed for low temperature oxygen isotope exchange between dolomite and water (Irwin et al, 1977):-

$$T(^{\circ}C) = 31.9 - 5.55\ (\delta d - \delta w) + 0.17\ (\delta d - \delta w)^2$$

Oceanic, magmatic, meteoric, geothermal and formation waters are all possible contributions to ore forming processes, and, in conjunction with H/D ratios, it is often possible to define the actual source or sources involved from the oxygen isotope composition of mineral phases or fluid inclusions. However, where hydrous phases are absent the problem becomes more difficult, as only one of the defining parameters is available.

The oceans at the present time have a very uniform oxygen isotopic composition of 0°/oo (SMOW) ±0.1°/oo. Small deviations from the norm occur in areas where evaporation is appreciable (up to +2°/oo) or where dilution by fresh waters has occurred (0 to -2°/oo), (Epstein and Mayeda, 1953). It is calculated that if all the world's ice caps melted, the $\delta^{18}O$ value of the oceans would be lowered by about 1°/oo (Taylor, 1974), and it is considered that at least throughout most of Phanerozoic time, the isotopic composition of the oceans may have fluctuated within these limits. However, marine limestones exhibit a progressive decrease in average ^{18}O content with increasing geologic age (Keith and Weber, 1964; Veizer and Hoefs, 1976). This has been interpreted as being due to increasing degrees of post-depositional oxygen isotope exchange, but recent work (M.L. Coleman - pers. comm.) suggests that this trend

may reflect variation in the oxygen isotope composition of the oceans with time.

Magmatic water is considered to have an isotopic composition of about +6 to +8°/oo (SMOW) (Taylor, 1974). As no water can be guaranteed to be uncontaminated magmatic water, this is a calculated value for water that would have co-existed with igneous minerals at magmatic temperatures.

Meteoric waters display a range in oxygen isotope compositions of +6°/oo to -55°/oo (SMOW) (Craig, 1961b; Dansgaard, 1964; Epstein et al, 1965, 1970). Isotopic variations in meteoric waters are extremely systematic, the higher the latitude or altitude, the lower the $\delta^{18}O$ (and δD) values. This variation is a product of the equilibrium isotope effect and the reservoir effect. Water vapour is depleted in ^{18}O with respect to co-existing liquid water, therefore any condensate from a vapour cloud will be enriched in the heavier isotope. As a vapour cloud is a finite reservoir, it will become increasingly depleted in ^{18}O as precipitation continues. As a consequence successive condensates will also be isotopically lighter than preceding ones. It can be seen, therefore, that as an air mass moves away from the equator and crosses the continents, rainfall will become progressively depleted in ^{18}O.

Geothermal and formation waters exhibit a similar range in isotopic compositions to meteoric waters with a shift towards magmatic values (see Taylor, 1974). This is because these waters are basically meteoric in origin, but have exchanged with the country rocks through which they have passed.

7.3 ISOTOPIC COMPOSITION OF HOST ROCK, ORE STAGE AND POST-ORE CARBONATES AT TYNAGH

7.3.1 Results

7.3.1.1 Introduction

Carbon and oxygen isotope analyses of samples collected from within the Tynagh deposit are presented in table 7.1. Analyses of unmineralized Waulsortian limestones are listed in table 7.2. Sampling of both the mineralized and unmineralized limestones was restricted to the micritic facies of the Waulsortian banks and associated diagenetic calcite infillings. Those samples labelled 'H707' in table 7.2 were collected from one of Lees' (1964) type localities - an isolated Waulsortian mound within lagoonal facies Lower Limestones. All other unmineralized limestones were collected from the main bank complex between the mine and the town of Loughrea, 12.5 km. W.N.W. of Tynagh.

7.3.1.2 The Waulsortian Limestones

Unmineralized Waulsortian micrites and associated diagenetic calcites display a narrow spread of carbon isotope compositions from +3.08°/oo to +4.12°/oo, mean: +3.83°/oo. $\delta^{18}O$ (SMOW) values range from +22.18°/oo to +28.11°/oo, mean: +26.29°/oo (fig. 7.4). Variation in isotopic composition is unrelated to proximity to the Tynagh orebody.

Mineralized, but physically unaltered Waulsortian limestones from within the ore zone, display a wider spread and are depleted in the heavier isotopes of carbon and oxygen with respect to the unmineralized examples:-$\delta^{13}C$ (PDB): +2.11°/oo to +4.00°/oo,

TABLE 7.1 ISOTOPIC COMPOSITION OF CARBON AND OXYGEN IN HOST ROCK, ORE STAGE AND POST-ORE CARBONATES, TYNAGH

Extraction No.	Location	Distance N of Fault (Metres)	Description	Stage No.	$\delta^{13}C$ (PDB) (°/oo)	$\delta^{18}O$ (SMOW) (°/oo)	$\delta^{18}O$ (PDB) (°/oo)
D882	5050 67+20W	55.0	pink, euhedral 'plug' dolomite	4	+2.05	+19.39	-11.13
C515	" "	"	calcite (overgrowing dolomite)	4	-2.72	+22.20	- 8.40
D834	" 66+80W	61.0	dolomite intergrown with sphalerite	2	+2.48	+25.11	- 5.58
D835	" "	"	" " " "	2	+2.41	+25.63	- 5.07
C429	" "	"	vein calcite	4	-2.97	+15.87	-14.54
D837	" 66+10W	67.0	dolomite intergrown with sphalerite	2	+2.40	+22.28	- 8.33
D876	" "	"	dolomitised micrite (0.2 cm.)	3	+2.79	+24.14	- 6.52
D877	" "	"	" " (0.6 cm.)	3	+2.75	+25.04	- 5.65
D878	" "	"	" " (0.9 cm.)	3	+2.80	+25.36	- 5.33
C1145	" "	"	calcitic micrite (2.2 cm.)	-	+2.75	+24.54	- 6.13
C366	" 66+00W	36.5	vein calcite	4	+2.57	+18.16	-12.32
C519	" "	"	" " (rpt.)	4	+2.35	+18.33	-12.16
D564	5000 67+10W	49.0	pink, euhedral 'plug' dolomite	4	+0.94	+18.41	-12.08
C509	" "	"	calcite (overgrowing dolomite)	4	-2.97	+22.48	- 8.13
C310	" 66+85W	39.5	vein calcite	4	+0.74	+20.44	-10.11
C1116	" 66+50W	30.5	calcitic micrite	-	+3.07	+24.37	- 6.29
C1117	" "	"	diagenetic calcite	-	+3.58	+26.07	- 4.65
D836	" "	"	dolomite intergrown with sphalerite	2	+2.69	+23.31	- 7.32
C317	" 66+00W	"	calcitic micrite	-	+2.11	+23.91	- 6.74
C318	" "	"	" "	-	+3.14	+24.19	- 6.47
C319	" "	"	" "	-	+3.30	+25.94	- 4.78
C320	" "	"	" "	-	+3.05	+23.68	- 7.00
C1147	" "	"	calcite intergrown with sphalerite	2	+2.23	+22.24	- 8.36
C1148	" "	"	" " " "	2	+2.13	+23.02	- 7.61
D840	" 65+00W	35.0	dolomite intergrown with sphalerite	2	+3.36	+26.17	- 4.55
C399	4912 65+35W	36.5	vein calcite	4	+0.39	+24.14	- 6.52
C398	" "	"	" "	4	-0.08	+24.09	- 6.57
C1139	" 64+85W	20.0	" "	4	-1.53	+23.29	- 7.34
D841	" 63+90W	15.0	dolomite intergrown with sphalerite	2	+2.36	+22.36	- 8.25
C511	" "	"	vein calcite	4	+0.72	+19.85	-10.69
C505	" "	24.5	calcite infilling cavity	4	+1.67	+20.54	-10.01
C1137	4890 62+65W	49.0	vein calcite (+ minor fluorite)	4	+2.06	+21.13	- 9.44
D567	4850 67+50W	61.0	pink dolomite from calcite/dolomite vein	4	+1.39	+18.50	-11.99
D884	" "	"	" " " " (rpt.)	4	+1.37	+18.53	-11.96
C425	" "	"	calcite from calcite/dolomite vein	4	+0.75	+17.81	-12.66
C174	4700 68+90W	30.5	" " " "	4	-0.27	+16.53	-13.90

cont. over

TABLE 7.1 cont.

Extraction No.	Location		Distance N of Fault (Metres)	Description	Stage No.	$\delta^{13}C$ (PDB) (°/oo)	$\delta^{18}O$ (SMOW) (°/oo)	$\delta^{18}O$ (PDB) (°/oo)
D880	4700	68+40W	26.0a	pink dolomite from calcite/dolomite vein	4	-0.34	+19.30	-11.22
D881	"	"	"	" " " " "	4	-0.43	+18.47	-12.02
D883	"	"	26.0b	" " " " "	4	-1.11	+18.85	-11.66
C424	"	"	"	calcite from calcite/dolomite vein	4	-1.54	+18.14	-12.34
C520	"	"	"	" " " " (rpt.)	4	-1.59	+18.13	-12.35
D565	"	"	32.0	pink dolomite from calcite/dolomite vein	4	-0.95	+18.09	-12.39
C172	"	"	"	calcite from calcite/dolomite vein	4	-1.62	+16.70	-13.74
D566	"	67+50W	"	pink dolomite from calcite/dolomite vein	4	+0.58	+19.17	-11.34
C171	"	"	"	calcite from calcite/dolomite vein	4	-0.69	+17.00	-13.44
D1153	4900	89+80W	41.0	dolomite intergrown with sphalerite	2	+3.43	+26.77	- 3.97
C395	"	89+00W	12.0	calcite infilling cavity	4	+1.26	+24.33	- 6.34
C428	"	"	"	" " "	4	+1.13	+23.10	- 7.53
C364	"	88+90W	7.5	vein calcite	4	-0.52	+17.95	-12.53
D560	"	"	24.5	dolomite intergrown with barytes	2	+2.05	+26.79	- 3.94
C1115	"	87+80W	46.0	calcitic micrite	-	+4.00	+27.11	- 3.64
C321	"	"	"	" "	-	+2.83	+25.79	- 4.92
C1133	"	"	"	calcite infilling cavity	4	+1.78	+21.66	- 8.93
C312	"	"	"	vein calcite	4	+2.54	+25.78	- 4.93
C1131	"	86+00W	23.0	calcitic micrite	-	+3.05	+24.83	- 5.85
C313	"	"	"	calcite infilling cavity	4	+1.28	+21.44	- 9.14
C390	"	85+20W	20.0	calcitic micrite (4.7 cm.)	-	+2.69	+17.62	-12.85
C393	"	"	"	fibrous calcite (2.7 cm.)	1	+3.17	+25.93	- 4.79
C391	"	"	"	" " (2.2 cm.)	1	+3.09	+26.23	- 4.49
C516	"	"	"	" " (rpt.)	1	+2.82	+26.30	- 4.42
D1157	"	"	"	sparry dolomite (2.0 cm.)	1	-2.76	+19.34	-11.18
C1124	"	"	"	fibrous calcite (1.8 cm.)	1	+3.04	+24.73	- 5.95
C392	"	"	"	" " (1.0 cm.)	1	+0.75	+21.58	- 9.01
C1122	"	"	"	" " (0.8 cm.)	1	+1.35	+22.19	- 8.41
C389	"	"	"	sparry calcite (0 cm.)	1	-2.77	+17.08	-13.37
C311	"	"	"	calcite infilling cavity	4	+0.54	+23.50	- 7.14
C1140	"	84+40W	49.0	black calcite enclosing pyrite	1	+0.96	+23.13	- 7.50
C502	"	"	"	calcite infilling cavity	4	+1.47	+21.75	- 8.84
D1158	4800	90+10W	12.0	black dolomite enclosing pyrite	1	+2.15	+26.88	- 3.86
C1129	"	"	21.0	calcitic micrite	-	+2.90	+26.79	- 3.94
D1159	"	"	"	black dolomite enclosing pyrite	1	+2.89	+23.60	- 7.04
C507	"	"	43.0	calcite infilling cavity	4	+2.32	+25.04	- 5.65
C1142	"	89+00W	21.0	black calcite enclosing pyrite	1	+0.66	+23.00	- 7.65
C1125	"	88+80W	"	calcitic micrite	-	+2.62	+22.26	- 8.34

cont. over

TABLE 7.1 cont.

Extraction No.	Location	Distance N of Fault (Metres)	Description	Stage No.	$\delta^{13}C$ (PDB) (°/oo)	$\delta^{18}O$ (SMOW) (°/oo)	$\delta^{18}O$ (PDB) (°/oo)
C1141	4800 88+80W	21.0	black calcite enclosing pyrite	1	+0.74	+20.75	- 9.81
C365	" "	"	vein calcite	4	-0.12	+19.96	-10.58
C514	" "	"	" " (rpt.)	4	-0.30	+20.04	-10.50
C506	" "	49.0	" "	4	+1.65	+25.46	- 5.24
C510	" 87+10W	27.5	" "	4	+1.58	+23.72	- 6.92
C517	" "	"	" " (rpt.)	4	+1.53	+24.09	- 6.57
C1130	" 82+90W	61.0	bleached/barytised calcitic micrite	3	+1.25	+23.96	- 6.69
C1113	" 82+20W	76.0	calcite infilling cavity	4	+1.35	+21.94	- 8.65
C1108	" 81+40W	84.0	vein calcite	4	+1.60	+22.99	- 7.63
C1109	" "	"	" "	4	+1.45	+25.19	- 5.50
C1110	" "	"	" "	4	+1.76	+21.99	- 8.60
C1111	" "	"	" "	4	+1.94	+20.71	- 9.84
C1112	" "	"	" "	4	+2.05	+20.14	-10.40
C1114	" 80+90W	64.0	" "	4	+1.77	+19.90	-10.63
D1152	" 80+80W	91.5	dolomitised/barytised micrite	3	+1.99	+25.75	- 4.96
D1154	" 80+30W	58.0	dolomite intergrown with sphalerite	2	+2.01	+25.93	- 4.79
D1156	" 79+80W	55.0	dolomitised micrite	3	+2.70	+24.24	- 6.43
D561	" 78+50W	39.5	dolomitised micrite (0.2 cm.)	3	+2.06	+24.40	- 6.27
D562	" "	"	" " (0.6 cm.)	3	+2.13	+22.99	- 7.63
D563	" "	"	" " (1.0 cm.)	3	+2.14	+21.59	- 8.99
C1138	" "	"	calcitic micrite (2.0 cm.)	-	+2.40	+22.11	- 8.49
D1404	" "	"	dolomitised micrite (0.2 cm.)	3	+2.21	+24.83	- 5.85
D1405	" "	"	" " (0.6 cm.)	3	+2.29	+23.50	- 7.14
D1406	" "	"	" " (1.0 cm.)	3	+2.20	+21.79	- 8.80
C513	4750 89+50W	126.5	vein calcite (+ minor fluorite)	4	-0.80	+24.33	- 6.33
D1151	4725 88+60W	91.5	dolomitised/barytised micrite	3	+0.97	+26.08	- 4.64
C1146	" 85+90W	116.0	bleached calcitic micrite	3	+2.45	+24.36	- 6.31
D1403	" 85+80W	128.0	dolomite intergrown with sphalerite	2	+1.25	+24.74	- 5.94
D879	" 85+50W	91.5	dolomitised micrite	3	+0.20	+26.51	- 4.22
C427	" "	"	calcite infilling cavity	4	+0.70	+24.65	- 6.03
C501	" "	"	" " "	4	+0.56	+21.18	- 9.39
C397	4700 92+00W	30.5	vein calcite	4	-4.03	+17.47	-12.99
C396	" "	"	" "	4	-3.14	+18.18	-12.30
D842	" 91+10W	9.0	dolomite intergrown with barytes	3	-1.09	+23.67	- 6.98
C504	" 90+00W	11.0	calcite infilling cavity	4	+0.14	+20.83	- 9.73
C508	" 89+00W	1.0	vein calcite	4	-4.04	+17.50	-12.96
C503	" 88+20W	17.0	" "	4	-2.87	+17.27	-13.18

cont. over

TABLE 7.1 cont.

Extraction No.	Location	Distance N of Fault (Metres)	Description	Stage No.	$\delta^{13}C$ (PDB) (°/oo)	$\delta^{18}O$ (SMOW) (°/oo)	$\delta^{18}O$ (PDB) (°/oo)
C368	4700 87+00W	30.5	calcite infilling cavity	4	+0.66	+22.14	- 8.46
D1155	4620 92+10W	24.5	dolomite intergrown with sphalerite	2	+0.25	+23.40	- 7.24
C367	" 86+30W	6.0	vein calcite	4	-0.50	+16.90	-13.54
C518	" "	"	" " (rpt.)	4	-0.61	+17.21	-13.24
C512	DDH 368 (123.5 m) 1.34 km. E of Zone III	"	calcite infilling cavity	4	-0.90	+21.41	- 9.16

TABLE 7.2

ISOTOPIC COMPOSITION OF CARBON AND OXYGEN IN UNMINERALISED WAULSORTIAN LIMESTONES

Extraction No.	Location	Description	$\delta^{13}C$ (PDB) (‰)	$\delta^{18}O$ (SMOW) (‰)	$\delta^{18}O$ (PDB) (‰)
C1345	12.5 km. W.N.W. Tynagh mine	calcitic micrite	+3.60	+22.18	-8.42
C1346	11.3 km. " " "	" "	+3.96	+26.84	-3.90
C1349	" " " "	diagenetic calcite	+4.02	+27.74	-3.02
C1343	8.9 km. " " "	calcitic micrite	+3.87	+26.40	-4.33
C1348	" " " "	diagenetic calcite	+4.08	+27.70	-3.06
C1344	8.0 km. " " "	calcitic micrite	+4.00	+28.01	-2.77
C1347	6.0 km. " " "	" "	+3.83	+28.11	-2.67
C1342	4.4 km. " " "	" "	+3.73	+23.42	-7.22
C1341	1.2 km. " " "	" "	+3.56	+25.12	-5.57
C400	9.7 km. W. " " (H707)	" "	+3.88	+25.58	-5.12
C401	" " " " "	diagenetic calcite	+3.08	+23.96	-6.69
C1128	" " " " "	calcitic micrite	+4.12	+27.40	-3.35
C1120	" " " " "	" "	+4.10	+27.02	-3.73
C1121	" " " " "	diagenetic calcite	+4.06	+27.95	-2.82
C1123	" " " " "	calcitic micrite	+3.79	+26.95	-3.79
C1132	" " " " "	diagenetic calcite	+3.53	+26.05	-4.67
C402	" " " " "	calcitic micrite	+3.94	+26.50	-4.23

TABLE 7.3 INFERRED OXYGEN ISOTOPE EQUILIBRIUM FRACTIONATION TEMPERATURES FOR POST-ORE DOLOMITE-CALCITE PAIRS

Location			Mineral Pair	1000 ln α	Inferred Temperature (^{o}C)*
4700	67+50W	(32 m)	dolomite-calcite	2.13	103
4700	68+40W	(32 m)	" "	1.37	207
4700	68+40W	(26 m) b	" "	0.70	441
4850	67+50W	(61 m)	" "	0.69	447

* Calculated from experimental calibrations of Matthews and Katz (1977), and O'Neil et al (1969)

mean: +2.96°/oo; $\delta^{18}O$ (SMOW): +17.62°/oo to +27.11°/oo, mean: +24.23°/oo (fig. 7.4).

7.3.1.3 Ore Stage Carbonates

Ore stage carbonates and altered micrites are again depleted in ^{13}C and to a lesser extent ^{18}O with respect to unmineralized Waulsortian limestones. With the exception of two samples, carbonates associated with each stage of sulphide mineralization display a similar spread in isotopic composition within the following range - $\delta^{13}C$ (PDB): -1.09°/oo to +3.43°/oo, mean: +1.99°/oo; $\delta^{18}O$ SMOW): +20.75°/oo to +26.88°/oo, mean: +24.21°/oo (fig. 7.5).

The above mentioned exceptions occur as the final infillings to a cavity that can be correlated with stage 1 sulphide mineralization (fig. 7.6). The cavity is lined with successive generations of dark fibrous calcite with minor conformable horizons of colloform pyrite. Sparry ferroan dolomite was precipitated from fluid injection between bands of the fibrous calcite, and subsequently displaced by microfaulting. Sparry calcite intergrown with minor amounts of euhedral and colloform pyrite formed the infilling to the centre of the cavity, and texturally identical discordant calcite veinlets cut both the fibrous calcite and the ferroan dolomite. The final event is recorded by a stylolite surface which can be seen to post-date all carbonate generations. Serial sampling through these successive generations of carbonate cement has revealed a comparatively wide variation in isotopic composition, the total spread in $\delta^{13}C$ (PDB) and $\delta^{18}O$ (SMOW) being -2.77°/oo to +3.17°/oo and +17.08°/oo to +26.27°/oo respectively. Although the relationship is not perfect, it becomes clear from examination of figure 7.6 that this variation is systematic,

the later generations being relatively depleted in the heavier isotopes of both carbon and oxygen.

Microsampling of dolomitised Waulsortian micrites in the zone of contact with stage 3 sulphide/sulphosalt veinlets reveals a contradictory picture of isotopic variation (fig. 7.7). There is no significant variation in $\delta^{13}C$ of the dolomite with distance from mineralization. In addition, the carbon isotope composition of the dolomite is identical or very close to that of the unaltered calcitic micrite. However, there are large systemic variations in oxygen isotope composition, in one example the carbonate being depleted (fig. 7.7A), and in another, enriched (fig. 7.7B) in the heavier isotope as the veinlet is approached.

7.3.1.4 Post-Ore Carbonates

Post-ore (stage 4) calcite veins and cavity infillings exhibit the greatest range in isotopic compositions ($\delta^{13}C$ (PDB): -4.04°/oo to +2.57°/oo; $\delta^{18}O$ (SMOW): +15.87°/oo to +25.78°/oo) and again are depleted in the heavier isotopes with respect to the host carbonates (fig. 7.8). 'Plug' dolomite and dolomite/calcite intergrowths from related veins fall within this range, but display a much smaller spread of values. Calcite overgrowths on 'plug' dolomite are isotopically distinct from calcite intergrown with vein dolomite, being relatively depleted in ^{13}C but enriched in ^{18}O. Co-precipitated calcite-dolomite pairs yield a wide range of fractionation factors and, therefore, cannot be considered to be in isotopic equilibrium (table 7.3). If interpreted as being so, they would infer unrealistic temperatures and temperature gradients. For example, a pair taken from a vein at the 4700

elevation, 68+40W would indicate a temperature of deposition of 441°C, whilst a similar pair from the same vein, but collected 6 m to the north, gives a temperature of 207°C.

In summary, when considered as a whole the carbon and oxygen isotope data exhibits a broad trend towards isotopically lighter compositions with time (fig. 7.9). Unmineralized Waulsortian micrites and diagenetic calcites define a heavy end member, carbonates coeval with sulphides occupy an intermediate position, whilst post-ore carbonates tend to be depleted in ^{13}C and ^{18}O with respect to the aforementioned.

7.3.2 Interpretation and Discussion

7.3.2.1 The Waulsortian Limestones

Both mineralized and unmineralized Waulsortian micrites and associated diagenetic calcites exhibit a range of isotopic compositions that falls within that displayed by other Carboniferous limestones (Keith and Weber, 1964; Veizer and Hoefs, 1976). However, the relative depletions in the heavier isotopes of carbon and oxygen in the mineralized examples, indicates either a differing depositional/diagenetic environment, or exchange with fluids other than normal sea-water.

The Great Bahama Banks probably represent the nearest modern day equivalent to the Waulsortian depositional environment. The mean annual surface temperature of the ocean in this area is 25°C (Milliman, 1974). Taking this temperature, and the mean $\delta^{18}O$ value for unmineralized Waulsortian micrites (excluding diagenetic calcites) an oxygen isotope composition of -2.55°/oo (SMOW) is obtained for Lower Carboniferous sea-water. If this value for

FIG.7.4 ISOTOPIC COMPOSITION OF WAULSORTIAN LIMESTONES.

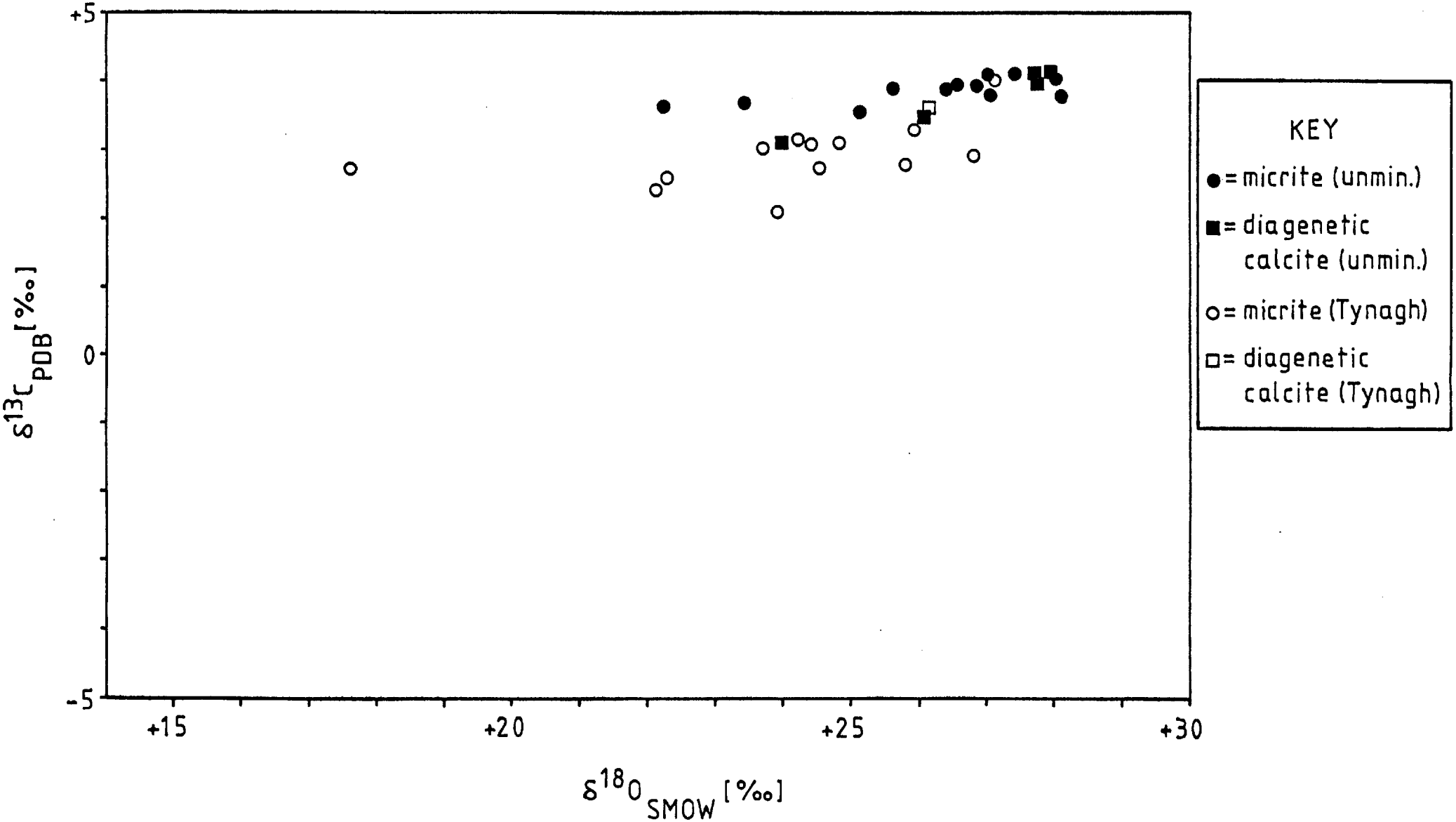

sea-water is in turn used to calculate the temperature of deposition of individual unmineralized micrite samples, a range of 16.4 to 45.2°C is indicated. This excessive spread of temperatures could be due to the non-equilibrium precipitation of the carbonate mud, or diagenetic modification. Consideration of isotopic data from the Bahama Banks, however, might suggest that the former situation is the case.

Lowenstam and Epstein (1957) found that the isotopic composition of Bahama aragonite mud falls within the range of algal carbonate, and concluded that this was the major source of the mud. In addition, some of the algal carbonate was shown to have been precipitated in disequilibrium with the ambient environment. The temperature range suggested by $\delta^{18}O$ values was 22.8 to 39.8°C, a spread incongruous with the maximum surface temperature of 30°C. As this temperature range is similar to that calculated for the Waulsortian micrites, it is considered that the $\delta^{18}O$ value suggested above for Lower Carboniferous sea-water is a close approximation.

Mineralized Waulsortian limestones occupy an intermediate range of isotopic compositions between, and overlapping with that of unmineralized limestones and ore stage carbonates. It is therefore apparent that the depletion in ^{13}C and ^{18}O occurred as a result of isotopic exchange between the host and the mineralizing fluids.

7.3.2.2 Ore Stage Carbonates

The Waulsortian limestones constitute a distinct end member to the isotopic variation displayed by dolomite and calcite cogenetic with the sulphide phases of stages 1, 2 and 3.

This suggests that the host was the major source of carbonate during mineralization. However, the displacement towards lighter carbon and to a lesser extent oxygen isotope compositions in both mineralized micrites and ore stage carbonates indicates the influence of an external contributor.

The two possible sources of light carbon already discussed are deep-seated carbon and organic carbon. However, as the sulphur isotope data indicates that bacterial reduction was taking place at the time of mineralization (see chapter 6), the incorporation of light CO_2 produced by bacterial oxidation of organic matter into both the ore stage carbonates and the mineralized limestones seems most likely. The absence of extremely light carbon values is not surprising as any bacterial CO_2 whether produced *in situ* or migrating out of off-bank facies, would be swamped by the vast reservoir of limestone derived carbonate. The trend towards lighter $\delta^{13}C$ values in later carbonate generations infilling the stage 1 cavity (fig. 7.6) could be a reflection of the incorporation of an increasing proportion of organic CO_2. As the host became locally more lithified it would have been less liable to interact with, and thus make a contribution to, passing fluids.

Any contribution of light carbon from deep-seated sources would be difficult to recognise against the prevailing background of organic and limestone derived carbon. As a contribution of sulphur from deep-seated sources has been demonstrated for stage 3 mineralization, dolomitised zones adjacent to veinlets of this stage would most likely show the effects of deep-seated carbon. However, the similarity of $\delta^{13}C$ values of these dolomites and the adjacent unaltered micrites (fig. 7.7) suggests that ^{13}C depletion

predates dolomitisation.

A reliable estimate of the oxygen isotope composition of the mineralizing fluid cannot be made without knowledge of the temperature of deposition. For example, the increasing depletions in ^{18}O within successive generations of stage 1 carbonate (fig. 7.6) could be due to deposition from increasingly warmer and/or isotopically lighter waters. Alternatively, the variation could be the result of isotopic exchange between previously precipitated carbonate generations and later hotter and/or lighter fluids passing through the cavity. An exchange mechanism seems unlikely though, as $\delta^{18}O$ (SMOW) varies as a function of paragenetic position rather than proximity to probable conduits.

An alternative approach would be to estimate the isotopic composition of the fluid, and thus calculate the probable temperature of deposition of the carbonate. It has been argued on the basis of the ore textures(chapter 3) and the sulphur isotope data (chapter 6), that stage 1 pyrite aggregates were precipitated during the early diagenetic history of the Waulsortian limestones, by bacterially reduced Lower Carboniferous sea-water sulphate. It is probable, therefore, that the oxygen isotope composition of the fluid was close to that of contemporaneous marine waters. If the $\delta^{18}O$ value of $-2.55^{o}/oo$ (SMOW) for Lower Carboniferous sea-water is accepted, a temperature range of 25 to 91°C would be implied for the successive generations of stage 1 carbonate illustrated in figure 7.6. The temperature range calculated for the fibrous calcite generations, (25 to 49°C) is within the range that can be survived by sulphate reducing bacteria (6.2.2.2) and, therefore, this interpretation would be consistent with the sulphur isotope data. However, the higher

FIG.7.5 ISOTOPIC COMPOSITION OF ORE STAGE CARBONATES.

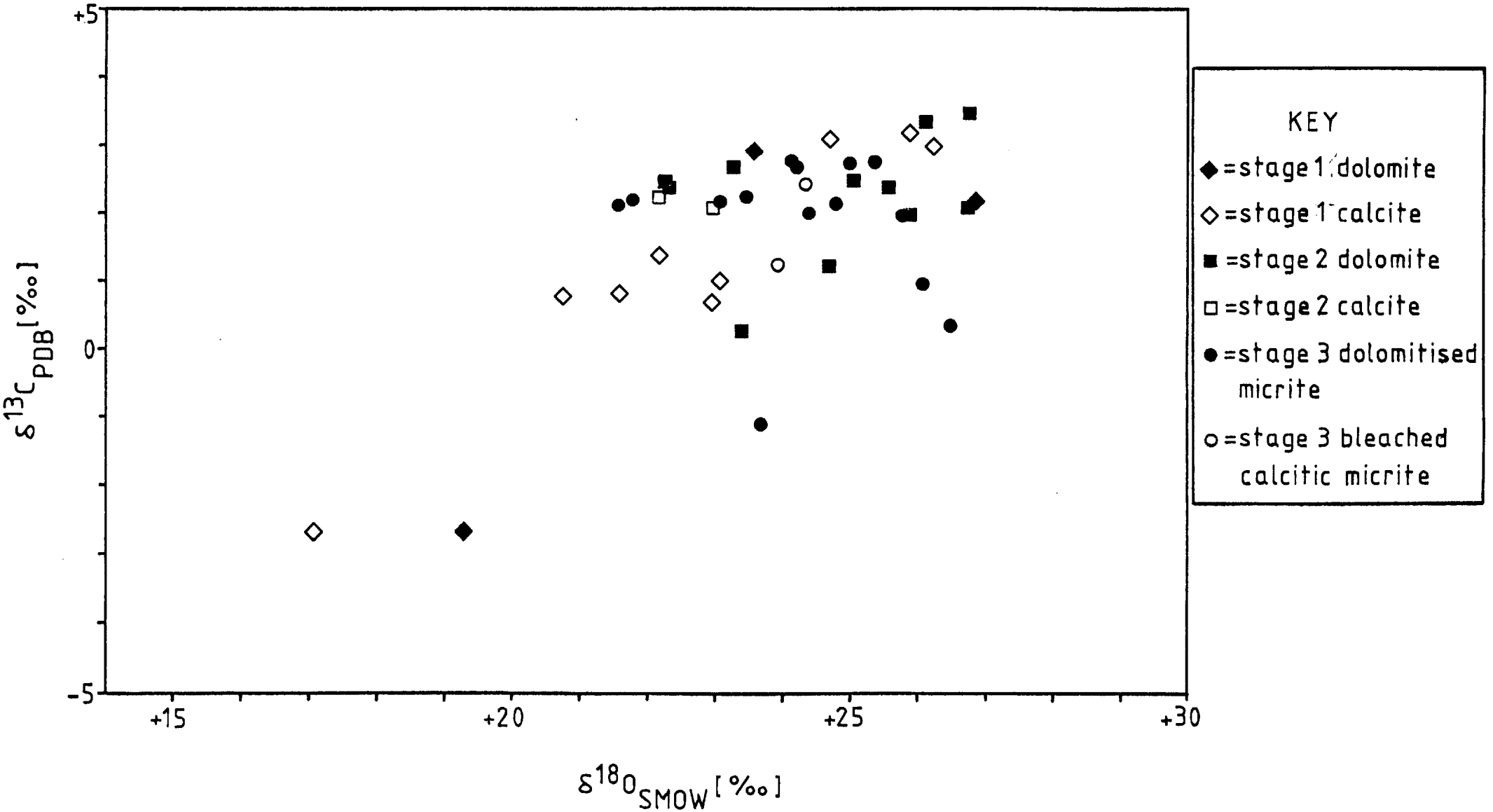

FIG.7.6 ISOTOPIC VARIATION IN SUCCESSIVE GENERATIONS OF STAGE 1 CARBONATE.

Temperature (°C) of deposition assuming equilibrium precipitation from -2·55‰ (SMOW) water. (Low T. calibration)

1 : 26·0, 2 : 24·8, 3 : 31·7, 4 : 48·7,

5 : 45·1, 6 : 90·7, 7 : 77·4.

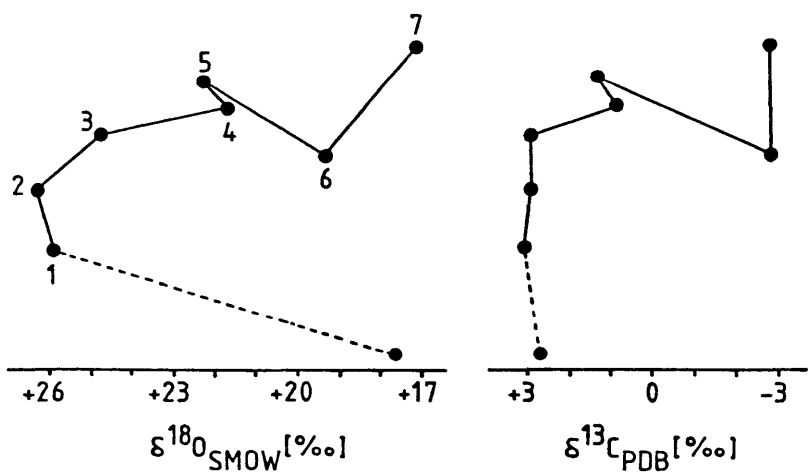

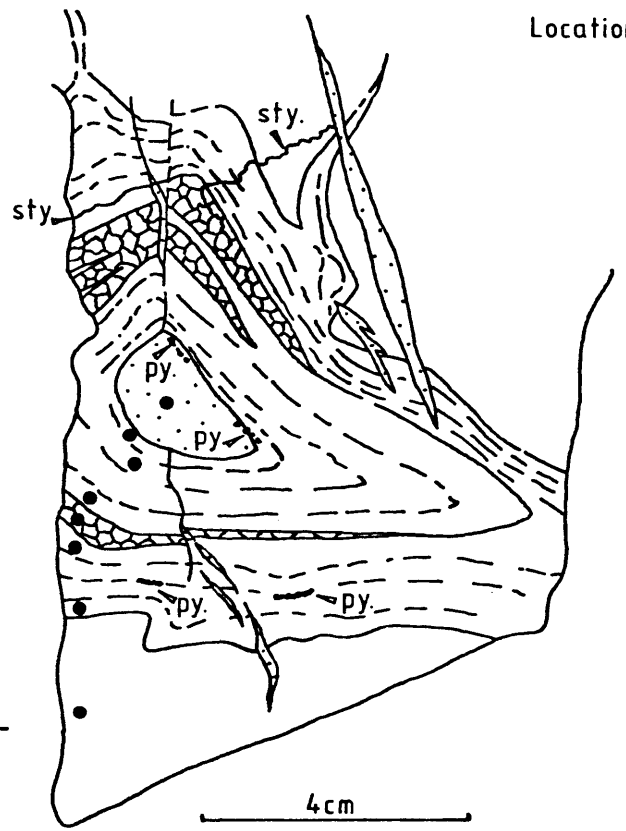

Location : 4900 85+20W.

= Sparry calcite.

= Ferroan dolomite.

= Fibrous calcite.

= Calcitic micrite.

sty.= Stylolite.

py.= Pyrite.

FIG.7.7 ISOTOPIC VARIATION WITHIN STAGE 3 DOLOMITE.

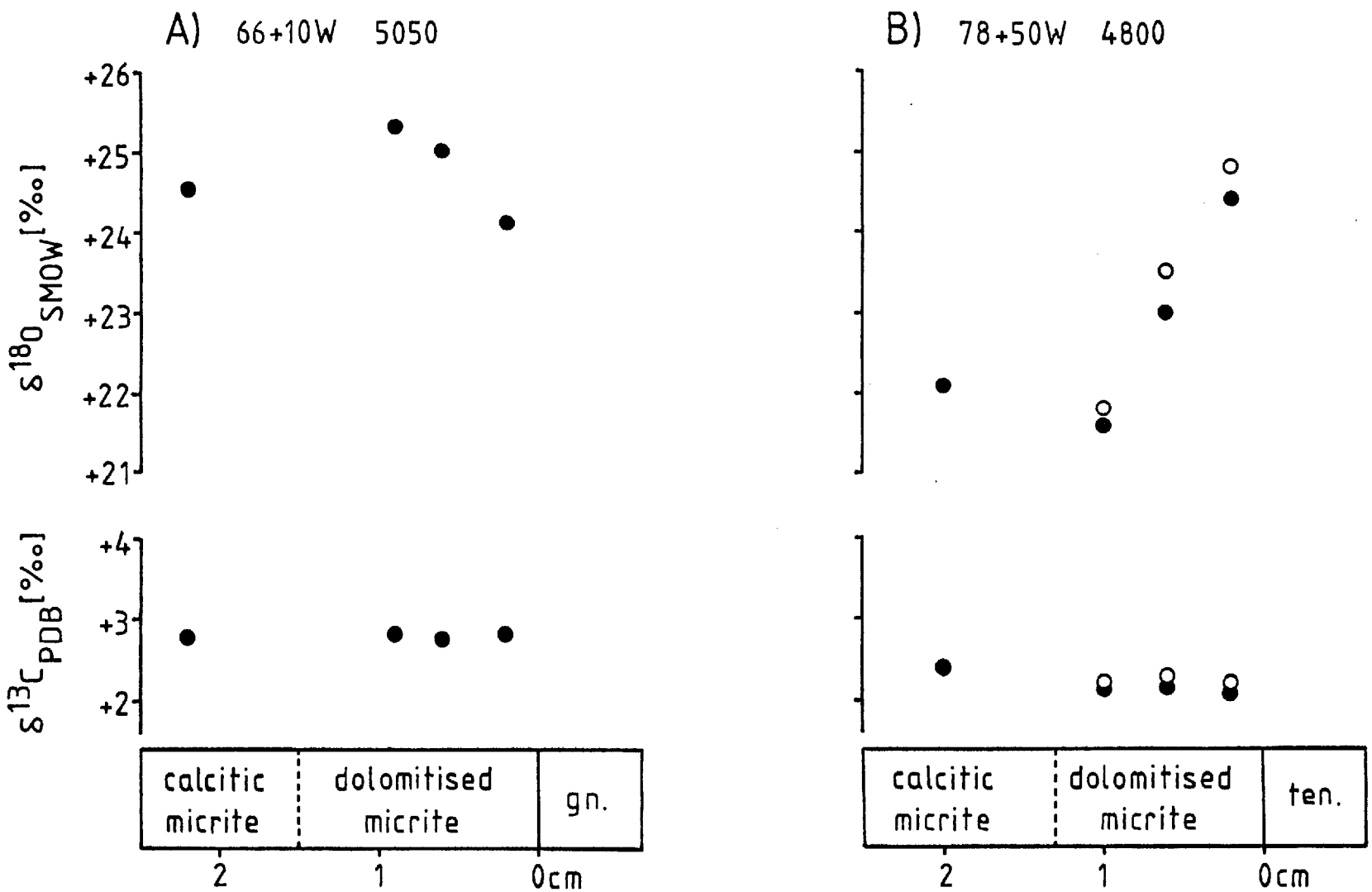

temperatures suggested by the oxygen isotope compositions of later sparry generations, would drastically reduce the activity of the anaerobes. These later generations of carbonate may, therefore, be coincident with the termination of in situ bacterial reduction. In addition, temperatures as high as 91°C at such shallow depths implies a considerable contribution of heat and thus heat transferring medium (water) from an external source. Circulation of sea-water to depth, or the influx of a totally unrelated fluid therefore has to be evoked. This would have mixed with normal sea-water and thus make the initial assumption of the oxygen isotope composition of the water less tenable.

A similar problem exists in the interpretation of oxygen isotope trends in dolomitised zones adjacent to stage 3 veinlets. An increase in $\delta^{18}O$ could be interpreted as reflecting a decrease in the temperature of deposition. However, if this were the sole cause of variation during dolomitisation, this would infer an increase in temperature towards the veinlet in one case (fig. 7.7A), but in the other example (fig. 7.7B), a decrease in temperature. In the latter instance the observed trend can only be explained satisfactorily by a mechanism involving isotopic exchange between the host carbonate and the mineralizing fluid. The dolomite towards the outer edge of the alteration zone has retained the isotopic composition of the pre-existing micrite, whilst samples nearer the vein represent increasing degrees of re-equilibration with the ore fluids. These fluids need not have been isotopically very different from sea-water. However, if the temperature of dolomitisation was above 31°C as seems likely, this would suggest a $\delta^{18}O$ value heavier than -2.55°/oo (SMOW) for the water.

7.3.2.3 Post-Ore Carbonates

The range of isotopic compositions displayed by post-ore carbonates again points to the mixing of carbonate derived from the Waulsortian limestones, with a source of light carbon and isotopically light and/or hot water. The greater extent of ^{13}C depletion as compared to ore stage carbonates possibly indicates an increased contribution from the light carbon source. However, if this is so, it is difficult to envisage how biogenic CO_2 could make a greater contribution than in earlier stages when bacterial sulphate reduction has been shown to be taking place.

The observed range of carbon isotope compositions could be produced from a solution with a constant $\Sigma\delta^{13}C$ composition by variations in fO_2 and pH. Fractionation between reduced and oxidised species is an unlikely mechanism as this would necessitate the presence of co-existing reduced carbon, either as graphite or methane. Graphite is not a phase that is noted at Tynagh, and investigation of present day geothermal areas has revealed that, neglecting steam., CO_2 dominates the vapour phase, whilst methane is usually present in quantities of less than 1 mole % (Ellis, 1967). In high fO_2 regions $\delta^{13}C$ is controlled by variations in pH alone (Ohmoto, 1972). However, wall rock reaction with the host limestones would probably counteract any large fluctuations in pH.

A wide variation in $\delta^{13}C$ could be produced from a limestone source of uniform isotopic composition, in response to temperature dependent equilibrium fractionation between various oxidised carbon species. However, examination of figure 7.2 shows that any calcite phase precipitated at temperatures up to 200°C will

FIG.7.8 ISOTOPIC COMPOSITION OF POST-ORE CARBONATES.

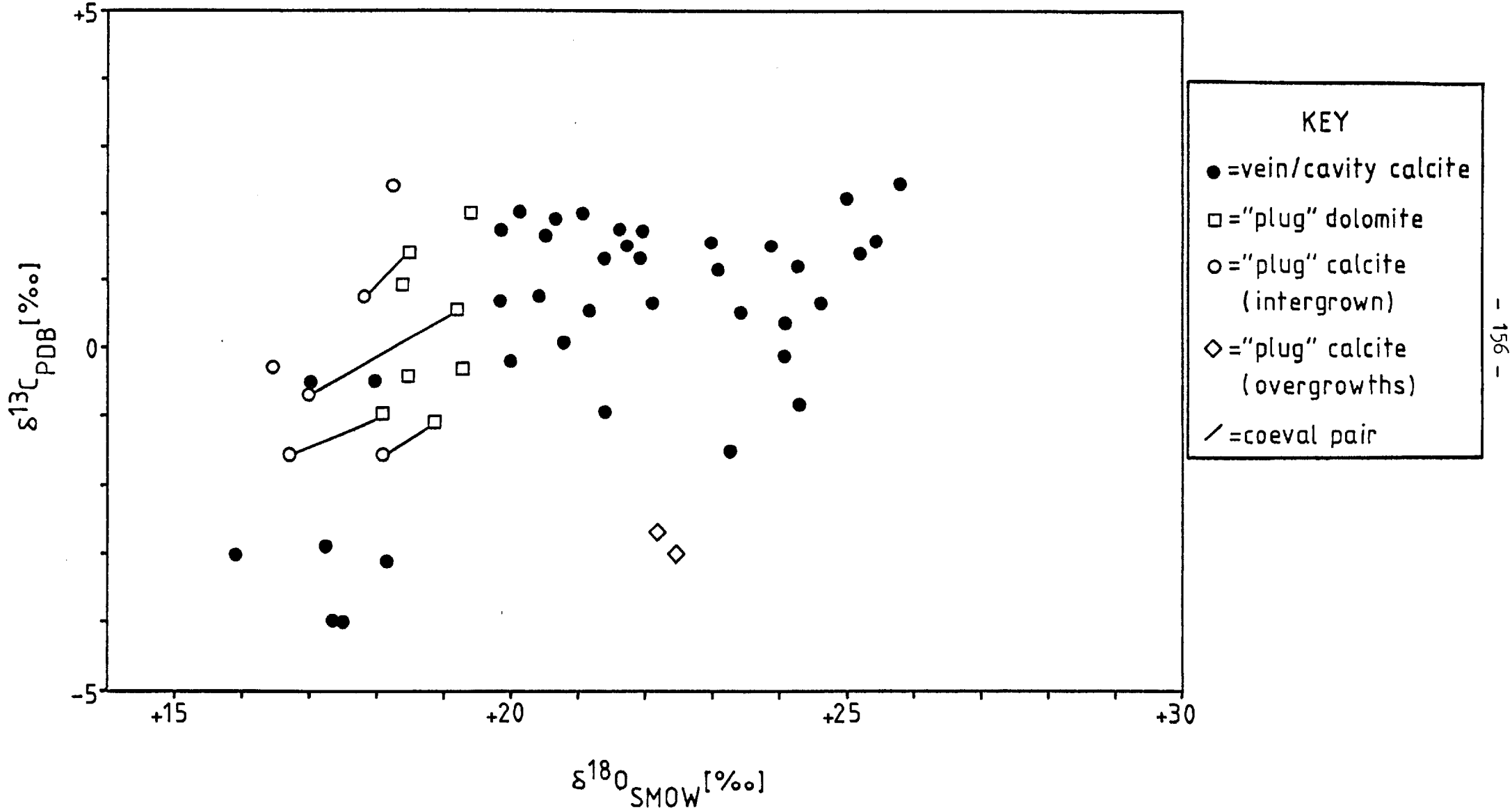

be either isotopically similar to, or heavier than the source carbon, which is clearly not the case at Tynagh.

An influx of deep-seated carbon provides the most probable explanation for the ^{13}C depletion in post-ore carbonates.

Unfortunately, due to the lack of precise information as to the temperature of deposition, the oxygen composition of these late stage fluids cannot be precisely defined. However, as the carbon isotope data indicate the influence of deep-seated sources, a contribution of magmatic water would seem likely. The assumption of a value of $+7^{o}/oo$ for the water (average magmatic water) would indicate a temperature range of 84 to 205°C for stage 4 carbonate precipitation. This would be in close agreement with the temperature range suggested by preliminary fluid inclusion studies (3.7.1).

7.4 ISOTOPIC COMPOSITION OF SILICATES ASSOCIATED WITH SULPHIDE MINERALIZATION

Due to the difficulties experienced in the separation of sufficient quantities of uncontaminated material, only three samples have been analysed (table 7.4).

Each of these has a $\delta^{18}O$ value that falls within the range exhibited by ore stage carbonates, and they are isotopically heavier than sedimentary, metamorphic and igneous silicates (Taylor, 1974). This confirms that they were precipitated from the ore fluids, and that they were not derived from detrial components within the sediment.

The quartz-albite pair yields an oxygen isotope fractionation temperature of 110°C which, if used in conjunction with the quartz-water calibration of Matsuhisa et al (1978), indicates a $\delta^{18}O$

TABLE 7.4

OXYGEN ISOTOPE COMPOSITION OF ORE-STAGE SILICATES

Extraction No.	Location	Distance N of Fault (Metres)	Description	Stage No.	$\delta^{18}O$ (SMOW) (°/oo)	1000lnα	Fractionation* Temp. (°C)
F432	5050 66+10W	67.0	Hyalophane intergrown with sphalerite	2	+17.82		-
F434a	4900 89+10W	1.5	Albite replacing micrite	3	+18.78	2.88	110
F434b	" "	"	Quartz replacing micrite	3	+21.72		

* Calculated from alkali feldspar - water calibration of O'Neil and Taylor (1967), and quartz - water calibration of Matsuhisa et al (1978).

FIG.7.9 SUMMARY OF CARBON AND OXYGEN ISOTOPE DATA.

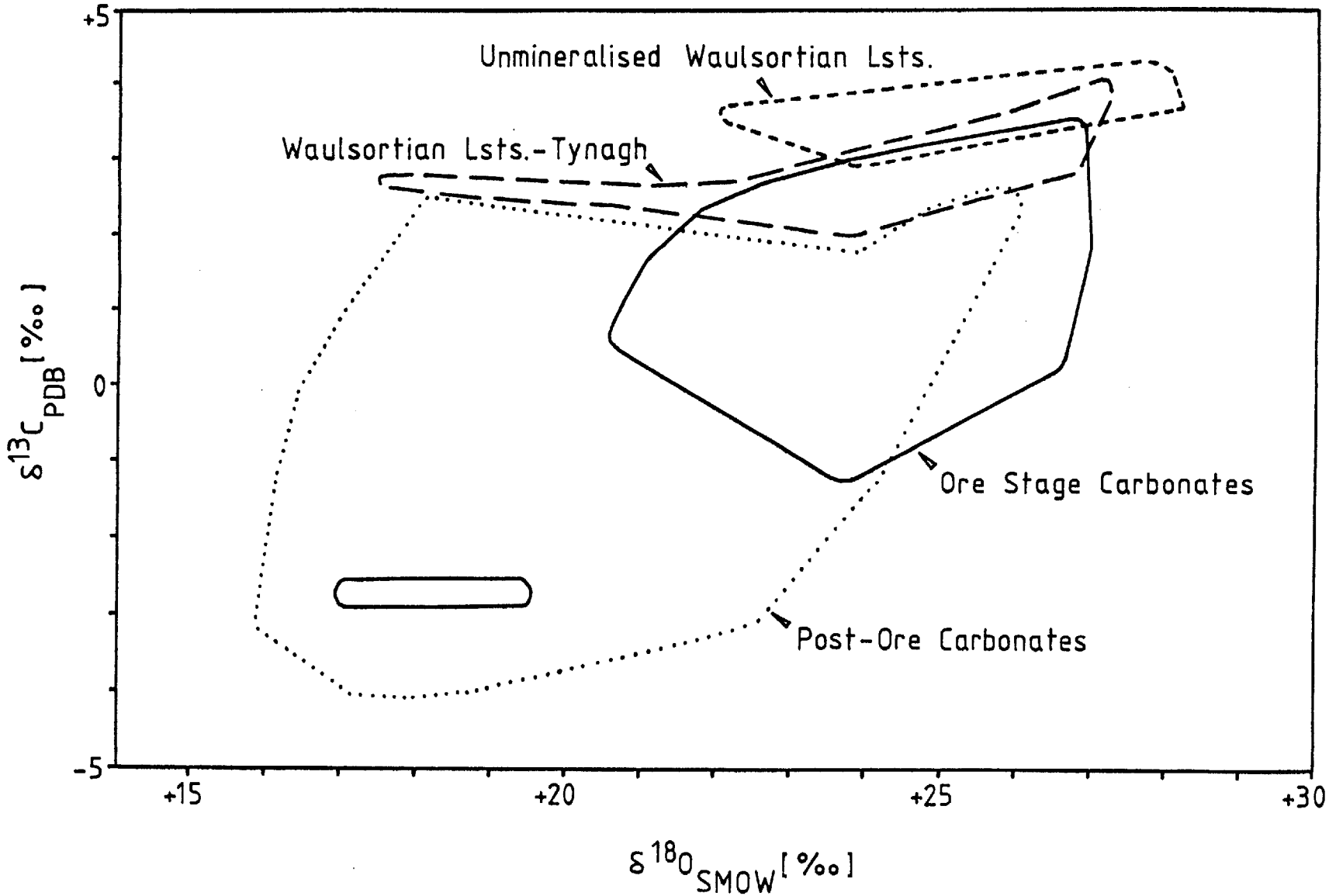

value of +2.4°/oo (SMOW) for stage 3 water. As this is based on only one mineral pair, and as the experimental calibrations have to be extrapolated to temperatures below 200°C, these values can only be considered as tentative. However they are in agreement with the conclusions drawn from the carbonate oxygen data which suggests an increase in temperature towards the end of stage 1 and during stage 3 $\delta^{18}O$ values heavier than those of contemporaneous sea-water. An increase in the $^{18}O/^{16}O$ ratio could have been produced by an influx of magmatic water or alternatively could be the result of high temperature exchange between ore fluids and the limestone host.

7.5 CONCLUSIONS

The host micritic limestones within the area of the Tynagh orebody are depleted in the heavier isotopes of carbon and oxygen with respect to local ummineralized Waulsortian limestones. The depletion in ^{13}C is due to the incorporation of isotopically light CO_2 produced from organic carbon during the bacterial reduction of sea-water sulphate. Depletion in ^{18}O is the result of exchange between the host and mineralizing fluids.

Dolomite and calcite coeval with sulphide deposition, and altered micrites are also depleted with respect to the Waulsortian limestones. However, the juxtaposition of the ranges in their isotopic composition suggests that the host limestones were a major source of carbonate. The incorporation of varying amounts of light organic carbon produced the observed range in $\delta^{13}C$. It is tentatively suggested that during the initial stages of sulphide mineralization temperatures did not exceed ~50°C, and that carbonates were precipitated from contemporaneous sea-water with a $\delta^{18}O$ value of -2.55°/oo (SMOW). Towards the end of stage 1 temperatures increased, possibly

to around 100°C. These higher temperatures probably persisted throughout the later stages of sulphide mineralization and, if so, must have been coincident with an increase in the $^{18}O/^{16}O$ ratio of the ore fluids. This increase could have been due to an influx of magmatic water or high temperature exchange between ore fluids and the host.

Post-ore carbonates display the greatest range in $\delta^{18}O$ and $\delta^{13}C$, which is again contiguous with that of the Waulsortian limestones. It is proposed that the range in carbon isotope compositions was produced by the mixing of limestone derived carbon with deep-seated carbon. The source of the water cannot be precisely defined from the oxygen isotope composition of the carbonates without independent evidence of the temperature of deposition. However, in view of the association with deep-seated carbon, a magmatic source is conjectured. This would indicate a temperature range of 84 to 205°C for post-ore carbonate precipitation, which would be in close agreement with the temperature range suggested by preliminary fluid inclusion studies.

CHAPTER 8

LEAD ISOTOPES

8.1 LEAD ISOTOPE MODELS

Variations in lead isotopic composition are the result of radioactive decay of ^{238}U and ^{235}U to ^{206}Pb and ^{207}Pb (uranogenic lead) respectively and ^{232}Th to ^{208}Pb (thorogenic lead). The fourth stable lead isotope, ^{204}Pb has no known radioactive parent and, therefore, provides an ideal index against which variations in other isotopes can be measured. The isotopes of Pb are not subject to significant fractionations in response to changing physico-chemical conditions, as are the light stable isotopes, the greatest equilibrium fractionation that would be expected being 0.05% of the $^{208}Pb/^{204}Pb$ ratio (see Doe, 1970). A single stage growth model based on the radioactive decay law to explain the increase in the Pb isotope ratios 206/204, 207/204 and 208/204 with decreasing geological age, was originally proposed by both Holmes (1946) and Houtermans (1946). The model is dependent upon a number of basic assumptions:-

(i) When the Earth was formed there was a unique set of isotopic proportions for all lead, throughout its mass, and probably within the solar system as a whole - primaeval lead.

(ii) From that time, all lead was contained within one or more closed systems, with constant proportion to uranium and thorium, apart from the effects of radioactive decay.

(iii) Lead extracted from this system or systems to form ore-bodies did not upset the U-Th-Pb proportions.

(iv) No contamination of the lead occurred between the source region and the deposition site.

This model can be displayed graphically as a plot of 207/204 against 206/204 for the U/Pb system, and 208/204 against 206/204 for the Th/Pb system. However, it is the U/Pb system (fig. 8.1) that is of most use because of the known consistency of the $^{238}U/^{235}U$ ratio at a given time, as opposed to the possible chemical fractionation of U and Th in nature.

Fig. 8.1 Single Stage Model

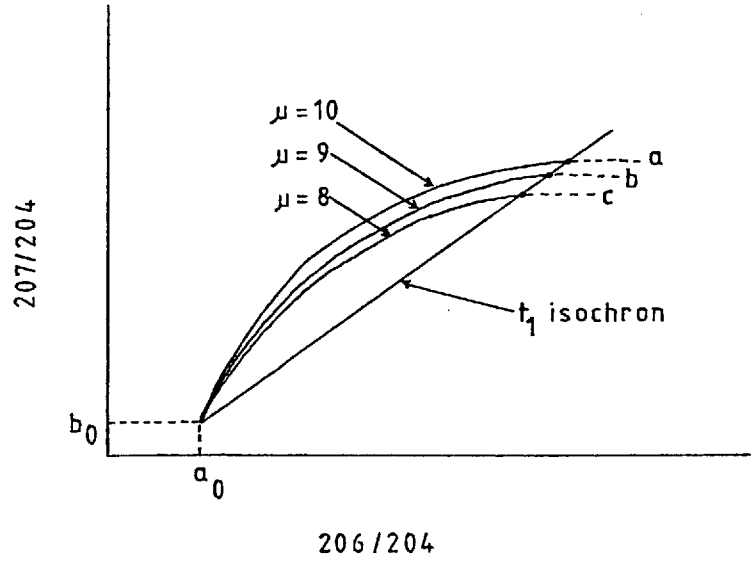

a, b and c are growth curves, which show how the isotope ratios change with time due to radioactive decay of the parent isotope (Appendix - 2a). They are curved due to the change in $^{238}U/^{235}U$ with time (at present this ratio is 137.88; 4.55 billion years ago it

was 3.33). The separate growth curves, a, b and c represent a group of locally closed systems with differing initial amounts of uranium (μ = present day ratio $^{238}U/^{204}Pb$). a_0 and b_0 are the primaeval ratios of lead at time t_0, the time of formation of the Earth. These are defined from meteoritic leads which contain negligible U and Th. If contemporaneous mineralization at time t_1 affected closed systems a, b and c, the extraction and concentration of lead into a lead mineral provides a "fossilised" record of the isotopic composition of the lead in the systems at t_1. The isotopic evolution of the lead ceases because it is separated from the radioactive parent isotope. The measured ratios of $^{206}Pb/^{204}Pb$ and $^{207}Pb/^{204}Pb$ of the lead minerals derived from the different closed systems, lie on a straight line called an isochron having a slope related to the age of the Earth (t_0) and the time of mineralization (t_1) - model age.

Stanton and Russell (1959) found that conformable ore leads of different ages fitted approximately to a single growth curve and proposed that this curve represented the development of the lead isotopic composition of the lower crust or upper mantle with time. However, recent revisions of the physical constants used in the model age equations have led to a re-assessment of the validity of a single stage growth curve developed from a closed U/Pb system. Oversby (1974) using the new constants, recalculated model ages and model μ values for a number of samples, and found that recent samples gave anomalous ages. The general trend of the data suggested a parent system which has had a small, rather steady increase in U/Pb ratio with time. Stacey and Kramers (1975) developed a two-stage model which gives good model ages for samples

of all ages. They postulated that lead developed initially from a primaeval composition beginning at 4.57 b.y. ago, in a system with average $^{238}U/^{204}Pb$ and $^{232}Th/^{204}Pb$ ratios of 7.19 and 32.21 respectively. At approximately 3.7 b.y. ago differentiation processes brought about the conditions of a second stage, in which $^{238}U/^{204}Pb \simeq 9.74$ and $^{232}Th/^{204}Pb \simeq 37.19$. Cumming and Richards (1975) propose a perhaps more reasonable model in which they postulate a steady growth in U/Pb accompanied by a slight decline in Th/U in the source region, without the necessity of a world-wide catastrophic event (Appendix - 2b). They additionally proposed a crustal source for ore leads on the basis that, in agreement with their model, it is generally accepted that U has migrated towards the upper crust faster than Th and that both have moved in preference to Pb.

Not all lead isotope ratios, however, can be explained by a single-stage model, some giving model ages which are clearly in conflict with the geological evidence. These are known as anomalous leads, and in certain instances (e.g. galenas from the Mississippi Valley deposits - Heyl et al, 1966) would give future ages if interpreted as having evolved in a single-stage system.

One way in which anomalous leads can be produced is by a two-stage process, in which the lead isotopic composition evolves in a single-stage system until some later event occurs that causes the initial $^{238}U/^{204}Pb$ ratio (μ_1) to be changed into a variety of values (μ_2). This results in lead isotope data that lie along a secondary isochron which intersects the growth curve at t_2 (age of mineralization) and t_1 (initiation of the second stage; i.e. age of the source, or age of an earlier mineralization of the source rock) -

fig. 8.2.

Fig. 8.2 Two-Stage Model

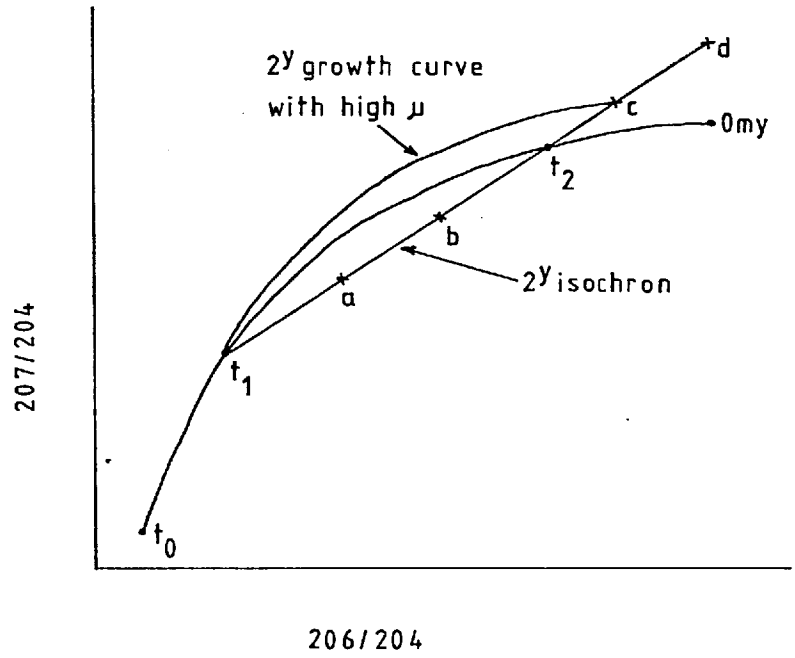

a and b = leads derived from source rocks in which $\mu_2 < \mu_1$

c and d = " " " " " " " $\mu_2 > \mu_1$

Multi-stage systems have also been recognised, but these can only be solved under certain special conditions (see Doe and Stacey, 1974).

8.2 LEAD ISOTOPE VARIATION WITHIN THE Pb-Zn DEPOSITS OF THE CENTRAL PLAIN OF IRELAND

8.2.1 Previous Studies

The first lead isotope studies of Irish galena occurrences were carried out at the University of Oxford, as part of a more extensive study of mineralization within the British Isles (Pockley,

1961; Moorbath, 1962). The samples analysed were representative of a variety of geological settings, and included a number that were hosted within Lower Carboniferous sediments. Model lead ages suggested a wide time span for mineralization within Ireland, but data from the Abbeytown deposit (the only large Lower Carboniferous hosted deposit known at the time) pointed to a possible Lower Carboniferous age of mineralization.

However, subsequent refinements in instrumentation, standardisation, and the amendment of geophysical constants and lead models, necessitated the revision of all earlier studies.

In an attempt to update the work of Pockley and Moorbath, Greig et al (1971) determined lead isotope ratios for 29 galena samples from 24 different localities, including Tynagh, Silvermines, Keel and Gortdrum. The data exhibited a wide scatter which they interpreted as being largely due to fractionation effects and ^{204}Pb measurement error. They concluded that the data could be adequately explained by a single-stage model which suggested ages of mineralization ranging from 270 to 75, or 215 to 20 m.y. depending on the decay constants used. A broad regional trend in isotope ratios was also revealed whereby leads became progressively more radiogenic (younger) southwards.

8.2.2 Aims of the Present Study

The current programme of lead isotope analysis was undertaken to further refine and extend the work of Greig and co-workers. By frequently analysing the NBS 981 standard and replicating analyses, it was hoped that measurement error would be reduced, thus enabling a more precise interpretation of the data to be achieved. In

addition, the revision of the uranium decay constants (Jaffey et al, 1971), and the proposal of the Linear Model for lead isotope evolution (Cummings and Richards, 1975) has necessitated the re-assessment of previously published model lead ages. Further, the discovery, and subsequent development of the vast Navan deposit has provided an ideal opportunity to re-examine the importance of regional lead isotope variations within the Irish Pb-Zn orefield.

8.2.3 Results

8.2.3.1 Introduction

All galena analyses are presented in table 8.1. Model ages and μ values are calculated according to the Linear Model of Cumming and Richards (1975). Where replicate analyses have been carried out, model ages are based on the mean values of the isotope ratios.

8.2.3.2 Tynagh

The samples analysed were chosen so as to cover as large a volume of the orebody as possible, and also to represent the two main stages of ore mineralization. However, examination of figures 8.3 and 8.4 reveals that galenas from the Tynagh deposit exhibit a very uniform lead isotope composition. There are no significant variations that can be related to either spatial or paragenetic position within the orebody. Mean model age (m.y.): $348^{+}_{-}22$ (2 standard deviations).

8.2.3.3 Silvermines

Galenas from Mogul's Upper G, Lower G and B zones

TABLE 8.1

GALENA LEAD ISOTOPE RESULTS

Run No.	Location								206/204	207/204	208/204	Model * Age (my)	μ
C437	Tynagh	5050	66+10W	67.0 m.	N of Fault	(Stage 2)			18.036	15.512	37.824	337.8	10.49
C402	"	"	65+80W	70.0 m.	"	(Stage 3)			18.052	15.537	37.884	354.8	10.55
C423	"	5000	64+85W	18.0 m.	"	(Stage 2)			18.045	15.518	37.909	338.5	10.50
C406	"	"	51+50W	30.5 m.	"	(Stage 3)			18.059	15.537	37.889	354.8	10.55
C420	"	"	"	5.5 m.	"	(Stage 3)			18.030	15.503	37.922	331.8	10.47
C439	"	4912	66+30W	21.0 m.	"	(Stage 2)			18.030	15.516	37.817	346.2	10.50
C426	"	"	64+40W	37.0 m.	"	(Stage 2)			18.036	15.518	37.902	344.4	10.51
C427	"	"	"	"	"	(Stage 3)			18.003	15.500	37.809	349.9	10.50
C442	"	"	"	"	"	(Replicate)			18.038	15.528	37.857		
C407	"	4900	86+00W	23.0 m.	"	(Stage 3)			18.039	15.543	37.874	371.4	10.57
C431	"	"	"	"	"	(Replicate)			18.041	15.547	37.914		
C432	"	4725	86+20W	122.0 m.	"	(Stage 3)			18.025	15.520	37.833	353.9	10.51
C440	"	4620	91+20W	40.0 m.	"	(Stage 2)			18.043	15.522	37.860	344.2	10.51
C414	Silvermines - Shallee Southwest								18.214	15.548	38.013	263.5	10.58
C441	"		"	"		(Replicate)			18.252	15.575	38.071		
C410	"	- Mogul Lower G Zone							18.246	15.570	38.087	263.9	10.59
C412	"	- Mogul Upper G Zone		307 RM					18.234	15.577	38.051	279.5	10.61
C433	"	- Mogul B Zone		4931 haulage					18.238	15.590	38.160	291.2	10.64
C411	"	- Mogul B Zone		4650 RM					18.247	15.567	38.135	259.9	10.59
C417	"	- Magcobar Barytes Pit							18.241	15.573	38.121	270.5	10.60
C467	Navan	1-5 Lens	827.0 NW	520.6 NE	1380 El	75 m.	from B Fault		18.221	15.573	38.169	279.8	10.59
C503	"	"	"	"	"	"	"	(Replicate)	18.208	15.559	38.011		
C494	"	"	822.3 NW	514.1 NE	1375 El	1 m.	"		18.286	15.633	38.199	307.1	10.73
C466	"	2-5 Lens	835.7 NW	494.8 NE	1388 El	83 m.	"		18.222	15.565	38.070	273.7	10.56
C499	"	"	"	"	"	"	"	(Replicate)	18.186	15.543	37.953		
C477	"	"	826.2 NW	492.7 NE	1350 El	90 m.	from A Fault		18.206	15.593	38.110	297.5	10.60
C504	"	"	"	"	"	"	"	(Replicate)	18.191	15.550	37.988		
C478	"	"	837.7 NW	483.0 NE	1398 El	3 m.	"		18.240	15.595	38.119	297.7	10.66
C501	"	"	"	"	"	"	"	(Replicate)	18.250	15.605	38.132		
C486	"	"	846.8 NW	496.8 NE	1388 El	5 m.	from B Fault		18.250	15.620	38.141	312.5	10.68
C492	"	"	"	"	"	"	"	(Replicate)	18.228	15.600	38.151		
C502	"	"	841.7 NW	495.2 NE	1375 El	45 m.	"		18.196	15.553	37.987	277.8	10.56
C487	"	1-4 Lens	822.2 NW	522.4 NE	1393 El	55 m.	"		18.210	15.568	38.052	285.3	10.59
C495	"	2-4 Lens	822.5 NW	498.0 NE	1348 El	110 m.	"		18.252	15.595	38.082	287.6	10.65
C489	"	2-3 Lens	820.0 NW	500.6 NE	1347 El	100 m.	"		18.409	15.737	38.473	344.4	10.96
C491	"	"	"	"	"	"	"	(Replicate)	18.415	15.749	38.496		
C482	"	2-1 Lens	812.0 NW	503.9 NE	1378 El	145 m.	"		18.366	15.692	38.310		
C488	"	"	"	"	"	"	"	(Replicate)	18.358	15.690	38.323	313.2	10.80
C496	"	"	"	"	"	"	"	(Replicate)	18.273	15.616	38.088		

* - Linear model - Cumming and Richards (1975)

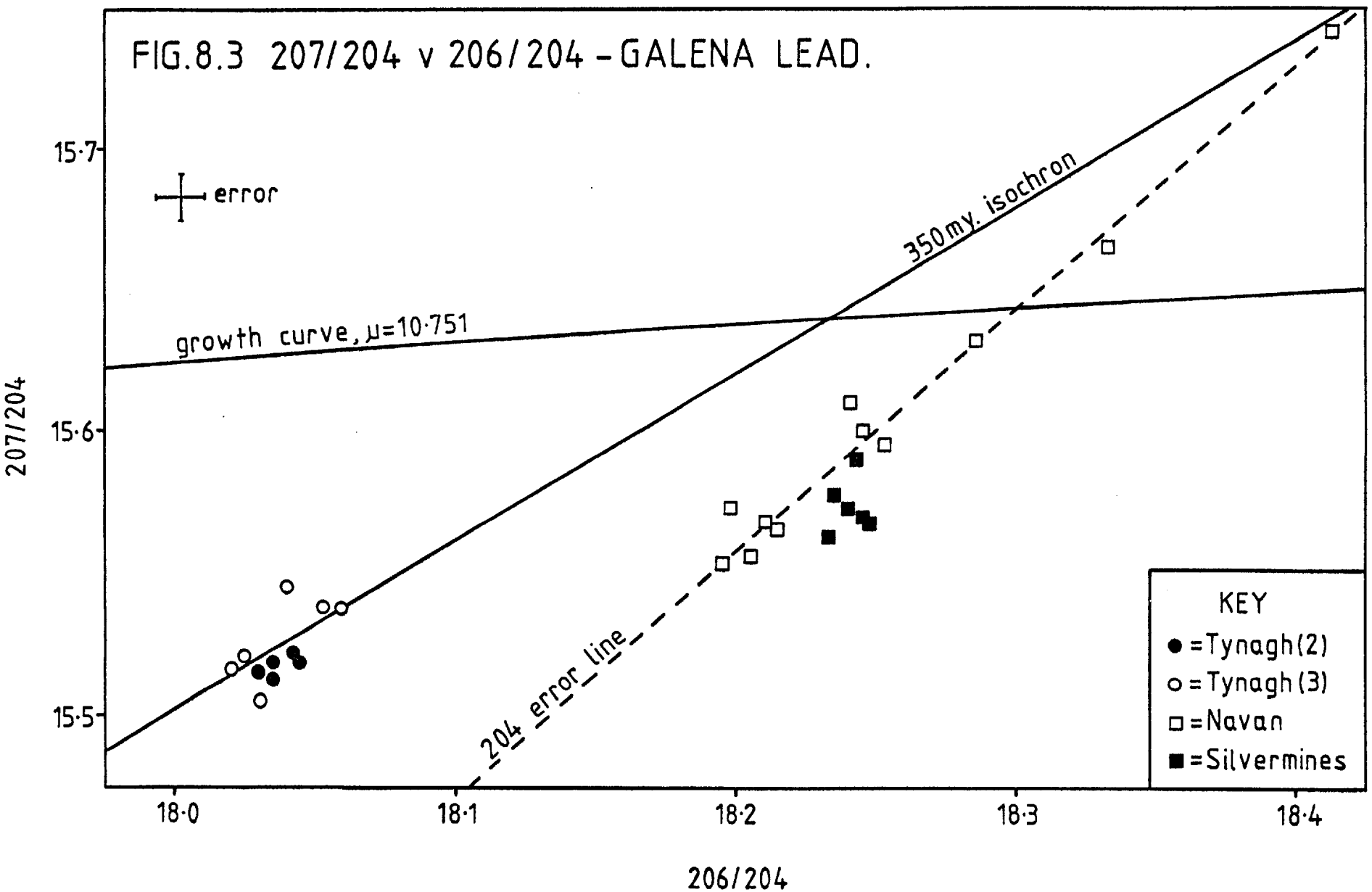
FIG.8.3 207/204 v 206/204 - GALENA LEAD.
15·7
15·6
15·5
207/204
error
350my. isochron
growth curve, μ=10·751
204 error line
KEY
● = Tynagh (2)
○ = Tynagh (3)
□ = Navan
■ = Silvermines
18·0
18·1
18·2
18·3
18·4
206/204

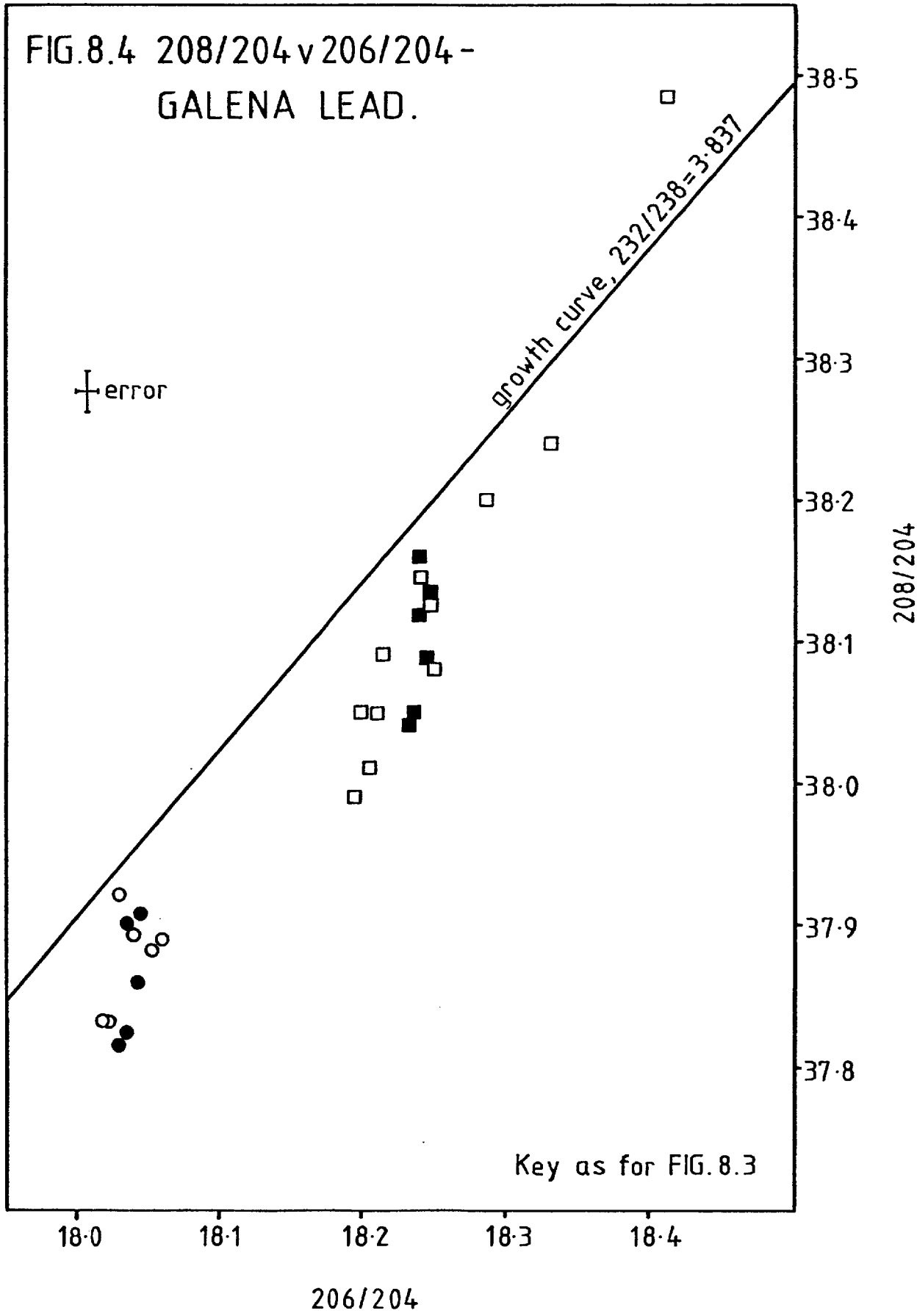
FIG.8.4 208/204 v 206/204 -
GALENA LEAD.
error
growth curve, 232/238=3.837
Key as for FIG.8.3
38·5
38·4
38·3
38·2
38·1
38·0
37·9
37·8
208/204
18·0
18·1
18·2
18·3
18·4
206/204

along with samples from the Magcobar barytes deposit and the O.R.S. hosted vein deposit at Shallee S.W. are almost identical in isotopic composition, (figs. 8.3, 8.4). This is in contrast to the data produced by Greig and co-workers (1971) which demonstrated wide ranges in lead isotope ratios for these same deposits. This confirms the view that much of the scatter in their data is due to analytical error. However, in agreement with their observations, the lead within the Silvermines deposits is clearly more radiogenic than that at Tynagh. Mean model age (m.y.): 271 ± 24 (2 standard deviations).

8.2.3.4 Navan

In contrast to Tynagh and Silvermines, galenas analysed from the Navan deposit exhibit a wide range in lead isotope ratios. The majority of the analyses cluster around, but are slightly less radiogenic than the Silvermines values (figs. 8.3, 8.4). However, three samples are distinct from the rest of the data. These have much higher ratios (and older model ages) and, together with the rest of the Navan data, define a linear trend that closely parallels a 204 error line. However, the replication of the two highest ratios, and the lack of any similar scatter in the standard analyses and analyses from the other deposits, rules out the possibility of 204 error. Moreover consideration of the spatial relationships of the samples indicates that this trend can be related to a number of important geological features.

Figure 8.5 is a more detailed plot of the Navan lead isotope data that indicates the ore horizon from which the sample was collected. For the 5 lens, the distance of the sample

FIG.8.5 LEAD ISOTOPE VARIATION WITHIN THE NAVAN DEPOSIT.

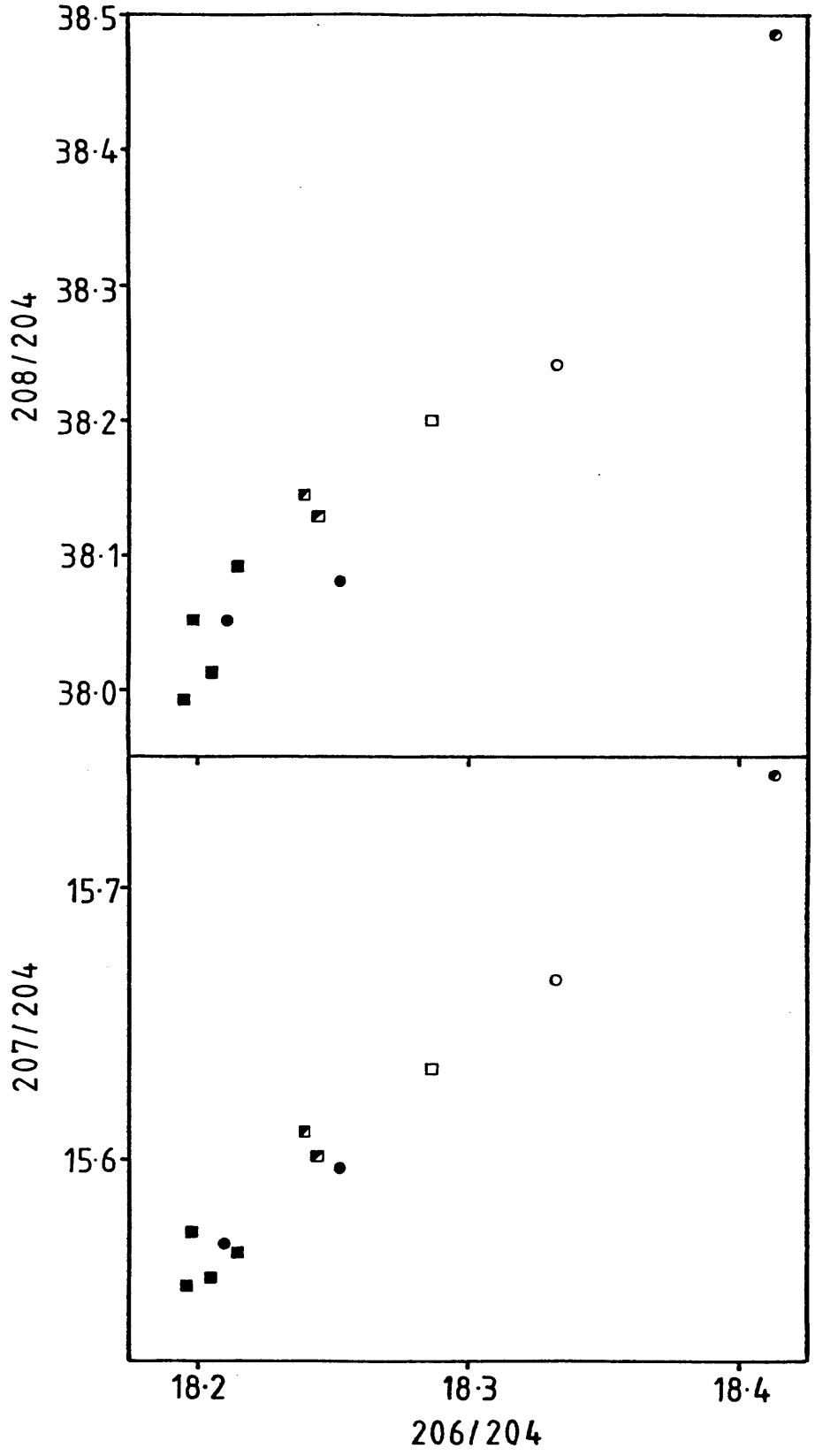

from either the A or the B fault is also shown. Considering samples from the 5 lens initially, it can be seen that there is a clear relationship between isotopic composition and proximity to either of the faults. Samples nearest the fault exhibit the highest ratios, while those in excess of 45 metres from the fault display lower ratios. Samples from the overlying ore horizons (4, 3 and 1 lens) were collected at distances in excess of 55 metres from the fault, but nearly all have higher ratios than their counterparts in the 5 lens . A possible explanation is discussed in the following section.

8.2.4 Interpretation and Discussion

8.2.4.1 Tynagh

The Galena model age for the Tynagh deposit agrees precisely with the age of mineralization inferred from the geological evidence. To recapitulate, it was argued in chapter 3 that mineralization at Tynagh was initiated during the early diagenetic history of the Waulsortian bank complex. These sediments are of Upper Tournaisian to Lower Visean in age, therefore a similar or possibly slightly younger age has to be inferred for the mineralization. George et al (1976) published a summary of radiometric dates for the British Dinantian stages (fig. 8.6), which suggests a date of approximately 350 m.y. for the Tournaisian-Visean boundary. The mean model age of $348^{+}_{-}22$ m.y. for the Tynagh deposit can, therefore, be safely interpreted at its face value as confirming an Upper Tournaisian/Lower Visean age for mineralization at Tynagh. Moreover, the similarity of the lead isotope ratios of stage 2 and 3 galenas indicates that the metals precipitated during these separate mineralizing events were derived from the same source.

Fig. 8.6 Summary of Published Radiometric Dates from the British Dinantian (after George et al, 1976)

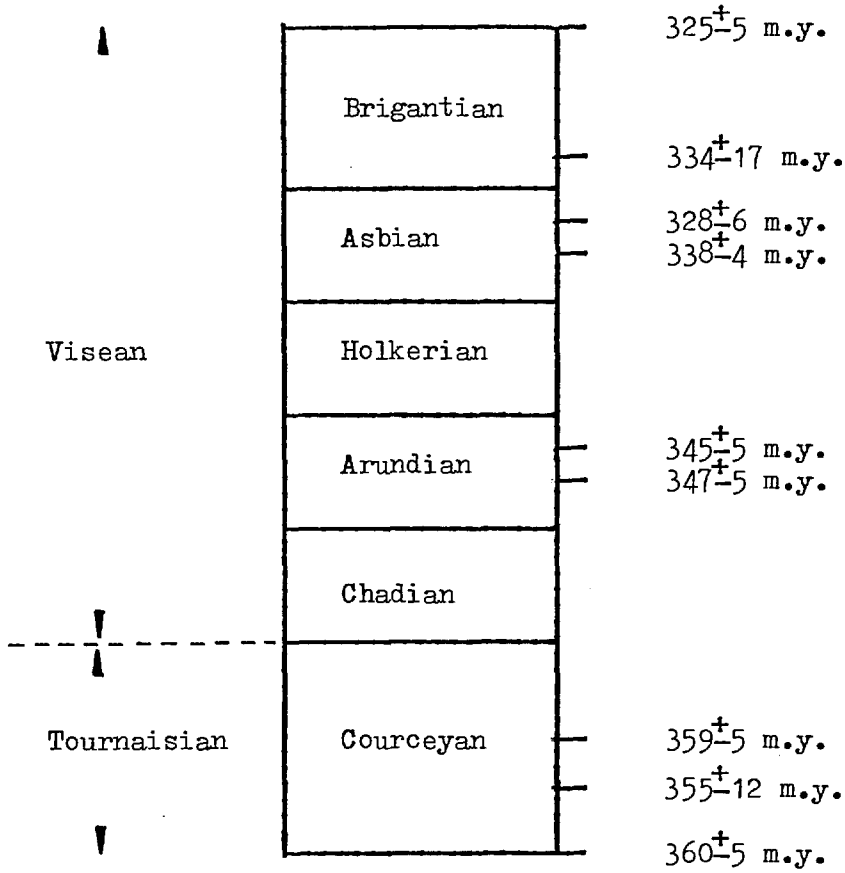

The agreement of the Tynagh model age with the age inferred from the geological evidence, raises important questions with regard to the source of the metals. The deep-seated, possibly mantle origin for this type of lead has been a feature of many interpretations in the past (e.g. Stanton and Russell, 1959; Cumming and Robertson, 1969). However lead in recent basic volcanics collected from sites where they would least likely have been contaminated during passage from the mantle, have heterogeneous isotopic compositions and do not fit a single stage growth curve (see Richards, 1971). Additionally, the Linear Model of Cummings and Richards (1975), favours a crustal source for ore leads. If single-stage

leads are indeed derived from a crustal source, a mechanism is called for that involved homogenisation of lead from large volumes of crust and its transport to the site of deposition with little or no contamination from radiogenic sources en route. The role of magmatism in such a process cannot be disregarded. Indeed, at Tynagh, the derivation of metals from an igneous source would be consistent with, and provide further support for, the recognition of deep-seated sulphur and carbon in the later stages of mineralization.

8.2.4.2 Silvermines

A model age of 271±24 m.y. for the Silvermines deposits would infer a Permian age for mineralization, if the lead had evolved in a single-stage system. This would support the views of Fillion (1973) and Barrett (1975) who considered that the Pb, Zn, Cu mineralization post-dated the deposition of the synsedimentary pyrite/barytes body. However, sample C433 (table 8.1) was taken from a stratiform sphalerite/galena horizon within the footwall Muddy "Reef" Limestone (see fig. 4.4). This horizon had undergone soft sediment deformation along with the host, and can, therefore, be dated stratigraphically as Upper Tournaisian. As it is isotopically identical, and thus undoubtedly related to galenas from the main ore horizon, a similar age is indicated for the economic mineralization. Galena lead from the Silvermines deposits is, therefore, anomalous in its isotopic composition and cannot be considered to have evolved in a single-stage system. In addition, the similarity in isotopic composition of the galena sample from the vein deposit at Shallee S.W., with galena from the stratiform Lower Carboniferous deposits indicates that they are

related to the same mineralizing episode.

Interpretation of the Silvermines and Tynagh data in terms of a two-stage model does not satisfactorily explain the anomalous Silvermines values. A least squares fit through the data, acceptance of the Tynagh model age as a close approximation to the age of mineralization, and adopting the average Tynagh μ value of 10.51 for the first stage, would infer an age of 3,175 m.y. for the source region. The existence of a basement as old as this is highly unlikely. The Inishtrahull gneiss complex of Co. Donegal has been correlated with the Lewisian of N.W. Scotland (Macintyre et al, 1975), but no isotope ages exceeding ~2,800 m.y. have been reported from the Scottish Precambrian (Chapman and Moorbath, 1977). Moreover, the basement underlying the Central Plain is considered to be much younger than Lewisian. Granulite-facies gneiss xenoliths within Lower Carboniferous agglomerates have been correlated with similar lithologies within the Ox Mountain inlier (Strogen, 1974). Phillips et al (1975) consider the Ox Mountain succession to resemble the Moine of Scotland, whilst Long and Max (1977) argue that it is Dalradian in age.

In recent years it has become accepted that hot concentrated chloride brines can leach metals from the formations through which they pass. The possibility has, therefore, arisen that radiogenic lead derived from local sedimentary sequences could explain the anomalous nature of many ore leads. In a radiogenic tracer study of lead and strontium in the Salton Sea geothermal brines Doe et al (1966) demonstrated that the bulk (50 - 100%) of the lead in the brines was leached from the host Quaternary and Tertiary sediments. Doe and Delevaux (1972) in a similar study of

ore and rock lead in the south east Missouri mining district, suggested that the radiogenic lead in the galenas could have been leached from the carbonate cement of the Lamotte Sandstone.

So as to ascertain whether or not a similar model could be proposed to explain the radiogenic nature of the Silvermines lead, a preliminary investigation of trace lead in some Palaeozoic sediments was carried out. Due to the limited time available only three samples were analysed (table 8.2), and even these are subject to large errors (see 5.3). Nevertheless it is evident that, even allowing for the error involved, Lower Palaeozoic and possibly Lower Carboniferous sediments can be regarded as a potential source of radiogenic lead. However, a contribution of single-stage lead, as exemplified by Tynagh, cannot be ruled out. Indeed, this would be necessary if the lead was derived from a source as radiogenic as the Ordovician or Silurian shales.

A more detailed and refined programme of whole rock analysis clearly needs to be undertaken to further define the radiogenic source. Such a study should include analysis of meta-sediments from the Ox Mountain inlier, as well as Palaeozoic sediments and volcanics from the Central Plain and adjacent massifs.

8.2.4.3 Navan

The scatter in the Navan data can be best explained by a model that involved the mixing of anomalous lead with single-stage, but high μ lead. The 5 lens was the first ore horizon to be deposited and at this time the metalliferous fluids had a similar lead isotope composition and were probably of similar provenance to those farther south at Silvermines. However, as

TABLE 8.2

WHOLE ROCK LEAD ISOTOPE ANALYSES

Run No.	Description	Location	ppm* U	ppm* Th	ppm* Pb	Measured Ratio[1]			Corrected Ratio[2]		
						206/204	207/204	208/204	206/204	207/204	208/204
C511	Lower Carboniferous Limestone shale (Lower Lst.)	11.3 km. W.N.W. of Tynagh mine	2.2	14.5	14.4	18.76	15.59	38.46	18.14	15.56	37.16
C510	Silurian slate	Slieve Bernagh inlier	2.0	8.7	10.5	24.39	16.18	39.65	23.53	16.14	38.47
C506	Ordovician black shale	Slieve Bernagh inlier	1.8	0.5	3.6	20.48	15.74	38.18	18.39	15.64	38.00

* Determined by X.R.F. analysis

1 Corrected for blank

2 Corrected for contribution of Radiogenic lead since time of mineralization (350 m.y.)

mineralization progressed at Navan, the lead isotope ratios of the metalliferous fluids increased resulting in the deposition of isotopically distinct galenas in the overlying (later) ore horizons. Contamination of previously precipitated sulphides in the vicinity of the main faults (the most probable conduits for these fluids), resulted in the displacement of their lead isotope ratios towards the values of the later fluids. The Navan sample with the highest ratio yields a model age of 344 m.y. which, if the same errors as on the Tynagh model age (± 22 m.y.) are adopted, would agree with the stratigraphic dating of the deposit. Therefore, the most likely cause for the shift towards higher ratios is the influx of single-stage magmatic lead that mixed with the Silvermines-type radiogenic lead.

One weakness in this argument is the widely differing μ values suggested for the source region. However, this could be accounted for by local variations in μ within the source region. Indeed, Cumming and Richards state that the Linear Model defines average behaviour and that variations in μ are to be expected.

8.2.5 The Role of Magmatism and the Source of Metals

In the preceding sections it was argued on the basis of the isotopic evidence that ore lead at Tynagh was derived from a magmatic source. Unfortunately, the apparent dearth of plutonic igneous activity of the appropriate age detracts from any model inferring a magmatic source for the metals. The Gortdrum Cu, Hg, Ag deposit displays the only known association with intrusions of Lower Carboniferous age. These consist of a number of minor basic plugs and dykes which cut the ore zone, but which have been

demonstrated to pre-date mineralization (Steed, 1975). However, gravity surveys have revealed anomalies (fig. 8.7) which have been interpreted as indicating the presence of a number of concealed acid plutons beneath central Ireland (Charlesworth, 1963). In addition, Schultz (1968) suggested that the broadly domal structure of the Slieve Aughty and associated Tynagh inlier may have been caused by vertical acting forces related to deep-seated magmatic activity.

Recent stable isotope studies have emphasised the importance of hydrothermal convection cells in the vicinity of igneous bodies intruded into the epizonal (upper 5 - 10 km.) continental environment (Taylor, 1974; Sheppard, 1977). In such circumstances the leaching of metals from the surrounding country rock and their incorporation into any embryonic mineralizing fluids has to be considered a possible consequence. As lead, and presumably other metals at Tynagh, was derived solely from a magmatic source, the effect of such a convection system has to be denied. Either permeability of the country rock was insufficient to allow significant circulation of pore waters, or magmatic activity occurred at depth. If the latter situation is the case then an explanation has to be proposed to account for the transport of lead to the site of ore precipitation with little or no contribution from radiogenic sources. An obvious answer lies in the Tynagh fault which may have provided a conduit for deep-seated hydrothermal fluids. Russell (1968) proposed that the intrusion of basic and intermediate magmas at the intersection of north-south geofractures with major east-west trending faults was intrinsic in controlling the location of the Lower Carboniferous hosted base metal deposits of Ireland.

FIG. 8.7 BOUGUER ANOMALY MAP OF CENTRAL IRELAND. (Based on Charlesworth, 1963).

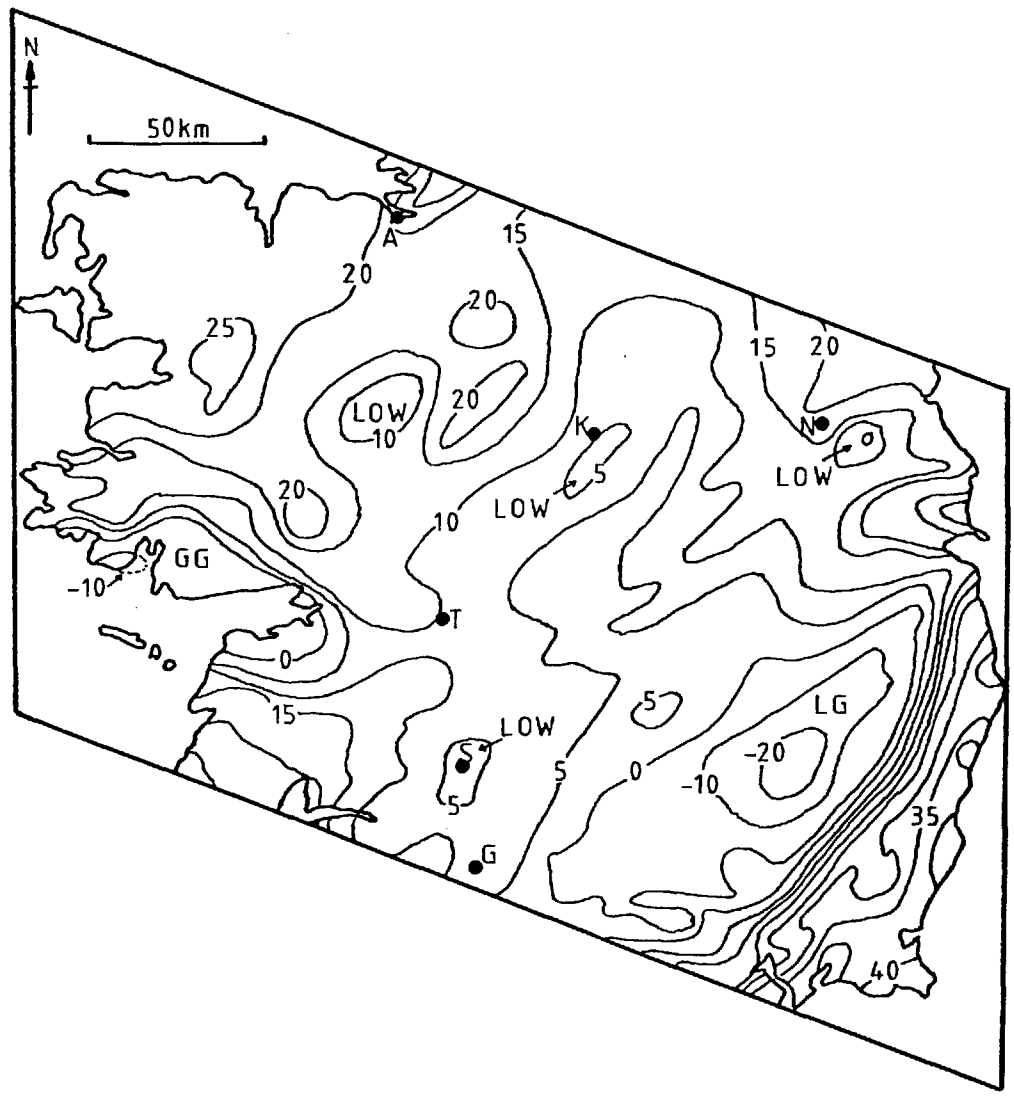

—= Bouguer anomaly in mgals.

GG = Anomaly related to outcrop & subsurface extension of Galway granite.

LG = Anomaly related to outcrop & subsurface extension of Leinster granite.

A = Abbeytown. G = Gortdrum. K = Keel.

N = Navan. S = Silvermines. T = Tynagh.

However, this is based entirely on conjecture. Indeed, such north-south structures are an unnecessary complication if the Tynagh and similar faults are themselves related to fundamental weaknesses in the basement.

Two of the most marked Bouguer "lows" within the Central Plain, excepting those associated with known outcropping granitic intrusions, occur in the immediate vicinity of the Navan and Silvermines deposits (fig. 8.7). No such anomaly is known at Tynagh. If these gravity "lows" are related to concealed granitic plutons of Lower Carboniferous age, then this would indicate that magma emplacement occurred at a higher level in the crust than that postulated beneath Tynagh. Consequently it is more likely that hydrothermal convection cells would have been established in their vicinity. If mineralization at Navan and Silvermines and high level intrusion were consanguineous, then no other mechanism need be sought to explain the circulation of waters through, and the leaching of radiogenic lead from surrounding sediments. In addition, a model involving derivation of metals from multiple source regions, both magmatic and sedimentary, goes far in explaining the differences in elemental composition between individual deposits.

8.3 Conclusions

Galena leads from the Tynagh deposit yield a model age for mineralization (348 ± 22 m.y.) that agrees precisely with that expected from the geological evidence. It is suggested that the lead evolved in a single-stage system, and that this indicates that the metals were derived from an igneous source.

Lead in galenas collected from the various deposits along

the Silvermines fault is isotopically uniform, and can be considered to have been deposited from the same metalliferous fluids. However, the lead is radiogenic in comparison to Tynagh lead, and the average model age is in conflict with the known stratigraphic age of the deposits. Therefore, the lead cannot have evolved solely within a single-stage system. Interpretation as a two-stage model predicts an age for the source region, that is older than any known basement in the British Isles. The Silvermines data can be best explained by a process that involved a contribution of radiogenic lead leached from a sedimentary or metasedimentary source.

Galenas from the Navan deposit exhibit a temporally related trend which indicates that initially the metalliferous fluids were of similar provenance to those at Silvermines. Later, mixing occurred with a high μ, single-stage lead, probably of magmatic origin.

A model is proposed whereby the Tynagh fault tapped metalliferous fluids generated by deep-seated magmatic activity, whilst at Navan and Silvermines higher level intrusion induced circulation of fluids through, and as a consequence leaching of lead from the surrounding country rocks.

CHAPTER 9

SUMMARY OF CONCLUSIONS AND GENETIC MODEL

9.1 SUMMARY

At Tynagh mine, Co. Galway, four major stages of mineralization can be recognised that span the diagenetic and post-lithification history of the host Waulsortian limestones:

Stage 1) Growth of colloform and granular pyrite (and marcasite) clots during early diagenesis.

Stage 2) Rapid geopetal precipitation of microcrystalline sphalerite, galena, dolomite and barytes, plus minor silicates within a dilatant fracture/breccia system. Tectonic disturbance in response to fault movement, combined with hydraulic fracturing, was responsible for creating the dilatant fracture/breccia system, and thus the space for stage 2 ore precipitation. The Waulsortian limestones had by this time reached an advanced stage of diagenesis and lithification. However, locally disruption extended to the sediment/rock interface where the host behaved in a semi-coherent manner. Injection of high pressure fluids maintained the fracture system and continuing tectonism resulted in the deformation and flow of previously precipitated sulphide muds.

Stage 3) An epigenetic stage of mineralization dominated by tennantite, medium to coarsely crystalline galena and sparry barytes, with subordinate chalcopyrite, bornite, arsenopyrite and sulphosalts. Under a regime of continuing sedimentation and diagenesis the host had become increasingly lithified and as a consequence the later Pb, Cu, As, Ba mineralization was emplaced as veinings and

replacements more typical of an epigenetic deposit.

Stage 4) Finally, precipitation of coarsely crystalline white calcite within veinlets and cavities, and dolomitisation of large volumes of unmineralized Waulsortian limestones.

The sulphur isotope data indicate that ore stage barytes was precipitated from Lower Carboniferous sea-water sulphate which had a $\delta^{34}S$ composition of approximately $+19^{o}/oo$. Stage 1 and 2 sulphides are isotopically light and were precipitated by reduced sulphur generated during open-system bacterial reduction of the sea-water sulphate reservoir. This is in agreement with mineral stability relationships which suggest that stage 2 metals and sulphur could not have been transported together to the site of ore deposition. Differences in the extent of the kinetic isotope effect between stages 1 and 2 are interpreted as being due to contrasting environmental conditions at the site of reduction. It is postulated that during stage 1 bacterial reduction occurred in situ, whilst during stage 2, reduced sulphur generated within the off-bank environment migrated into the Waulsortian limestones.

Stage 3 sulphides and sulphosalts display a much wider range of $\delta^{34}S$ values and exhibit a distinct trend towards $0^{o}/oo$ as the fault is approached. This is interpreted as indicating that deep-seated sulphur was introduced from the fault zone along with the metals, and that mixing occurred with bacteriogenic sulphur migrating into the Waulsortian limestones. The transport of sulphur along with lead implies that later metalliferous fluids were fairly acid, which in turn would account for the importance of replacement during stage 3.

Mineralized limestones, ore stage and post-ore carbonates

are depleted in the heavier isotopes of carbon and oxygen with respect to unmineralized limestones. The depletion in ^{13}C is attributed to the mixing of host derived carbon with bacterially oxidised organic carbon, and, during stage 4, deep-seated carbon. Calculated oxygen isotope fractionation temperatures for stage 1 fibrous calcites (25-49°C), assuming equilibrium deposition from Lower Carboniferous sea-water, are within the range tolerated by sulphate reducing anaerobes. A trend towards lighter $\delta^{18}O$ values in later generations of stage 1 sparry carbonate indicates either an increase in temperature towards 90°C or an influx of isotopically lighter water. However, as a stage 3 quartz-albite pair yield a fractionation temperature of 110°C, and because oxygen isotope variation in dolomitised zones adjacent to a stage 3 veinlet can only be explained as being due to exchange with water isotopically heavier than sea-water, this trend is interpreted as indicating an increase in temperature.

Galenas representative of both second and third stages of mineralization display a narrow range of lead isotope ratios and yield an average model age of 348 ± 22 m.y. (2σ). This agrees precisely with the stratigraphic dating of the deposit. On this basis a deep-seated, magmatic source is postulated for the metals.

A preliminary sulphur isotope investigation of banded stratiform ores from the Navan deposit indicates their precipitation from bacterially reduced Lower Carboniferous sea-water sulphate. However, further work is needed to refine the model. Nevertheless, the similarity of $\delta^{34}S$ values from Tynagh and Navan, with previously published analyses from Silvermines, provides further evidence for a genetic link between these major Lower Carboniferous hosted

deposits.

In contrast to the sulphur isotope data, lead from the Navan and Silvermines deposits is isotopically distinct from that at Tynagh. Silvermines lead is radiogenic in comparison to Tynagh lead, and the average model age is in conflict with the known stratigraphic age of the deposit. The data can be best explained by a model that involves a contribution of radiogenic lead leached from a sedimentary or metasedimentary source. Galenas from the Navan deposit exhibit a secular trend which indicates that initially, the metalliferous fluids were of similar provenance to those at Silvermines, and that later, mixing occurred with a high μ, single stage, magmatic lead.

A model is proposed whereby the Tynagh fault tapped hydrothermal metalliferous fluids generated by deep-seated magmatic activity. This fluid rose along the line of the Tynagh fault as a discrete body with little or no interaction with country rocks en route. It is postulated that mineralization at Navan and Silvermines may be related to higher level granites, and that radiogenic lead was leached from the surrounding country rocks by hydrothermal convection cells established in their immediate vicinity.

9.2 A MODEL FOR ORE EMPLACEMENT

9.2.1 Tynagh

In Upper Tournaisian to Lower Visean times, metalliferous hydrothermal fluids generated by deep-seated magmatic activity rose along the line of the Tynagh fault. Initially, these fluids were rich in iron and silica and on encountering the mid-Lower Carboniferous sea floor were precipitated as a sedimentary iron formation

in a basinal region to the north of the Waulsortian carbonate mud bank complex. Fault movements synchronous with these exhalations led to syn-sedimentary slumping of Waulsortian carbonates, and the rapid burial of organic matter. Local centres of anaerobic bacterial activity were established, and iron diffusing through the sediment was precipitated by bacterially reduced contemporaneous sea-water sulphate (stage 1). The ambient temperature within the sediment at the time of iron sulphide deposition did not exceed 50°C.

During the later stages of Waulsortian bank accumulation fault movement in league with hydraulic fracturing resulted in the formation of a dilatant fracture/breccia system. The utilisation of all available organic matter and an increase in the temperature, possibly to in excess of 100°C, had resulted in the destruction of the local anaerobe population. Nevertheless, bacteriogenic sulphur generated within the argillaceous off-bank facies was by this time migrating into the Waulsortian limestones. Metals, now largely zinc, contained within the hydrothermal fluid mixed with the bacterially reduced sulphur and were rapidly precipitated as microcrystalline sulphides within the fracture system (stage 2). Continuing tectonism resulted in the detachment of limestone fragments from the walls of the fractures, and the disruption, fluidisation and flow of previously precipitated sulphide muds.

Throughout the second stage of sulphide mineralization dissolution of the host rock was minimal. The small amount of carbonate that was derived from the Waulsortian limestones mixed with the lesser quantities of bacterial CO_2 and was re-precipitated as fine grained dolomite within the sphalerite muds. However, the third and final stage of sulphide mineralization not only marked the

influx of a metalliferous fluid rich in Cu, Pb, Ba and As, but was also accompanied by a change in pH. Whereas before the ore solutions were probably neutral to mildly alkaline, they may now have been slightly acid, resulting in the dissolution and replacement of the host limestones. Although deep-seated sulphur was introduced from the fault zone along with the metals, the mixing with bacteriogenic reduced sulphur and Lower Carboniferous sea-water sulphate was fundamental in controlling the precipitation of stage 3 sulphides, sulphosalts and barytes.

The waning stage of mineralization was marked by the dolomitisation of unmineralized ground, and the precipitation of calcite within cavities and post-ore fractures (stage 4).

9.2.2 Broader Implications

The similarities in sulphur isotope variation at Navan, Silvermines and Tynagh suggests that the generation and accumulation of bacteriogenic sulphur was a key factor in controlling the deposition of the major Lower Carboniferous base metal deposits. Future exploration philosophy should, therefore, take into consideration the location of sites that were favourable for bacterial reduction of contemporaneous sea-water sulphate. At Tynagh the palaeo-hydrogeologic situation and availability of a near surface reservoir were additional factors instrumental in creating a suitable environment for ore precipitation. Barrett (1975) demonstrated that the footwall topography beneath the stratiform deposits at Silvermines was important in controlling water circulation, the Eh and pH conditions, and thus the nature of mineralization at the sediment/water interface. Research into the palaeoenvironmental controls on ore deposition at Navan may further

define the parameters influencing ore emplacement in the Central Plain of Ireland.

APPENDIX 1

ISOTOPE RATIO CORRECTION FACTORS

a) Valve leakage correction - worked example

True isotopic composition of reference gas = $0^{o}/oo$

True isotopic composition of sample gas = $+20^{o}/oo$

$\therefore$ actual difference in isotopic composition (δ a) = $+20^{o}/oo$

Valve leakage from reference → sample = 0.07%

Valve leakage from sample → reference = 0.08%

Total valve leakage = 0.15%

i.e. When the sample gas is being analysed, 0.07% of the gas measured is reference, and 99.93% of the gas measured is sample.

$\therefore$ value of gas in source when switched to sample =

$+20^{o}/oo - (\delta a \times 0.07\%) = +19.986^{o}/oo$

value of gas in source when switched to reference =

$+0^{o}/oo + (\delta a \times 0.08\%) = +0.016^{o}/oo$

$\therefore$ measured difference in isotopic composition (δ m) = $+19.97^{o}/oo$

To correct for valve leakage:-

$\delta a = \delta m + (\delta m \times \text{total valve leakage correction})$

$= +19.97^{o}/oo + (19.97^{o}/oo \times 0.15\%) = +20^{o}/oo$

b) Isobaric corrections (Craig, 1957)

General equations:-

$$\delta^{13}C \text{ corrected} = \delta^{45}\left[\frac{R^{45}(std)}{R^{13}(std)}\right] - \left[\frac{R^{17}(std)}{2R^{13}(std)}\right]\delta^{18}O \qquad (1)$$

$$1 + \delta m = \frac{\left[(1 + \delta c) + \frac{(1 + \delta^{13}C)\, R^{13}(std)\, (1 + \frac{\delta c}{2})\, R^{17}(std)}{R^{18}(std)}\right]}{\left[1 + \frac{R^{13}(std)\, R^{17}(std)}{R^{18}(std)}\right]} \qquad (2)$$

$$\times \quad \frac{\left[1 + R^{13}(std) + R^{17}(std)\right]}{\left[1 + (1 + \delta^{13}C)\, R^{13}(std) + (1 + \frac{\delta c}{2})\, R^{17}(std)\right]}$$

Where:-

$\delta m = \delta^{46}$; $\delta c = \delta^{18}O$ corrected

Isotopic ratios of standards:-

$R^{13}PDB = 0.0112372$ (Craig, 1957)

R^{18} SMOW (as CO_2) = 0.0040104 (Baertschi, 1976)

R^{17} SMOW (as CO_2) = 0.0007385 (Calculated from Baertschi, 1976).

However, for correction of measurements made against the laboratory reference gas, the isotopic ratios of the reference gas have to be known. These can be obtained from its δ value with respect to the laboratory standard, which is calibrated with respect to the international standards:-

$$\delta^{*}\ (ref) = \left[\frac{R^{*}(ref)}{R^{*}(std)} - 1\right] \times 1000$$

$$\therefore\ R^{*}\ (ref) = \left[\frac{\delta^{*}(ref)}{1000} + 1\right] \times R^{*}(std)$$

The δ values of the laboratory standard calcite (MCS) are:-

$\delta^{13}C$ (PDB) = $-0.70^{o}/oo$

$\delta^{18}O$ (SMOW) = $+21.40^{o}/oo$

Applying the fractionation factor (α) of 10.25°/oo for CO_2 prepared from calcite at 25.18°C, (Sharma and Clayton, 1965):-

δ^{18} (SMOW) of CO_2 prepared from MCS = +31.87°/oo

$$\delta^{17}\ (SMOW) \simeq \frac{\delta^{18}O\ (SMOW)}{2}$$

∴ the isotopic ratios of the laboratory standard gas prepared from MCS are:-

$R^{13} = 0.0112293$

$R^{18} = 0.0041382$

$R^{17} = 0.0007503$

$R^{45} = R^{17} + R^{13}$

Substituting these values in equations (1) and (2) above, and ignoring products of δ:-

$$\delta^{13}C \text{ corrected} = 1.0668\ \delta^{45} - 0.0334\ \delta^{18}O \qquad (3)$$

$$\delta^{18}O \text{ corrected} = 1.0014\ \delta^{46} + 0.009\ \delta^{13}C \qquad (4)$$

Equations (3) and (4) can be solved by combining as simultaneous equations:-

$$\delta^{13} \text{ corrected} = 1.0665\ \delta^{45} - 0.0334\ \delta^{46} \qquad (5)$$

$$\delta^{18} \text{ corrected} = 0.0097\ \delta^{45} + 1.0011\ \delta^{46} \qquad (6)$$

Substituting values for δ^{45} and δ^{46} obtained by measurements against CO_2 prepared from MCS and corrected for valve leakage, will give $\delta^{13}C$ and $\delta^{18}O$ (corrected) for the sample CO_2, with respect to CO_2/MCS.

For conversion with respect to the standards, PDB and SMOW:-

$$\delta\,^{13}C\ \text{SAMPLE}_{(PDB)} = \left[\frac{R^{13}\ CO_2/\text{SAMPLE}}{R^{13}\ CO_2/\text{MCS}} \times \frac{R^{13}\ CO_2/\text{MCS}}{R^{13}\ \text{PDB}} - 1\right] \times 1000$$

$$\delta\,^{18}O\ CO_2/\text{SAMPLE}_{(SMOW)} = \left[\frac{R^{18}CO_2/\text{SAMPLE}}{R^{18}CO_2/\text{MCS}} \times \frac{R^{18}\ CO_2/\text{MCS}}{R^{18}\ \text{SMOW}} - 1\right] \times 1000$$

$$\therefore\ \delta\,^{18}O\ \text{SAMPLE}_{(SMOW)} = \left[\frac{R^{18}CO_2/\text{SAMPLE}}{\text{SMOW}} \times \frac{1}{^{18}\alpha\ \text{Calcite} - CO_2} - 1\right] \times 1000$$

c) Lead isotope blank correction

$$\frac{206}{204}\ \text{actual} = \frac{206\ \text{measured} - 206\ \text{blank}}{204\ \text{measured} - 204\ \text{blank}}$$

$$= \frac{\left[\frac{(\mu g\ \text{sample} + \text{blank})}{\text{A.W. meas.}} \times \%\ 206\ \text{meas.}\right] - \left[\frac{\mu g\ \text{blank}}{\text{A.W. blank}} \times \%\ 206\ \text{blank}\right]}{\left[\frac{(\mu g\ \text{sample} + \text{blank})}{\text{A.W. meas.}} \times \%\ 204\ \text{meas.}\right] - \left[\frac{\mu g\ \text{blank}}{\text{A.W. blank}} \times \%\ 204\ \text{blank}\right]}$$

and similarly for the other radiogenic masses.

Atomic weights and atomic percentages are determined from the isotope ratios.

Ratios assumed for the blank are those of atmospheric lead (Chow, 1968):-

206/204	207/204	208/204
18.41	15.64	38.66

APPENDIX 2

LEAD ISOTOPE MODELS

a) Holmes/Houtermans Model

The equations employed in the mathematical treatment of common lead data can be derived from the basic radioactive decay equation:-

$$Nt = Np\ e^{\lambda t} \qquad (1)$$

Where Nt is the number of atoms of a radioactive parent at time t in the past, that would be reduced to Np atoms at the present time; λ is the decay constant.

The number of ^{206}Pb atoms generated from the beginning of geological time (t_0), to some arbitary time (t_1) is given by

$$^{206}Pbt_1 = {}^{238}Ut_0 - {}^{238}Ut_1 = {}^{238}Up\ (e^{\lambda t_0} - e^{\lambda t_1}) \qquad (2)$$

To obtain the total ^{206}Pb in a closed system at time t_1, the ^{206}Pb present in primaeval lead must be added to the radiogenic ^{206}Pb. Expression as a ratio with respect to ^{204}Pb (a constant in a closed system), removes the necessity of knowing the absolute quantities involved.

$$\left[\frac{^{206}Pb}{^{204}Pb}\right]_{t_1} = \left[\frac{^{206}Pb}{^{204}Pb}\right]_{t_0} + \left[\frac{^{238}U}{^{204}Pb}\right]_{present} (e^{\lambda t_0} - e^{\lambda t_1}) \qquad (3)$$

Primaeval Lead — Radiogenic Lead

Similarly for the other radiogenic isotopes:-

$$\left[\frac{^{207}Pb}{^{204}Pb}\right]_{t_1} = \left[\frac{^{207}Pb}{^{204}Pb}\right]_{t_0} + \frac{1}{137.88}\left[\frac{^{238}U}{^{204}Pb}\right]_{p} (e^{\lambda' t_0} - e^{\lambda' t_1}) \qquad (4)$$

$$\left[\frac{^{208}Pb}{^{204}Pb}\right]_{t_1} = \left[\frac{^{208}Pb}{^{204}Pb}\right]_{t_0} + \left[\frac{^{232}Th}{^{204}Pb}\right]_{p} (e^{\lambda'' t_0} - e^{\lambda'' t_1}) \qquad (5)$$

Equations (3) and (4) can be combined to give

$$\left[\frac{\left[\frac{207}{204}\right]t_1 - \left[\frac{207}{204}\right]t_0}{\left[\frac{206}{204}\right]t_1 - \left[\frac{206}{204}\right]t_0}\right] = \frac{(e^{\lambda' t_0} - e^{\lambda' t_1})}{137.88\,(e^{\lambda t_0} - e^{\lambda t_1})} \qquad (6)$$

and similarly (3) and (5) to give

$$\left[\frac{\left[\frac{208}{204}\right]t_1 - \left[\frac{208}{204}\right]t_0}{\left[\frac{206}{204}\right]t_1 - \left[\frac{206}{204}\right]t_0}\right] = \left[\frac{Th^{232}}{U^{238}}\right] \frac{(e^{\lambda'' t_0} - e^{\lambda'' t_1})}{(e^{\lambda t_0} - e^{\lambda t_1})} \qquad (7)$$

Where:- $\lambda = 0.155125 \times 10^{-9}$ yr.$^{-1}$ (Jaffey et al, 1971)

$\lambda' = 0.98485 \times 10^{-9}$ yr.$^{-1}$ (" ")

$\lambda'' = 0.049475 \times 10^{-9}$ yr.$^{-1}$ (Le Roux and Glendenin, 1963)

$$\left.\begin{aligned} (^{206}Pb/^{204}Pb)t_0 &= 9.307 \\ (^{207}Pb/^{204}Pb)t_0 &= 10.294 \\ (^{208}Pb/^{204}Pb)t_0 &= 29.476 \end{aligned}\right\} \text{ (Tatsumoto et al, 1973)}$$

(6) and (7) are the equations for the primary growth curves which can be solved by substituting values for t_0 and t_1. For the calculation of a secondary growth curve, the isotope ratios and age of the source rocks are substituted for those of the Earth at t_0.

b) Linear Model

In Cummings and Richards model an additional factor is introduced to allow for a linear increase in the U/Pb and U/Th ratio with geological time:-

$$\left[\frac{^{206}Pb}{^{204}Pb}\right]t_1 = \left[\frac{^{206}Pb}{^{204}Pb}\right]t_0 + \left[\frac{^{238}U}{^{204}Pb}\right]p \left\{ e^{\lambda t_0}\left[1 - \epsilon\left(t_0 - \frac{1}{\lambda}\right)\right] - e^{\lambda t_1}\left[1 - \epsilon\left(t_1 - \frac{1}{\lambda}\right)\right]\right\}$$

with similar equations for 207/204 and 208/204

Where:-

ϵ (U system) = 0.050×10^{-9} yr.$^{-1}$

ϵ (Th system) = 0.037×10^{-9} yr.$^{-1}$

t_0 = 4.509×10^{9} years.

ϵ was obtained by fitting the conformable ore data to a curve that yielded reasonable geological ages i.e. ages in agreement with those obtained by other dating methods.

REFERENCES

ANDERSON, G.M., 1973, The hydrothermal transport and deposition of galena and sphalerite near 100°C: Econ. Geol., V. 68, p. 480 - 492.

ANDERSON, G.M., 1975, Precipitation of Mississippi - Valley type ores: Econ. Geol., V. 70, p. 937 - 942.

ASHBY, D.F., 1939, The geological succession and petrology of the Lower Carboniferous volcanic area of Co. Limerick: Proc. Geol. Ass., V. 50, p. 324 - 330.

BAERTSCHI, P, 1976, Absolute ^{18}O content of Standard Mean Ocean Water: Earth Planet. Sci. Lett., V. 31, p. 341 - 344.

BARRETT, J.R., 1975, Genesis of the Ballynoe barite deposit, Ireland and other British stratabound barite deposits: Unpub. PhD. thesis, London Univ.

BATHURST, R.G.C., 1971, Carbonate Sediments and their Diagenesis. Developments in Sedimentology, V. 12: Amsterdam, Elsevier.

BEALES, F.W., 1975, Precipitation mechanisms for Mississippi Valley - type ore deposits: Econ. Geol., V. 70, p. 943 - 948.

BERNER, R.A., 1969, The synthesis of framboidal pyrite: Econ. Geol., V. 64, p. 383 - 384.

BIGELEISEN, J., 1952, The effects of isotopic substitution on the rates of chemical reactions: J. Phys. Chem., V. 56, p. 823 - 828

BUERGER, N.W., 1934, The unmixing of chalcopyrite from sphalerite: Am. Mineralogist, V. 19, p. 525 - 530.

BYRNE, B., DOWNING D., and ROMER D., 1971, Some aspects of the genesis of the zinc - lead orebody at Navan, in Skevington, D., ed., The genesis of base metal deposits in Ireland - Irish Geol. Assoc., Proc. Galway Symp.

CAMERON, A.E., SMITH, D.H., and WALKER, R.L., 1969, Mass spectrometry of nanogram - size samples of lead: Anal. Chem., V. 41, p. 525 - 526

CATANZARO, E.J., MURPHY T.J., SHIELDS, W.R., and GARNER, E.L., 1968, Absolute isotopic abundance ratios of common, equal - atom, and radiogenic lead isotopic standards: J. Res. Natn. Bur. Stand.- A. Physics and Chemistry, V. 72, p. 261 - 267.

CHAPMAN, H.J., and MOORBATH, S., 1977, Lead isotope measurements from the oldest recognised Lewisian gneisses of north - west Scotland: Nature, V. 268, p. 41 - 42.

CHARLESWORTH, J.K., 1963, Historical Geology of Ireland: Edinburgh and London, Oliver and Boyd.

CHOW, T.J., 1968, Isotope analysis of sea water by mass spectrometry: J. Water Pollution Control Federation, V. 40, p. 399 - 411.

CLAYPOOL, G., PRESLEY, B.J., and KAPLAN, I.R., 1973, Gas analyses of sediment samples from Legs 10, 11, 13, 14, 15, 18 and 19: Initial Reports of the Deep Sea Drilling Project, V. 19, p. 879 - 884.

CLAYTON, R.N., and MAYEDA, T.K., 1963, The use of bromine pentafluoride in the extraction of oxygen from oxides and silicates for isotopic analysis: Geochim. Cosmochim. Acta, V. 27, p. 43 - 52.

COLEMAN, M.L., 1977, Sulphur isotopes in petrology: Jl. Geol. Soc. Lond., V. 133, p. 593 - 608.

COOMER, P.G., and ROBINSON, B.W., 1976, Sulphur and sulphate - oxygen isotopes and the origin of the Silvermines deposits, Ireland: Mineral. Deposita, V. 11, p. 155 - 169.

CRAIG, H., 1954, Carbon 13 in plants and their relationships between Carbon 13 and Carbon 14 variations in nature: J. Geol., V. 62, p. 115 - 149.

CRAIG, H., 1957, Isotopic standards for carbon and oxygen and correction factors for mass spectrometric analysis of carbon dioxide: Geochim. Cosmochim. Acta, V. 12, p. 133 - 149.

CRAIG, H., 1961a, Standards for reporting concentrations of deuterium and oxygen - 18 in natural waters: Science, V. 133, p. 1833 - 1834.

CRAIG, H., 1961b, Isotopic variations in meteoric waters: Science, V. 133, p. 1702 - 1703.

CRAIG, H., 1965, Measurement of oxygen isotope palaeotemperatures: Proc. Spoleto. Conf. on Stable Isotopes in Oceanographic Studies and Palaeotemperatures, V. 3, p. 7.

CUMMING, G.L., and ROBERTSON, D.K., 1969, Isotopic composition of lead from the Pine Point Deposit: Econ. Geol., V. 64, p. 731 - 732

CUMMING, G.L. and RICHARDS, J.R., 1975, Ore lead isotope ratios in a continuously changing Earth: Earth Planet. Sci. Lett., V. 28, p. 155 - 171.

CZAMANSKE, G.K., and RYE, R.O., 1974, Experimentally determined sulphur isotope fractionations between sphalerite and galena in the temperature range 600° to 275°C: Econ. Geol., V. 69, p. 17 - 25.

DANSGAARD, W., 1964, Stable isotopes in precipitation: Tellus, V. 16, p. 436 - 468.

DEINES, P., 1970, Mass spectrometer correction factors for the determination of small isotopic composition variations of carbon and oxygen: Int. J. Mass Spectrom. Ion Phys., V. 4, p. 283 - 295.

DERRY, D.R., CLARK, G.R., and GILLATT, N., 1965, The Northgate base-metal deposit at Tynagh, County Galway, Ireland: Econ. Geol., V. 60, p. 1218 - 1237.

DOE. B.R., 1970, Lead Isotopes: Berlin, Springer - Verlag.

DOE, B.R., HEDGE, C.E., and WHITE, D.E., 1966, Preliminary investigation of the source of lead and strontium in deep geothermal brines underlying the Salton Sea area: Econ. Geol., V. 61, p. 462 - 483.

DOE, B.R., and DELEVAUX, M.H., 1972, The source of lead in south-east Missouri galena ores: Econ. Geol., V. 67, p. 409 - 439.

DOE, B.R., and STACEY, J.S., 1974, The application of lead isotopes to the problems of ore genesis and ore prospect evaluation - a review: Econ. Geol., V. 69, p. 757 - 776.

ECKELMANN, W.R., BROECKER, W.S., WHITLOCK, D.W., and ALLSUP, J.R., 1962, Implications of carbon isotopic composition of total organic carbon of some recent sediments and ancient oils: Am. Assoc. Petrol. Geol. Bull., V. 46, p. 699 - 704.

ELLIS, A.J., 1967, The chemistry of some explored geothermal systems, in Barnes, H.L., ed., Geochemistry of Hydrothermal Ore Deposits: New York, Holt, Rhinehart and Winston, Inc., p. 465 - 514.

EPSTEIN, S., 1970, Antarctic ice sheet - Stable isotope analyses of Byrd station cores and interhemispheric climatic implications: Science, V. 168, p. 1570 - 1572.

EPSTEIN, S., and MAYEDA, T., 1953, Variations of ^{18}O content of waters from natural sources: Geochim. Cosmochim. Acta, V. 4, p. 213 - 224.

EPSTEIN, S., BUCHSBAUM, R., LOWENSTAM, H.A., and UREY, H.C., 1953, Revised carbonate - water isotopic temperature scale: Geol. Soc. Am. Bull., V. 64, p. 1315 - 1325.

EPSTEIN, S., SHARP, R.P., and GOW, A.J., 1965, Six-year record of oxygen and hydrogen isotope variations in South Pole firn: J. Geophys. Res., V. 70, p. 1809 - 1819.

FILLION, M., 1973, Economic geology and geostatistics of base metal mineralization at Silvermines, Ireland: Unpub. Ph.D. thesis, London Univ.

GEORGE, T.N., JOHNSON, G.A.L., MITCHELL, M., PRENTICE, J.E., RAMSBOTTOM, W.H.C., SEVASTOPULO, G.D., and WILSON, R.B., 1976, A correlation of Dinantian rocks in the British Isles: Geol. Soc. Lond. Spec. Report No. 7.

GINSBURG, R.N., 1957, Early diagenesis and lithification of shallow - water carbonate sediments in south Florida, in Le Blanc, R.J., and Breeding, J.G., eds., Regional Aspects of Carbonate Deposition: Soc. Palaeontologists Mineralogists Spec. Publ. 5, p. 80 - 100.

GOLDHABER, M.B., and KAPLAN, I.R., 1974, Controls and consequences of sulphate reduction in recent marine sediments: Soil Sci., V. 119, p. 42 - 55.

GRAHAM, R.A.F., 1970, The Mogul base metal deposits, Co. Tipperary, Ireland: Unpub. Ph.D. thesis, Univ. Western Ontario.

GREIG, J.A., BAADSGAARD, H., CUMMING, G.L., FOLINSBEE, R.E., KROUSE, H.R., OHMOTO, H., SASAKI, A., and SMEJKAL, V., 1971, Lead and sulphur isotopes of the Irish base metal mines in Carboniferous carbonate host rocks: Soc. Mining Geologists Japan, Spec. Issue 2 (Proc. IMA - IAGOD Mtgs. 1970, Joint Symp. Vol.), p. 84 - 92.

HALLS, C., 1975, Syndiagenetic emplacement in Irish ore deposits and the tectonic implications: Mineral Deposits Studies Group Geol. Soc. Lond., Leicester Mtg., 1975, Abstracts.

HAMANN, R.J., and ANDERSON, G.M., 1978, Solubility of galena in sulphur rich NaCl solutions: Econ. Geol. V. 73, p. 96 - 100.

HARRISON, A.G., and THODE, H.G., 1957, The kinetic isotope effect in the chemical reduction of sulphate: Trans. Faraday Soc., V. 53, p. 1648 - 1651.

HEYL, A.V., DELEVAUX, M.H., ZARTMAN, R.E., and BROCK, M.R., 1966, Isotopic study of galenas from the Upper Mississippi Valley, the Illinois - Kentucky and some Appalachian Valley mineral districts: Econ. Geol., V. 61, p. 933 - 961.

HOLMES, A., 1946, An estimate of the age of the Earth, Nature, V. 157, p. 680 - 684.

HOLSER, W.T., 1977, Catastrophic chemical events in the history of the ocean: Nature, V. 267, p. 403 - 408.

HOLSER, W.T., and KAPLAN, J.R., 1966, Isotope geochemistry of sedimentary sulphates: Chem. Geol., V. 1, p. 93 - 135.

HOUTERMANS, F.G., 1946, The isotope ratios in natural lead and the age of uranium: Naturwiss, V. 33, p. 185 - 186, 219.

HUNT, J.M., 1967, The Origin of petroleum in carbonate rocks, in Chilingar, G.V., Bissel, H.J., and Fairbridge, R.W., eds., Carbonate Rocks. Developments in Sedimentology V. 9B: Amsterdam, Elsevier.

IRWIN, H., CURTIS, C., and COLEMAN, M., 1977, Isotopic evidence for source of diagenetic carbonates formed during burial of organic rich sediments: Nature, V. 269, p. 209 - 213.

JAFFEY, A.H., FLYNN, K.F., GLENDENIN, L.E., BENTLEY, W.C., and ESSLING, A.M., 1971, Precision measurements of half-lives and specific activities of ^{235}U and ^{238}U: Phys. Rev. C., V. 4, p. 1889 - 1906.

JENSEN, M.L., 1967, Sulphur isotopes and mineral genesis, in Barnes, H.L., ed., Geochemistry of Hydrothermal Ore Deposits: New York, Holt, Rhinehart and Winston Inc., p. 143 - 165.

JENSEN, M.L., and NAKAI, N., 1963, Sulphur isotope meteorite standards, results and recommendations, in Biogeochemistry of Sulphur Isotopes: Natl. Sci. Foundation Symposium Volume, p. 30 - 35.

KAJIWARA, Y., and KROUSE, H.R., 1971, Sulphur isotope partitioning in metallic sulphide systems: Canadian Jour. Earth Sci., V. 8, p. 1397 - 1408.

KAPLAN, I.R., EMERY, K.O., and RITTENBERG, S.C., 1963, The distribution and isotopic abundance of sulphur in recent marine sediments off southern California: Geochim. Cosmochim. Acta, V. 27, p. 297 - 331.

KAPLAN, I.R., and HULSTON, J.R., 1966, The isotopic abundance and content of sulphur in meteorites: Geochim. Cosmochim. Acta, V. 30, p. 479 - 496.

KASTNER, M., 1971, Authigenic feldspars in carbonate rocks: Am. Mineralogist, V. 56, p. 1403 - 1442.

KEITH, M.L., and WEBER, J.N., 1964, Carbon and oxygen isotopic composition of selected limestones and fossils: Geochim. Cosmochim. Acta, V. 28, p. 1787 - 1816.

KEMP, A.L.W., and THODE, H.G., 1968, The mechanism of the bacterial reduction of sulphate and of sulphite from isotope fractionation studies: Geochim. Cosmochim. Acta, V. 32, p. 71 - 91.

LEBEDEV, L.M., 1967, Metacolloids in Endogenic Deposits: New York, Plenum Press.

LEES, A., 1961, The Waulsortian "reefs" of Eire - a carbonate mud-bank complex of Lower Carboniferous age: J. Geol., V. 69, p. 101 - 109.

LEES, A., 1964, The Structure and origin of the Waulsortian (Lower Carboniferous) "reefs" of West - Central Eire: Phil. Trans. R. Soc. B, V. 247, p. 483 - 531.

LELEU, M. and GONI, J., 1974, Sur la formation biogéochemique de stalactites de galène: Mineral. Deposita, V. 9, p. 27 - 32.

Le ROUX, L.J., and GLENDENIN, L.E., 1963, Half-life of thorium - 232: Proc. Natl. Conf. on Nuclear Energy, Pretoria, April, 1963.

LINDBLOOM, G.P., and LUPTON, M.D., 1961, Microbiological aspects of organic geochemistry: Develop. Ind. Microbiol., V. 2, p. 9 - 22.

LONG, C.B., and MAX, M.D., 1977, Metamorphic rocks in the S.W. Ox Mountains inlier, Ireland; their structural compartmentation and place in the Caledonian orogen: Jl. Geol. Soc. Lond., V. 133, p. 413 - 432.

LOVE, L.G., 1957, Micro-organisms and the presence of syngenetic pyrite: Q. Jl. Geol. Soc. Lond., V. 113, p. 429 - 440.

LOVE, L.G., 1964, Early diagenetic pyrite in fine-grained sediments and the genesis of sulphide ores, in Amstutz, G.C., ed., Sedimentology and Ore Genesis. Developments in Sedimentology V. 2: Amsterdam, Elsevier.

LOWENSTAM, H.A., and EPSTEIN, S., 1957, On the origin of sedimentary aragonite needles of the Great Bahama Bank: J. Geol., V. 65, p. 364 - 375.

MacDERMOT, C.V., and SEVASTOPULO, G.D., 1972, Upper Devonian and Lower Carboniferous stratigraphical setting of Irish mineralization: Geol. Surv. Ireland Bull., V. 1, p. 267 - 280.

MacINTYRE, R.M., VAN BREEMAN, O., BOWES, D.R., and HOPGOOD, A.M., 1975, Isotopic study of the gneiss complex, Inishtrahull, Co. Donegal: Scient. Proc. R. Dubl. Soc. A, V. 5, p. 301 - 309.

MATSUHISA, Y., GOLDSMITH, J.R., and CLAYTON, R.N., 1978, Oxygen isotope fractionation in the system quartz - albite - anorthite - water: Geol. Soc. Am. Abstr., V. 8, p. 999.

MATTHEWS, A., and KATZ, A., 1977, Oxygen isotope fractionation during the dolomitisation of calcium carbonate: Geochim. Cosmochim. Acta, V. 41, p. 1431 - 1438.

McCREA, J.M., 1950, On the isotopic chemistry of carbonates and a palaeotemperature scale: J. Chem. Phys., V. 18, p. 849 - 857.

McCREADY, R.G.L., 1975, Sulphur isotope fractionation by Desulfovibrio and Desulfotomaculum species: Geochim. Cosmochim. Acta, V. 39, p. 1395 - 1401.

MILLIMAN, J.D., 1974, Recent Sedimentary Carbonates, pt. 1, Marine carbonates: Berlin, Springer - Verlag.

MOORBATH, S., 1962, Lead isotope abundance studies on mineral occurrences in the British Isles and their geological significance: Phil. Trans. R. Soc. A, V. 254, p. 295 - 360.

MOORE, J., 1975, Fault tectonics at Tynagh mine, Ireland: Trans. Instn. Min. Metall. (Sect. B: Appl, earth sci.), V. 84, p. 141 - 145.

MORRISSEY, C.J., 1970, The mineralogy, structure and origin of the lead - zinc - copper residual orebody at Tynagh, Co. Galway, Ireland: Unpub. Ph.D. thesis, London Univ.

MORRISSEY, C.J., and WHITEHEAD, D., 1970, Origin of the Tynagh residual orebody, Ireland, in Mining and Petroleum Geology. (Proc. 9th Commonw. Min. Metall. Congr. 1969, V. 2): London, Instn. Min. Metall., p. 131 - 145.

MORRISSEY, C.J., DAVIS, G.R., and STEED, G.M., 1971, Mineralization in the Lower Carboniferous of Central Ireland: Trans. Instn. Min. Metall. (Sect. B: Appl. earth sci.), v. 80, p. 174 - 184.

NAKAI, N., and JENSEN, M.L., 1964, The kinetic isotope effect in the bacterial reduction and oxidation of sulphur: Geochim. Cosmochim. Acta, V. 28, p. 1893 - 1912.

NELSON, F., and KRAUS, K.A., 1954, Anion – exchange studies. xi. Lead (II) and bismuth (III) in chloride and nitrate solutions: J. Am. Chem. Soc., V. 76, p. 5916 - 5920.

NORTHROP, D.A., and CLAYTON, R.N., 1966, Oxygen - isotope fractionations in systems containing dolomite: J. Geol., V. 74, p. 174 - 196.

OANA, S., and ISHIKAWA, H., 1966, Sulphur isotope fractionation between sulphur and sulphuric acid in the hydrothermal solution of sulphur dioxide: Geochem. J., V. 1, p. 45 - 50.

OHMOTO, H., 1972, Systematics of sulphur and carbon isotopes in hydrothermal ore deposits: Econ. Geol. V. 67, p. 551 - 578

O'NEIL, J.R., and TAYLOR, H.P., 1967, The oxygen isotope and cation exchange chemistry of feldspars: Am. Mineralogist, V. 52, p. 1414 - 1437.

O'NEIL, J.R., CLAYTON, R.N. and MAYEDA, T.K., 1969, Oxygen isotope fractionation in divalent metal carbonates: J. Chem. Phys., V. 51, p. 5547 - 5558.

ORR, W.L., 1974, Changes in sulphur content and isotopic ratios of sulphur during petroleum maturation – study of Big Horn Basin Palaeozoic oils: Am. Assoc. Petrol. Geol. Bull., V. 58 p. 2295 - 2318.

OVERSBY, V.M., 1974, New look at the lead isotope growth curve: Nature, V. 248, p. 132 - 133.

PATTERSON, J.M., 1971, The Keel, Co. Longford, Zinc – lead – cadmium deposit, in Skevington, D., ed., The genesis of base metal deposits in Ireland - Irish Geol. Assoc., Proc. Galway Symp.

PHILLIPS, W.E.A., TAYLOR, W.E.G., and SANDERS, I.S., 1975, An analysis of the geological history of the Ox Mountain inlier: Scient. Proc. R. Dubl. Soc. A, V. 5, p. 311 - 329

PHILLIPS, W.E.A., STILLMAN, J., and MURPHY, T., 1976, A Caledonian plate tectonic model: Jl. Geol. Soc. Lond., V. 132, p. 579 - 609.

PHILLIPS, W.J., 1972, Hydraulic fracturing and mineralization: Jl. Geol. Soc. Lond., V. 128, p. 337 - 359.

PINEAU, F., JAVOY, M., and BOTTINGA, Y., 1976, $^{13}C/^{12}C$ ratios of rocks and inclusions in popping rocks of the mid-Atlantic Ridge and their bearing on the problem of isotopic composition of deep-seated carbon: Earth Planet. Sci. Lett., V. 29, p. 413 - 421.

POCKLEY, R.P.C., 1961, Lead isotope and age studies of uranium and lead minerals from the British Isles and France: Unpub. Ph.D. thesis, Oxford Univ.

POWELL, R.A., and KINSER, C.A., 1958, Dithizone method for determination of lead in monazite: Anal. Chem., V. 30, p. 1139 - 1141.

RAFTER, T.A., 1957, Sulphur isotope variations in nature, Part 1 - The preparation of sulphur dioxide for mass spectrometer examination: N.Z. Jl. Sci. Technol. Sect. B, V, 38, p. 849 - 857.

RAMDOHR, P., 1969, The Ore Minerals and their Intergrowths: New York, Pergamon Press.

REES, C.E., 1970, The sulphur isotope balance of the ocean: an improved model: Earth Planet. Sci. Lett. V. 7, p. 366 - 370.

REES, C.E., 1973, A steady - state model for sulphur isotope fractionation in bacterial reduction processes: Geochim. Cosmochim. Acta, V. 37, p. 1141 - 1162.

REES, C.E., JENKINS, W.J., and MONSTER, J., 1978, The sulphur isotopic composition of ocean water sulphate: Geochim. Cosmochim. Acta, V. 42, p. 377 - 381.

RHODEN, H.N., 1958, The geology and mineralization of the Silvermines area, north Tipperary, Eire: Unpub. Ph.D. thesis, London Univ.

RICHARDS, J.R., 1971, Major lead orebodies - mantle origin ?: Econ. Geol., V. 66, p. 425 - 434.

RIEDEL, D., 1977, Zur geochemie und genese der lagerstatte Tynagh, Ireland: Dr. - Ing dissertation, Rheinisch - Westfalischen Technischen Hochschule, Aachen.

ROBINSON, B.W., and KUSAKABE, M., 1975, Quantitative preparation of sulphur dioxide, for $^{34}S/^{32}S$ analyses, from sulphides by combustion with cuprous oxide: Anal. Chem., V. 47, p. 1179 - 1181.

ROEDDER, E., 1968, The noncolloidal origin of "colloform" textures in sphalerite ores: Econ. Geol. V. 63, p. 451 - 471.

ROGERS, A.F., 1917, A review of the amorphous minerals: J. Geol., V. 25, p. 515 - 541.

RUSSELL, M.J., 1968, Structural controls of base metal mineralization in Ireland in relation to continental drift: Trans. Instn. Min. Metall. (Sect. B: Appl. earth sci.), V. 77, p. 117 - 128.

RUSSELL, M.J., 1974, Manganese halo surrounding the Tynagh ore deposits, Ireland; a preliminary note: Trans. Instn. Min. Metall. (Sect. B: Appl. earth sci.), V. 83, p. 65 - 66.

RUSSELL, M.J., 1975, Lithogeochemical environment of the Tynagh base - metal deposit, Ireland, and its bearing on ore deposition: Trans. Instn. Min. Metall. (Sect. B: Appl. earth sci.), V. 84, p. 128 - 133.

RYE, R.O., and OHMOTO, H., 1974, Sulphur and carbon isotopes and ore genesis - a review: Econ. Geol., V. 69, p. 826 - 842.

SAKAI, H., 1968, Isotopic properties of sulphur compounds in hydrothermal processes: Geochem. J., V. 2, p. 29 - 49.

SCHLANGER, S.O., 1964, Petrology of the limestones of Guam: U.S. Geol. Survey Prof. Papers, 403 - D, p. 1 - 52.

SCHULTZ, R.W., 1966a, Lower Carboniferous cherty ironstones at Tynagh, Ireland: Econ. Geol. V. 61, p. 311 - 342.

SCHULTZ, R.W., 1966b, The Northgate base - metal deposit at Tynagh, County Galway, Ireland (Discussion): Econ. Geol. V. 61, p. 1443 - 1449.

SCHULTZ, R.W., 1968, The geology of the primary sulphide - barite deposit at Tynagh, Ireland: Unpub. Ph.D. thesis, Dublin Univ. (TCD).

SCHWARCZ, H.P., 1969, The stable isotopes of carbon, in Wedepohl, K.H., ed., Handbook of Geochemistry: Berlin, Springer - Verlag, 6B1 - 6B15.

SCHWARCZ, H.P., and BURNIE, S.W., 1973, Influence of sedimentary environments on sulphur isotope ratios in clastic rocks - a review: Mineral. Deposita., V. 8, p. 264 - 277.

SHARMA, T., and CLAYTON, R.N., 1965, Measurement of $^{18}O/^{16}O$ ratios of total oxygen of carbonates: Geochim. Cosmochim. Acta, V. 29, p. 1347 - 1353.

SHEPPARD, S.M.F., 1977, Identification of the origin of ore-forming solutions by the use of stable isotopes, in Volcanic Processes in Ore Genesis: Geol. Soc. Lond. Spec. Publication No. 7, p. 25 - 41.

SHERIDAN, D.J.R., HUBBARD, W.P., and OLDROYD, R.W., 1967, A note on Tournaisian strata in northern Ireland: Scient. Proc. R. Dubl. Soc. A, v. 3, p. 33 - 37.

SMEJKAL, V., COOK, F.D., and KROUSE, H.R., 1971, Studies of sulphur and carbon isotope fractionation with micro-organisms isolated from springs of western Canada: Geochim. Cosmochim. Acta, V. 35, p. 787 - 800.

STACEY, J.S., and KRAMERS, J.D., 1975, Approximation of terrestrial lead isotope evolution by a two - stage model: Earth Planet. Sci. Lett., V. 26, p. 207 - 221.

STANTON, R.L. and RUSSELL, R.D., 1959, Anomalous leads and the emplacement of lead sulphide ores: Econ. Geol., V. 54, p. 588 - 607.

STEED, G.M., 1975, The geology and mineralization of the Gortdrum district Ireland: Unpub. Ph.D. thesis, London Univ.

STROGEN, P., 1974, The sub-Palaeozoic basement in central Ireland: Nature, V. 250, p. 562 - 563.

TATSUMOTO, M., KNIGHT, R.J. and ALLEGRE, 1973, Time differences in the formation of meteorites as determined from the ratio of lead -207 to lead -206 ! Science, V. 180, p. 1279 - 1283.

TAYLOR, H.P., 1974, The application of oxygen and hydrogen isotope studies to problems of hydrothermal alteration and ore deposition: Econ. Geol. V. 69, p. 843 - 883.

TAYLOR, H.P., FRENCHEN, J. and DEGENS, E.T., 1967, Oxygen and carbon isotope studies of carbonatites from the Laacher Sea district, West Germany, and the Alno district, Sweden: Geochim. Cosmochim. Acta, V. 31, p. 407 - 430.

THODE, H.G., MONSTER, J., and DUNFORD, H.B., 1961, Sulphur isotope geochemistry: Geochim. Cosmochim. Acta, V. 25, p. 159 - 174.

THODE, H.G., and MONSTER, J., 1965, Sulphur isotope gechemistry of petroleum, evaporites and ancient seas: Am. Assoc. Petrol. Geol. Mem. 4, p. 367 - 377.

TOLAND, W.G., 1960, Oxidation of organic compounds with aqueous sulphate: J. Am. Chem. Soc., V. 82, p. 1911 - 1916.

UREY, H.C., LOWENSTAM, H.A., EPSTEIN, S., and McKINNEY, C.R., 1951, Measurement of palaeotemperatures of the Upper Cretaceous of England, and the south-eastern United States: Bull. Geol. Soc. Am., V. 62, p. 399 - 416.

UYTENBOGAARDT. W., and BURKE, E.A.J., 1971, Tables for Microscopic Identification of Ore Minerals, 2nd edition: Amsterdam, Elsevier.

VALLENTYNE, J.R., 1963, Isolation of pyrite spherules from recent sediments: Limnol. Oceanogr., V. 8, p. 16 - 30.

VEIZER, J., and HOEFS, J., 1976, The nature of $^{18}O/^{16}O$ and $^{13}C/^{12}C$ secular trends in sedimentary carbonate rocks: Geochim. Cosmochim. Acta, V. 40, p. 1387 - 1395.

WEST, I.M., BRANDON, A., and SMITH, N., 1968, A tidal flat evaporitic facies in the Visean of Ireland: J. Sedim. Petrol., V. 38, p. 1079 - 1093.

WHITEHEAD, D., 1971, Base metal sulphides at Tynagh, in Skevington D., ed., The genesis of base metal deposits in Ireland - Irish Geol. Assoc., Proc. Galway Symp.

YODER, H.S., and EUGSTER, H.P., 1955, Synthetic and natural muscovite: Geochim. Cosmochim. Acta, V. 8, p. 255 - 280.

ZoBELL, C.E., 1963, Organic geochemistry of sulphur, in Berger, I.A., ed., Organic Geochemistry: New York, Pergamon Press.

APPENDIX 3.

UNDERGROUND DEVELOPMENT PLAN - TYNAGH.